Synthesis, Spectroscopy and Reactivity of Phenyl-Substituted 1,3-Biradicals

Thesis by

Frank D. Coms

In Partial Fulfillment of the Requirements
for the Degree of
Doctor of Philosophy

California Institute of Technology
Pasadena, California

1989

(Submitted May 5, 1989)

To Judi and Carly

Acknowledgement

I would first like to thank my advisor, Dennis Dougherty, for the support, encouragement, and guidance he has provided during my stay at Caltech.

Very special thanks go to my wife, Judi, for her unfailing love, patience, and support; and to Carly, for the joy she brings to my life every day.

I would also like to thank all the members of the Dougherty group for their friendship and support. Special thanks go to fellow "biradical guys" Rakesh Jain, Mike Sponsler, and Gary Snyder for their unselfish assistance in numerous areas including matrix-isolation EPR spectroscopy.

Thanks also go to Janet Nelson and Mark Trimmer for their invaluable help with the magnetization transfer experiments and for providing their computer programs for the data analysis.

I would also like to thank Debbie Chester for typing this thesis. I am also very grateful to Linda Clark who came through with some much-needed help as the end drew near. Finally, I would like to thank Rakesh Jain again for his invaluable proofreading of this thesis.

Abstract

Irradiation of frozen MTHF solutions of 1,4-diphenyl- and 1-methy-4-phenyl-2,3-diazabicyclo[2.1.1]hex-2-enes (**14** and **15**) at cryogenic temperatures produces the corresponding triplet 1,3-diphenyl- and 1-methyl-3-phenylcyclobutanediyls (**24-Ph** and **24-MP**) as monitored by EPR spectroscopy. The spectra of **24-Ph** and **24-MP** exhibit zero-field splitting (zfs) parameters of $|D/hc| = 0.060$ cm^{-1}, $|E/hc| = 0.001$ cm^{-1} and $|D/hc| = 0.082$ cm^{-1}, $|E/hc| = 0.003$ cm^{-1}, respectively. The triplet EPR spectra provide valuable information concerning biradical geometry and spin distribution. The trends in the observed D values can be quantitatively modeled using a relatively simple scheme for zfs calculations. Analysis of the hyperfine splitting pattern observed in the $\Delta m_s = 2$ transition of ^{3}**24-Ph** reveals that the four-membered ring is planar.

Upon warming biradicals ^{3}**24-Ph** and ^{3}**24-MP** to 20-50 K, nonexponential decay to the corresponding bicyclobutanes commence. The decay kinetics of ^{3}**24-Ph** were quantitatively studied from 27 to 54 K with the explicit inclusion of matrix-site effects. The kinetics analysis revealed that the variation of the decay rates with temperature follows the Arrhenius law, producing activation parameters of $\log A = 7.8$, $E_a° = 2.29$ kcal/mol. These activation parameters are compared with those of other cyclobutanediyls.

Photolysis of matrix-isolated 1,4-diphenyl-2,3-diazabicyclo[2.2.1]-hept-2-ene (**21**) in the cavity of an EPR spectrometer at 3.8 and 77 K produces the triplet spectrum of 1,3-diphenylcyclopentanediyl **20**. The zfs parameters of the spectrum are $|D/hc| = 0.045$ cm^{-1}, $|E/hc| = 0.001$ cm^{-1}. The observed zfs parameters and hyperfine splitting pattern are completely in line with expectation and are consistent with a planar cyclopentanediyl geometry.

Biradical ^{3}**20** is considerably more persistent than its four-membered ring analog ^{3}**24-Ph**.

1,4-Diphenylbicyclo[2.1.0]pentane (**22**), the closed-shell isomer of **20**, possesses a very weak C1-C4 bond. This weak bond is manifested in the low activation barrier for a degenerate bridge-flip process. Through a combination of ^{1}H NMR complete lineshape analysis and magnetization transfer studies, the activation parameters for this process are determined to be $\Delta H^\ddagger = 12.2$ kcal/mol, $\Delta S^\ddagger = -16.4$ eu. At room temperature, bicyclopentane **22** reacts rapidly to form 2,3-dioxa-1,4-diphenylbicyclo[2.2.1]heptane (**23**). Using the activation parameters for the bridge-flip reaction along with other data results in the development of a detailed model of the kinetic and thermodynamic relationships among ^{1}**20**, ^{3}**20**, and **22**.

Table of Contents

Chapter 3 – 1,3-Diphenyl-1,3-cyclopentanediyl 109

List of Figures

List of Tables

List of Schemes

Chapter 1

Introduction

Biradicals are molecules that possess one fewer bond than allowed by the standard rules of valence. These bond-broken species have been invoked as reactive intermediates in numerous thermal and photochemical reactions.[1] The chemical reactivity of biradicals is also of great importance as a source of information on the fundamental issues of structure and bonding. In recent years, biradicals have been recognized as interesting molecules in their own right, especially when viewed as potential building blocks for new materials possessing novel magnetic and electrical properties.[2]

Theoretical Description of Biradicals

In valence bond terminology, a biradical may be defined as an even-electron molecule that has two distinct radical centers. The spins may be oriented either antiparallel to give a singlet (S = 0), or parallel to give a triplet (S = 1). The discussion here will be limited to homosymmetric biradicals[3] in which the unpaired electrons reside in two *p*-type orbitals, χ_l and χ_r (Figure 1-1). From these basis orbitals, we can construct two formally nonbonding molecular orbitals (NBMOs), ϕ_s which is symmetric to mirror inversion and slightly bonding, and ϕ_a which is antisymmetric and slightly antibonding

$$\phi_s = (2 + 2\,S_{lr})^{-1/2}(\chi_l + \chi_r) \qquad (1\text{-}1)$$

$$\phi_a = (2 - 2\,S_{lr})^{-1/2}(\chi_l - \chi_r) \qquad (1\text{-}2)$$

(eq 1-1,2). In the limit where the overlap between χ_l and χ_r is zero ($S_{lr} = 0$), ϕ_s and ϕ_a will be exactly degenerate.[3-5] In molecular orbital terms, then, a

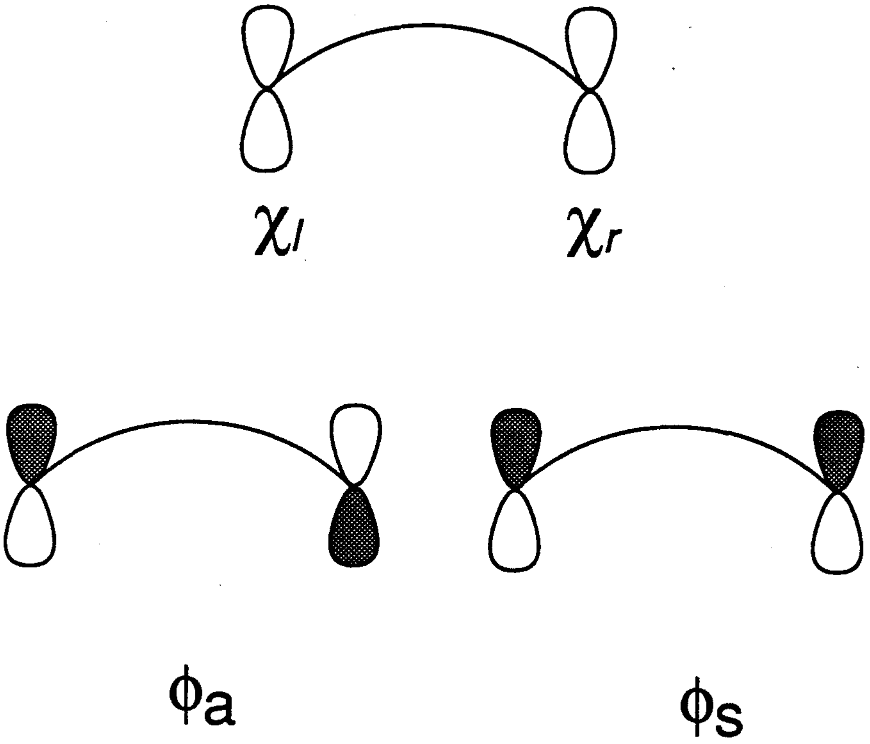

Figure 1-1. Nonbonding molecular orbitals of a homosymmetric biradical.

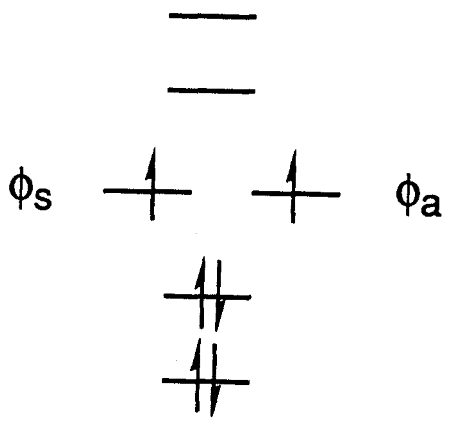

Figure 1-2. Molecular orbital representation of a biradical.

biradical is defined as a molecule that contains two electrons in two degenerate or nearly-degenerate nonbonding molecular orbitals[3] (Figure 1-2).

Upon assigning of two electrons to two NBMOs, six possible configurations arise. Three of these configurations comprise the three components of the triplet state, while the three remaining configurations give rise to three singlet states. The configuration where both electrons occupy the symmetric NBMO, $\phi_S{}^2$, is a good description of the ground state of the singlet function when S_{lr} is large (*i.e.*, strong bonding between χ_l and χ_r). However, in biradicals, where S_{lr} is very small or zero, $\phi_S{}^2$ provides a poor description of the singlet biradical ground state. This can be seen by expanding $\phi_S{}^2$ in terms of χ_l and χ_r when $S_{lr} = 0$ (eq 1-3). The ionic terms in eq 1-3, where both electrons

$$\phi_s^2 = \frac{1}{2}\left[\chi_l(1)\chi_r(2) + \chi_r(1)\chi_l(2) + \chi_l(1)\chi_l(2) + \chi_r(1)\chi_r(2)\right] \qquad (1\text{-}3)$$

occupy the same atomic orbital, lead to unfavorable Coulomb repulsions. A proper description of the covalent singlet biradical can be constructed by mixing $\phi_S{}^2$ with $\phi_a{}^2$ such that the ionic terms cancel. This is accomplished by taking the negative combination

$$\lambda\phi_s^2 - (1 - \lambda^2)^{1/2}\phi_a^2 \qquad (1 \geq \lambda > 1/\sqrt{2}).$$

This two-configuration wavefunction can contain a variable amount of ionic character depending on the value of the mixing coefficient λ. In the limit where S_{lr} goes to zero ($\lambda = 1/\sqrt{2}$), the purely covalent singlet function is obtained (eq 1-4). The opposite combination of the $\phi_S{}^2$ and $\phi_a{}^2$ configurations

$$ {}^{1}\psi = \frac{1}{\sqrt{2}}\left[\phi_s^2 - \phi_a^2\right] = \frac{1}{\sqrt{2}}\left[\chi_l(1)\chi_r(2) + \chi_r(1)\chi_l(2)\right] \qquad (1\text{-}4) $$

gives rise to a purely ionic wavefunction in the limit where S_{lr} goes to zero (eq 1-5). This wavefunction describes the doubly-excited singlet state. The two remaining configurations, the singly-excited singlet state and the triplet state, can be described by single configuration wavefunctions and are independent of the value of S_{lr}. The singlet configuration is purely ionic (eq 1-6). The triplet wavefunction is properly described by equation 1-7.

$$ {}^{1}\psi = \frac{1}{\sqrt{2}}\left[\phi_s^2 + \phi_a^2\right] = \frac{1}{\sqrt{2}}\left[\chi_l(1)\chi_l(2) + \chi_r(1)\,\chi_r(2)\right] \qquad (1\text{-}5) $$

$$ {}^{1}\psi = \frac{1}{\sqrt{2}}\left[\phi_s(1)\,\phi_a(2) + \phi_a(1)\phi_s(2)\right] = \frac{1}{\sqrt{2}}\left[\chi_l(1)\chi_l(2) - \chi_r(1)\,\chi_r(2)\right] \qquad (1\text{-}6) $$

$$ {}^{3}\psi = \frac{1}{\sqrt{2}}\left[\phi_s(1)\,\phi_a(2) - \phi_a(1)\phi_s(2)\right] = \frac{1}{\sqrt{2}}\left[\chi_l(1)\chi_r(2) - \chi_r(1)\chi_l(2)\right] \qquad (1\text{-}7) $$

Summarizing, the biradical configurations give rise to four states: a low-lying singlet-triplet pair of covalent states (eq 1-4,7) and a pair of excited ionic states (eq 1-5,6). The covalent singlet state (eq 1-4) is described by a two configuration wavefunction, whereas the triplet (eq 1-7) is described as a single configuration.

When discussing the chemically relevant states of homosymmetric biradicals, the ionic states can be removed from consideration because of their high energy relative to the covalent singlet and triplet.[3,6] The relative ordering of the covalent singlet and triplet is strongly correlated to the magnitude of S_{lr}.[4,5] The magnitude of S_{lr} can contain contributions from both through-space and through-bond effects. When S_{lr} is close to zero, ϕ_S and ϕ_a become very nearly degenerate. In this situation, the two-electron exchange integral (K_{lr}) favors the triplet state. The key to obtaining a strong triplet preference, then, is to have a zero or near-zero overlap *and* maintain a strong exchange interaction. In contrast, as S_{lr} becomes large, ϕ_S is stabilized and ϕ_a is destabilized as a bond forms between the radical centers. Thus, increasing S_{lr} leads to a strong singlet preference.

General Considerations. The reactivity of the two covalent states of homosymmetric biradicals differ dramatically. As a consequence of its parallel spins, the triplet biradical must invert a spin and cross to the singlet surface before it can undergo any unimolecular reaction to give a closed-shell molecule. This intersystem crossing (ISC) is, in general, a highly inefficient process for hydrocarbon biradicals and, in turn, imparts an extended lifetime to the triplet biradicals. The singlet biradicals do not experience such a spin barrier and hence have a much shorter lifetime. The triplet also possesses a permanent magnetic moment which allows its direct detection by electron paramagnetic resonance (EPR) spectroscopy.[8] For the above mentioned reasons, studies aimed at the direct detection of biradicals have focussed mainly on the triplet state, although recent studies have reported the direct detection of an exceptionally long-lived singlet biradical by solid-state nuclear magnetic resonance (NMR) spectroscopy.[9]

Biradicals may be classified as either localized or delocalized, the latter class representing the overwhelming majority of directly observed biradicals. Delocalized biradicals have been referred to as non-Kekulé molecules because their unpaired electrons occupy a classical π system but are topologically forbidden from forming a π bond. Examples of delocalized biradicals include trimethylenemethane (**1**),[10] tetramethyleneethane (**2**),[11] 2,4-dimethylene-1,3-cyclobutanediyl (**3**)[12] and *m*-quinodimethane (**4**).[13] The non-Kekulé nature and, to a considerable extent, the spin preferences of such structures are set by the toplogies of the π systems.[14]

1

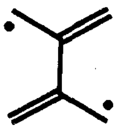

2

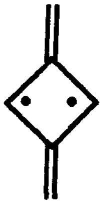

3

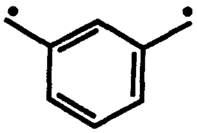

4

In contrast, direct spectroscopic studies of localized biradicals are rare. Localized biradicals contain two well-defined radical substructures which are not in classical π conjugation with one another. The radical units themselves can be classically delocalized, such as allyl or benzyl. A typical example of a localized biradical is trimethylene **5**. For over 50 years, this 1,3-biradical has been invoked as either a transition state or an intermediate in the thermal reactions of cyclopropane. Unlike non-Kekulé molecules, there

5

are no simple topological rules for the prediction of the ground state of localized biradicals. Instead, a subtle and sometimes complicated interplay among factors such as ring strain, steric effects and second-order electronic effects (e.g., through-bond coupling) determines the electronic ground state.[3-5]

Localized Biradicals. The first direct spectroscopic study of a localized hydrocarbon biradical was reported in 1975 by Buchwalter and Closs when they observed the triplet state of 1,3-cyclopentanediyl (**6**) by EPR spectroscopy.[15] This trimethylene derivative was generated by photolysis of 2,3-diazabicyclo[2.2.1]hept-2-ene (**7**) in frozen organic solutions at cryogenic temperatures. Biradical **6** was assigned to have a triplet ground state based on the fact that it could be observed at temperatures as low as 1.3 K. *Ab initio*

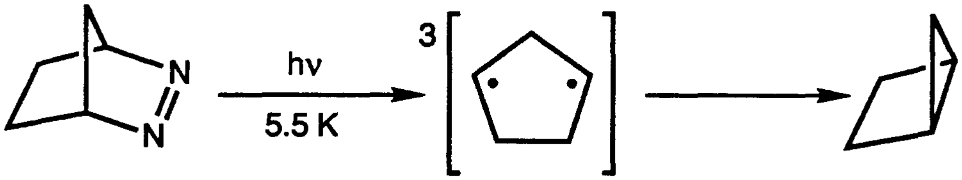

7 **6** **8**

calculations also confirmed this experimental observation, finding the triplet state 0.9 kcal/mol below the singlet state (S-T gap = 0.9 kcal/mol) at the planar geometry.[7] The EPR signal exhibited nonexponential decay from 1.3 to 40 K. The decay process was assigned to be the closure reaction to give bicyclo[2.1.0]-pentane (**8**). It was also found that the decay rate was quite insensitive to temperature from 5-20 K, indicating that reaction was proceeding via a heavy-atom tunneling mechanism. Assuming a preexponential factor of 10^8, the fit of the kinetic data to the Bell tunneling model indicated an activation energy of 2.3 kcal/mol. This initial investigation appeared to pave the way for other, more comprehensive, studies of this important class of reactive intermediates. Unfortunately, the cyclopentanediyl framework proved to be quite sensitive. For example, simple methyl substitutions led to very weak EPR signals or no signals at all.[16] Thus, a systematic study of the role of substituents on biradical spectroscopy and reactivity was not possible.

Subsequently, Goldberg and Doughtery undertook an *ab initio* study of the next smaller homolog of **6**, 1,3-cyclobutanediyl (**9**).[4] They found that **9** should also possess a triplet ground state, and in fact, the triplet preference of **9**

9

was found to be roughly twice that of **6** (1.7 *vs.* 0.9 kcal/mol). The calculations showed that in both **6** and **9** a fortuitous balance between through-space and through-bond effects gives rise to very nearly degenerate NBMOs (*i.e.* $S_{lr} \approx 0$). Therefore, because exchange repulsions in both **6** and **9** are large, triplet ground states result.

Given the predicted strong triplet preference of **9**, the azoalkane precursor 2,3-diazabicyclo[2.1.1]hex-2-ene (**10**) was prepared by Chang and Dougherty.[16] Upon photolysis of **10** at cryogenic temperatures, however, no triplet EPR signal was observed. Rationalizing that the likelihood of observing a triplet cyclobutanediyl may be increased by stabilizing the radical centers, 1,4-dimethyl-2,3-diazabicyclo[2.1.1]hex-2-ene (**11**) was synthesized. Photolysis of **11** at cryogenic temperatures in an organic matrix produced

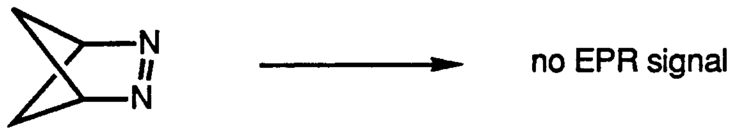

10

triplet 1,3-dimethylcyclobutanediyl (**12**).[17] Like **5**, this cyclobutanediyl also exhibited temperature independent nonexponential decay between 4 and 10 K indicating tunneling.[17] The decay process was also shown to be closure, giving 1,3-dimethylbicyclo[1.1.0]butane (**13**).

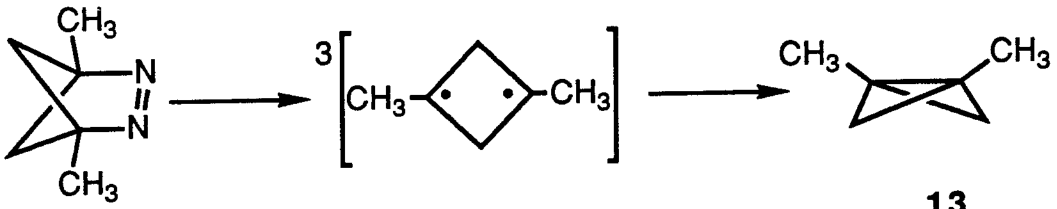

11 **12** **13**

More recent theoretical work indicates a likely cause of the failure to observe ^{3}**9**.[18] A careful geometry optimization of ^{3}**9** reveals that the ground state is not planar (D_{2h}) but rather C_{2h}. In this ground-state structure, the cyclobutane ring is planar, but the hydrogens attached to the radical centers have moved out of the plane of the ring. Furthermore, it was found that there is a rapid interconversion ($k \sim 10^{12}$ s^{-1}) to a C_{2v} form via H-atom tunneling. It was also found that singlet-triplet surface crossings can be readily achieved simply by the motion of a hydrogen atom attached to the radical center. This process results in relatively fast ISC ($k \sim 10^{7}$ s^{-1}) and very short triplet lifetimes. Triplet **9** simply tunnels to the singlet too rapidly to be observed. Methyl groups appended to the radical centers greatly reduce the tunneling rate and allow the observation of ^{3}**12**.

The present work is concerned with the synthesis, spectroscopy and reactivity of phenyl-substitued 1,3-biradicals.[19] At the outset of this work several questions concerning the effect of phenyl substitution arose. What effect will delocalizing substituents have on the S-T gap? If the triplet biradicals are observable, will they be more or less stable than those with simple alkyl group substituents? What factors govern the stability: sterics (*i.e.*, matrix effects) or electronics? To answer these questions the appropriate diazene precursors were required.

A general synthetic scheme for the synthesis of bridgehead-substituted 2,3-diazabicyclo[2.1.1]hex-2-enes **14-16** was developed. Photolysis of **14** or **15** in a 2-methyltetrahydrofuran (MTHF) matrix at 4 K produced the corresponding triplet cyclobutanediyls **17** and **18** which, unlike **6** and **12**, were indefinitely stable up to roughly 20 K. Photolysis of diazene **16** did not produce an EPR signal. The observed zero-field splitting parameters of **17** and **18** are completely in agreement with the assignments and provide valuable information about the distribution of spin density in biradicals. The hyperfine splittings observed in the half-field transition of **17** supplied structural information which revealed that the cyclobutanediyl ring is planar.

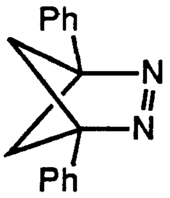

14

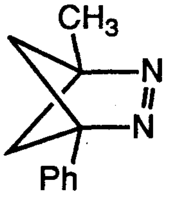

15

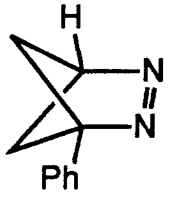

16

The nonexponential decay of the EPR signal of **17** was quantitatively studied from 27-54 K. By employing our previously described protocol for analyzing such dispersive decay kinetics, we have determined that the decay of

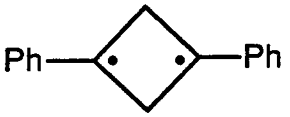

17

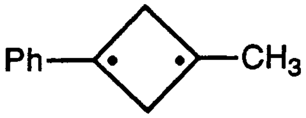

18

17 to 1,3-diphenylbicyclo[1.1.0]butane (19) follows conventional Arrhenius behavior. This, and other work from these laboratories,[19ab] has established that 1,3 cyclobutanediyls constitute a general class of observable localized 1,3-biradicals.

17 **19**

Noting the marked stability increase observed in the cyclobutanediyl series when phenyl is substituted for methyl, we rationalized that 1,3-diphenyl-1,3-cyclopentanediyl 20 merited investigation. A synthesis of 1,4-diphenyl-2,3-diazabicyclo[2.2.1]hept-2-ene (21) was developed and, upon photolysis in an MTHF matrix at 77 K, a strong EPR signal attributable to 20 was observed. The observed zero-field splitting parameters and hyperfine splitting pattern were completely in accord with theoretical predictions. Thus,

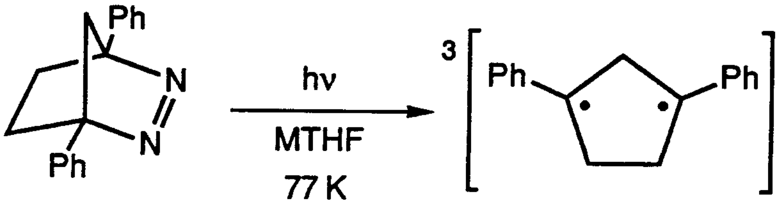

21 **20**

despite the apparent capriciousness of the cyclopentanediyl framework, **20** is readily observable at 77 K and is orders of magnitude more stable than ^{3}**17**. Biradicals **17** and **20** constitute the first set where direct comparisons between cyclobutanediyls and cyclopentanediyls can be made and allows us to better determine what factors govern biradical stability/reactivity.

The EPR spectroscopy of two deuterated derivatives of **20** were also studied. The EPR decay kinetics of ^{3}**20**-d_2 were observed to exactly parallel ^{3}**20** . However, the rate of decay of tetradeutero biradical ^{3}**20**-d_4 was found to be a factor of five slower than ^{3}**20** at 77 K. Furthermore, the matrix effect observed for the decay of ^{3}**20**-d_4 is substantially larger than that of ^{3}**20**.

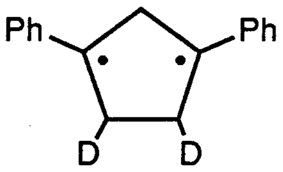

20-d_2

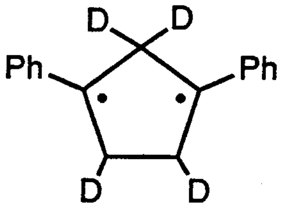

20-d_4

Photolysis or gentle heating of diazene **21** cleanly produces 1,4-diphenylbicyclo[2.1.0]pentane (**22**). Compound **22** is a quite unusual molecule in that it possesses an extremely weak C1-C4 bond and yet it is indefinitely stable at room temperature. This weak bond is manifest in the very low barrier for the degenerate bridge-flip process which proceeds via the singlet biradical ^{1}**20**. Through a combination of ^{1}H NMR complete lineshape analysis and magnetization transfer studies we have determined the activation parameters for this process.

Bicyclopentane **22** is also observed to undergo a rapid reaction with oxygen at room temperature to give predominantly endoperoxide **23**. This reaction is believed to proceed via ^{1}**20**. The kinetics of this trapping reaction

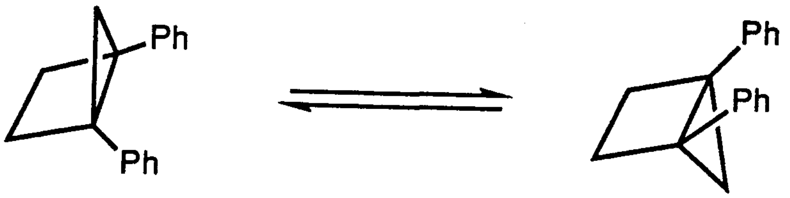

22

have been quantitatively studied by Adam and Wirz.[20] Their data, combined with our activation parameters for the bridge-flip reaction, result in a remarkably detailed model of the kinetic and thermodynamic relationships among **22**, ^{1}**20**, and ^{3}**20**.

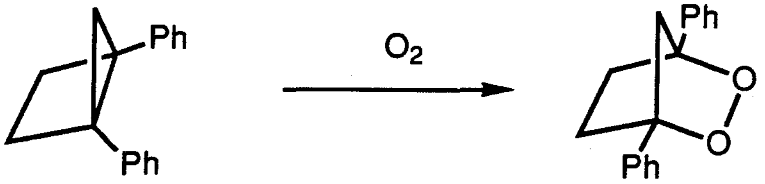

22 **23**

References and Notes

1. For an overview of biradical chemistry see: *Diradicals*; Borden, W. T., Ed.; Wiley: New York, 1982.
2. Pranata, J.; Dougherty, D. A. *J. Am. Chem. Soc.* **1987**, *109*, 1621-1627.
3. Salem, L; Rowland, C. *Angew. Chem., Int. Ed. Engl.* **1972**, *11*, 92-111. Salem, L. *Pure Appl. Chem.* **1973**, *33*, 317-328.
4. Goldberg, A. H.; Dougherty, D. A. *J. Am. Chem. Soc.* **1983**, *105*, 284-290.
5. Doubleday, C., Jr.; McIver, J. W., Jr.; Page, M. *J. Am. Chem. Soc.* **1982**, *104*, 6533-6542.
6. *Ab initio* calculations[7] have placed these ionic states some 90 kcal/mol above the covalent states.
7. Conrad, M. P.; Pitzer, R. M.; Schafer, H. F., III *J. Am. Chem. Soc.* **1979**, *101*, 2245-2246.
8. Dougherty, D. A. in *Kinetics and Spectroscopy of Carbenes and Biradicals;* Platz, M. S., Ed.; Plenum Press: New York, in press.
9. Zilm, K. W. ; Merrill, R. A.; Greenberg, M. M.; Berson, J. A. *J. Am. Chem. Soc.* **1987**, *109*, 1567-1569. Zilm, K. W.; Merrill, R. A.; Webb, G. G.; Greenberg, M. M.; Berson, J. A. *J. Am. Chem. Soc.* **1989**, *111*, 1533-1535.
10. Dowd, P. *Acc. Chem. Res.* **1972**, *5*, 242-248.
11. Dowd, P.; Chang, W.; Paik, Y. H. *J. Am. Chem. Soc.* **1986**, *108*, 7416-7417.
12. Snyder, G. J.; Dougherty, D. A. *J. Am. Chem. Soc.* **1985**, *107*, 1774-1775. Snyder, G. J.; Dougherty, D. A. *J. Am. Chem. Soc.* **1986**, *108*, 299-300.

13. Wright, B. B.; Platz, M. S. *J. Am. Chem. Soc.* **1983**, *105*, 628-630. Haider, K.; Platz, M. S.; Despres, A.; Lejeune, V.; Migirdicyan, E.; Bally, T.; Haselbach, E. *J. Am. Chem. Soc.* **1988**, *110*, 2318-2320.

14. For recent discussions of such rules, see: (a) Ovchinnikov, A. A. *Theor. Chim. Acta* **1978**, *47*, 297-304. (b) Klein, D. J.; Nelin, C. J.; Alexander, S.; Matsen, F. A. *J. Chem. Phys.* **1982**, *77*, 3101-3108. (c) Borden, W. T.; Davidson, E. R. *J. Am. Chem. Soc.* **1977**, *99*, 4587-4594.

15. Buchwalter, S.L.; Closs, G.L. *J. Am. Chem. Soc.* **1975**, *97*, 3857-3858. Buchwalter, S.L.; Closs, G.L. *J. Am. Chem. Soc.* **1979**, *101*, 4688-4694.

16. Chang, M. H.; Dougherty, D. A. *J. Org. Chem.* **1981**, *46*, 4092-4093. Chang, M. H.; Dougherty, D. A. *J. Am. Chem. Soc.* **1982**, *104*, 2333-2334.

17. Jain, R.; Snyder, G. J. ; Dougherty, D. A. *J. Am. Chem. Soc.* **1984**, *106*, 7294-7295.

18. Pranata, J.; Dougherty, D. A. *J. Phys. Org. Chem.* **1989**, in press.

19. Much of the present work has been reported in the following publications: (a) Jain, R.; Sponsler, M. B.; Coms, F. D.; Dougherty, D. A. *J. Am. Chem. Soc.* **1988** *110*, 1356-1366. (b) Sponsler, M. B., Jain, R.; Coms, F. D.; Dougherty, D. A. *J. Am. Chem. Soc.* **1989**, *111*, 2240-2252. (c) Coms, F. D.; Dougherty, D. A. *Tetrahedron Lett.* **1988**, *29*, 3753-3756. (d) Coms, F. D.; Dougherty, D. A. *J. Am. Chem. Soc.* submitted for publication.

20. Adam, W.; Wirz, J. personal communication. Adam, W.; Platsch, H.; Wirz, J. *J. Am. Chem. Soc.* submitted for publication.

Chapter 2

Phenyl-Substituted 1,3-Cyclobutanediyls

A wide variety of biradicals and related structures have been directly observed by EPR spectroscopy in the last 25 years.[1,2] The majority of such studies have involved delocalized biradicals.[2] In 1975, the first direct spectroscopic study of a localized, hydrocarbon biradical was reported by Buchwalter and Closs.[3] They observed the triplet state of 1,3-cyclopentanediyl (**6**) by EPR spectroscopy upon photolysis of diazene **7** at cryogenic temperatures in organic matrices. The triplet signal of **6** can be observed at temperatures as low as 1.3 K where thermal population of a triplet is highly unlikely. This observation strongly suggests that the triplet state is the ground state. This study remained the only successful effort of its kind until 1984 when workers from these laboratories reported the observation of the triplet state of 1,3-dimethylcyclobutanediyl (**24-Me**) when diazene **11** was photolyzed at 4 K.[4] We have subsequently found that cyclobutanediyls constitute a general class of directly observable, localized 1,3 biradicals and that their spectroscopy and reactivity can be directly probed as a function of structure. The work described herein is primarily concerned with the

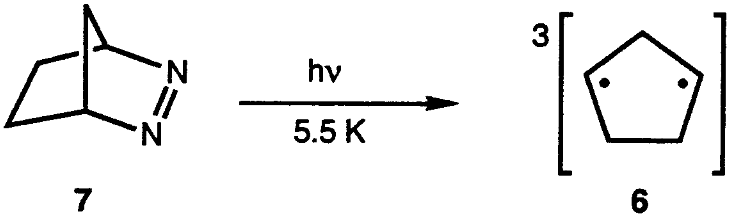

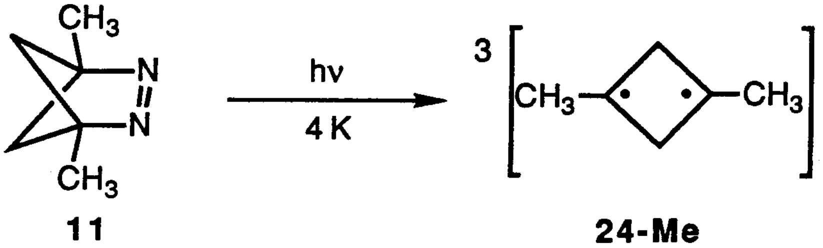

synthesis, spectroscopy and reactivity of phenyl substituted cyclobutanediyls, specifically 1,3-diphenylcyclobutanediyl **24-Ph**, 1-methyl-3-phenylcyclobutanediyl **24-MP** and 1-phenylcyclobutanediyl **24-PhH**.[5] Other cyclobutanediyls (**24**) will also be included in much of the discussion for the purpose of comparison (Table 2-1).

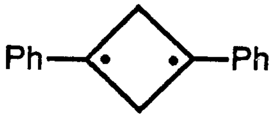

24-Ph

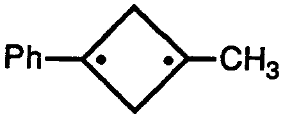

24-MP

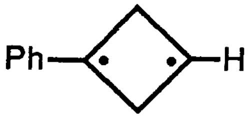

24-PhH

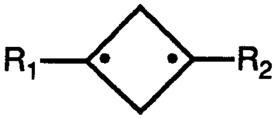

Table 2-1. Cyclobutanediyls

R_1	R_2	Label
H	H	**24-H**
CH_3	CH_3	**24-Me**
C_2H_5	C_2H_5	**24-Et**
H	Ph	**24-PhH**
CH_3	Ph	**24-MP**
Ph	Ph	**24-Ph**
C_2H_5	$CH{=}CH_2$	**24-EV**
$CH{=}CH_2$	$CH{=}CH_2$	**24-Vin**
$CD{=}CD_2$	$CD{=}CD_2$	**24-Vin-**d_6

Synthesis

The immediate precursors to the biradicals **24** are the substituted 2,3-diazabicyclo[2.1.1]hex-2-enes which, in turn, are prepared from the appropriate urazoles. Earlier work in these laboratories[6] demonstrated that addition of N-methyltriazolinedione (MTAD) across the strained central bond of a bicyclobutane provides a convenient method for the synthesis of such urazoles.[7] One key to the synthesis of the diazenes, then, is to obtain the appropriately functionalized bicyclobutanes for the MTAD addition.

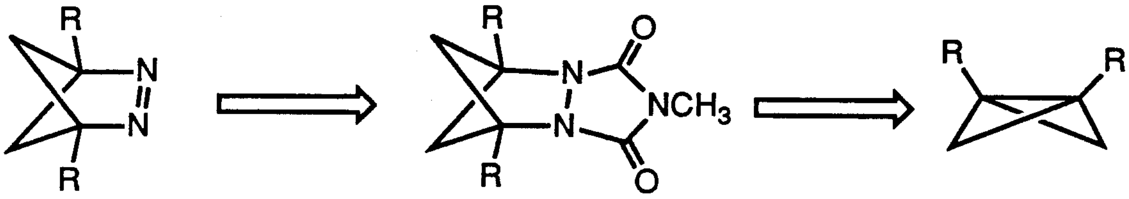

A fairly general route to substituted bicyclobutanes is based on the reductive coupling of 1,3-dihalocyclobutanes. The synthesis of the diphenyl urazole **25**, then, began with α-truxillic acid[8] which was converted in four steps to the known 1,3-dibromo-1,3-diphenylcyclobutane[9] as a 1:1 mixture of diastereomers (Scheme 2-1). Closure of the dibromides to 1,3-diphenylbicyclobutane (**19**) is efficiently accomplished by treatment with lithium amalgam. The thermal addition of MTAD to **19** in refluxing *n*-hexane then afforded urazole **25** in good yield.

Bicyclobutane **19** proved to be rather sensitive to dioxygen. For example, left unprotected from air at room temperature a sample of **19** reacts with oxygen to give epoxyketone **26** and an ill-defined polymer over a period of 12 h. One reasonable mechanism for the formation of **26** involves reaction of **19** to give the endoperoxide **27** followed by rearrangement to the epoxyketone.

Scheme 2-1

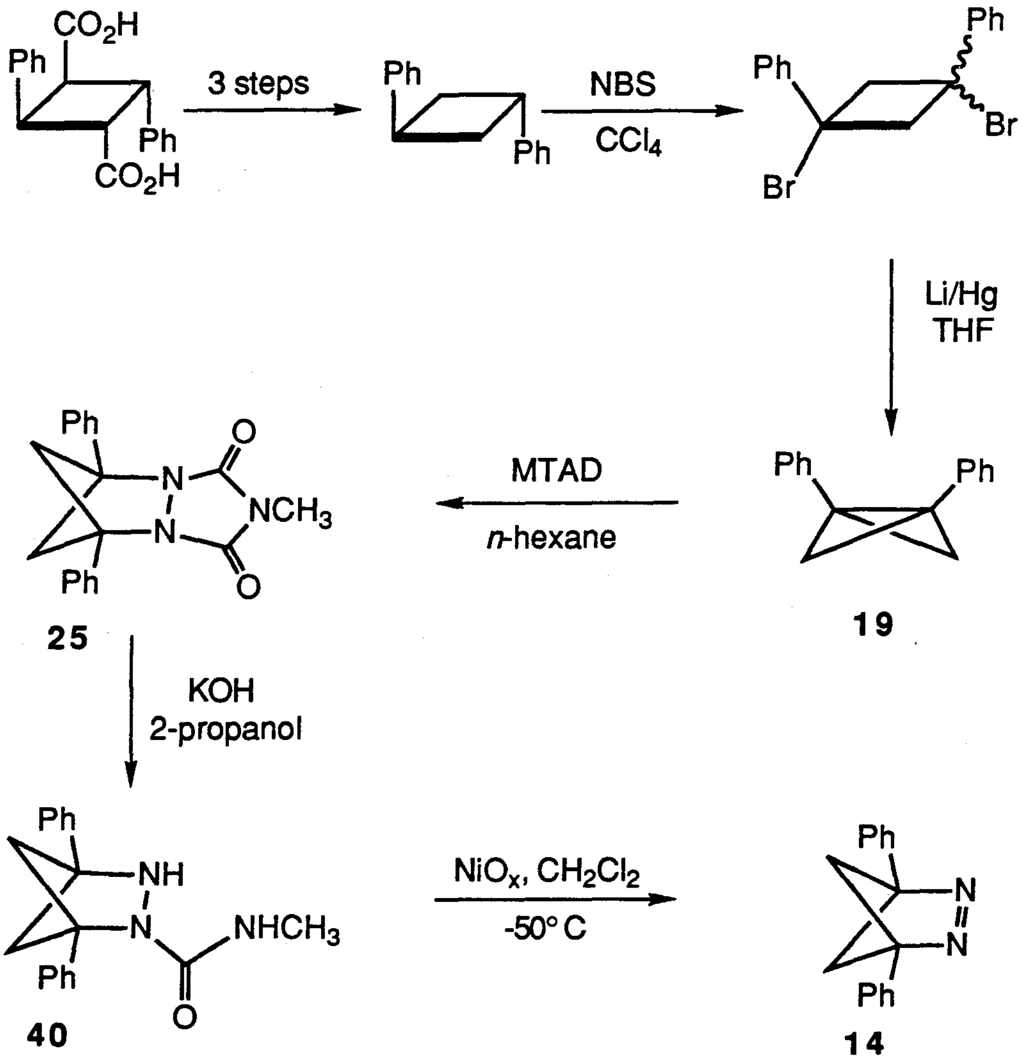
CO$_2$H
Ph
Ph
CO$_2$H
3 steps
Ph
Ph
NBS
CCl$_4$
Ph
Ph
Br
Br
Li/Hg
THF
Ph
Ph
19
MTAD
n-hexane
Ph
O
N
N
NCH$_3$
O
Ph
25
KOH
2-propanol
Ph
NH
N
NHCH$_3$
O
Ph
40
NiO$_x$, CH$_2$Cl$_2$
-50° C
Ph
N
N
Ph
14

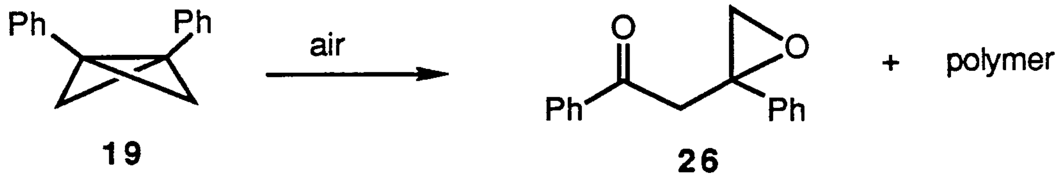

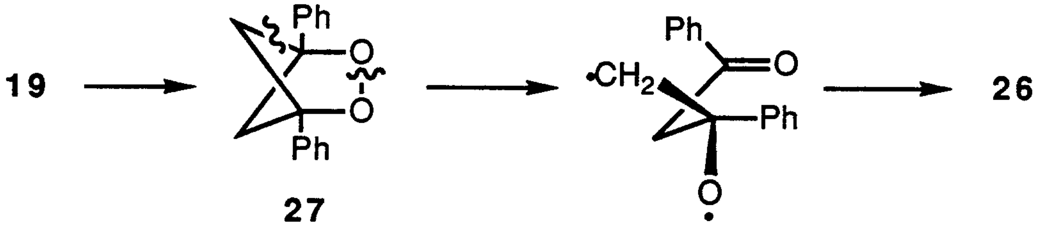

Analogous rearrangements have been observed for a number of 1,2-dioxolanes.[10] For example, 2,3-dioxabicyclo[2.2.1]heptane **28** undergoes a rearrangement to epxoyaldehyde **29** via simultaneous homolytic cleavages of the O-O and β C-C bonds.[10a] The existence of endoperoxide **27** should, at best, be only transient because the strain energy of the bicyclo[2.1.1]hexane skeleton (*ca.* 35 kcal/mol)[11] is nearly equal to the O-O bond strength of peroxides.

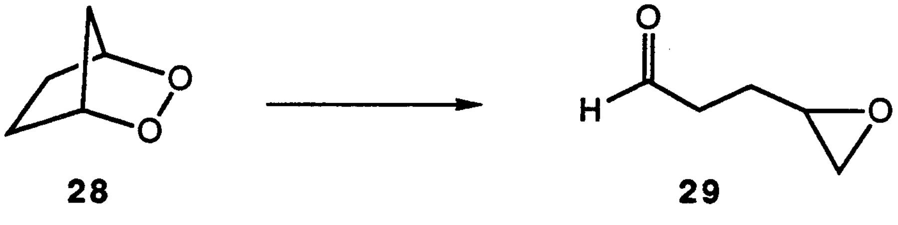

The syntheses of the methyl-phenyl and monophenyl urazoles (**30** and **31**) follow parallel paths that begin with 3-phenylcyclobutanone[12] (Scheme 2-2). The syntheses differ only in the first step wherein the ketone is reduced with either methyllithium or sodium borohydride to afford

Scheme 2-2

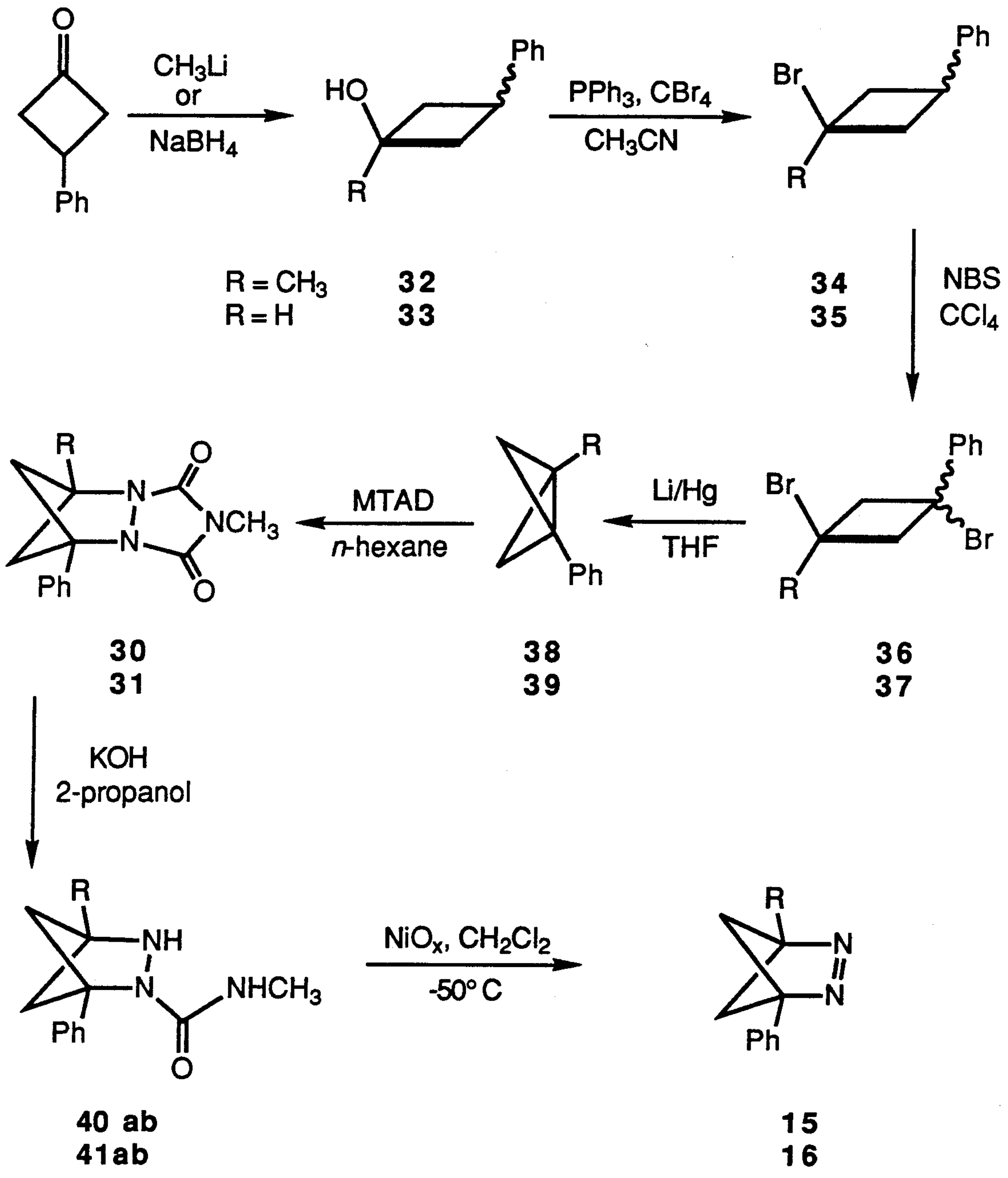
O
Ph
CH3Li
or
NaBH4
HO
Ph
R
R = CH3
R = H
32
33
PPh3, CBr4
CH3CN
Br
Ph
R
34
35
NBS
CCl4
Br
Ph
Br
R
36
37
Li/Hg
THF
R
Ph
38
39
MTAD
n-hexane
R
O
N
NCH3
N
Ph
O
30
31
KOH
2-propanol
R
NH
N
NHCH3
Ph
O
40 ab
41ab
NiOx, CH2Cl2
-50° C
R
N
N
Ph
15
16

diastereomeric mixtures of alcohols. Converting the hydroxyls to bromides using triphenylphosphine-carbon tetrabromide followed by benzylic bromination gives the dibromides **36** and **37** in very good yield. Of course, from the dibromides, the synthesis of urazoles **30** and **31** is identical to **25**.

Bicyclobutanes **38** and **39** did not exhibit the severe oxygen sensitivity that plagued **19**, but both were quite prone to rearrangement to the corresponding cyclobutenes under mildly acidic conditions.

The standard method of converting urazoles to 1,2-diazenes involves basic hydrolysis followed by an oxidation via copper complexes.[13] Several attempts to convert diphenyl urazole **25** to diazene **14** using this method, however, produced only very low yields of an unmanageable copper complex. We then turned our attention to an alternative hydrolysis-oxidation procedure recently developed in these laboratories.[6c,14] This procedure involves partial hydrolysis of the urazoles and isolation of the product semicarbazides. Oxidation of the semicarbazides with nickel peroxide then cleanly affords the desired diazenes. One valuable advantage this procedure holds over the previous one is that the oxidation can be performed at temperatures as low as −78°C, thereby accommodating thermally labile diazenes. Treatment of urazoles **25**, **30** and **31** with potassium hydroxide in refluxing isopropanol gave the corresponding semicarbazides **40**, **41ab** and **42ab** (urazoles **30** and **31** gave equal amounts of both isomers of their respective semicarbazides). An

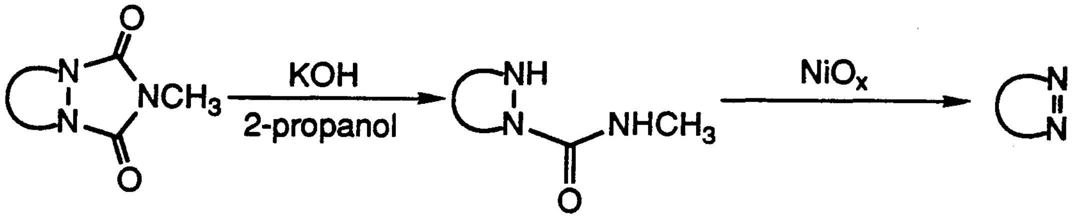

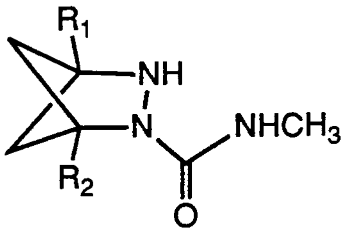

R_1	R_2	Label
Ph	Ph	**40**
Ph	CH_3	**41a**
CH_3	Ph	**41b**
Ph	H	**42a**
H	Ph	**42b**

obstacle to the success of the nickel peroxide method was the propensity of semicarbazides **40** and **41a** to rearrange under the reaction conditions and at room temperature to give heterocycles **43** and **44**, respectively. These rearrangements were not studied extensively, but they appear to involve cleavage of a C-C bond on the "amine nitrogen" side of the molecule. This mode of reactivity, which relieves at least 30 kcal/mol of strain,[11] has been previously observed in the photochemistry of various diazabicyclo[2.1.1]hex-2-enes.[15] It is interesting to note that only one of the semicarbazide isomers derived from **30** gives a rearrangement product and semicarbazides **42ab** do not rearrange at all under the same conditions.[16] Attempts to purify semicarbazides **40** and **41ab** led to complete decomposition. With careful handling the extent of these rearrangements could be minimized to 10% or less. Treatment of the semicarbazides with nickel peroxide at -50°C in CH_2Cl_2 solution then cleanly afforded diazenes **14**, **15**, and **16** (Schemes 2-1,2). The rearranged semicarbazides were not affected by treatment with nickel peroxide.

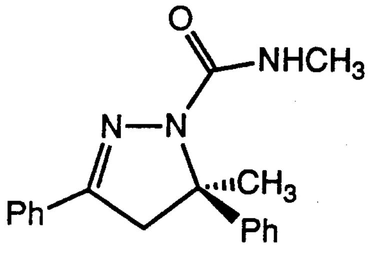

43

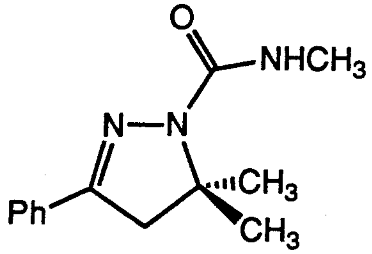

44

Diazene Reactivity

Thermal Chemistry. All three diazabicyclohexenes thermally decompose to afford the corresponding bicyclobutanes as the sole product. Of course, the thermal stability of the diazenes is strongly dependent upon the radical-delocalizing ability of the bridgehead substituents.[19] Diphenyldiazene 14 is the least stable, decomposing rapidly ($k > 10^{-4}\ s^{-1}$) above -30°C. Diazenes **15** and **16** are indefinitely stable at 0°C but decompose rapidly above 40°C.

Photochemistry. Diazabicyclohexenes **14**, **15**, and **16**, upon either direct or sensitized photolysis, give the corresponding bicyclobutane as the sole product. The photolyses of **15** and **16** were performed at 5°C in C_6D_6 solution, whereas the photolysis of **14** was carried out in CD_2Cl_2 solution at -78 °C and 77 K. These results are in marked contrast with the results obtained upon photolysis of diazenes **10** and **11**.[15] These diazenes, give mainly the corresponding bicyclobutane upon direct photolysis, but triplet-sensitized photolysis gives nitrogen retained products, 1,2-diazabicyclo[3.1.0]hex-2-enes. Apparently, one delocalizing group is enough to turn off this mode of reactivity.

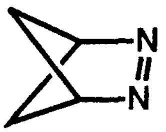

10

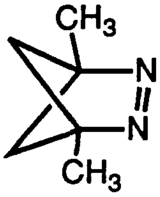

11

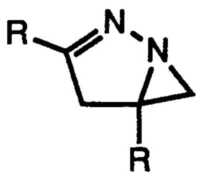

EPR Spectroscopy

General Considerations. The EPR spectroscopy of organic triplets is highly informative but somewhat different from the more common EPR of doublets (free radicals). Herein, we provide a brief overview of triplet EPR spectroscopy.[20-24]

One major difference between doublet and triplet EPR concerns the energy level pattern. At zero field, the two spin states ($m_s = \pm 1/2$) of a doublet are degenerate. Application of an external field splits these levels via the Zeeman effect, and an allowed ($\Delta m_s = 1$) transition can be observed between them (Figure 2-1). The spectrum consists of a single line which may be extensively split by hyperfine coupling. In contrast, the three spin states of a triplet ($m_s = 0, \pm 1$) are nondegenerate, even in the absence of an external magnetic field. This zero-field splitting is a consequence of a spin-dipolar interaction. That is, the effective magnetic field (H_{eff}) experienced by an electron is composed of the applied magnetic field (H_o) plus the magnetic field created by the other electron. The magnitude of this spin-dipolar interaction is strongly orientation dependent and classically is described by eq 2-1, where θ

$$H_{eff} = H_o + \frac{\mu_e(3\cos^2\theta - 1)}{r^3} \qquad (2\text{-}1)$$

is the angle between the applied field and the vector (r) connecting the two electron spin dipoles (e_1 and e_2), and μ_e is the magnetic moment of the electron (see Figure 2-2a). From inspection of eq 2-1 it is clear that the dipolar interaction, and hence zfs, is strongly dependent on the average distance, r, between the unpaired spins. The relative energies of the three triplet levels at

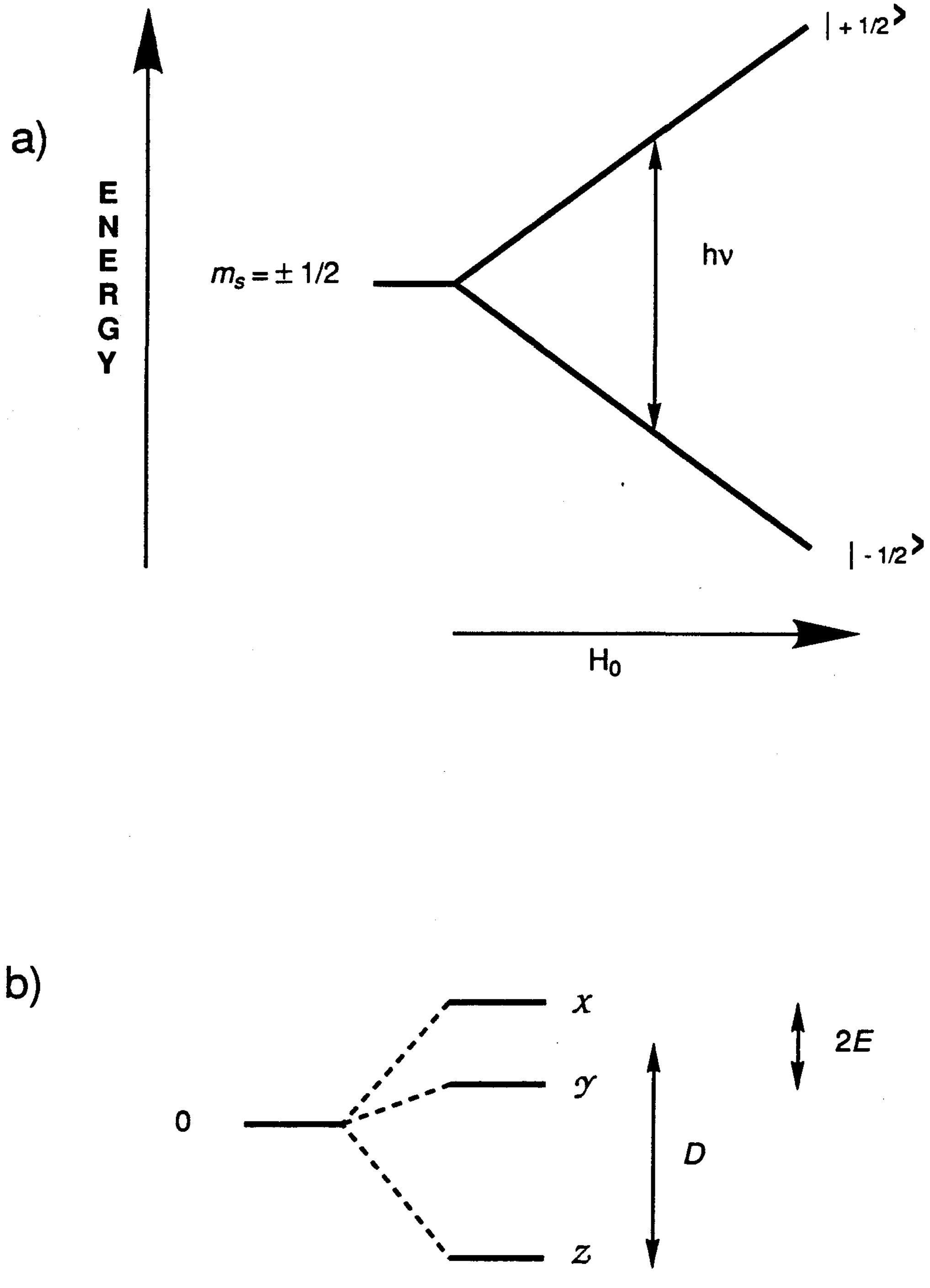

Figure 2-1. (a) Splitting of the two spin states of a doublet in an applied magnetic field. (b) Zero-field splitting of the three magnetic sublevels of the triplet state.

zero field are typically described by two zfs parameters D and E. The D value provides a measure of the average propinquity of the two spins, while E can be viewed as a probe of biradical symmetry such that, if there is three-fold or higher symmetry, E is zero. Thus, triplet EPR provides an extremely informative probe of biradical structure.

The second major difference between doublet and triplet EPR is that, typically, the former is obtained in fluid media, while the latter obtained in frozen glasses or solids. Thus, doublet spectra are isotropic, but triplet spectra are highly anisotropic. Because there are three magnetic sublevels, one would expect two allowed ($\Delta m_s = 1$) transitions in a triplet. However, in a sample of randomly oriented, but non-reorienting triplets, each orientation produces its own pair of resonances. This leads to an essentially limitless number of lines in the absorption spectrum. Fortunately, due to the $3\cos^2\theta$-1 orientation dependence of the dipolar interaction, one can effectively observe only those molecules which have one of their principal magnetic axes aligned or nearly-aligned with the external magnetic field. The reason for this behavior can be seen by examining the function $3\cos^2\theta$-1 and recognizing that the value of this function changes very little near $\theta = 0°$ and near $\theta = 90°$ (Figure 2-2b). Near each of these angles there will be an unusually wide range of orientations, all of which correspond to the same value of $3\cos^2\theta$-1. This "gathering" of resonances causes an abrupt increase in the absorption spectrum of the fields where these canonical orientations occur. These discontinuities in the absorption spectrum become peaks in the derivative spectrum[21] (Figure 2-3). While the non-canonical orientations contribute to the absorption, they give rise to a more gradual change in the signal intensity and they consequently produce no prominent feature in the derivative spectrum. Because, in effect, only three orientations contribute to the spectrum, the maximum number of

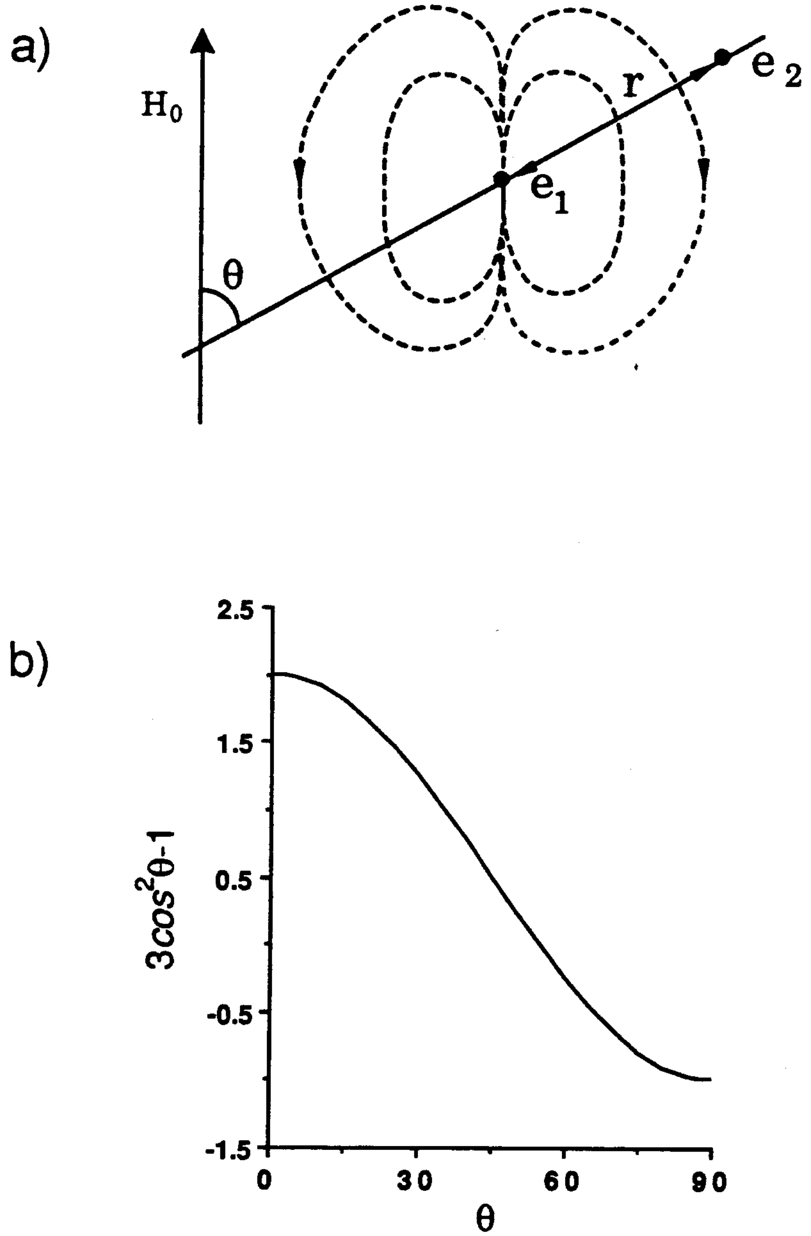

Figure 2-2. (a) Spin-dipolar interaction of two electrons in an applied field H_0 showing the magnetic lines of force emanating from electron 1. (b) The function $3\cos^2\theta - 1$.

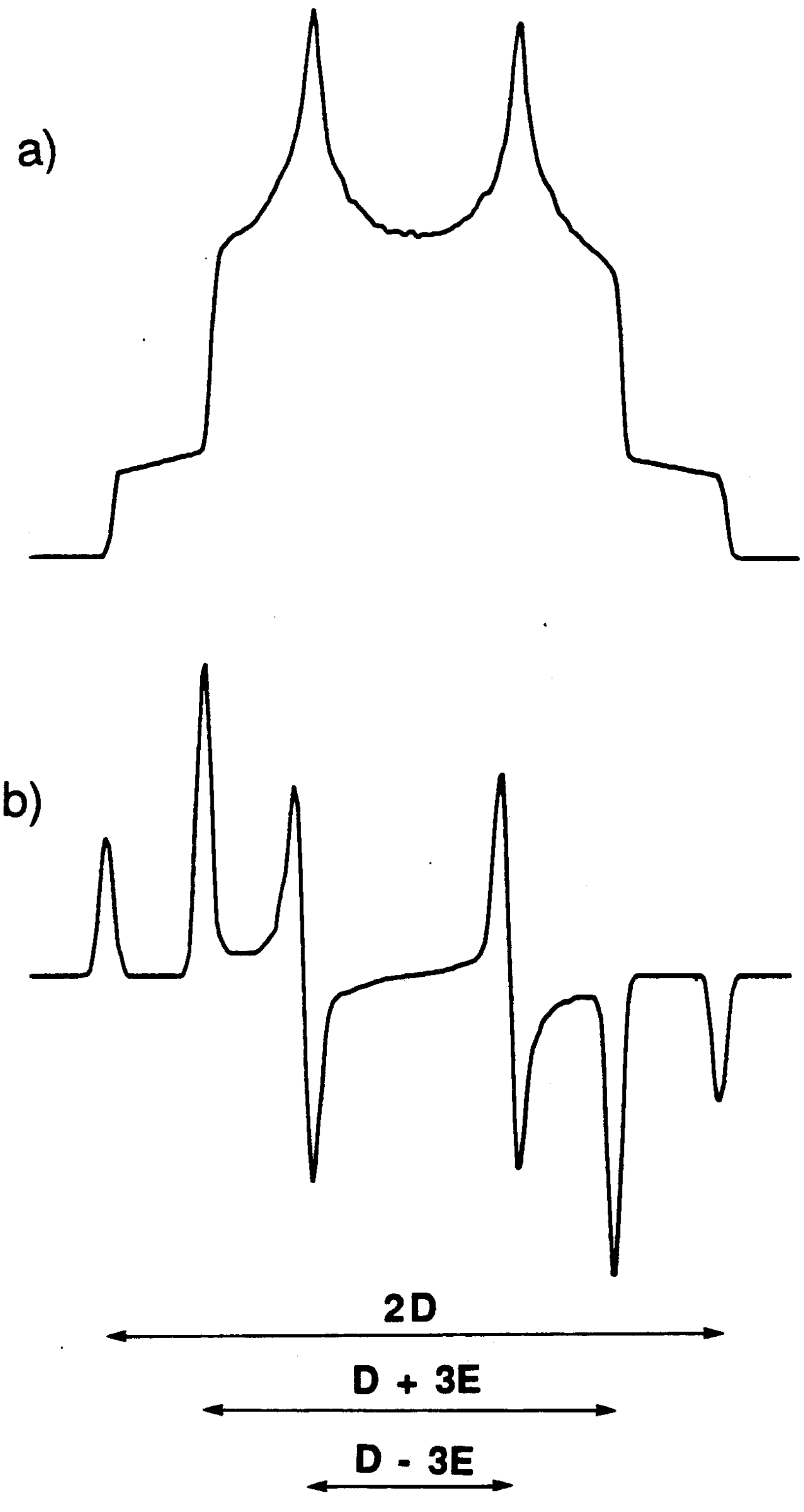

Figure 2-3. Theoretical (a) absorption and (b) derivative EPR spectra ($\Delta m_S = 1$ region) for a randomly oriented triplet.

lines observed in the $\Delta m_s = 1$ region of a triplet EPR spectrum is 3 x 2 = 6. In cases where E is very small or zero because of coincidence or symmetry, the number of lines is reduced to four. As shown in Figure 2-3, it is a simple matter to extract the zfs parameters D and E from such spectra,[20-23] and thereby obtain an estimate of the average separation of spins.

In addition to the $\Delta m_s = 1$ transitions, a formally '"forbidden" $\Delta m_s = 2$ transition is frequently observed at half-field near 1600 G.[24] This transition, which is highly diagnostic of a triplet state, is intrinsically less anisotropic then the $\Delta m_s = 1$ transition, and so only a single, broad line is observed.

Zero-Field Splittings. Photolysis of frozen solutions of diazenes **14** and **15** in MTHF at 4K produces EPR spectra of the corresponding triplet cyclobutanediyls **24-Ph** and **24-MP**. Diazene **16** did not give rise to an EPR signal upon either direct or benzophenone-sensitized photolysis. Figure 2-4 shows the EPR spectra of **24-Ph** and **24-MP** along with the spectra of three other cyclobutanediyls observed in these laboratories. Table 2-2 lists the observed zfs parameters.[5a] The anticipated six lines of the $\Delta m_s = 1$ region are clearly visible in the spectrum of **24-Me** along with the $\Delta m_s = 2$ transition. For the other structures, the value of E is quite small and this leads to an apparent four-line spectrum. Qualitatively it is evident that the D value, or equivalently, the magnetic field range spanned by the $\Delta m_s = 1$ transitions, steadily decreases as delocalizing substituents are appended to the radical centers. The "most-localized" cyclobutanediyl **24-Me** exhibits a zfs of $|D/hc| = 0.112\ \text{cm}^{-1}$. This D value has been compared[4] with $|D/hc| = 0.084\ \text{cm}^{-1}$, which has been reported for 1,3-cyclopentanediyl (**6**).[3] The larger D value of **24-Me** is a consequence of the $1/r^3$ dependence of D, since the four-membered ring

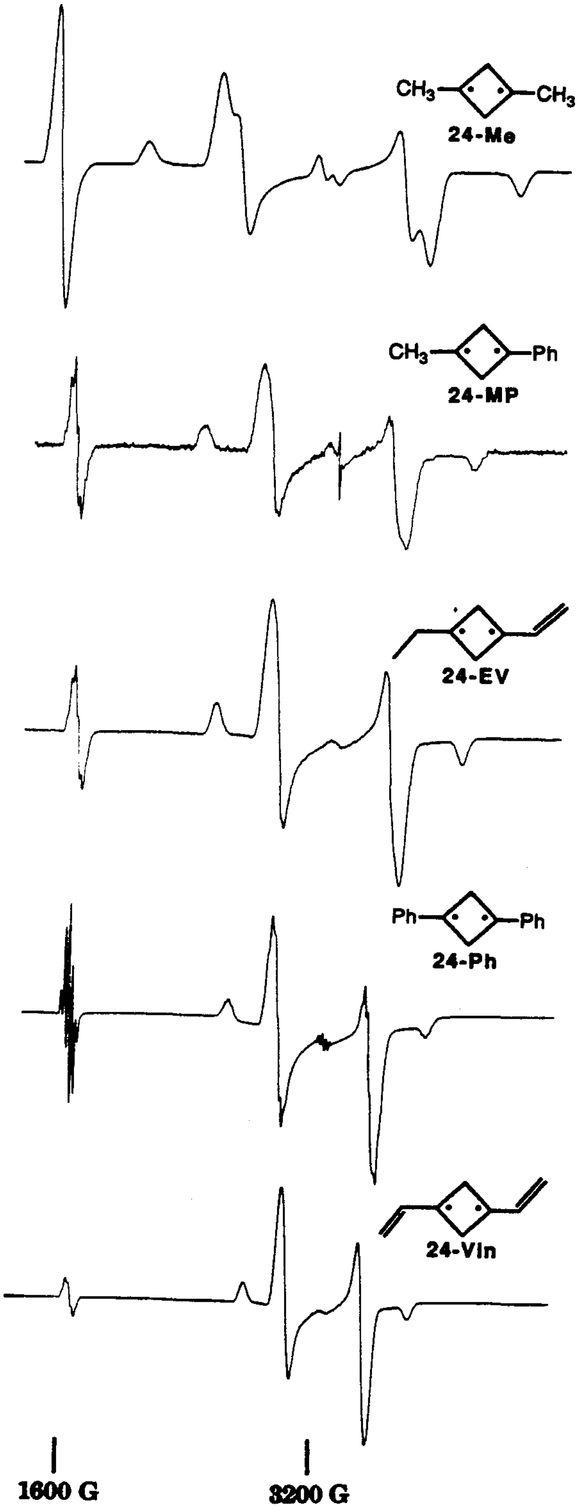

Figure 2-4. EPR spectra (first derivative) of several cyclobutanediyls (24) in order of decreasing *D* value. The biradicals were generated by irradiation of the corresponding diazenes in an MTHF matrix at 4 K. Lines in the region of 3200 G arise from free radicals and from double quantum transitions.[23]

Table 2-2. Zero-Field Splitting Parameters for Cyclobutanediyls

	obsd[a]		calcd[a,b]	
biradical	$\|D/hc\|$	$\|E/hc\|$	$\|D/hc\|$	$\|E/hc\|$
24-Me	0.112	0.005	0.112	0.005
24-CD$_3$	0.112	0.005	0.112	0.005
24-Et	0.112	0.005	0.112	0.005
24-MP	0.082	0.003	0.081	0.003
24-EV	0.074	0.003	0.074	0.003
24-Ph	0.060	0.002	0.061	0.002
24-Vin	0.050	0.001	0.050	0.001
24-Vin-d_6	0.050	0.001	0.050	0.001

[a] In cm^{-1}. [b] Calculated D values are derived from the fit of Figure 2-5.

brings the radical centers closer than the five-membered ring. Turning to the cyclobutanediyls which possess delocalizing substituents, it may at first seem surprising that **24-Ph** exhibits a significantly larger *D* value than **24-Vin**. Recall, however, that the Hückel coefficient at the CH_2 group in the NBMO of benzyl radical ($2/\sqrt{7}$) is *larger* than that in allyl radical ($1/\sqrt{2}$). Thus, the spin density at the ring carbons is greater in the diphenyl structure. Given the $1/r^3$ dependence, this effect dominates the *D* value. It is also important to note that for cyclobutanediyls, the observed percentage drop in *D* value upon substituting a delocalizing group for an alkyl group is identical for the first and second substitutions. For example, substituting a phenyl group for one methyl group of **24-Me** to give **24-MP** decreases the *D* value from 0.112 cm^{-1} to 0.082 cm^{-1}, a factor of 0.732. A subsequent substitution of phenyl for methyl decreases the *D* value of **24-MP** by *exactly* the same factor to give a *D* value of 0.060 cm^{-1} for **24-Ph**. The same effect is observed upon vinyl substitution. In this case, the *D* value multiplier is 0.668.

The experimental *D* values of Table 2-2 can be quantitatively correlated to theoretical values obtained by employing a semiempirical method based on the point-charge approximation.[25] The distance between the radical centers in the ring were taken from *ab initio* optimized geometries of the parent cyclobutanediyl (**24-H** 2.10 Å)[26] and of **6** (2.37 Å).[27] The use of Hückel spin densities in the calculations allowed semi-quantitative reproduction of the *D* values. However it is well known that in delocalized monoradicals such as allyl or benzyl, spin polarization effects produce spin densities that deviate significantly from those predicted by Hückel theory.[28] We have approximated such spin polarization effects in our calculations by using "experimental" spin densities from hyperfine measurements determined for allyl and benzyl radicals.[29] We assumed complete localization for alkyl-substituted radicals. With this approach, very good agreement between theory and experiment was obtained. A plot of experimental vs calculated D values (Figure 2-5) shows an excellent correlation, giving a least-squares line with a near-zero intercept. The calculated value for cyclopentanediyl (**6**) was not included in the least-squares fit, but as shown in Figure 2-5, it falls very close to the line. It is important to emphasize that, in these calculations, the delocalizing substituents (phenyl and vinyl) are coplanar with the cyclobutanediyl ring. Given the excellent correlation of Figure 2-5, this strongly suggests that the delocalizing substituents of **24-Ph, -MP -Vin** and **-EV** are also coplanar with the ring and that they are in full conjugation with the radical p orbitals. Also, given the "multiplicative" substituent effects described above, it seems clear that the spin distribution in these localized biradicals is simply the same as would be observed upon placing two of the corresponding radicals 2.10Å apart (*i.e.*, there is no special "biradical effect").

Hyperfine Coupling. Six of the cyclobutanediyls display splittings due to hfc in their half-field ($\Delta m_S = 2$) transitions (Figure 2-6). It was at first surprising to see these splittings, some of them quite well resolved, because of the anisotropies involved in powder spectra. Indeed, the observation of interpretable hyperfine in triplet EPR is relatively rare,[6c,30] except for single-crystal samples.[31] We have found, however, that these splittings can be readily interpreted, providing values for the hfc constants (a_H) of several protons in these structures. Of course, these coupling constants provide important structural information through standard relationships[20,32] such as the McConnell equation (eq 2-2) for α protons (those directly attached to radical centers) and a related expression (eq 2-3) for β protons (those on

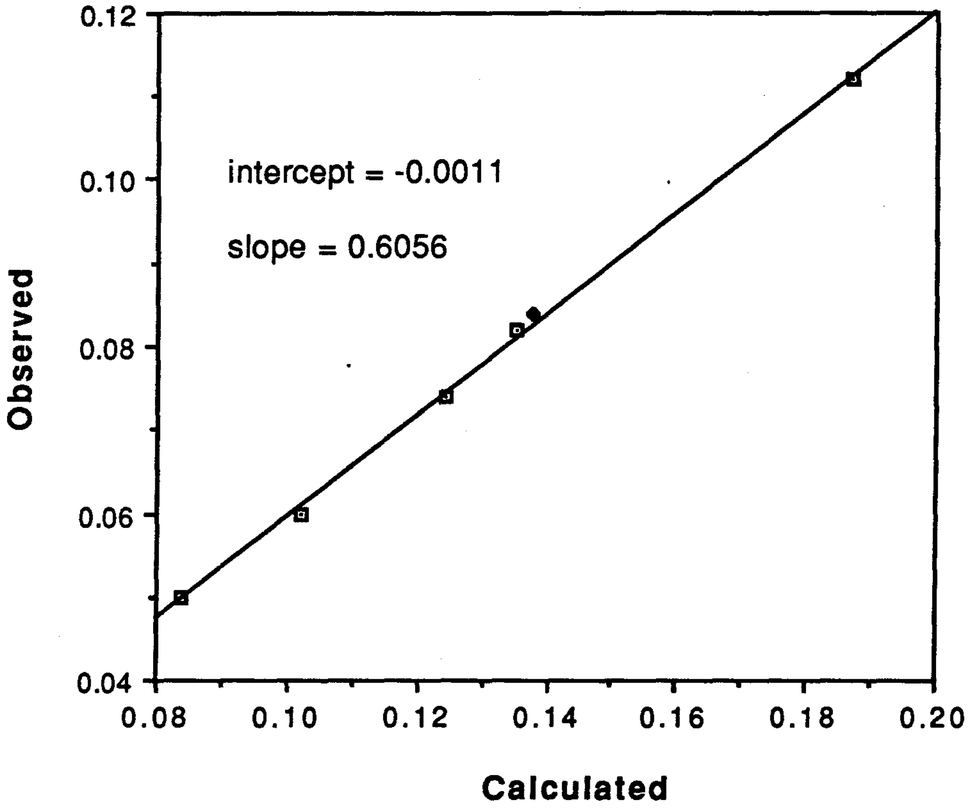

Figure 2-5. Observed vs calculated |*D*/hc|=values (cm^{-1}) for cyclobutanediyls **24** (open boxes). The value for **6** (filled diamond) was not included in the least-squares analysis.

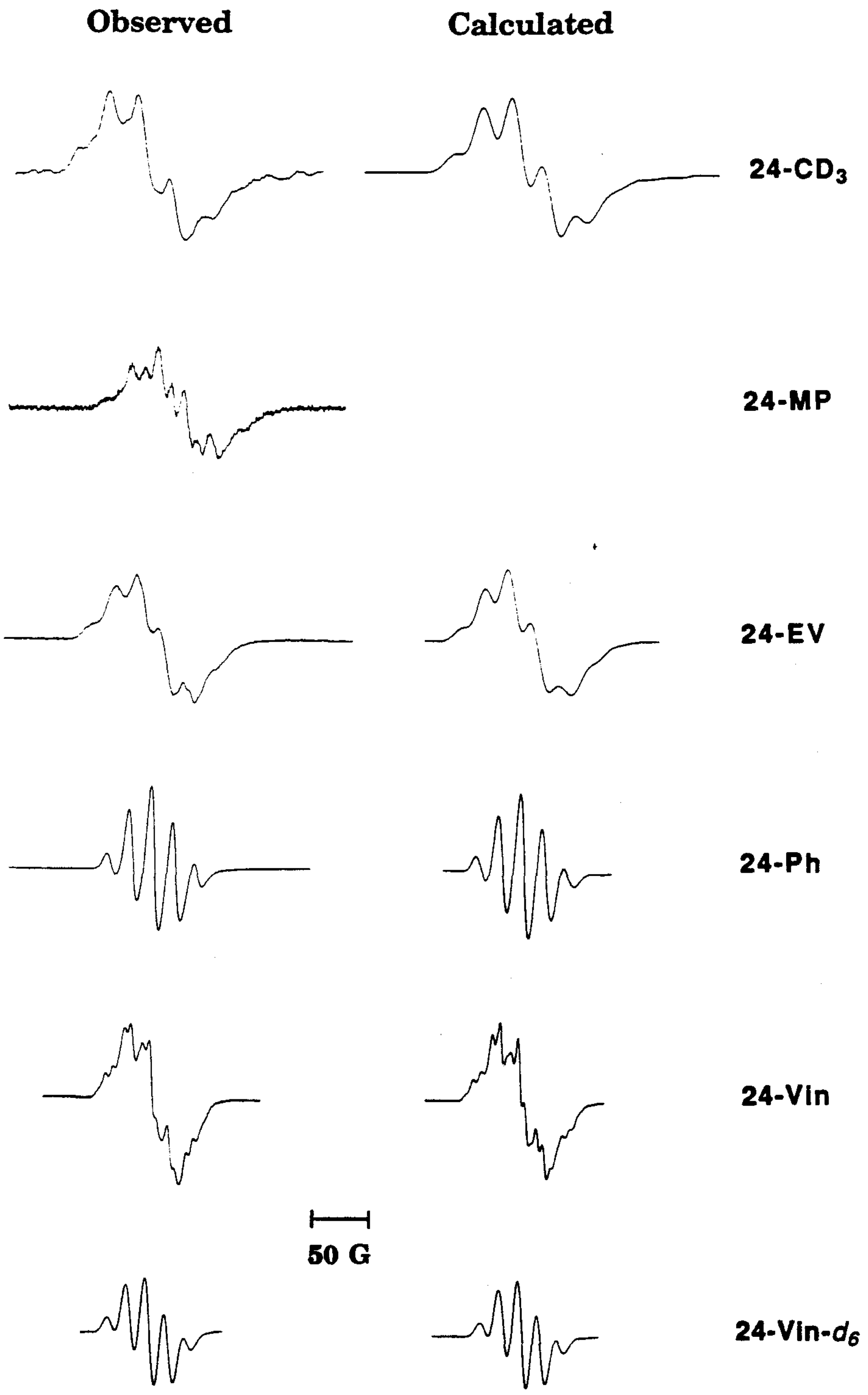

Figure 2-6. Hyperfine structure in the $\Delta m_s = 2$ region of several cyclobutanediyls.

$$a_H^{\alpha} = Q\rho \tag{2-2}$$

$$a_H^{\beta} = A + \rho C \cos^2\theta \tag{2-3}$$

carbons adjacent to radical centers). In these equations, ρ is the spin density at a radical center; Q, A, and C are empirical constants with typical values of 20-30, 0-5, and 40-45 G, respectively; and θ is the angle between the axis of the radical p orbital on the α carbon and the β C-H bond.

A first source of anisotropy to be considered is that which is intrinsic to the hfc tensor, and α and β couplings are different in this regard. It is generally recognized that the hfc tensor for β couplings is relatively isotropic,[32,33] and so splittings due to β couplings can be directly related to isotropic $a^{\beta}{}_{H}$ values. In contrast, the α hfc tensor is generally quite anisotropic.[33] However, Sternlicht[34] has shown that for planar organic radicals in randomly oriented, nonreorienting (powder) samples, the splittings observed from α hfc are approximately equal to the isotropic hfc constants ($a^{\alpha}{}_{H}$) and the lines are fairly symmetrical. Thus, anisotropies introduced by the hfc tensors should be relatively small in our spectra.

Our goal, of course, is to relate the splittings we observe in our triplet spectra to spin densities, as is done for radical spectra. There is, however, an important difference between biradicals and simple radicals. A typical magnetic nucleus in a localized biradical will effectively interact with only one of the two spins of the triplet. This is always true for α protons and will be true for β protons in the R groups of **24**. When electron-exchange terms are much greater than the hyperfine interaction, nuclei of this type are expected to produce couplings which are half those seen in analogous free radicals.[35-37] For example, in allyl radical, the magnitudes of the α couplings are *ca.* 14 G for the terminal (CH_2) hydrogens and ca. 4 G for the central hydrogen. On the basis of the above arguments, one would expect the analogous hydrogens in **24-Vin** to produce 7 and 2 G splittings, respectively, and this is what is observed (see below). The exception to this rule is the set of β hydrogens that are on the four-membered ring of **24**. These can couple directly to both radical centers, and so the splittings that arise from them should be of the same magnitude as analogous splittings in simple radicals. As described below our simulations fully support this analysis.

There is another source of anisotropy in these triplet spectra, namely, the intrinsic orientational anisotropy of the $\Delta m_s = 2$ transition.[24] Just as there are, in effect, two observable $\Delta m_s = 1$ transitions for each of the three canonical orientations of a triplet, so there is *one* $\Delta m_s = 2$ transition for each canonical orientation. In addition, a fourth $\Delta m_s = 2$ transition, termed H_{min}, occurs at lower field than the other three (H_x, H_y, and H_z). The positions of these transitions can be calculated easily from the zfs parameters.[24] In addition, the intensities of these transitions decrease through the series H_{min}, H_x, H_y, H_z (Figure 2-7). Thus, the largest contributions to the line shape come from resonances at H_{min}, H_x, *and* H_y. From Figure 2-7, it is clear that for biradicals with relatively small D values (e.g., **24-Vin** and **24-Ph**) the separation between H_{min} and H_x is on the order of the spectral line width (5-6 G). Thus, the spectra are very nearly isotropic, and simple splitting patterns can be observed. In contrast, biradicals with large D values (e.g., **24-CD$_3$**) have a large separation between H_{min} and H_x (30 G), and as a result the line shape for the $\Delta m_s = 2$ transition should be broad and unsymmetrical, even in

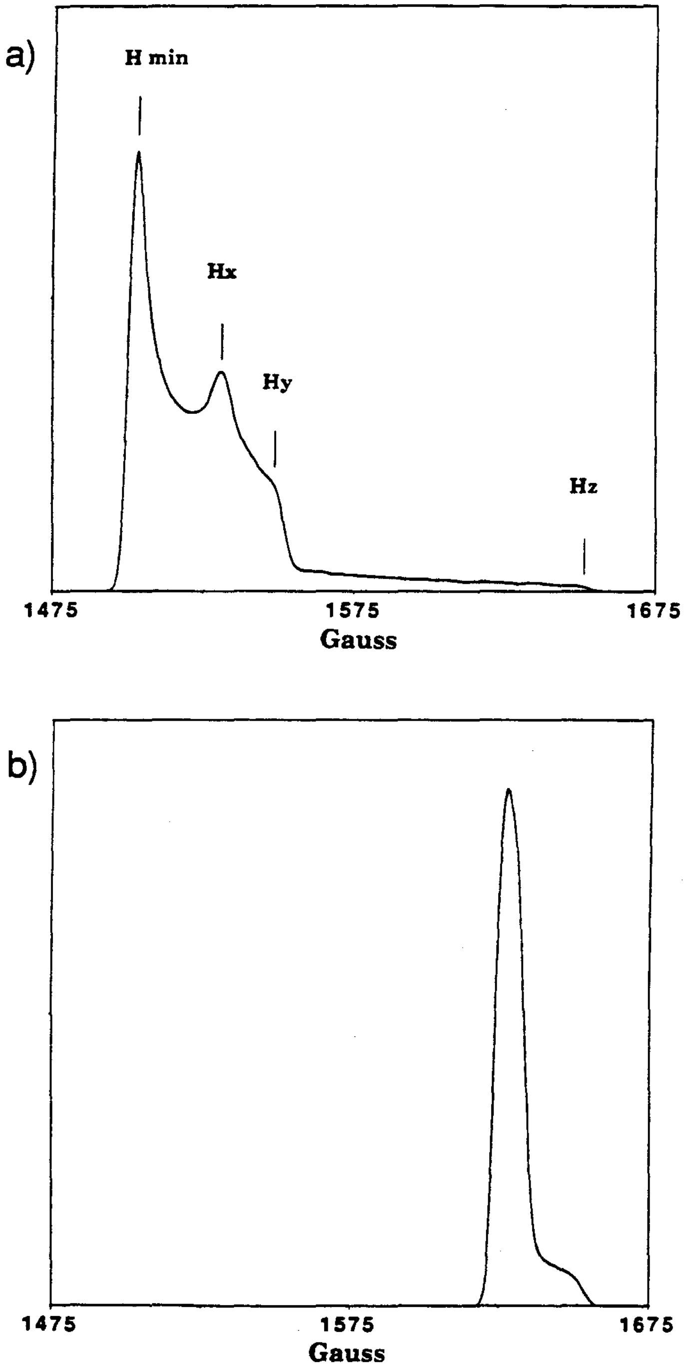

Figure 2-7. Simulated absorbance spectra in the $\Delta m_S = 2$ region of **24-Me** (a) and **24-Vin** (b) in the absence of hyperfine coupling.

the absence of any hfc. If there is hfc, it is superimposed onto the patterns of Figure 2-7.

Quantitative interpretation of the hyperfine splitting patterns of Figure 2-6 required spectral simulation. Our program, based on the algorithm of Kottis and Lefebvre,[24] assumes isotropic hfc and equal transition probabilities for all orientations. The simulations explicitly include the orientational anisotropy of the $\Delta m_s = 2$ transition. The resulting calculated spectra are shown for the five cyclobutanediyls which exhibit interpretable hyperfine in Figure 2-6. The agreement between experiment and theory is quite satisfactory, given the approximations involved. In Table 2-3 we list the coupling constants used in the simulations.

Two of the biradicals, **24-Ph** and **24-Vin**-d_6, display well-defined five-line patterns in their half-field transitions, which may be attributed to the dominant hyperfine interaction with the four β protons of the cyclobutanediyl ring. But despite the apparent simplicity of the patterns, simulations show that the β-hyperfine interaction alone does not account for the observed spectrum. *Accurate simulations* required the inclusion of the smaller couplings to other nuclei. Due to the dominant β-hyperfine interaction, **24-Ph** and **24-Vin**-d_6 also exhibit hyperfine splitting patterns in the $\Delta m_s = 1$ transitions that are identical with those in the $\Delta m_s = 2$ region, though they are less well resolved. Shown in Figure 2-8 is the $\Delta m_s = 1$ region of **24-Ph**. For both **24-Ph** and **24-Vin** the α couplings observed in the substituents are as expected -- they are half the value seen for analogous protons in the benzyl and allyl radicals. In **24-CD$_3$**, a simple five-line pattern as for **24-Ph** is not observed because of the anisotropy of the $\Delta m_s = 2$ transition. The simulation, though, treats this spectrum well, although the line broadening required to

Table 2-3. Hyperfine Simulation Parameters

biradical	$a_{\beta H}$[a,b]	other[a,b]
24-CD$_3$	32	3 (2D), 1.5 (4D)
24-EV	23	vinyl; 2(1H), 7(2H) ethyl; 5 (1H), 21 (1H)
24-Ph	22.5	3 (4H; ortho); 3 (2H; para); 0.5 (4H; meta)
24-Vin	19	2 (2H), 7 (4H)
24-Vin-*d*$_6$	19	1.5 (4D)

[a] In gauss. [b] Coupling constants rounded to the nearest 0.5 G.

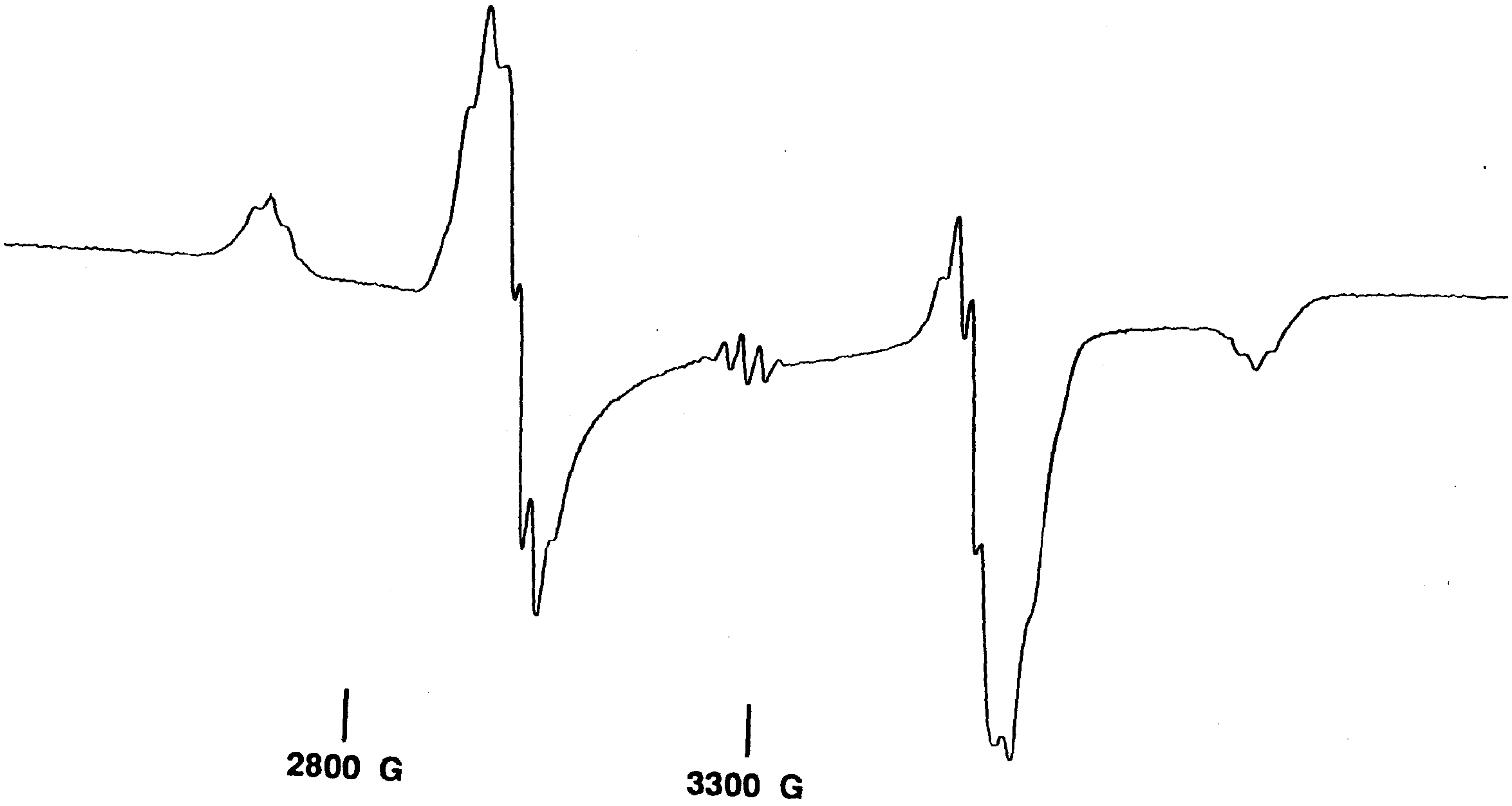

Figure 2-8. Hyperfine splitting in the $\Delta m_s = 1$ region.

achieve a good fit was much greater for **1-CD$_3$** than for other spectra.

An important feature of these spectra is the fact that the ring CH$_2$ protons of a given biradical all have identical coupling constants. Given the dependence of a $a^{\beta}{}_{H}$ on θ this requires that *the cyclobutanediyl ring is planar* in all these structures. This is the first structural information of this kind for a localized biradical and is in accord with earlier theoretical predictions.[37] The observation of equivalent couplings would also be consistent with a pair of rapidly interconverting nonplanar forms, but this would seem to be unlikely at 3.8 K. Also, the intrinsic broadness of triplet EPR lines introduces some uncertainty, in that small differences in hfc constants would be absorbed into the line widths. Our simulations, though, indicate that differences as small as 1.0 G, implying differences in θ of *ca.* 2°, could be detected in the spectra of **24-Ph**. The uncertainty is greater in a more complex spectrum, such as that from **24-CD$_3$**. Thus, it is perhaps best to say that cyclobutanediyls are planar, or nearly so. Note that in the biradical precursors, the cyclobutane moiety is very highly puckered (flap angle ca. 58°). Clearly, a considerable structural reorganization occurs within the matrix site after N$_2$ loss from the diazenes. Apparently, the restraining forces of the matrix material are not overwhelming, an observation that is quite relevant to efforts to characterize the matrix decay kinetics of such biradicals (see below).

As indicated in eq 2-3, the values of $a^{\beta}{}_{H}$ for the ring protons provide another gauge of spin density at the cyclobutanediyl radical carbons. It is apparent from Table 2-3 that $a^{\beta}{}_{H}$ does decrease with increasing delocalization, just as the zfs D value does. We have only three accurately determined values for $a^{\beta}{}_{H}$, but if we plot them according to eq 2-3, the result of Figure 2-9 is obtained. The intercept is 1.2 G, a quite reasonable value for A. The slope is

30.9 G. If we set $C = 42.5$ G, the value of θ is 31°, which is in good agreement with our theoretically determined[26b] value of 27°. Of course, three data points are hardly enough to provide an accurate determination of θ. However, the results summarized in Figure 2-9 again show that the spectral data we have obtained for the cyclobutanediyls agree both in absolute magnitude and in trends along the series with expectations based upon analogies to conventional radical chemisty.

The level of complexity in the hyperfine patterns of triplet spectra that can be interpreted is limited. For example, only a broad featureless $\Delta m_s = 2$ line is observed for **24-Me**, and the pattern for **24-MP** (Figure 2-6) has not yielded to simulation. This could be a consequence of multiple conformations for the methyl groups. Remembering the angle dependence of eq 2-3, this could greatly complicate the spectra. Even if the methyls are rapidly rotating at 4 K (perhaps via tunneling), the number of lines they would produce, superimposed on the quintet from the ring β protons, would create a poorly resolved spectrum. We have been able to simulate the spectrum for **24-EV**, but the simulations required five large couplings, instead of the usual four due to the ring protons. This could indicate that one of the CH_2 protons of the ethyl group has $\theta \approx 0°$, which, after application of the factor of one-half, would produce a coupling similar to the ring protons. This uncertainty, coupled with the fact that it is not completely clear what value of ρ should be used for the ring protons, is the reason that the value of $a\beta_H$ for **24-EV** was not included in the fit of Figure 2-9.

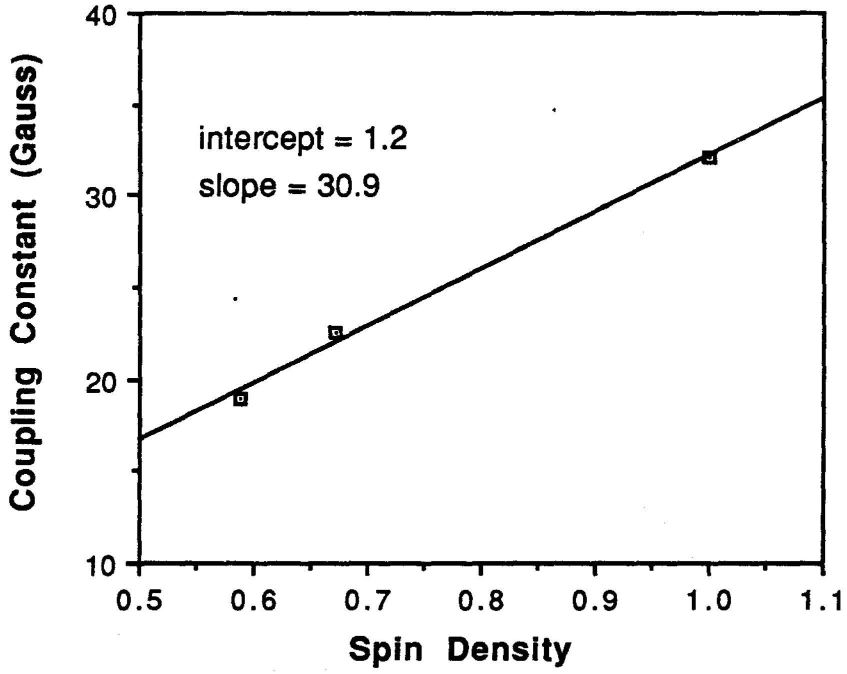

Figure 2-9. Correlation of $a\beta_H$ for cyclobutanediyls 24 with spin densities according to eq 2-3, using the coupling constants of Table 2-3.

Decay Kinetics

All triplet cyclobutanediyls **24** undergo thermal decay in some temperature range between 4 and 65K. The rate of decay of a particular cyclobutanediyl at a given temperature is strongly dependent on the substitution at the radical centers. The goal of this work is to quantitatively examine the effects of various substituents on the stability of triplet cyclobutanediyls and to identify the decay process. Quantifying the decay kinetics of the matrix-isolated species is quite difficult, however, due to the matrix-site effect. In nonfluid media at cryogenic temperatures, different molecules in a sample experience different microenvironments. These matrix perturbations generally lead to complex (dispersive) kinetic behavior, because, in principle, each site has its own intrinsic decay rate. Previous work in these laboratories has led to the development of a highly useful method for the analysis of such dispersive kinetics.[26b] This section first describes the application of this method to the quantitative analysis of the decay kinetics of 1,3-diphenylcyclobutanediyl (**24-Ph**) in MTHF and then compares the decay behavior of this biradical with other cyclobutanediyls studied in these laboratories. For the purpose of discussion, it is convenient to divide the cyclobutanediyls into two classes, those with delocalizing substituents, and those without. We shall refer to the first group (**24-Ph, 24-Vin, 24-EV**) as stabilized and the second (**24-Me, 24-Et**) as fully localized.

Decay Products. Prior to describing the analysis of the decay kinetics, it is important to establish the nature of the decay process. We have considered three possibilities, shown in Figure 2-10. Radical hydrogen-abstraction from the solvent matrix, probably the most commonly studied reaction at cryogenic temperatures,[38-40] was ruled out by several lines of

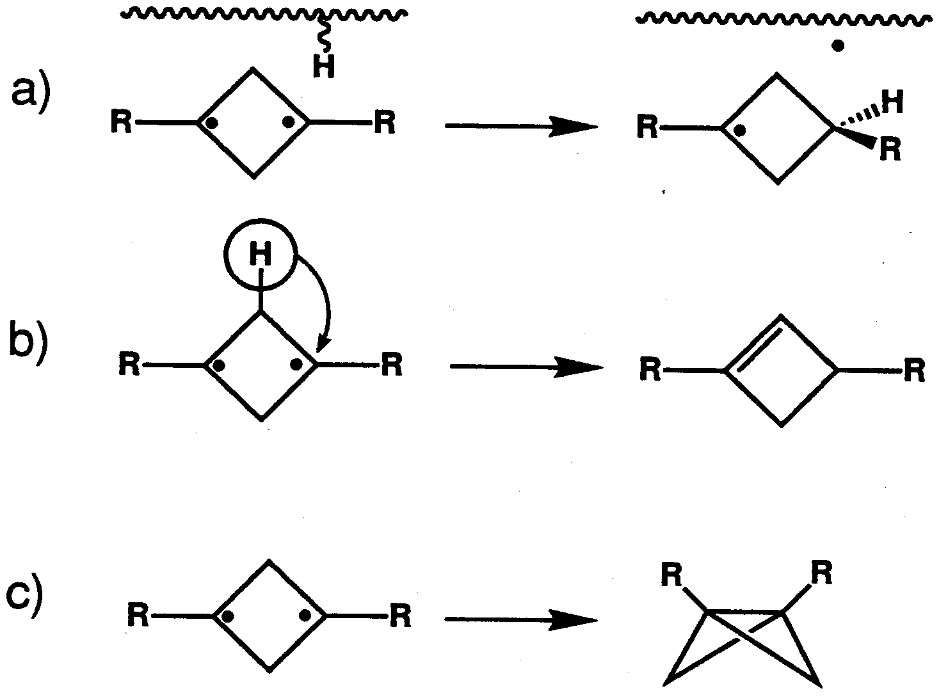

Figure 2-10. Possible decay pathways for cyclobutanediyls: (a) abstraction of H atom from solvent, (b) intramolecular 1,2-H shift, and (c) intramolecular coupling of two radical centers.

evidence. First, the observed decay of the cyclobutanediyls is much faster than any known abstraction process. Hydrogen abstraction by radicals and carbenes is most often studied at 77 K or higher, whereas all our studies on cyclobutanediyls have been carried out below 65 K. Second, decay of the triplet signals corresponding to **24** is *not* accompanied by growth of any doublet signals, which would be expected from the resulting cyclobutyl and solvent radicals. Finally, comparison of decay rates in protio *vs.* deuterio solvents shows no difference in rates. Such an abstraction reaction should show a large kinetic isotope effect at such low temperatures, especially if tunneling is involved.[40]

The other two possible decay processes, closure to give bicyclobutanes and 1,2-hydrogen shift to give cyclobutenes (Figure 2-10) will be considered together. Compelling evidence comes from product analysis of EPR samples. High-field ^{1}H NMR analysis of a sample of **14** which had been photolyzed many times in EPR experiments showed conversion to the bicyclobutane closure product **19** with no signs of a cyclobutene. Similar results were obtained for other diazabicyclohexenes. In addition, in all of our extensive studies of the solution-phase thermal chemistry and photochemistry of various diazabicyclohexenes we have seen no evidence of cyclobutene products.[6b,15a] We feel this rules out cyclobutene formation as the decay path for cyclobutanediyls.

In support of this, we note that Fisher and Michl[41] have recently observed both processes in the same biradical, a naphthoquinodimethane (**45**), under different conditions. The hydrogen-shift reaction, producing **46**, occurred in a purely exponential fashion, and a conventional analysis produced activation parameters. In contrast, the closure process, giving **47**, was characterized by nonexponential kinetics attributed to a matrix effect resulting from a larger geometrical change. Cyclobutanediyls 24 display *strongly* nonexponential decay. This behavior is more consistent with the closure pathway, given Michl's work.

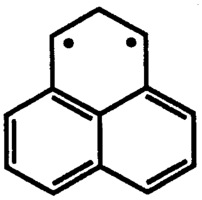

45

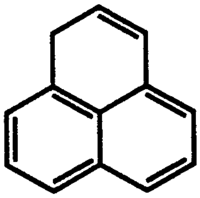

46

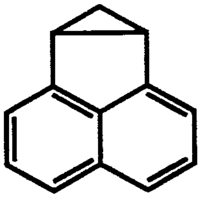

47

Thus, the process we are observing represents perhaps the most fundamental of organic reactions – the direct coupling of two radical centers to make a new C–C bond. Concomitant with bond formation, intersystem crossing must occur, as this is the spin-forbidden, triplet → singlet incarnation of radical coupling.

Anticipated Decay Patterns. Before discussing our results, consideration of typical kinetic behavior at cryogenic temperatures, with and without a matrix effect, would be helpful. Presuming, for the moment, that the reaction under study shows exponential and Arrhenius (non-tunneling) behavior, the temperature range in which the reaction would occur on a convenient time scale would be quite small. For example, Figure 2-11a shows predicted decay traces for a process with $\log A = 8.0$ and $E_a = 1.5$ kcal/mol at 25, 30 and 35 K. Over a range of 10 degrees, the reaction rate varies by nearly four orders of magnitude. This illustrates the much greater sensitivity of reaction rates to small temperature changes at very low temperatures. Such a reaction would present severe obstacles to anyone attempting to accurately measure its activation parameters, since temperatures would have to be maintained with high precision and measured with high accuracy, both difficult tasks below 77 K.

Suppose next that the reaction has a distribution of activation energies, but still displays Arrhenius behavior. Simulated decays (obtained as described below) are shown in Figure 2-11b, assuming the same activation parameters as in Figure 2-11a and a Gaussian E_a distribution with a standard deviation (σ) of 0.5 kcal/mol. The temperature range over which decay is observable is much larger, even though the most probable rates are the same at a given temperature. Note that the signal intensities are never 100% due to decay during the photolysis interval. For a distribution over E_a that extends toward zero activation energy, decay during the short photolysis interval is inevitable above a given threshold temperature because an appreciable fraction of the sites have low activation barriers which can be surmounted during the photolysis interval. As the temperature is increased, a greater fraction of sites will have activation barriers that can be surmounted during the photolysis interval and therefore the absolute intensity will decrease with increasing temperature. This situation represents a trade-off for the experimentalist in search of activation parameters; in return for the expanded temperature range, the complexity of the problem has increased enormously. As shown in Figure 2-12, the experimental data observed for **24-Ph** are consistent with such a distribution over E_a.

An important point illustrated by Figures 2-11 and 2-12 is the fact that all the decay traces in a composite first-order system are similar in shape, differing mainly in intensity. This observation can be explained by dividing the distribution into three components for any given decay trace, as done for the 20 and 40 K traces in Figure 2-13. The three components are (1) the "fast sites," which have rate constants too high to allow observation at the given

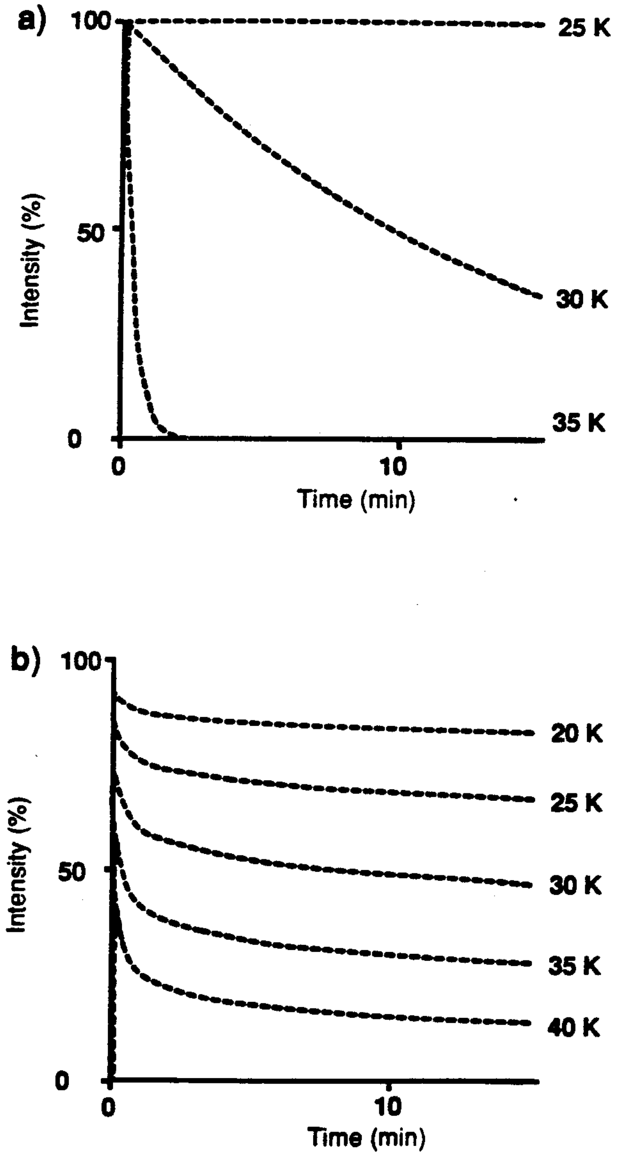

Figure 2-11. Simulated decay of an Arrhenius process ($\log A = 8.0$) with (a) $E_a{}^\circ = 1.5$ kcal/mol, and (b) Gaussian distribution over energy of activation, $E_a = 1.5$ kcal/mol and standard deviation (σ) $= 0.5$ kcal/mol. The rates (s^{-1}) involved (single rates in (a), most probable rates in (b)) are the following: 20 K, 4.0×10^{-9}; 25 K, 7.7×10^{-6}; 30 K, 1.2×10^{-3}; 35 K, 4.3×10^{-2} and; 40 K, 6.4×10^{-1}. Photolysis time is 5 s in all cases.

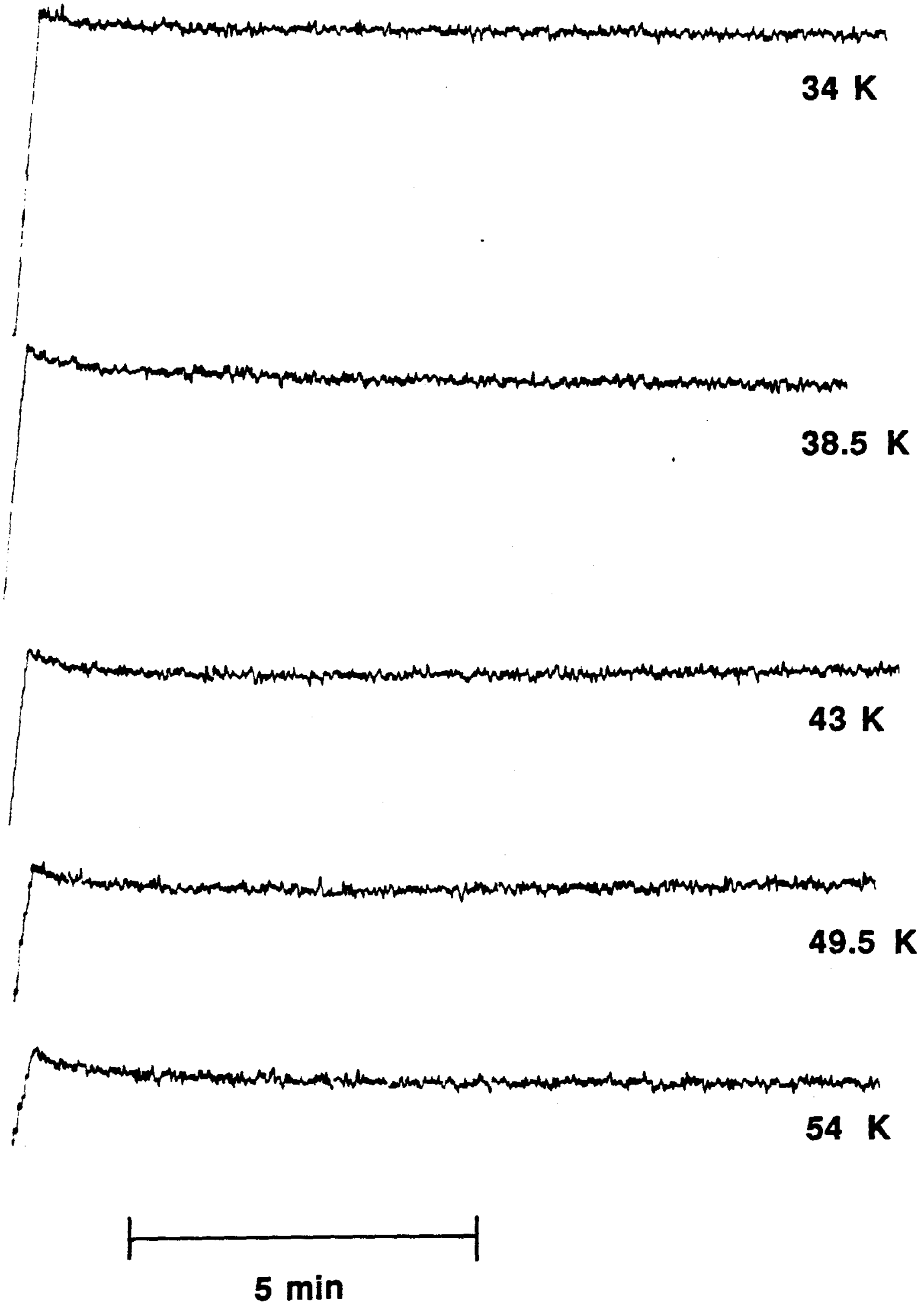

Figure 2-12. Experimental decay traces for 24-Ph in MTHF.

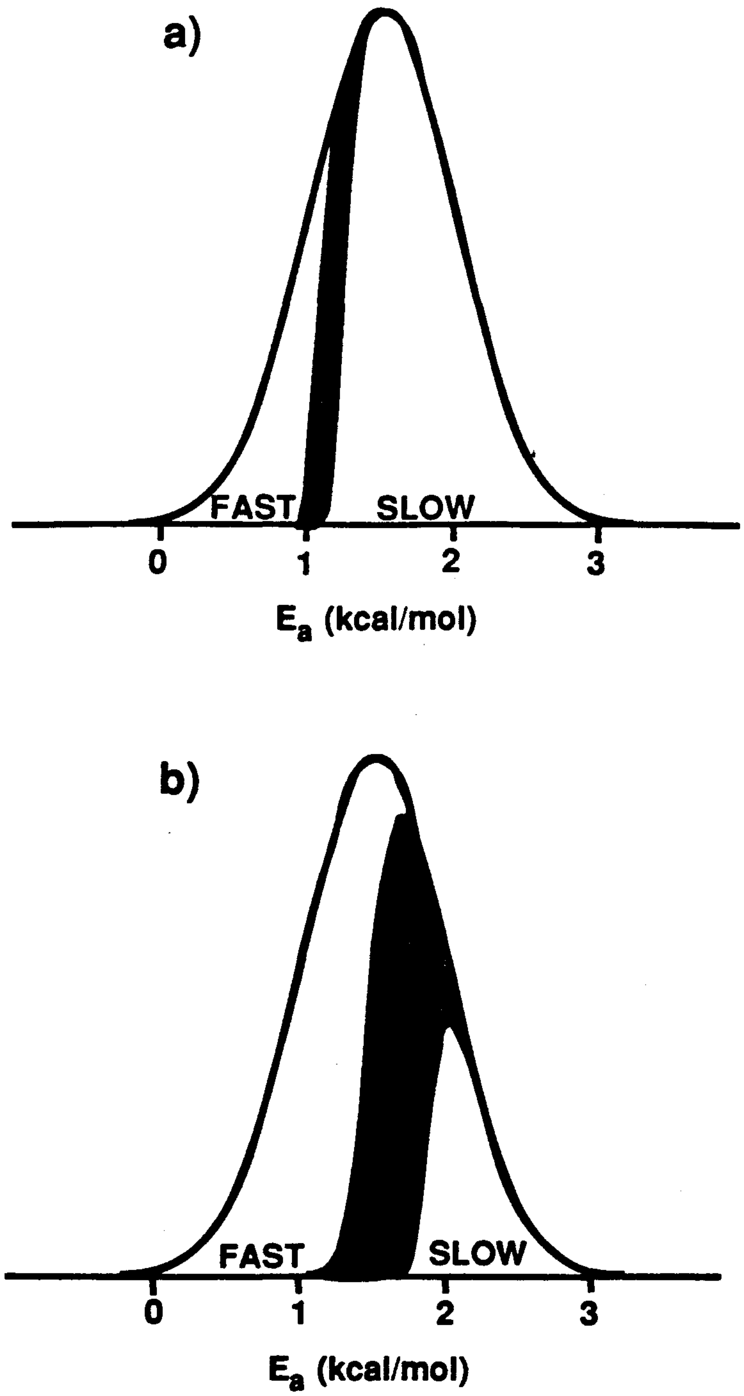

Figure 2-13. Division of a distribution into fast, intermediate (shaded) and slow sites at (a) 20 K and (b) 40 K. The observed decay corresponds to the shaded portions of the distribution.

temperature, (2) the "slow sites," which are completely stable on the time scale of the experiment, and (3) the "intermediate sites" (shaded in Figure 2-13), which account for all of the observed decay. The intermediate sites for the two temperatures have the same range of rate constants, which explains the similarity in the shape of the decay traces. The important feature in determining shape, then, is simply the ratio of intermediate sites to slow sites.

Methodologies for Modeling Dispersive Kinetics. This section describes the implementation of various modeling techniques we have used to analyze the decay behavior of triplet cyclobutanediyls.

In all experiments, the EPR samples were prepared by immersing a degassed solution of the diazene into liquid nitrogen to form a glassy or polycrystalline matrix. Thus, regardless of the conditions of a particular kinetics experiment, we assume that all samples of **24-Ph** have the same initial distribution of diazene sites.

Distribution Slicing. The first kinetics technique to be described is called distribution slicing.[26b] This extremely valuable technique provides a wealth of information that is crucial to the quantitative analysis of dispersive kinetics. In particular, distribution slicing provides (1) distribution shape information, (2) independent evidence for the existence for a distribution over E_a, (3) a means to normalize decay traces.

Conceptually and experimentally, the distribution slicing method is relatively simple. A signal that represents an intact E_a distribution is generated by photolysis at a temperature low enough to ensure that no decay occurs, usually 3.8 K. Then, by warming the matrix to successively higher temperatures, fast sites are in effect sliced off the distribution in layers (see

Figure 2-14). By recooling to 3.8 K in-between warming cycles and measuring the signal intensity, the size of each "slice" (relative to the intact distribution) can be obtained. Reconstruction of the distribution from the constituent slices (Figure 2-14f) then produces a crude image of the distribution.

As shown in Figure 2-15, even the boundary line of a slice spans a significant range in E_a, which defines a "resolution" of the method. Our objective in the experiment is to assign a single E_a value to the slice so that the overall E_a distribution may be reconstructed directly. Starting with the

$$E_a = -RT \, \ell n(\frac{k}{A}) \tag{2-4}$$

Arrhenius equation (eq 2-4), the rate, k, is assigned to the sites which experience 50% decay during the warming interval (see Figure 2-15). In other words, the warming interval corresponds to exactly one half-life for these sites. Therefore,

$$\text{warming interval} = t = \frac{(\ell n \, 2)}{k} \; . \tag{2-5}$$

Substituting into equation 2-4 gives

$$E_a = -RT \, \ell n\left(\frac{(\ell n \, 2)}{At}\right) . \tag{2-6}$$

The value of T is known from the experiment, and we must assume a value for A (see below). Thus, E_a is easily calculated.

Reconstruction of the distribution from the slicing experiment, as shown in Figure 2-14f, involves conversion of the intensity data into areas under the distribution, and as such constitutes a form of numerical differentiation. This type of process always results in magnification of errors, and for this reason it is perhaps preferable to present the results in the

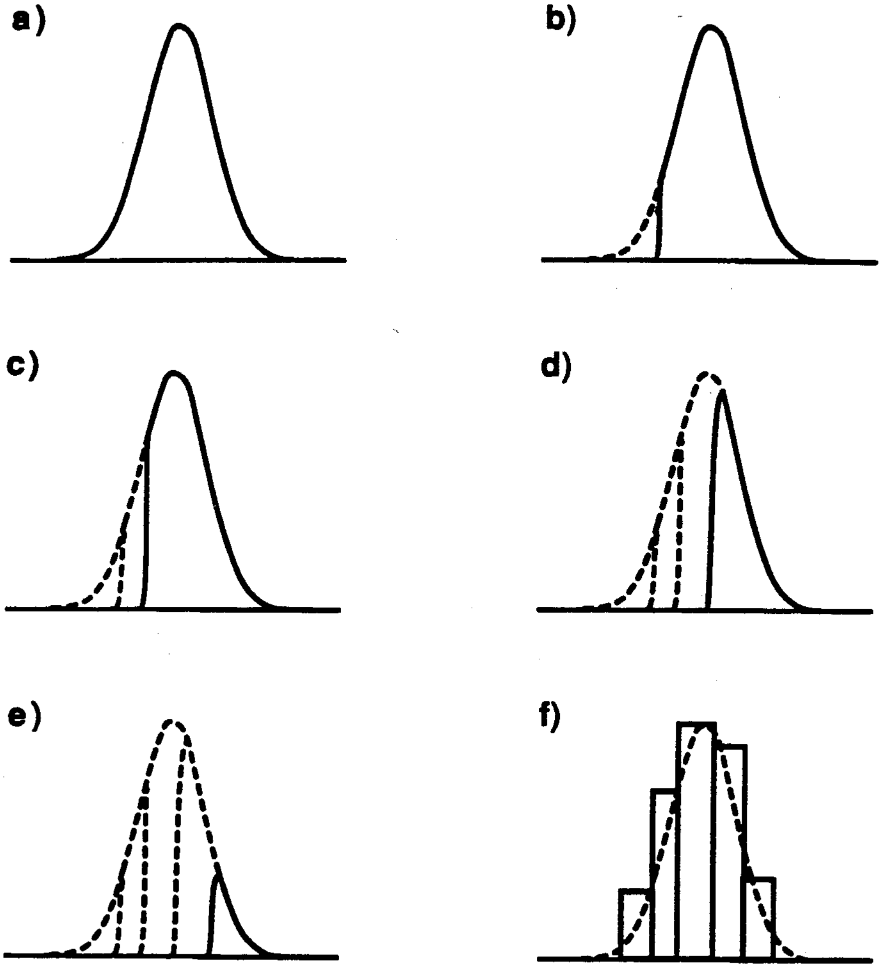

Figure 2-14. A distribution-slicing experiment, on an E_a scale: (a) intact distirbution; (b-e) evolution of the distribution during warmings to successively higher temperatures [the area bounded by the solid line represents the sites that remain (and thus the signal intensity) after warming]; (f) reconstruction of the distribution.

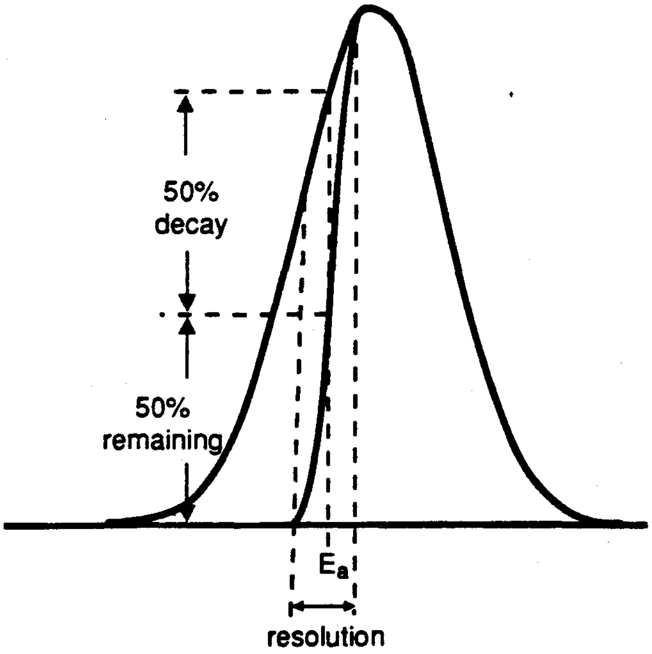

Figure 2-15. Assignment of a representative E_a to a given slice.

integrated (intensity *vs.* E_a) form. Distribution-shape information is still available in this format, as shown in Figure 2-16 for Gaussian, box, and right-triangle distributions.

The raw data for each cycle include the temperature to which the matrix was warmed, the warming interval, and the intensity recorded upon recooling. The data from the distribution-slicing experiment for **24-Ph** in MTHF are listed in Table 2-4. In order to plot the data, the temperature and time values were first converted to E_a values using equation 2-6 and assuming $\log A = 8.0$. (The choice of $\log A$ affects only the E_a values and the width, not the distribution shape.) The plot of intensity *vs.* E_a for **24-Ph** is shown in Figure 2-17. This graph, when compared to the curves in Figure 2-16, agrees best with the Gaussian distribution curve. Thus, the distribution shape, which completely eludes decay-fitting procedures (see below), is in effect "photographed" by this comparatively simple procedure.

In addition to providing shape information, this method serves to verify the distribution model itself through simple, qualitative observations. For example, whenever consecutive warming cycles involve the same temperature, the majority of the decay always occurs during the first cycle. Subsequent cycles show very little decay, since the fast sites and many of the sites in the intermediate region have already been depleted. Furthermore, any subsequent warming cycles to lower temperatures show no decay at all on a reasonable time scale. Note also that the data of Table 2-4 are *not* consistent with a distribution over A, with a relatively constant E_a. In such a case decay behavior is essentially invariant to temperature. As far as we are aware, these observations constitute the most direct evidence to date in support of a distribution model.[42]

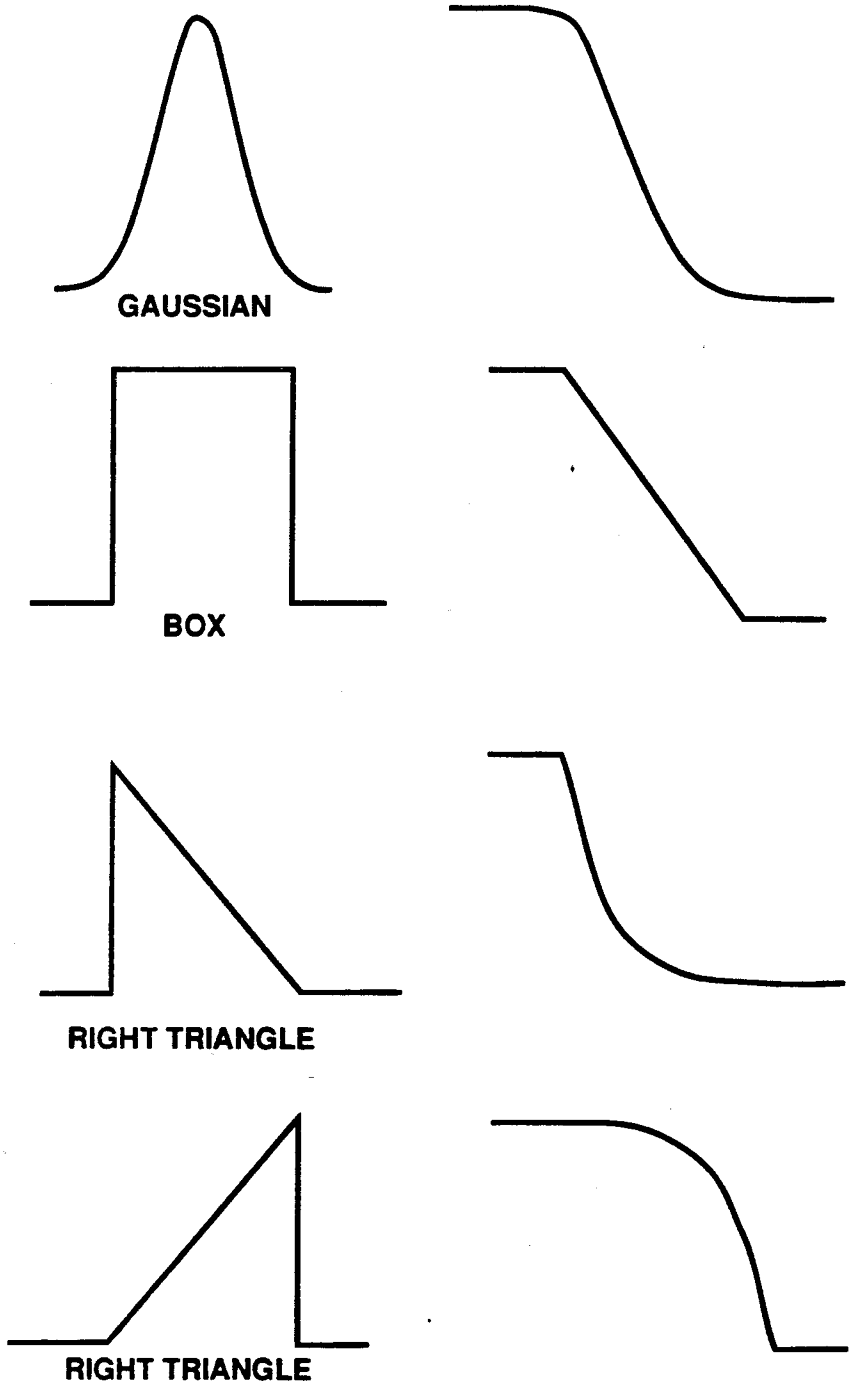

Figure 2-16. Distribution shapes (probability vs E_a, left) and integrated form of the distributions (intensity vs E_a, right).

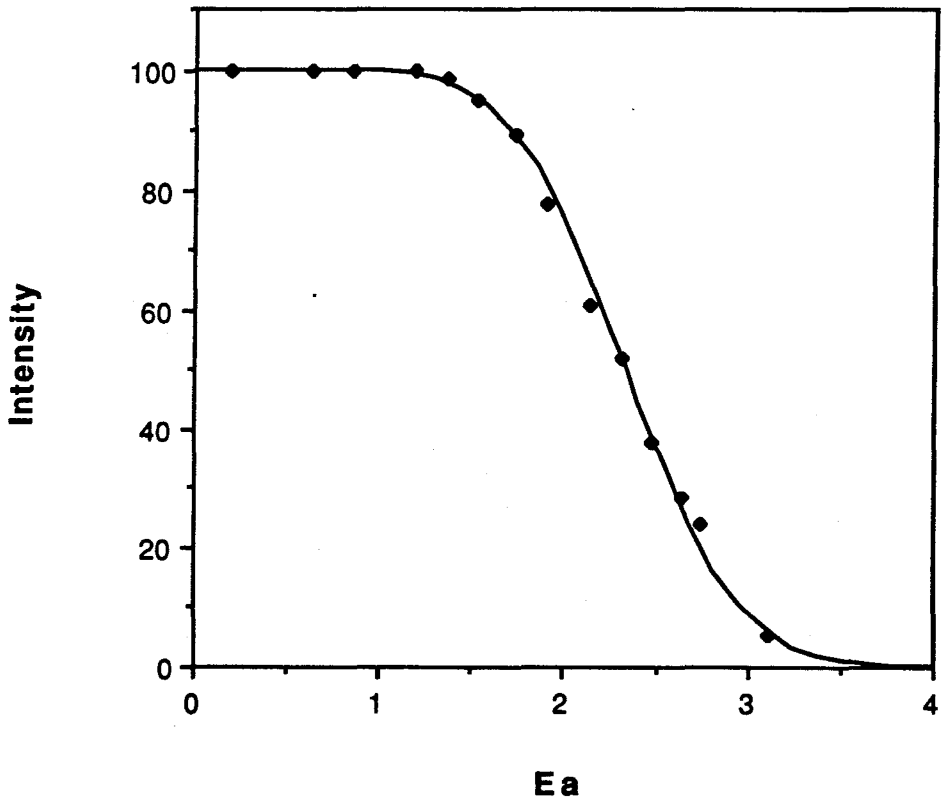

Figure 2-17. Distribution-slicing results (from DSFIT) for 24-Ph in MTHF, assuming log $A = 8.0$ (Table 2-4).

Table 2-4. Distribution Slicing Data for **24-Ph** in MTHF[a]

T,K	intensity, %	E_a, kcal/mol[b]
3.8	100	0.19
13.0	100	0.63
17.5	100	0.85
24.5	100	1.19
28.0	98.6	1.36
31.5	94.9	1.53
35.5	89.1	1.73
39.3	77.4	1.91
44.0	61.0	2.14
47.5	51.9	2.31
51.0	37.9	2.48
54.0	28.6	2.63
56.3	24.0	2.74
64.0	5.3	3.11

[a] Calculated using equation 2-6 with $\log A = 8.0$. [b] The warming interval (t) was 300 s for all points.

Our results (such as the example in Figure 2-17) closely resembled the Gaussian model, and we have used this distribution shape in our analyses. However, it should be noted that satisfactory fits to the *decay traces* can be obtained using other distributions, including all those of Figure 2-16.[26b] We choose the Gaussian because of the results of Figure 2-17, and because it seems like a relatively unbiased shape. Previous work in these laboratories led to the development of a computer program that fits the distribution slicing data to the Gaussian model.[26b] The program, called DSFIT, accepts as input from a data file the raw temperature, time, and intensity data (*e.g.*, Table 2-4). The only additional input necessary is log A. The most probable E_a and distribution width (expressed as the standard deviation implied by the Gaussian, σ) are optimized. The fit obtained for the **24-Ph** using log $A = 8.0$ is shown in Figure 2-17.

The experimental procedure used in distribution slicing has several intrinsic advantages when compared to normal decay kinetics. A significant advantage is that even though the decay may be probed over a large temperature range, all intensity measurements are made at the *same* temperature. This is crucial because in EPR, absolute signal intensity varies considerably with temperature in the 4-65 K range (Curie Law). Furthermore, the measurement temperature, usually 3.8 K, is the easiest temperature to attain accurately when using a liquid helium cryostat.

The method also has several drawbacks. One is that the temperatures must be equilibrated quickly and without overshooting. At such low temperatures, kinetic behavior for a distribution of sites is characterized by a much greater dependence on temperature than on time, so temperature equilibration is a crucial issue. The precise control of liquid helium cryostats and maintenance of a viable temperature calibration also complicate the analysis. Further simulations[26b] suggest two other limitations of the method. First, the width of the *rate* distribution at any given temperature must be quite substantial, although, as discussed above, this is a common situation at cryogenic temperatures. Second, the total width of the E_a distribution should be large relative to the most probable E_a. In other words, the distribution should extend nearly to zero on the E_a axis. Therefore, the range of reactions for which distribution slicing may be used effectively may be somewhat limited.

Decay-Trace Fitting. We have also used decay-trace fitting, the usual method of analysis for rate-dispersive kinetics. Extraction of useful rate information from matrix-perturbed kinetic traces has proven to be highly challenging to chemists and physicists, though several methods have been used with success.[39,40,43-45] A convenient and common assumption in the distribution model, and one that we will use, is that the rate dispersion arises from a distribution of activation energies (E_a), *i.e.,* that the Arrhenius pre-exponential term (log A) is a constant. We have already shown that the distribution slicing data support this assumption. Also, at very low temperatures, the rate is much more sensitive to small variations in E_a than in log A. For example, at 20 K a change of 0.1 kcal/mol in E_a is equivalent to a change of more than one log A unit. Therefore, a distribution that covers a small range over both log A and E_a can usually be approximated by a distribution over E_a alone.

The goal of all methods using a distribution model is to obtain the initial rate-constant distribution, or at least its maximum, the most probable rate constant ($k°$). If we denote the distribution at a given time as $F(k,t)$, then it is well known that the decay-trace kinetic observable $f(t)$ is related to the initial distribution, *F(k,0)*, by the Laplace transform (eq 2-7).

$$f(t) = \int_0^\infty F(k,0)e^{-kt}\,dk \tag{2-7}$$

This relationship implies that the desired distribution can be obtained by Laplace inversion of

$$F(k,0) = L^{-1}[f(t)] \tag{2-8}$$

the kinetics trace, as indicated in equation 2-8. Unfortunately, numerical Laplace inversion is an ill-conditioned transformation; *i.e.* very small changes in *f(t)* can result in very large changes in *F(k,0)*. As a consequence of this instability, no general procedure is available for numerically inverting the Laplace transform.

The only decay-trace analysis method that we have used successfully is a simple numerical approach based on the forward Laplace transform.[43,45] The procedure calls for an initial assumption of distribution shape, then adjustment of parameters to produce the simulated decay trace that best fits the actual trace. Typically, distributions have two adjustable parameters, one relating to width and one relating to position on the rate axis.

This method has a disadvantage in that the distribution shape is chosen *a priori*. However, in the present case, we already know from the distribution-slicing experiments that the shape is Gaussian (or very nearly Gaussian), so the requirement of a shape assumption is no longer a disadvantage.

Using a previously developed algorithm,[26b] the decay-trace fitting procedure involves computing the simulated decay trace point-by-point in a chronological sense. The distribution at each point is calculated from the distribution at the previous point, accounting for the decay occurring over the intervening time interval. The intensity at each point is simply the area under the current distribution. With this procedure, the photochemical generation period can be included explicitly, accounting for both growth and decay during photolysis.

This approach correctly models the shapes of the decay traces we observe. However, as Figure 2-11b shows, the major feature that distinguishes different rates is the absolute intensity of the signal, rather than the shape. Thus, one needs a way to "normalize" the decay trace, *i.e.*, to put it on an absolute intensity scale. The distribution slicing data described above provide the necessary information. That is, any point in a distribution slicing experiment corresponds to an *absolute* intensity for a given time at a given temperature. For example, Table 2-4 reveals that after 300 *s* at 44 K, 61.0% of the sites will remain for **24-Ph** in MTHF. Thus, a decay trace determined at 44 K is normalized so that it crosses 61.0% at 300 *s* into the decay. Note that this procedure uses the raw time, temperature and intensity data, and so does not introduce any assumption concerning log A or E_a.

The important point is that in exponential kinetics, knowledge of initial intensity or even when the reaction started is unnecessary, since the $ln f(t)$ versus t plot gives the same rate constant no matter when reaction monitoring is begun. However, *in nonexponential kinetics, knowledge of the absolute intensity is crucial, because this is the main feature that differentiates decay traces at various temperatures* (see Figure 2-11).

The decay algorithm has been incorporated into two programs: a simulation program, DECAY, and a fitting program, FIT. DECAY serves two purposes: (1) simulated growth/decay traces are produced given log A, the most probable E_a, the choice of distribution shape and its width, and the temperature; and (2) the E_a distribution at any point during the growth or decay can be displayed. (This program was used to produce the simulations in Figures 2-11 and 2-13.)

FIT produces growth/decay trace simulations in the same manner as DECAY, but the results are compared to an experimental trace. The distribution is handled on a logarithmic rate scale, which is proportional to E_a, so that log A input is not necessary. The distribution width and/or position on the axis can be optimized to produce the best fit.[47]

At this point, the relationship between the E_a and rate axes should be clarified. The rate constant of the most probable site, $k°$, can be related to

$$ln\left(\frac{k}{k^\circ}\right) = \frac{(\Delta E_a)}{RT} \qquad (2\text{-}9)$$

that of any other site in the distribution, k, by equation 2-9, where $\Delta E_a = E_a{}^\circ - E_a$. Equation 2-9 shows that the $\ell n(k/k^\circ)$ and ΔE_a scales are directly proportional. Further, whereas ΔE_a is temperature-independent, $\ell n(k/k^\circ)$ varies inversely with temperature. The effect of this relationship is that an E_a distribution remains constant at all temperatures, while the corresponding $\ell n(k/k^\circ)$ distribution becomes narrower as the temperature increases.

EPR-signal growth and decay curves were recorded for **24-Ph** in the 27-54 K temperature range using photolysis intervals of 10-20 seconds. The signal decays, digitized and stored for later analysis, were followed for 8 to 13 minutes, even though at the lower temperatures only a small fraction of the signal decayed during this interval (see Figures 2-11,12). Monitoring signal decay over several half-lives, as is always desirable in quantitative kinetics, was impractical in our experiments. In most cases, this would have required experiments lasting days or weeks. Though experiments on the order of several hours may have been possible, these would not have resulted in significant improvement.

Once the decay traces have been normalized using the distribution slicing data, the fitting procedure is straightforward and can proceed in one of two manners. These are summarized in Figure 2-18. The first procedure, termed σ_{av}, uses the simulation package (FIT) to simultaneously optimize $k°$ and σ for each observed decay trace. This produces a different value of σ for each decay, but the observed variation is usually small. Since our model assumes that all initial distributions are the same, we average the various σ values to produce the one σ_{av} for a given biradical/solvent combination. We then refit the decays using σ_{av} and optimizing only $k°$. These $k°$ values (Table 2-5) for the various temperatures are then plotted in an Arrhenius fashion to produce activation parameters. For **24-Ph** in MTHF the value of σ_{av} is 0.600 kcal/mol. The fits to the experimental decay traces are shown in Figure 2-19. The resulting Arrhenius plot Figure 2-20a yielded activation parameters log A $= 7.8, E_a° = 2.29$. Note that the kinetic point at 27 K was not included in the least squares fit of the Arrhenius plot. This point was not included because the extent of its decay is very small and therefore its associated error must be relatively large. But as shown in Figure 2-20, this point is quite close to the line, a remarkable validation of the fitting scheme.

The alternative approach, termed σ_{DS}, first assumes a value for log A (Figure 2-18). With this in hand, the distribution slicing data can be fit using DSFIT to produce a value for σ_{DS}. The rest of the procedure is then the same as for the σ_{av} approach (Figure 2-18). The choice of log A in the first step can be based on several types of evidence. One can use the log A determined from the σ_{av} approach (Table 2-6). One can invoke experimental precedent, in that a variety of studies of spin-forbidden processes in hydrocarbons have been

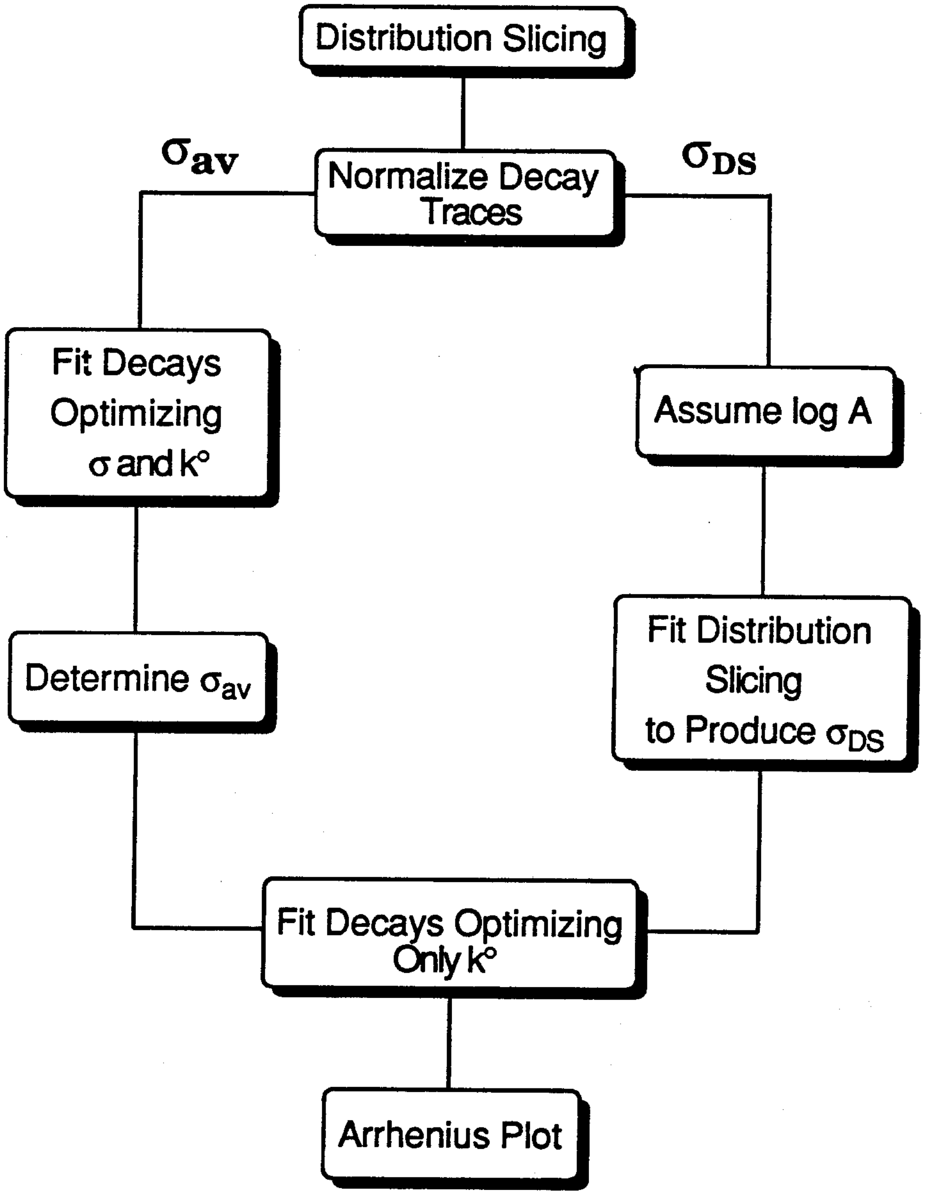

Figure 2-18. Flow chart depicting the two methods used to obtain activation parameters from experimental decay traces.

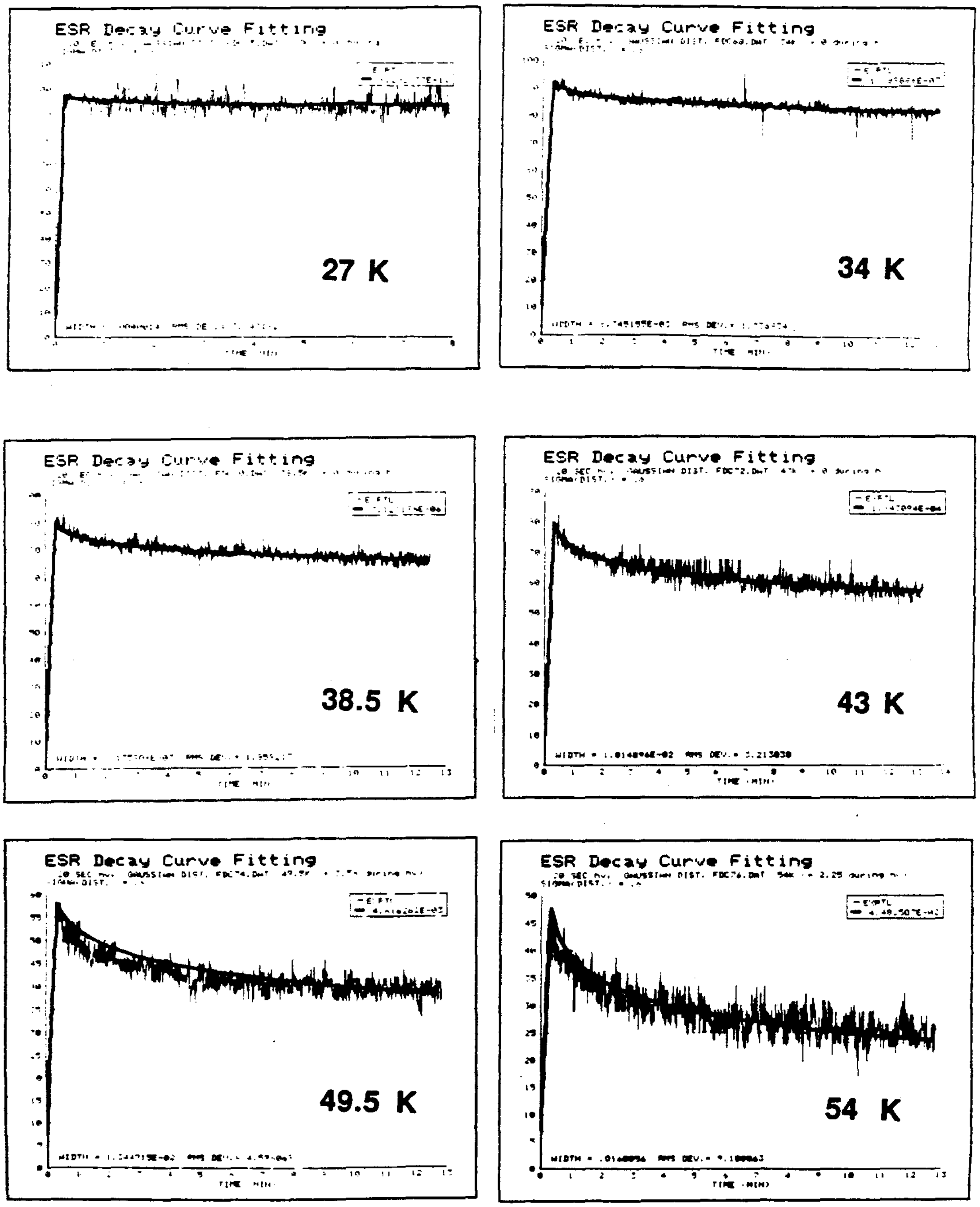

Figure 2-19. Experimental and calculated decay traces for 24-Ph in MTHF using the σ_{av} procedure. The fits were obtained with $\sigma_{av}=0.600$ kcal/mol. The optimized rate constants ($k°$) are shown in Table 2-5.

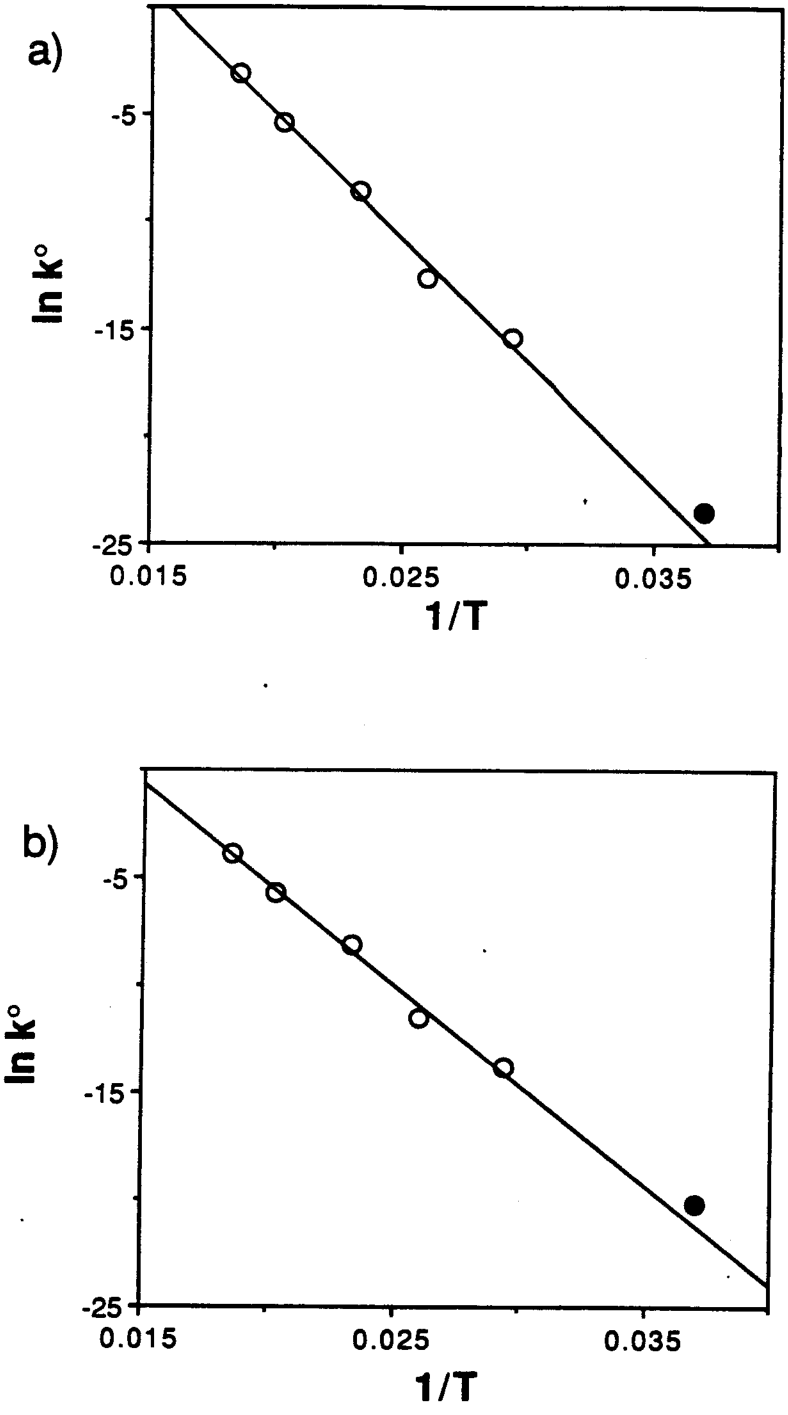

Figure 2-20. Arrhenius plots for 24-Ph in MTHF. The rates were obtained by using (a) the σ_{av} procedure (b) the σ_{DS} procedure (Table 2-5). Data points corresponding to rate constants with *ln* $k° < -20$ (filled markers) were not included in the least-squares analysis.

Table 2-5. Most Probable Rate Constants for **24-Ph** in MTHF.

T,K	$k°_{av}$, s^{-1}	$k°_{DS}$, s^{-1}
27	6.20×10^{-11}	1.62×10^{-9}
34	1.89×10^{-7}	9.76×10^{-7}
38.5	3.13×10^{-6}	9.86×10^{-6}
43	1.94×10^{-4}	2.98×10^{-4}
49.5	4.62×10^{-3}	3.38×10^{-3}
54	4.48×10^{-2}	2.03×10^{-2}

Table 2-6. Activation Parameters for Cyclobutanediyls.

Biradical	Solvent	σ_{av}			DSFIT log $A = 8$		σ_{DS}	
		σ_{av}	E_a°	log A	E_a°	σ_{DS}	E_a°	log A
24-Ph	MTHF	0.600	2.29	7.8	2.34	0.488	1.85	5.7
24-Vin[a]	MTHF	0.554	1.80	8.3	1.74	0.523	1.70	7.6
24-EV[a]	MTHF	0.432	1.16	6.0	1.44	0.533	1.40	7.8

[a] Sponsler, M.B., Ph.D. Thesis, California Institute of Technology, 1987.

examined, as shown in Table 2-7. Both approaches indicate that spin-forbidden processes have low *A* values. We have chosen a log *A* of 8.0, which is consistent with precedent (Table 2-7), and with the σ_{av} analysis (Table 2-6).

For **24-Ph**, assuming a log *A* of 8.0, DSFIT gives $E_a{}^\circ$ = 2.34 kcal/mol and σ_{DS} = 0.488 kcal/mol (see Figure 2-17). Shown in Figure 2-21 are the fits obtained to the data using a σ of 0.488 kcal/mol. The correlation between the experimental and calculated traces is noticably poorer for this method relative to the σ_{av} procedure. The derived activation parameters are log *A* = 5.7, $E_a{}^\circ$=1.85 (Figure 2-20b). These results are in poor agreement with the log A of 8.0 assumed for DSFIT. When this value of log *A* (5.7) was input to DSFIT, the resulting parameters were $E_a{}^\circ$=1.86 kcal/mol and σ_{DS}=0.365 kcal/mol. Fitting the decay traces with this new width led to poor results again (log *A* = 3.5, $E_a{}^\circ$=1.37 kcal/mol). This is quite unusual because with all other cyclobutanediyls studied by this method, the log *A* obtained from the Arrhenius plot is very near (less than one log *A* unit) that used with DSFIT. Thus, because of the poor agreement between the Arrhenius plot and the assumed log *A* and the less satisfactory decay fits, we believe the results obtained from the σ_{av} procedure are more reliable and our discussion will emphasize them.[48]

The two fitting schemes, σ_{av} and σ_{DS}, are in some sense complementary. An advantage of the σ_{av} approach is that *no assumption of log A is involved.* The raw distribution slicing data are used only to normalize the decay traces, and log *A* is obtained directly from the Arrhenius plot. A disadvantage to this approach is that it requires simultaneous optimization of two tightly coupled parameters (σ and k°) using curves that have a relatively low information content (Figure 2-12). The σ_{DS} procedure avoids this problem, but it requires an assumption of log *A*.

Table 2-7. Activation Parameters for Triplet Biradical Reactions

Reaction	log *A* (s^{-1})	E_a (kcal/mol)	Ref.
	7.7–9.9	6–8	*a*
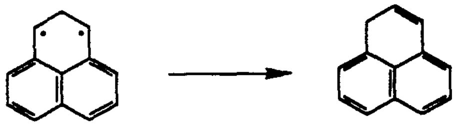	5.1 ±1.0	5.3 ±1.0	*b*
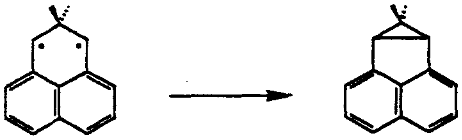	8.4 ±0.15	6.8 ±0.2	*c*
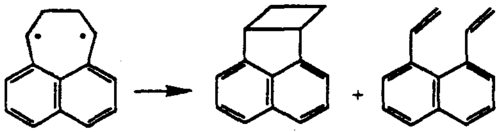	6.9 ±0.3	4.5 ±0.3	*d*
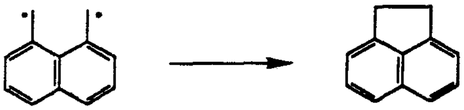	10.4 ±0.5	6.4 ±0.3	*e*
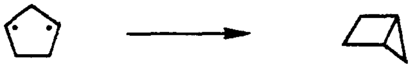	8.0	2.3	*f*
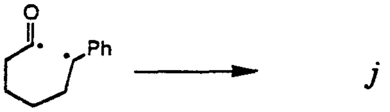	8.2 ±0.1 7.7 ±0.3	1.2 ±0.1 0.8 ±0.2	*g* *h*
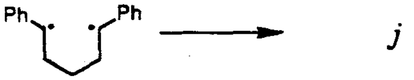	6.7 ±0.2	0.85 ±0.15	*i*

a Dowd, P.; Chow, M. *Tetrahedron* **1982**, *38*, 799-807. *b* Ref. 10. *c* Hasler, E.; Gassman, E.; Wirz, J. *Helv. Chim. Acta.* **1985**, *68*, 777-788. *d* Gisin, M.; Rommel, E.; Wirz, J.; Burnett, M.N.; Pagni, R.M. *J. Am. Chem. Soc.* **1979**, *101*, 2216-2218. *e* Platz, M.S. *J. Am. Chem. Soc.* **1980**, *102*, 1192-1194. *f* Ref. 3. *g* Weir, D.; Scaiano, J.C. *Chem. Phys. Lett.* **1985**, *118*, 526-529. *h* Zimmt, M.B.; Doubleday, C.Jr.; Turro N.J. *J. Am. Chem. Soc.* **1986**, *108*, 3618-3620. *i* Zimmt, M.B.; Doubleday, C., Jr.; Gould, I.R.; Turro, N.J. *J. Am. Chem. Soc.* **1985**, *107*, 6724-6726. *j* products not determined.

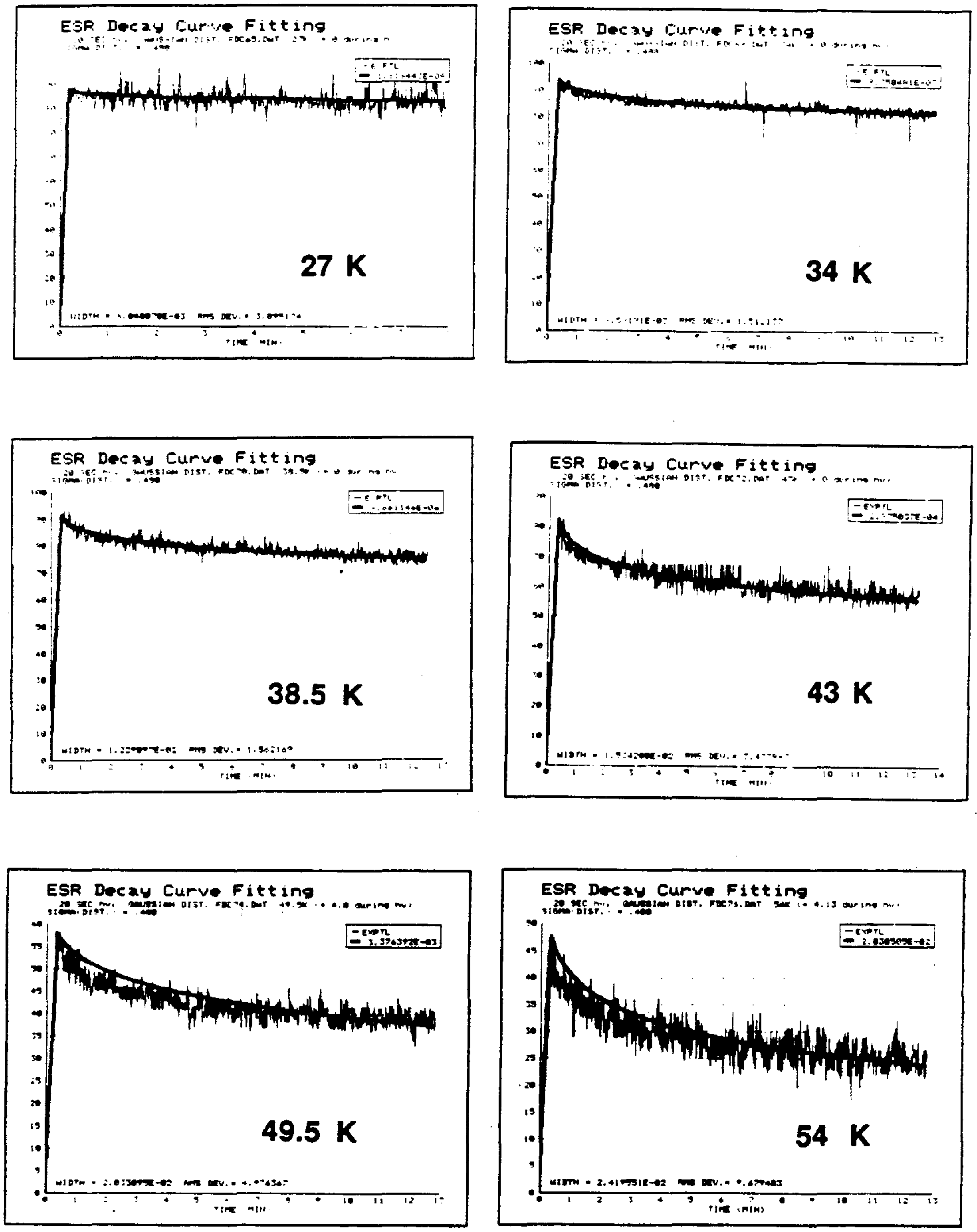

Figure 2-21. Experimental and calculated decay traces for 24-Ph in MTHF using the σ_{DS} procedure. The fits were obtained with σ_{DS} = 0.488 kcal/mol. The optimized rate constants ($k°$) are shown in Table 2-5.

It is worth emphasizing that *neither model assumed that the variation of k° with temperature would follow the Arrhenius law.* Yet, excellent correlations (Figure 2-20) are obtained over a very large temperature range (a *factor* of two) and a huge rate range (over nine orders of magnitude). Given the difficulties of accurate temperature measurement and the complex analysis required to obtain k°, we consider these results to be quite compelling.

At this point, it is instructive to compare the observed decay behavior of **24-Ph** with other localized 1,3-biradicals. First, we will consider stabilized cyclobutanediyls **24-EV** and **24-Vin** which have one and two vinyl groups appended to the radical centers, respectively. Like **24-Ph**, these triplet cyclobutanediyls are indefinitely stable at 4 K and only at temperatures near 20 K does nonexponential decay commence. Analysis of the decay kinetics of these biradicals in MTHF matrices by the σ_{av} procedure described above, reveals that they too exhibit Arrhenius behavior (Table 2-6). The derived activation parameters for **24-EV** are log A = 6.0, $E_a{}^{\circ}$ = 1.16 kcal/mol. The divinyl biradical is noticably more stable, yielding log A = 8.3, $E_a{}^{\circ}$ = 1.80 kcal/mol.

Unfortunately, we were unable to study the decay kinetics of **24-MP** because it failed to produce strong EPR signals. Qualitative studies, however, revealed that the biradical is indefinitely stable at temperatures up to *ca.* 20 K.

The matrix isolation decay behaviors of the fully localized biradicals **24-Me**, **24-Et** and Closs' biradical **6** are fundamentally different from those observed for the other (stabilized) structures discussed above. Even at 4 K, the EPR signals of the fully localized biradicals decay significantly.

In analyzing the decay of **6**, Closs considered only initial decay rates[3] and found that they were relatively temperature insensitive. Similarly, when workers in these laboratories studied the decays of **24-Me, 24-Et** and **6** by analyzing the *entire* decay profile using the above-described method, they also found that the decay rates were very temperature insensitive.[15b] For example, consider the representative data for **6** in MTHF. A decay trace recorded at 4 K produced k° of 1.6×10^{-2} s^{-1} when subjected to the decay-trace fitting procedure. Assuming a log A of 8.0, this rate implies an E_a of 170 cal/mol. If this process follows Arrhenius behavior, the predicted k° at 42 K would then be 4.1×10^{6} s^{-1}, but the observed value is only 8.2×10^{-2} s^{-1}. Very similar behavior is observed for **24-Me** and **24-Et**. The relative insensitivity of k° to temperature is, of course, the hallmark of a tunneling event.

Closs showed[3] that the initial rates he obtained for the decay of **6** could be readily modeled using Bell's simple scheme for tunneling through a parabolic barrier.[49] The same was found to be true for **24-Me, 24-Et** and **6** when the most probable rate constant, k°, was used in the modeling.[15b] The results of the tunneling calculations are shown in Table 2-8. The tunneling calculations assumed a log A = 8.0 and a mass (m) of the tunneling particle equal to the entire mass of the biradical. These calculations show that significant tunneling rates through chemically meaningful barriers (2a) can be obtained for even very heavy particles.[50]

Discussion. At this stage it is appropriate to consider the absolute accuracy of the parameters we have obtained. There is some uncertainty in the A values. This is important because for a given set of decay data, A and $E_a{}^{\circ}$ are strongly correlated. That is, a low A leads to a low $E_a{}^{\circ}$ and vice versa (Table 2-6). For **24-Ph**, we feel the log A value of 7.8 obtained from σ_{av} procedure is quite reasonable for a spin forbidden process in a hydrocarbon. Evidence for this comes from the data of Table 2-7 and a variety of laser-flash

Table 2-8. Tunneling Parameters [a,b]

Structure	Solvent	E_a (kcal/mol)	$2a$ (Å)
24-Me	Acetone	0.75	0.38
24-Et	Acetone	0.825	0.325
6	MTHF	2.35	0.25
6	Cyclohexane	1.60	0.29

[a] For all calculations $A = 10^8$ s^{-1} and the mass of the whole structure is used. [b] Jain, R., Ph.D. Thesis, California Institute of Technology, 1987.

photolysis studies of triplet biradicals that indicate lifetimes of tens to hundreds of nanoseconds.[51]

It should be remembered that our model assumes that all matrix sites have identical A values. This is almost certainly untrue. However, attempts to simultaneously optimize A and $E_a°$ would introduce yet another adjustable parameter to a scheme that already involves fitting curves with fairly low information content. The distribution-slicing results require a variation in E_a, and as discussed above, relatively modest variations in E_a have much more profound consequences for rates than do comparable variations in A, at cryogenic temperatures. Thus we feel the assumption of constant A is the best course for this system.

We are now in a position to assess, to some degree, the influence of the matrix on the ring-closure reaction. A reasonable gauge of the magnitude of the matrix effect is the standard deviation of the Gaussian distribution, σ. The σ values of the three stabilized cyclobutanediyls (**24-Ph**, **24-Vin** and **24-EV**) are all quite consistent, falling in the range of 0.4 to 0.6 kcal/mol. It is actually a small effect. The only reason we see such profound rate variations over different sites is the low E_a of the process we are investigating. For instance, simulations clearly show that for a process that has $E_a° = 25$ kcal/mol and a Gaussian distribution width of $\sigma = 0.5$ kcal/mol, the observed decays (at temperatures around 300K) are not perceptibly different from those obtained with a single E_a.[52]

In many other studies of matrix-isolation decays, it is not difficult to imagine that in fact one is actually probing the nature of the matrix environment rather than the intrinsic reactivity of the species of interest. However, such studies almost invariably involve hydrogen abstraction from the matrix. Thus, the matrix material is one of the reactants in the system, so of course "matrix effects" are profoundly important. We feel there is good reason to believe that the *trends* we have observed in the present work are indicative of the intrinsic reactivities of the biradicals. The most compelling evidence in support of this is the fact that the steric interactions of a matrix with **24-Et**, **24-EV** and **24-Vin** must be extremely similar, yet the three biradicals display qualitatively different behaviors. At present we cannot dissect the activation energies we obtain into a component due to matrix forces and a component that reflects the intrinsic reactivities of the biradicals. We think it is reasonable, though, to propose that the matrix effect is relatively constant for such closely related molecules. Thus, we feel that comparisons among the biradicals are chemically meaningful.

As mentioned previously, the molecules studied in the present work fall into two classes: stabilized and fully localized. The stabilized biradicals are persistent[53] at 4 K and undergo thermally activated decay at higher temperatures in accord with the Arrhenius law. Biradical **24-EV**, with only one stabilizing group, is less stable than those with two. Qualitatively, **24-Ph** is the most persistent cyclobutanediyl, observable at significantly higher temperatures than **24-Vin**, which is reflected in the larger $E_a°$ obtained for **24-Ph**. This stability ordering is the reverse of what one would expect on the basis of resonance stabilization energies of allyl *vs* benzyl radicals (11.9 *vs* 10.2 kcal/mol).[54] The enhanced stability of **24-Ph** may arise from increased resistance offered by the matrix to structural reorganization involving motions of the much larger phenyl substituents. In other words, the phenyl groups are more tightly anchored in the matrix. This argument is also consistent with the standard deviation observed for **24-Ph**, $\sigma_{av} = 0.600$ kcal/mol, the largest of the cyclobutanediyls. The data set we have at present is limited, but the trend across the series of stabilized structures is satisfyingly consistent with one's chemical intuition.

Fully localized cyclobutanediyls decay via quantum mechanical tunneling. The process is qualitatively similar to that seen for cyclopentanediyl **6**, although the onset of Arrhenius behavior occurs at a lower temperature for the cyclobutanediyls. This factor is reflected in the smaller barrier heights E relative to **6** (Table 2-8). We have made a related observation, in that 1,3-diphenylcyclopentanediyl (**20**) is much more stable than **24-Ph** (Chapter 3). For instance, $k°$ for **20** at 77 K is *ca.* 10^{-4} s^{-1}, much less than what one would expect for **24-Ph** (see Table III). This suggests that, despite the apparent capriciousness of the cyclopentanediyl framework observed in early studies, there is some generality for the greater stability of cyclopentanediyls *vs.* cyclobutanediyls (Chapter 3).

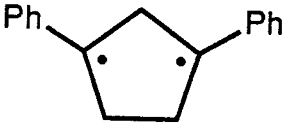

20

An important aspect of the cyclobutanediyl decay is that there are no H-shift (cyclobutene) products. In studies of **6** there are always small amounts of cyclopentene in the product mixtures.[3] This left open the possibility that in fact the tunneling process was a hydrogen shift, a type of reaction for which tunneling is precedented. The present studies greatly strengthen the conclusion that fully localized, triplet 1,3-biradicals can undergo C–C bond formation via tunneling.

More recent theoretical work[55] on cyclobutanediyls has revealed that the tunneling process may only involve motions of the substituents attached to the radical centers and that these motions can bring the singlet and triplet surfaces into coincidence. Using semiclassical periodic orbit theory, the calculations show that for 1,3-cyclobutanediyl (**24-H**), where the tunneling particle is a hydrogen atom, the rate of this tunneling process can be very fast ($k \sim 10^7\ s^{-1}$). This finding provides an explanation for the failure to observe the triplet state of **24-H** at cryogenic temperatures -- it simply decays too fast to allow detection. Also, using the same approach, it was shown that the calculated tunneling rates of bond formation for **24-Me** are quite comparable to the observed experimental values (*ca.* $10^{-2}\ s^{-1}$). Rapid tunneling is also indicated when the decay of **24-H** is simulated with the Bell tunneling model (using the entire mass of the biradical) described above. In the present work, we have been unable to observe **24-PhH** under cryogenic, matrix-isolation conditions. It seems likely that, as in **24-H**, the hydrogen atom attached to the radical center in **24-PhH** also undergoes a rapid tunneling reaction that brings the singlet and triplet surfaces into coincidence and leads to irreversible bond formation. Thus, from the above mentioned results, it appears that only those cyclobutanediyls with substituents more massive than hydrogen (*i.e.* methyl) can be observed by triplet EPR spectroscopy.

One might ask why there is a qualitative difference in decay behavior between the stabilized cyclobutanediyls and the fully localized ones. An interesting parallel exists in the cyclopropane thermal rearrangement literature.[51a,56] Theory suggests that the parent 1,3-biradical, trimethylene (**5**), should have no barrier to ring closure on the singlet surface, and so is not a true intermediate. Thermal rearrangement studies on 1,2-d_2-cyclopropane are consistent with this prediction, in that double methylene rotation is the dominant mode of stereomutation. In contrast, vinylcyclopropane, phenylcyclopropane and other cyclopropanes with radical stabilizing substituents display more conventional thermal behavior that is consistent with the intervention of a singlet 1,3-biradical as a true intermediate.

In light of these arguments, we can construct a model for cyclobutanediyl decay. Consider the contrasting behaviors of **24-Et** and **24-Vin**. We assume that delocalizing substituents preferentially stabilize the planar form of the biradical. This will introduce a well, or deepen a pre-existing well, at the biradical geometry on the singlet (S) surface (Figure 2-22). In fact, in their classic analysis of biradicals, Salem and Rowland[57] proposed that the introduction of stabilizing substituents may be the only way to introduce a biradical minimum on the singlet surface. For the sake of argument, we shall assume that there is no singlet well for **24-Et**, but that there is for **24-Vin**. However, the analysis would be unchanged by the existence of a small barrier to closure for **24-Et**. We also assume that the S-T gap ($E_{S\text{-}T}$) in **24-Vin** is smaller than in **24-Et**. The T preference in these structures results from exchange repulsions, which depend upon the separation distance between the two radicals.[26a,57] Our spectroscopic studies clearly show that delocalization keeps the spins further apart which should diminish the exchange repulsions and the S-T gap in **24-Vin**.

The model is summarized in Figure 2-22. We assume that it is the spin forbiddeness of ring closure that is primarily responsible for the stabilitiy of the biradicals, and that intersystem crossing requires a near degeneracy of the S and T surfaces brought about by some geometric distortion. For **24-Et**, with no singlet biradical well, the transition state is approximated by the S-T crossing point.[55] Note that $E_a < E_{S\text{-}T}$, and one has a small, narrow barrier. In **24-Vin**, both the S and T surfaces are stabilized by *ca.* 20 kcal/mol[54] relative to **24-Et** at biradical geometries. The introduction of a singlet well could move the surface crossing as shown to a point after the maximum on S. In this case,

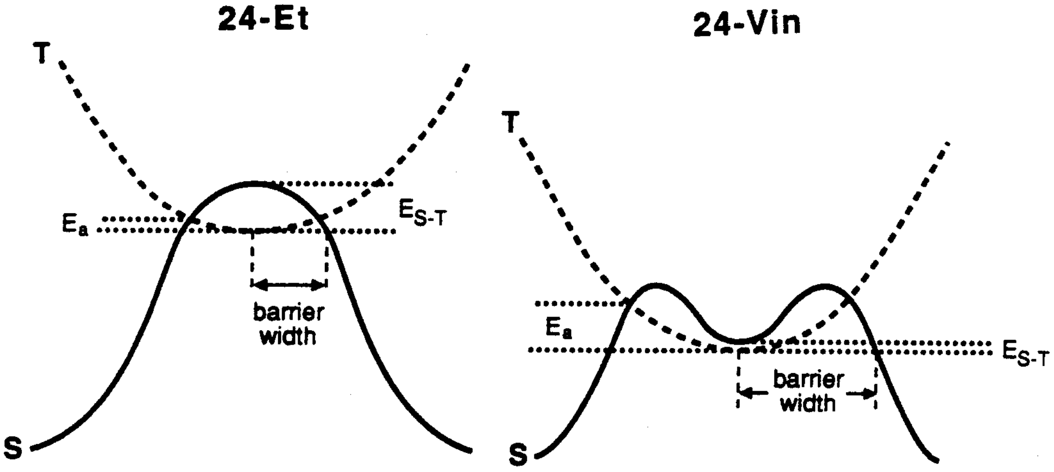

Figure 2-22. Schematic potential energy surfaces for the closure of cyclobutanediyls **24-Et** and **24-Vin** to the corresponding bicyclobutanes.

$E_a > E_{S\text{-}T}$ and the barrier width is substantially increased. In all tunneling models, the most important parameter is the barrier width, $2a$, with the height, E, and mass, m, being less important. In our model for biradical decay, the width is essentially determined by how steeply the S surface falls. Introducing a well (or deepening an existing well) on S means that it initially rises and then falls, and this can increase the barrier width. Thus, **24-Et** and **24-Me** are presented with a fairly narrow barrier, through which tunneling is feasible, but **24-Vin**, **24-EV** and **24-Ph** face too wide a barrier for tunneling. The model also nicely explains the increase in E_a on going from **24-Et** to **24-Vin** and why E for **24-Et** is smaller than 1.5 kcal/mol, the computed value of $E_{S\text{-}T}$.[55] Of course, at this point the model outlined in Figure 2-22 is strictly conjecture, and it will be interesting to see whether further examples support the basic scheme.

Conclusion

We have found that cyclobutanediyls constitute a general class of triplet ground state, localized 1,3-biradicals. The EPR spectra of the cyclobutanediyls provide valuable structural information. The *D* value is a sensitive probe of spin distribution, and we have shown that the trends in the data can be quantitatively modeled by using a relatively simple scheme for zfs calculations. Similarly, hfc to the ring CH_2 protons was observed to be quantitatively correlated to the spin densities at the ring radical centers. Importantly, the hfc shows that the cyclobutanediyls are effectively planar.

We have studied the decay kinetics of the cyclobutanediyls with the explicit inclusion of matrix-site effects. Cyclobutanediyls bearing stabilizing substituents such as phenyl or vinyl on the radical centers are indefinitely stable at 4 K. On warming to 20-50 K, ring closure commences, and the variation of the decay rates with temperature follows the Arrhenius law. In contrast, cyclobutanediyls that are devoid of stabilizing substituents decay even at 4 K. The reaction rates are very insensitive to temperature and quantum mechanical tunneling is involved in the ring closure.

A model has been developed to rationalize the contrasting behaviors of stabilized *vs.* fully localized cyclobutanediyls. Delocalizing substituents are thought to deepen the potential energy well in which the singlet biradical lies. This widens the barrier to ring closure, and thus suppresses tunneling. The model rationalizes the observed trends in activation parameters and appears to be consistent with cyclopropane thermal rearrangement chemistry.

Experimental

General. Fourier transform NMR spectra (^1H and ^{13}C) were obtained on a JEOL GX-400 or Varian XL-200 spectrometer. An INEPT[58] pulse sequence was employed to determine carbon-hydrogen coupling constants. Ultraviolet spectra were recorded on a Hewlett-Packard 8451A diode array spectrophotometer. Mass spectra were obtained at the University of California, Riverside Analytical Facility. Analytical gas chromatography was performed on a Hewlett-Packard 5880 chromatograph equipped with a flame ionization detector. Melting points are uncorrected.

Tetrahydrofuran was distilled from benzophenone ketyl prior to use. All other solvents were reagent grade or better and used as purchased unless otherwise noted. Column chromatography was performed by the method of Still[59] employing 230-400 mesh silica gel.

1,3-Diphenylbicyclo[1.1.0]butane (19). To a solution of 1,3-dibromo-1,3-diphenylcyclobutane[9] (203 mg, 0.55 mmol) in 4 mL of tetrahydrofuran was added 1.0 g of freshly pulverized 2% lithium amalgam.[60] The heterogeneous mixture was allowed to stir for 2 h under an argon atmosphere. After the dark gray slurry was filtered through Celite, tetrahydrofuran (5 mL), CH_2Cl_2 (10 mL), and 5% sodium bicarbonate (30 mL) were added to the filtrate and thoroughly mixed. The organic solution was dried over Na_2SO_4 and concentrated to afford 104 mg of waxy yellow crystals, which were immediately used in the next step. ^1H NMR ($CDCl_3$) δ 1.60 (s, 2 H), 2.80 (s, 2 H), 7.22 (m, 10 H); ^{13}C NMR ($CDCl_3$) δ 28.72 (s), 32.59 (tdd, $^1J_{CH}$ = 160 Hz, $^3J_{CH}$ = 13.9, 4.4 Hz), 124.93 ($^1J_{CH}$ = 161 Hz), 124.96 (d, $^1J_{CH}$ = 160 Hz), 127.86 (d, $^1J_{CH}$ = 159 Hz), 135.53 (s).

1,3-Diphenyl-3-oxiranylpropan-1-one (26). Upon standing overnight in air, bicyclobutane **19** formed epoxy-ketone **26** and a polymer. The epoxy-ketone was purified by flash chromatography (CH_2Cl_2) to give a colorless oil. ^1H NMR ($CDCl_3$) δ 2.97 (dd, 1 H, J = 5.3, 1.2 Hz), 3.12 (d, 1 H, J = 5.3 Hz), 3.57 (d, 1 H, J = 16.5 Hz), 3.77 (dd, 1 H, J = 16.5, 1.2 Hz), 7.4 (m, 8H), 7.95 (m, 2 H); mass spectrum (EI) *m/e* 238, 224, 210, 105 (100), 77; exact mass calcd for $C_{16}H_{14}O_2$ 238.0994, found 238.0984.

1,7-Diphenyl-4-methyl-2,4,6-triazatricyclo[5.1.1.0^{2,6}]nonane-3,5-dione (25). To a refluxing solution of 1,3-diphenylbicyclobutane (**19**) (225 mg, 1.1 mmol) in *n*-hexane was added a solution of MTAD (140 mg, 1.2 mmol) in 40 mL of diethyl ether over 45 min while under stream of argon. The solvent was then removed under reduced pressure, and the crude material was purified by flash chromatography (4:1 benzene-ethyl acetate) to give 103 mg (28% from the dibromide) of **25** as a white crystalline solid: mp 207.5-208.5°C; ^1H NMR ($CDCl_3$) δ 2.52 (m, 4 H), 2.86 (s, 3 H), 7.33 (m, 10 H); ^{13}C NMR ($CDCl_3$) δ 25.76 (q, J_{CH} = 140 Hz), 47.38 (t, J_{CH} = 143 Hz), 73.72 (s), 126.84 (d, J_{CH} = 157 Hz), 128.18 (d, J_{CH} = 166 Hz), 128.73 (d, J_{CH} = 160 Hz), 132.99 (s), 159.15 (s); mass spectrum (El), *m/e* 319, 234, 206, 205 (100), 169, 117; exact mass calcd for $C_{19}H_{17}N_3O_2$ 319.1321, found 319.1318.

Semicarbazide 40. To a 5 mL flask containing **25** (15 mg, 47 mmol) were added 23 mg of KOH and 1.5 mL of degassed 2-propanol. The contents of the flask were brought to reflux under an argon atmosphere for 10 min. The cooled solution was then carefully acidified by dropwise addition of degassed 3 N HCl until CO_2 evolution ceased (250 µL). The solution was then neutralized by dropwise addition of degassed 1 N NH_3. Degassed water was added to dissolve the salts and then the solution was extracted with two 1.5 mL portions of degassed CH_2Cl_2 (distilled from CaH_2). The extracts were dried by filtration through $MgSO_4$. The solvent was removed by passing a stream of argon over the solution and then subjecting the residue to high vacuum to leave a yellow oil. High-field ^1H NMR analysis shows that the product consists of 90% semicarbazide **40** and 10% rearranged semicarbazide **43**. All attempts to purify **40** failed. **40:** ^1H NMR ($CDCl_3$) δ 2.40 (m, 4 H), 2.75 (d, 3 H, J = 5 Hz), 6.63 (bs, 1 H), 7.4 (m, 10 H), **43:** ^1H NMR ($CDCl_3$) δ 2.05 (s, 3 H), 2.86 (d, 3 H, J = 5 Hz), 3.42 (m, 2 H), 6.17 (bs, 1 H), 7.4 (m, 8 H), 7.70 (m, 2 H).

1,4-Diphenyl-2,3-diazabicyclo[2.1.1]hex-2-ene (14). A 10-mL two necked oven-dried pear flask was fitted with an addition ampule charged with 130 mg of nickel peroxide.[61] The atmosphere was replaced with argon, and **40** (16 mg, 0.054 mmol) in 3.5 mL of dry CH_2Cl_2 (distilled from CaH_2) was added via syringe. After the solution was cooled to -50°C, the contents of the ampule were added over 2 min. After 2 h of stirring, the slurry was transferred via a Teflon cannula to precooled (-78°C) filtration frit and vacuum filtered into a cold receiving flask. The CH_2Cl_2 was removed under high vacuum at -50°C to leave a white crystalline solid: ^1H NMR (CD_2Cl_2, -70°C) δ 2.55 (m, 2 H), 3.00 (m, 2 H), 7.4 (m, 10 H); UV (MTHF) λ_{max} 345 nm.

1-Methyl-3-phenylcyclobutanol (32). A solution of 3-phenylcyclobutanone[12] (200 mg, 1.37 mmol) in 3 mL of dry ether was added dropwise to an ice-cold ether solution of methyllithium (1.3 mL, 2.0 mmol) over 20 min. After stirring at room temperature for 20 min, the reaction was quenched by addition of water (*ca.* 10 mL). The ether solution was dried over $MgSO_4$, concentrated, and purified by flash chromatography (7:3 petroleum ether-ethyl acetate) to give 195 mg (88%) of a diastereomeric mixture (83:17 syn:anti) of the alcohols as a colorless oil. Syn isomer: ^{1}H NMR (CDCl$_3$) δ 1.50 (s, 3 H), 2.00 (bs, 1 H), 2.22 (m, 2 H), 2.51 (m, 2H), 3.06 (quintet, 1 H, J = 8.8 Hz), 7.27 (m, 5 H); ^{13}C NMR (CDCl$_3$) δ 27.33, 30.24, 45.52, 68.96, 125.70, 126.31, 128.01, 128.05. Anti isomer: ^{1}H NMR (CDCl$_3$) δ 1.36 (s, 3 H), 1.69 (bs, 1 H), 2.25 (m, 2 H), 2.50 (m, 2 H), 3.75 (quintet, 1 H, J = 8.5 Hz), 7.24 (m, 5 H).

1-Bromo-1-methyl-3-phenylcyclobutane (34). To a solution of **32** (112 mg, 0.691 mmol) in 6.5 mL of dry acetonitrile under argon were added triphenylphosphine (615 mg, 2.35 mmol) and carbon tetrabromide (780 mg, 2.35 mmol). After stirring at room temperature for 16 h, the mixture was filtered and concentrated to give a yellow oil. Careful flash chromatography (petroleum ether-benzene, 0-5%, gradient) gave 80 mg (45%) of **34** as a mixture of diastereomers (65:35 anti:syn). Anti isomer: ^{1}H NMR (CDCl$_3$) δ 1.90 (s, 3 H), 2.45 (m, 2 H), 3.0 (m, 2 H), 4.05 (quintet, 1 H, J = 8.5 Hz), 7.3 (m, 5 H). Syn isomer: ^{1}H NMR (CDCl$_3$) δ 2.10 (s, 3 H), 2.90 (m, 2 H), 3.0 (m, 2 H), 3.45 (quintet, 1 H, J = 8.5 Hz), 7.3 (m, 5 H).

1,3-Dibromo-1-methyl-3-phenylcyclobutane (36). A solution containing **34** (72 mg, 0.32 mmol), *N*-bromosuccinimide (57 mg, 0.32 mmol), and dibenzoyl peroxide (3 mg) in 3 mL of carbon tetrachloride was allowed to reflux under argon until the NBS had been consumed (1.5 h). The cooled solution was filtered and concentrated to afford 97 mg of a 1:1 diastereomeric mixture of **36** as a viscous oil. Syn isomer: ^{1}H NMR (CDCl$_3$) δ 1.60 (s, 3 H), 3.5 (m, 2 H), 3.8 (m, 2 H), 7.4 (m, 5 H). Anti isomer: ^{1}H NMR (CDCl$_3$) δ 2.30 (s, 3 H), 3.5 (m, 2 H), 3.8 (m, 2 H), 7.4 (m, 5 H).

1-Methyl-3-phenylbicyclo[1.1.0]butane (38). To a solution of dibromide **36** (95 mg, 0.31 mmol) in 2 mL of tetrahydrofuran was added 1.5 g of freshly pulverized 2% lithium amalgam.[60] The heterogeneous mixture was allowed to stir at room temperature under argon for 12 h. After the dark gray slurry had been filtered through Celite, tetrahydrofuran (3 mL), CH_2Cl_2 (10 mL), and 5% sodium bicarbonate were added to the filtrate and thoroughly mixed. The organic solution was dried over Na_2SO_4 and concentrated to afford 40 mg of a volatile oil, which was used immediately in the next step. ^{1}H NMR ($CDCl_3$) δ 1.20 (s, 2 H), 1.35 (s, 3 H), 2.05 (s, 2 H), 7.25 (m, 5 H); ^{13}C NMR ($CDCl_3$) δ 11.60 (q, J = 127 Hz), 16.02 (s), 20.08 (s), 34.60 (t, J = 161 Hz), 124.41 (d, J = 161 Hz), 125.27 (d, J = 158 Hz), 128.111 (d, J = 159 Hz), 138.33 (s).

1,4-Dimethyl-7-phenyl-2,4,6-triazatricyclo[5.1.1.0^{2,6}]nonane-3,5-dione (30). To a solution of bicyclobutane **38** (45 mg, 0.31 mmol) in 30 mL of refluxing *n*-hexane under a stream of argon was added a solution of MTAD (47 mg, 0.42 mmol) in 5.5 mL of ether until the red color of MTAD persisted (*ca.* 3.5 mL). After the hexane was removed, the crude solid was triturated with CH_2Cl_2. The dichloromethane solution was then concentrated and purified by flash chromatography (4:1 benzene-ethyl acetate) to afford **30** (30 mg, 37% from **34**) as a white crystalline solid: mp 143.5-145.5°C; ^{1}H NMR (C_6D_6) δ 1.42 (m, 2 H), 1.57 (s, 3 H), 1.76 (m, 2 H), 2.51 (s, 3 H), 7.15 (m, 5 H); 13C NMR ($CDCl_3$) δ 16.10 (q, J = 128 Hz), 25.79 (q, J = 141 Hz), 47.87 (t, J = 145 Hz), 69.81 (s), 74.20 (s), 126.78 (d, J = 158 Hz), 128.12 (d, J = 159 Hz), 128.62 (d, J = 162 Hz), 133.18 (s), 159.20 (s), 159.74 (s); mass spectrum (EI), *m/e* 257, 242, 199, 185, 143 (100), 129, 103, 91, 77; exact mass calcd for $C_{14}H_{15}N_3O_2$ 257.1164, found 257.1167.

Hydrolysis of 30. A suspension of urazole **30** (9.5 mg, 0.037 mmol) and freshly crushed KOH (19 mg, 0.3 mmol, 87%) in 2 mL of degassed 2-propanol was allowed to reflux for 10 min under argon. The cooled solution was then acidified by dropwise addition of degassed 3 N HCl until decarboxylation ceased (*ca.* 250 µL). The solution was then neutralized with degassed 1 N NH_3. Degassed water (1 mL) was added to dissolve the salts, and then the solution was extracted with degassed CH_2Cl_2 (2 x 2.5 mL). The organic solution was dried with Na_2SO_4, filtered, and concentrated to leave 8.5 mg of a light yellow oil. High-field ^{1}H NMR analysis revealed that >90% of the product consisted of a 1:1 mixture of semicarbazides **41a** and **41b** and <10% consisted of a rearranged semicarbazide **44**. All attempts to purify this mixture failed. **41a:** ^{1}H NMR ($CDCl_3$) δ 1.90 (s, 3 H), 1.98 (bs, 4 H), 2.82 (d, 3 H, *J* = 5 Hz), 4.30 (bs, 1 H), 6.75 (bs, 1 H), 7.28 (m, 5 H). **41b:** ^{1}H NMR ($CDCl_3$) δ 1.44 (s, 3 H), 1.98 (bs, 4 H), 2.70 (d, 3 H, *J* = 5 Hz), 4.30 (bs, 1 H), 6.50 (bs, 1 H), 7.28 (m, 5 H). **44:** ^{1}H NMR ($CDCl_3$) δ 1.62 (s, 6 H), 2.88 (d, 3 H, *J* = 5 Hz), 3.08 (s, 2 H), 6.04 (bs, 1 H), 7.28 (m, 3 H), 7.64 (m, 2H).

1-Methyl-4-phenyl-2,3-diazabicyclo[2.1.1]hex-2-ene (15). To a cooled solution of (-50°C) of semicarbazides **41a** and **41b** (*ca.* 8 mg, 0.035 mmol) in 3.5 mL of distilled CH_2Cl_2 under argon was added nickel peroxide[61] (130 mg, 0.60 mmol of active oxidant). After 1 h of stirring, the cold slurry was transferred via a Teflon cannula onto a cold filtration frit and vacuum filtered into a cold receiving flask. The solvent was removed at -50°C under high vacuum to leave a slightly yellow, crystalline solid: ^{1}H NMR ($CDCl_3$) δ 1.89 (s, 3 H), 2.12 (m, 2 H), 2.59 (m, 2 H), 7.45 (m, 5 H); UV ($CDCl_3$) δ λ_{max} 344 nm.

3-Phenylcyclobutanol (33). To a 0°C solution of 3-phenylcyclobutanone (100 mg, 0.68 mmol) in 5 mL of absolute ethanol was added sodium borohydride (16 mg, 0.34 mmol). After the addition, the reaction mixture was allowed to warm to room temperature. After stirring at room temperature for 20 min, the reaction was quenched by dropwise addition of 0.1 N HCl (*ca.* 0.5 mL). The solution was then extracted with CH_2Cl_2 (3 x 7 mL). After washing with 10 mL of water, the organic solution was then dried over $MgSO_4$ and concentrated to afford 99 mg of a light yellow oil. ^{1}H NMR ($CDCl_3$) δ 2.0 (m, 3 H), 2.75 (m, 2 H), 2.96 (m, 1 H), 4.38 (m, 1 H), 7.2 (m, 5H).

1-Bromo-3-phenylcyclobutane (35). To a solution of triphenylphosphine (393 mg, 1.5 mmol) and carbon tetrabromide (500 mg, 1.5 mmol) in 3 mL of dry acetonitrile was added a solution of 3-phenylcyclobutanol (121 mg, 0.82 mmol) in 4 mL of acetonitrile. The heterogeneous mixture was then heated to reflux for 3 h. After cooling to room temperature, the solvent was removed to leave a brown solid. The solid was dissolved in CH_2Cl_2 and then absorbed onto silica gel. The crude product was then purified by flash chromatography (19:1 pet. ether-benzene) to yield 146 mg (0.69 mmol, 85%) of **35** as a colorless oil. ^{1}H NMR ($CDCl_3$) δ 2.87 (dd, 4 H, J = 6, 8 Hz), 4.02 (quintet, 1 H, J = 8 Hz), 4.67 (quintet, 1 H, J = 6 Hz), 7.3 (m, 5 H).

1,3-Dibromo-3-phenylcyclobutane (37). A solution containing 35 (146 mg, 0.69 mmol), N-bromosuccinimide (124 mg, 0.69 mmol) and dibenzoyl peroxide (4 mg) in 5 mL of carbon tetrachloride was allowed to reflux under argon until the NBS had been consumed (2 h). The cooled solution was filtered and concentrated to leave 182 mg of an oily solid (**37**) as an approximately 3:2 mixture of diastereomers. ^{1}H NMR ($CDCl_3$) Major isomer δ 3.20 (m, 2 H), 3.55 (m, 2 H), 5.08 (quintet, 1 H, J = 8 Hz), 7.4(m, 5 H). Minor isomer δ 3.55 (m, 2 H), 3.78 (m, 2 H), 4.14 (quintet, 1 H, J = 7 Hz), 7.4 (m, 5 H).

1-Phenylbicyclo[1.1.0]butane (39). To a solution of dibromide **37** (180 mg, 0.62 mmol) in 5 mL of tetrahydrofuran was added 1.0 gram of freshly-pulverized 2% lithium amalgam.[60] The heterogeneous mixture was allowed to stir for 12 h while under argon. The resulting dark gray slurry was vacuum filtered through a pad of celite and concentrated under aspirator vacuum to leave 79 mg of a volatile yellow oil. ^{1}H NMR (C_6D_6) δ 0.91 (d, 2 H, J = 1.5 Hz), 1.40 (m, 1 H), 1.97 (d, 2 H, J = 3.2 Hz), 7.1 (m, 5 H).

4-Methyl-1-phenyl-2,4,6-triazatricyclo[5.1.1.0^{2,6}]nonane-3,5-dione (31). To a solution of bicyclobutane **39** (65 mg, 0.5 mmol) in 30 mL of refluxing n-hexane under a stream of argon was added a solution of MTAD (70 mg, 0.62 mmol) in 10 mL of anhydrous ether until the red color of MTAD persisted (*ca.* 9 mL). The hexane was then removed and the solid dissolved in CH_2Cl_2. The dichloromethane solution was absorbed onto silica and the crude material purified by flash chromatography (3:1 benzene-ethyl acetate) to afford 53 mg (35% from **35**) of **31** as a white crystalline solid: mp 147-149°C. ^{1}H NMR ($CDCl_3$) δ 2.18 (m, 2 H), 2.42 (m, 2 H), 3.02 (s, 3 H), 4.76 (t, 1 H, J = 2 Hz), 7.4 (m, 4 H); ^{13}C NMR (CD_2Cl_2) δ 25.98 (q, J = 141 Hz), 44.16 (d, J = 143 Hz), 59.80 (d, J = 174 Hz), 77.21 (s), 127.16 (d), 128.29 (d), 128.83 (d), 133.79 (s), 160.01 (s), 160.68 (s); mass spectrum (EI) *m/e* 243, 185, 129 9100), 115, 103, 77; exact mass calcd for $C_{13}H_{13}N_3O_2$ 243.1008, found 243.1011.

Hydrolysis of 31. A suspension of urazole **31** (8.0 mg, 33 µmol) and freshly-crushed KOH (17.5 mg, 0.26 mmol, 87%) in 1.0 mL of degassed isopropanol was allowed to stir at 45°C under an argon atmosphere for 1 h (after 20 min the solution was homogeneous). The cooled solution was then acidified with degassed 3 N HCl until decarboxylation ceased (*ca.* 250 µL). The solution was then neutralized with degassed 1 N NH_3. Degassed water (1 mL) was added to dissolve the salts, and the solution extracted with degassed CH_2Cl_2 (2 x 2.5 mL). The organic solution was then dried over MgSO4, filtered and concentrated under a stream of argon to yield 6.6 mg (93%) of a 7:3 mixture of semicarbazides **42a** and **42b**. ^1H NMR ($CDCl_3$) major isomer δ 1.95 (bm, 2 H), 2.20 (bm, 2 H), 2.70 (d, 3 H, J = 5 Hz), 4.03 (t, 1 H, J = 2 Hz), 4.56 (bs, 1 H), 6.50 (bs, 1 H), 7.4 (m, 5 H). Minor isomer δ 1.95 (bm, 2 H), 2.20 (bm, 2 H), 2.88 (d, 3 H, J = 5 Hz), 4.22 (bs, 1 H), 4.86 (t, 1 H, J = 2 Hz), 6.50 (bs, 1 H), 7.4 (m, 5 H).

1-Phenyl-2,3-diazabicyclo[2.1.1]hex-2-ene (16). To a cooled solution (-50°C) of semicarbazides **41a** and **41b** (17 mg, 70 µmol) in 3.5 mL of distilled CH_2Cl_2, was added nickel peroxide[61] (170 mg, 0.8 mmol of active oxidant) under an argon atmosphere. After 1 h of stirring, the cold slurry was transferred via a teflon cannula onto a cold filtration frit and vacuum filtered into a cold receiving flask. The solvent was removed at -50°C to leave a slightly yellow oil. ^1H NMR ($CDCl_3$) δ 2.33 (m, 2 H), 2.57 (m, 2 H), 5.02 (t, 1 H, J = 1.5 Hz), 7.45 (m, 5 H); UV (MTHF) λ_{max} 345 nm.

Photolysis Experiments. The photolyses of diazenes **14**, **15**, and **16** were performed with degassed samples in sealed 5 mm quartz NMR tubes using an Oriel 1000-W Mercury-Xenon arc lamp. Various optical filter combinations (Schott) were employed to obtain the desired wavelength range. Sensitized photolyses were performed by using either benzophenone or thioxanthone. All experiments gave the corresponding bicyclobutane as the sole product as monitored by high field ^{1}H NMR.

EPR Experiments. A varian E-line Century Series X-band spectrometer equipped with an Oxford Instruments ESR-900 liquid helium continuous-flow cryostat was used to obtain EPR spectra at low temperature. The temperature at the sample was calibrated with a carbon-glass resistance sensor (Lakeshore Cryotronics) placed inside a sample tube. During each experiment the temperature was monitored continuously by a gold-chromel thermocouple fixed 1 cm below the sample in the quartz dewar. The temperature was varied by using either the helium flow rate or the automatic DTC2 temperature controller.

An Oriel 1000-W mercury-xenon arc lamp was focused into the microwave cavity for photolysis. Various optical filters (Schott) were used to obtain narrow bands of light in the desired wavelength range.

Samples were prepared from solutions of 1-3 mg of diazene in 300 µL of solvent (MTHF was freshly vacuum-transferred from benzophenone ketyl). The solution was placed in 4- or 4.5-mm-o.d. quartz EPR tubes equipped with high vacuum stopcocks. The samples were then degassed (three freeze-pump-thaw cycles), frozen in liquid nitrogen, and cooled to 3.8 K in the EPR cavity.

Distribution Slicing

A strong triplet signal was generated by prolonged photolysis (*ca.* 5-10 min) of the sample in the EPR cavity at 3.8 K. The intensity was recorded continuously throughout the experiment with occasional reference to an off-resonance baseline. Care was taken to ensure that the signal was not saturated. At 3.8 K this was only possible for the $\Delta m_S = 2$ transition, typically at power settings of 0.02 mW or less. Warming of the matrix was accomplished either by restricting helium flow or by using the heater and automatic temperature control. In either case, equilibration was completed as quickly as possible without overshooting the desired temperature. Calibration of temperature was generally performed before and after the experiment, the experimental temperatures being determined by interpolation of the available calibration points. The intensity after each cycle was measured following re-equilibration to 3.8 K.

Decay-Trace Fitting

Decay traces were recorded by first equilibrating the sample in the EPR cavity to the desired temperature, which was determined by calibration immediately before and/or after the trace. With the spectrometer set to the field of the strongest transition, a signal was generated by photolysis. Baseline measurements at an off-resonance field were recorded before the generation and after the decay to allow later correction for any observed drift. The traces were digitized and stored on disk as collected using a Compaq Plus computer. Each data file contained 1000 intensity measurements. Decay traces were normally recorded at a nonsaturating microwave power, but higher power was sometimes used to allow shorter photolyses. No difference was distinguishable between saturated and nonsaturated traces, and the two types were fitted equally well in the analysis.

Simulation of Triplet EPR Spectra. Our computer programs, used to simulate powder EPR spectra, are based on the algorithm of Kottis and Lefebvre.[24] We have also incorporated isotropic hyperfine coupling into these simulations. Instead of introducing a new term into the Hamiltonian, we have taken the much simpler route of splitting each resonance line into the appropriate number of lines with intensities following Pascal's triangle. Multiple coupling constants can be introduced by repeating this process, and then intensities for each field strength are added. A consistent line-width factor of 5 G was used for all spectra, except for the $\Delta m_S = 2$ lines of **24-EV** and **24-CD$_3$**, which required line widths of 15 and 26 G, respectively. Due to the limited number of data points (250), the accuracy of the coupling constants used in the simulations was limited by the width of the individual $\Delta m_S = 2$ transition. Typical G/point ratios varied from 0.72 to 1.6. We must emphasize here that this approach is by no means a rigorous treatment of hfc.

References and Notes

1. For an overview of biradical chemistry see: *Diradicals*; Borden, W. T., Ed.; Wiley: New York, 1982.
2. Dougherty, D. A. in *Kinetics and Spectroscopy of Carbenes and Biradicals;* Platz, M. S., Ed., Plenum Press: New York, in press.
3. Buchwalter, S. L.; Closs, G. L. *J. Am. Chem. Soc.* **1975**, *97*, 3857-3858. Buchwalter, S. L.; Closs, G. L. *J. Am. Chem. Soc.* **1979**, *101*, 4688-4694.
4. Jain, R.; Snyder, G. J. ; Dougherty, D. A. *J. Am. Chem. Soc.* **1984**, *106*, 7294-7295.
5. Much of the work described in this chapter has been reported in the following publications: (a) Jain, R.; Sponsler, M. B.; Coms, F. D.; Dougherty, D. A. *J. Am. Chem. Soc.* **1988** *110*, 1356-1366. (b) Sponsler, M. B., Jain, R.; Coms, F. D.; Dougherty, D. A. *J. Am. Chem. Soc.* **1989**, *111*, 2240-2252.
6. (a) Chang, M. H.; Dougherty, D. A. *J. Org. Chem.* **1981**, *46*, 4092-4093. (b) Chang, M. H.; Jain, R.; Dougherty, D. A. *J. Am. Chem. Soc.* **1984**, *106*, 4211-4217. (c) Snyder, G. J.; Dougherty, D. A. *J. Am. Chem. Soc.* **1985**, *107*, 1774-1775.
7. See also, Amey, R. L.; Smart, B. E. *J. Org. Chem.* **1981**, *46*, 4090-4092.
8. Farnum, D. G.; Mostashari, A.J. in *Organic Photochemical Synthesis*; Srinivasan, R., Ed.; Wiley: New York, 1971; Vol 1.
9. Farnum, D. G.; Mostashari, A. J.; Hagedorn, A. A., III, *J. Org. Chem.* **1971**, *36*, 698-702.
10. (a) Coughlin, D. J.; Salomon, R. G. *J. Am. Chem. Soc.* **1979**, *101*, 2761-2763. (b) Wilson, R. M.; Rekers, J. W. *J. Am. Chem. Soc.* **1981** *103*, 206-207.

11. Wiberg, K. B. *Angew. Chem. Int. Ed. Engl.* **1986**, *25*, 312-322.

12. Falmagne, J.-B.; Escudero, J.; Taleb-Sahraoui, S.; Ghosez, L. *Angew. Chem., Int. Ed. Engl.* **1981**, *20*, 870-880. We have found that 3-phenylcyclobutanone can be easily prepared in multi-gram quantities by reductive dechlorination of 2,2-dichloro-3-phenyl-cyclobutanone (Krepski, L. R.; Hassner, A. *J. Org. Chem.* **1978**, *43*, 2879-2882) with zinc in refluxing acetic acid (Bak, D. A.; Brady, W. T. *J. Org. Chem.* **1979**, *44*, 107-110. Stewart, E. G., unpublished results.)

13. Gassman, P. G.; Mansfield, K. T. *Org. Synth* **1969**, *49*, 1-6.

14. Snyder, G. J., Ph.D. Thesis, California Institute of Technology, 1988.

15. (a) Chang, M. H.; Dougherty, D. A *J. Am. Chem. Soc.* **1982**, *104*, 2333-2334. (b) Jain, R., Ph.D. Thesis, California Institute of Technology, 1987.

16. It is quite possible that the semicarbazide rearrangement is mediated via a nitrogen-centered radical at the "amine" nitrogen. The rearrangement of the analogous hydrocarbon radical, bicyclo[2.1.1]-hex-2-yl, has been reported to proceed at a rate of *ca.* 10^2 s^{-1} near room temperature.[17] There is also precedent which suggests that the rearrangments of nitrogen-centered radicals are considerably more facile than their carbon-centered counterparts.[18] Thus, such a rearrangement of these semicarbazides could be very fast once the nitrogen centered radical is formed.

17. Walton, J. C. *J. Chem. Soc., Perkin Trans 2* **1988**, 1989-1993.

18. Maeda, Y.; Ingold, K. U. *J. Am. Chem. Soc.* **1980** *102*, 328-331. Ingold, K. U.; Maillard, B.; Walton, J. C. *J. Chem. Soc., Perkin Trans 2* **1981**, 970-974.

19. Engel, P. S. *Chem. Rev.* **1980**, *80*, 99-150.

20. Wertz, J. E.; Bolton, J. R. *Electron Spin Resonance: Elementary Theory and Practical Applications;* McGraw-Hill: New York, 1972; pp. 223-257.

21. Berson, J. A. in *The Chemistry of Quinonoid Compounds*, Vol II; Patai, S.; Rappaport, Z., Ed.; Wiley: New York, 1988; pp 455-536.

22. Weltner, W., Jr., *Magnetic Atoms and Molecules*, Scientific and Academic Editions: New York, 1983.

23. Wasserman, E.; Snyder, L. C.;Yager, W. A. *J. Chem. Phys.* **1964**, *41,* 1763-1772.

24. (a) Kottis, P.; Lefebvre, R. *J. Chem. Phys.* **1963**, *39*, 393-403. (b)Kottis,P.; Lefebvre, R. *J. Chem. Phys.* **1964**, *41*, 379-393.

25. Rule, M.; Matlin, A. R.; Seeger, D. E.; Hilinski, E. F.; Dougherty, D. A.; Berson, J. A. *Tetrahedron* **1982**, *38*, 787-798.

26. (a) Goldberg, A. H.; Dougherty, D. A. *J. Am. Chem. Soc.* **1983**, *105,* 284-290. (b) Sponsler, M. B., Ph.D. Thesis, California Institute of Technology, 1987.

27. Conrad, M. P.; Pitzer, R. M.; Schafer, H. F., III *J. Am. Chem. Soc.* **1979**, *101*, 2245-2246.

28. Salem, L. *The Molecular Orbital Theory of Conjugated Systesm;* W. A. Benjamin: New York, 1966; Chapter 5.

29. Snyder, L. C.; Amos, T. *J. Chem. Phys.* **1965**, *42*, 3670-3683.

30. Muller, J.-F.; Muller, D.; Dewey, H. J.; Michl, J. *J. Am. Chem. Soc.* **1978**, *100*, 1629-1630. Yamaguchi, T.; Irie, M.; Yoshida, H. *Chem. Lett.* **1973**, 975-978. Grivet, -Ph., *Mol. Phys.* **1970**, *19,* 389-398. Dowd, P.; Chang, W.; Paik, Y. H. *J. Am. Chem. Soc.* **1986**, *108*, 7416-7417. Jain, R.; McElwee-White, L.; Dougherty, D. A. *J. Am. Chem. Soc.* **1988**,

110, 552-560. Wagner, P. J.; May, M. J. *Chem. Phys. Lett.* **1976**, *39*, 350-352.

31. See for example: Claesson, O.; Lund, A.; Gillbro, T.; Ichikawa, T.; Edlund, O.; Yoshida, H. *J. Chem. Phys.* **1980**, *72*, 1463-1470.
32. Fischer, H. In *Free Radicals*, Kochi, J. K. Ed.; Wiley: New York, 1973; Vol. 2, p. 435-491.
33. Morton, J. R. *Chem. Rev.* **1964**, *64*, 453-471.
34. Sternlicht, H. *J. Chem. Phys.* **1960**, *33*, 1128-1132.
35. McConnell, H. M. *J. Chem. Phys.* **1960**, *33*, 115-121.
36. Reitz, D. C.; Weissman, S. I. *J. Chem. Phys.* **1960**, *33*, 700-704.
37. Glarum, S. H.; Marshall, J. H. *J. Chem. Phys.* **1967**, *47*, 1374-1378.
38. French, W. G.; Willard, J. E. *J. Phys. Chem.* **1968**, *72*, 4604-4608. Williams, F.; Sprague, E. D. *Accts. Chem. Res.* **1982**, *15*, 408-415.
39. Doba, T.; Ingold, K. U.; Siebrand, W.; Wildman, T. A. *J. Phys. Chem.* 1984, *88*, 3165-3167. Doba, T.; Ingold, K. U.; Siebrand, W. *Chem. Phys. Lett.* **1984**, *103*, 339-342.
40. See, for example, Platz, M.S.; Senthilnathan, V.P.; Wright, B.B.; McCurdy, C.W., Jr. *J. Am. Chem. Soc.* **1982**, *104*, 6494-6501, and references therein.
41. Fisher, J. J.; Michl, J. *J. Am. Chem. Soc.* **1987**, *109*, 583-584.
42. Less-direct evidence has been based upon variation of the photolysis intervals and hence the number of fast sites. See reference 43. In addition, "site-clearing" behavior has been seen by Chapman: McMahon, R. J.; Chapman, O. L. *J. Am. Chem. Soc.* **1987**, *109*, 683-692.
43. Siebrand, W.; Wildman, T. A. *Acc. Chem. Res.* **1986**, *19*, 238-243
44. Austin, R. H.; Beeson, K.; Eisenstein, L.; Frauenfelder, H.; Gunsalus, I. C.; Marshall, V. P. *Phys. Rev. Lett.* 1974, *32*, 403-405.

45. Jankowiak, R.; Richert, R.; Bassler, H. *J. Phys. Chem.* **1985**, *89*, 4569-4574. Albery, W.J.; Bartlett, P.N.; Wilde, C.P.; Darwent, J.R. *J. Am. Chem. Soc.* **1985**, *107*, 1854-1858. Richert, R. *J. Chem. Phys.* **1987**, *86*, 1743-1747. Plonka, A. "Time-Dependent Reactivity of Species in Condensed Media," Spring-Verlag: Berlin, 1986. Hoffman, W.F., III; Shirk, J.F. *J. Mol. Struct.* **1987**, *157*, 275-287.

46. Bellman, R.; Kalaba, R.E.; Lockett, J.A. "Numerical Inversion of the Laplace Transform," American Elsevier: New York, 1966.

47. The last operation performed by FIT is a heating-optimization to account for heating during photolysis (typically 1-3 K). Often times, the heating amount is larger than 1-3 degrees. This may be because the errors from other sources, such as temperature, width, and intensity normalization, are funneled into the heating optimization, since it is the last operation of the simulation.

48. The poor results obtained with the σ_{DS} method seem to lie in the width calculated for the distribution slicing data by DISFIT. Numerous attempts to obtain "more satisfactory" distribution slicing data were unsuccessful.

49. (a) Bell, R.P. "The Tunnel Effect in Chemistry," Chapman and Hall: New York, 1980. (b) The rate expression must be modified to incorporate a tunneling correction factor Q. Thus,

$$k = QAe^{-E/RT}$$

where

$$Q = \frac{e^{\alpha}}{\beta - \alpha}\left(\beta e^{-\alpha} - \alpha e^{-\beta}\right),$$

and

$$\alpha = \frac{E}{RT}$$

$$\beta = \frac{2\pi^2 a\,(2mE)^{\frac{1}{2}}}{h}\,.$$

50. Carpenter, B.K. *J. Am. Chem. Soc.* **1983**, *105*, 1700-1701. Huang, M.-J.; Wolfberg, M. *J. Am. Chem. Soc.* **1984**, *106*, 4039-4040. Dewar, M. J. S.; Merz, K. M., Jr.; Stewart, J. J. P. *J. Am. Chem. Soc.* **1984**, *106*, 4040-4041. Goldanskii, V. I.; Fleurov, V. N.; Trakhtenberg, L. I. *Sov. Sci. Rev. B.* **1987**, *9*, 59-124.

51. (a) Dervan, P. B.; Dougherty, D. A. in ref 1, Chapter 3. (b) Scaiano, J. C. *Acc. Chem. Res.* **1982**, *15*, 252-258. Caldwell, R. A.; Majima, T.; Pac, C. *J. Am. Chem. Soc.* **1982**, *104*, 629-630. Scaiano, J. C.; Wagner, P. J. *J. Am. Chem. Soc.* **1984**, *106*, 4626-4627. Johnston, L. J.; Scaiano, J. C.; Sheppard, J. W.; Bays, J.P. *Chem. Phys. Lett.* **1986**, *124*, 493-498. Akiyama, K.; Ikegami, Y.; Tero-Kubota, S. *J. Am. Chem. Soc.* **1987**, *109*, 2538-2539. Caldwell, R. A.; Sakuragi, H.; Majima, T. *J. Am. Chem. Soc.* **1984**, *106*, 2471-2473. Johnston, L. J.; Scaiano, J. C. *J. Am. Chem. Soc.* **1986**, *108*, 2349-2353. Closs, G. L.; Forbes, M. D. E. *J. Am. Chem. Soc.* **1987**, *109*, 6185-6187. Mizuno, K.; Ichinose, N.; Otsuji, Y.; Caldwell, R. A. *J. Am. Chem. Soc.* **1985**, *107*, 5797-5798. Sugawara, T.; Bethell, D.; Iwamura, H. *Tetrahedron Lett.* **1984**, *25*, 2375-2378. Burnett, M. N.; Boothe, R.; Clark, E.; Gisin, M.; Hassaneen, H. M.; Pagni, R. M.; Persy, G.; Smith, R. J.; Wirz, J. *J. Am. Chem. Soc.* **1988**, *110*, 2527-2538.

52. It has recently been demonstrated that at room temperature in fluid media there is a distribution of sites that show nonexponential decays on the femtosecond time scale. However, such fluctuations would be

averaged out on the time scale of conventional kinetic studies. See for example, Cruz, C. H. B.; Fork, R. L.; Knox, W. H.; Shank, C .V. *Chem. Phys. Lett.* **1986,** *132*, 341-344. Barbara, P.F.; Jarzeba, W. *Accts. Chem. Res.* **1988,** *21*, 195-199.

53. Griller, D.; Ingold, K. U. *Acc. Chem. Res.* **1976,** *9*, 13-19.
54. McMillen, D. F.; Golden, D. M. *Ann Rev. Phys. Chem.* **1982,** *33*, 493.
55. Pranata, J.; Dougherty, D. A. *J. Phys. Org. Chem.* **1989**, in press.
56. Berson, J. A.; Pedersen, L. D.; Carpenter, B. K. *J. Am. Chem. Soc.* **1976,** *98*, 122-143. Baldwin, J. E.; Barden, T. C. *J. Am. Chem. Soc.* **1984,** *106*, 5312-5319.
57. Salem, L.; Rowland, C. *Angew. Chem., Int. Ed. Engl.* **1972,** *11*, 92-111.
58. Morris, G. A.; Freeman, R. *J. Am. Chem. Soc.* **1979** *101*, 760-762. Benn, R.; Günther, H. *Angew. Chem., Int. Ed. Engl.* **1983,** *22,* 350-380.
59. Still, W. C.; Kahn, M.; Mitra, A. *J. Org. Chem.* **1978,** *43*, 2923-2925.
60. Alexander, J.; Krishna Rao, G. S. *J. Chem. Educ.* **1970,** *47*, 277.
61. George, M. V.; Balachandran, K. S. *Chem. Rev.* **1975,** 75, 491-519.

Chapter 3

1,3-Diphenyl-1,3-cyclopentanediyl

The report of the first directly observable, localized hydrocarbon biradical, triplet 1,3-cyclopentanediyl (**6**), by Buchwalter and Closs in 1975 generated great interest and appeared to signal a turning point in the study of this important class of reactive intermediates.[1] Unfortunately, further work showed that the cyclopentanediyl ring system was quite sensitive to substitution and apparently, that cyclopentanediyls did not constitute a general class of localized 1,3-biradicals.[1,2] For example, the 1-methyl derivative gave a much weaker EPR signal than **6**, and the 1,3-dimethyl derivative gave no EPR signal at all. This trend is opposite to that observed in the cyclobutanediyl series where substitution at the radical centers is a prerequisite to triplet biradical observation. One possible explanation for the capricious behavior of cyclopentanediyls is that substituents may alter the conformation of the ring enough (from its ideal planar geometry) to produce a singlet ground state or greatly increase T→S intersystem crossing (ISC) rates. This unpredictable nature of cyclopentanediyls is somewhat of a paradox when one considers that **6** is observable at temperatures up to 42 K, but fully localized cyclobutanediyls such as **24-Me** can only be observed as high as 25 K[3] (Chapter 2). This lone example of reactivity comparison between cyclobutanediyls and cyclopentanediyls led us to wonder if, in general, cyclopentanediyls are more stable than their cyclobutanediyl counterparts. Of course, to address this issue, a new cyclopentanediyl would have to be synthesized, preferably one analogous to a known cyclobutanediyl. We chose

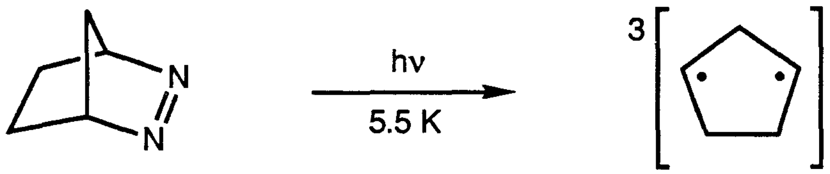

7 **6**

1,3-diphenyl-1,3-cyclopentanediyl (**20**) as a target because phenyl substitution at the radical centers leads to the most persistent biradical of the cyclobutanediyl series **24-Ph**, and because conjugation with the benzene ring may help to maintain the cyclopentanediyl ring rigid and planar. Therefore, 1,4-diphenyl-2,3-diazabicyclo[2.2.1]hept-2-ene (21) was synthesized as described in detail below. This study of 1,3-diphenylcyclopentanediyl has provided a wealth of information on the nature of localized 1,3-biradicals.[4]

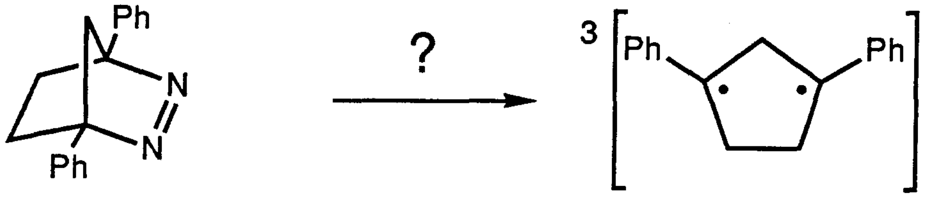

21 **20**

Synthesis

The synthesis of **21** is quite simple and straightforward (Scheme 3-1), and it is surprising that it had not been previously reported in the literature.[5] The synthesis begins with a Diels-Alder reaction between 1,4-diphenylcyclopentadiene (**48**) and MTAD in *n*-hexane to cleanly give the unsaturated urazole **49**. This olefin, when in solution, is quite prone to undergo a retro Diels-Alder reaction so care must be exercised during its use. Urazole **49** is reduced to saturated urazole **50** under three atmospheres of hydrogen employing 5% rhodium-on-alumina as catalyst.[6] Semicarbazide **51** is produced by hydrolysis of the urazole with potassium hydroxide in refluxing 2-propanol. In contrast to some of the semicarbazides employed as precursors to the diazabicyclo[2.1.1]hexenes (Chapter 2), **51** is quite stable and is amenable to purification by recrystallization or chromatography. The robust nature of **51** is probably due to the decreased strain energy of a bicyclo[2.2.1] system (*ca.* 17 kcal/mol)[8] relative to a bicyclo[2.1.1] system (*ca.* 37 kcal/mol)[8]. Oxidation of **51** to **21** is cleanly affected by treatment with nickel peroxide[9] at 0°C. As described below in detail, diazene **21** is somewhat thermally labile, and loses nitrogen with first order kinetics as monitored by ^{1}H NMR between 25 and 45°C. This decomposition, in the absence of air, affords 1,4-diphenylbicyclo[2.1.0]pentane (**22**).

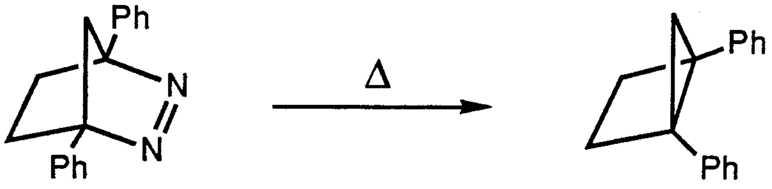

21 **22**

Scheme 3-1

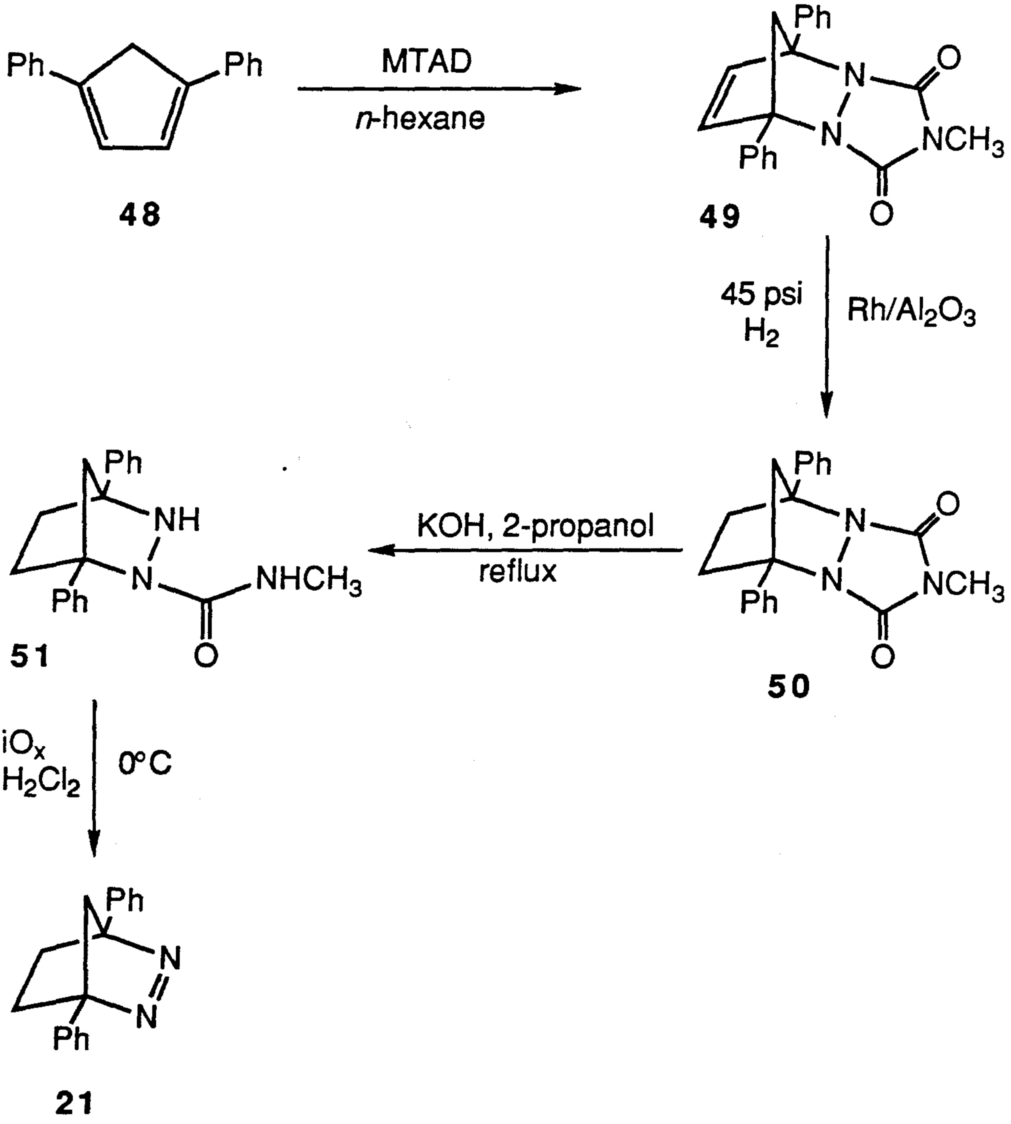
Ph
Ph
48
MTAD
n-hexane
Ph
N
O
N
NCH3
Ph
O
49
45 psi
H2
Rh/Al2O3
Ph
N
O
N
NCH3
Ph
O
50
KOH, 2-propanol
reflux
Ph
NH
N
NHCH3
Ph
O
51
NiOx
CH2Cl2
0°C
Ph
N
N
Ph
21

We also required deuterated diazenes **21**-*d*$_2$ and **21**-*d*$_4$ for various spectroscopic and kinetics studies. Urazole **50**-*d*$_2$ was prepared as shown below. The two *exo* deuteria were introduced by reduction of **49** under three atmospheres of deuterium using 5% palladium-on-carbon as catalyst. Interestingly, whenever this reduction was conducted using 5% rhodium-on-alumina as the catalyst, only perprotio material (**50**) was obtained. This suggests that rhodium may also be a very good dehydrogenation catalyst, by removing H_2 from the solvent, ethyl acetate. Urazole **50**-*d*$_2$ could also be obtained by performing a diimide reduction using hexadeutero hydrazine hydrate in air but, because the retro Diels-Alder reaction of **49** was rapid under these conditions, the yields were very low.

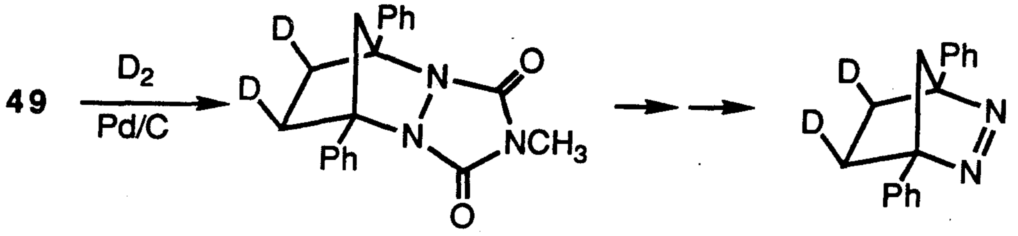

50-*d*$_2$ **21**-*d*$_2$

For the synthesis of **21**-*d*$_4$, tetradeutero diene **48**-*d*$_4$ was required. This was readily obtained by treatment of a benzene/hexane solution of **48** with a 5N NaOD solution and benzyltriethylammonium chloride as phase-transfer catalyst.[10] Surprisingly, only one such cycle was required to achieve >95% incorporation of deuterium.

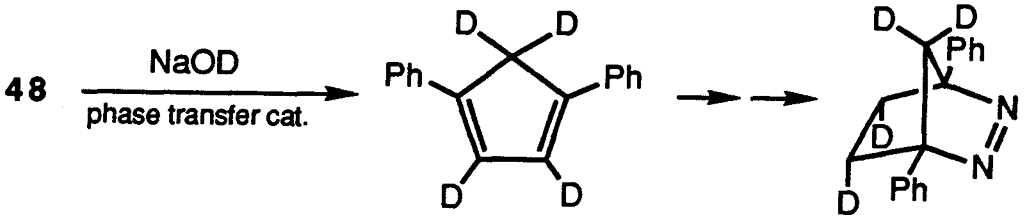

48-*d*$_4$ **21**-*d*$_4$

Diazene Photochemistry. Direct or benzophenone-sensitized photolysis of diazene **21** in CD_2Cl_2 solution at 0°C gives 1,4-diphenylbicyclo[2.1.0]pentane (**22**) as the sole product. These results are strictly analogous to those obtained upon photolysis of the corresponding diazabicyclohexene (**14**, Chapter 2), but are in marked contrast to the results obtained for the parent diazene **7** where the photolysate consists of cyclopentene (*ca.* 10%) and bicyclopentane **8** (*ca.* 90%).[11] Direct photolysis of *exo*-labeled diazene **21**-d_4 at -78°C in CD_2Cl_2 solution gives rise to a slight excess (*ca.* 60%) of the bicyclopentane isomer which exhibits retention of configuration (*i.e., endo* protons).

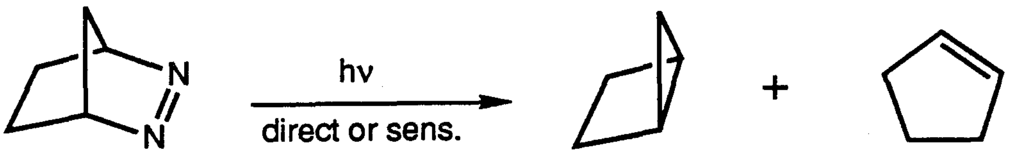

7 **8**

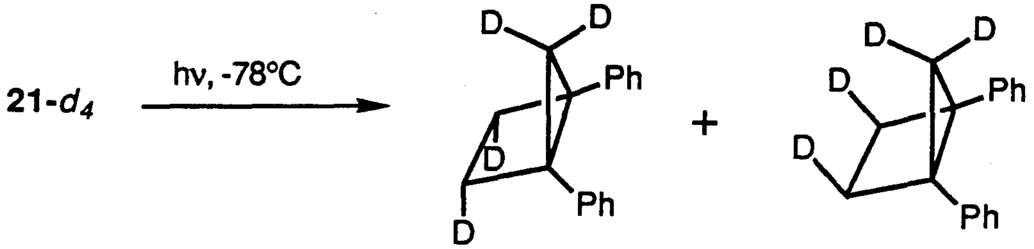

60% **22**-d_4 40%

EPR Spectroscopy

Photolysis ($324 \leq \lambda \leq 346$ nm) of a frozen 2-methyltetrahydrofuran (MTHF) solution of diazene **21** at 3.8 or 77K in the cavity of an EPR spectrometer produces the spectrum of triplet 1,3-diphenylcyclopentanediyl (**20**) (Figure 3-1). The spectrum can be described by the zero-field splitting (zfs) parameters $|D/hc| = 0.045$ cm^{-1}, $|E/hc| = 0.001$ cm^{-1} (Table 3-1). Intense spectra of the deuterated biradicals **20**-d_2 and **20**-d_4, which exhibit zfs parameters identical to **20**, are also generated upon photolysis of **21**-d_2 and **21**-d_4, respectively (Figures 3-2,3). The small E value of these spectra leads to an apparent four line pattern in the $\Delta m_s = 1$ region, even for tetradeutero biradical **20**-d_4 where hyperfine line broadening is significantly decreased relative to **20**.

The observed zfs values obtained for **20** are completely in line with expectation. In fact, a D value for **20** of $|D/hc| = 0.048$ cm^{-1} was calculated using a semiempirical method[12] long before the spectrum was observed.[13] Intuitively, it makes sense that the D value of **20** is smaller than that of **24-Ph** because the five-membered ring places the spins farther apart (2.37Å)[15] than the four-membered ring (2.10Å).[16] Additionally, upon close inspection of the zfs values of Table 3-1, one can see that the ratios of D values **24-Me** to **6** and **24-Ph** to **20** are identical, with a value of 0.75. This is equivalent to the observation that the D values of the completely localized biradicals, **24-Me** and **6**, both decrease by precisely the same amount (53.6%) upon phenyl substitution at both radical centers. Thus, the delocalizing effects of phenyl groups are identical in the two ring systems.

A most remarkable aspect of this study of **20** is that intense EPR signals of the biradical can be generated at liquid nitrogen temperature (77 K). As described in detail below, ^{3}**20** does decay very slowly and

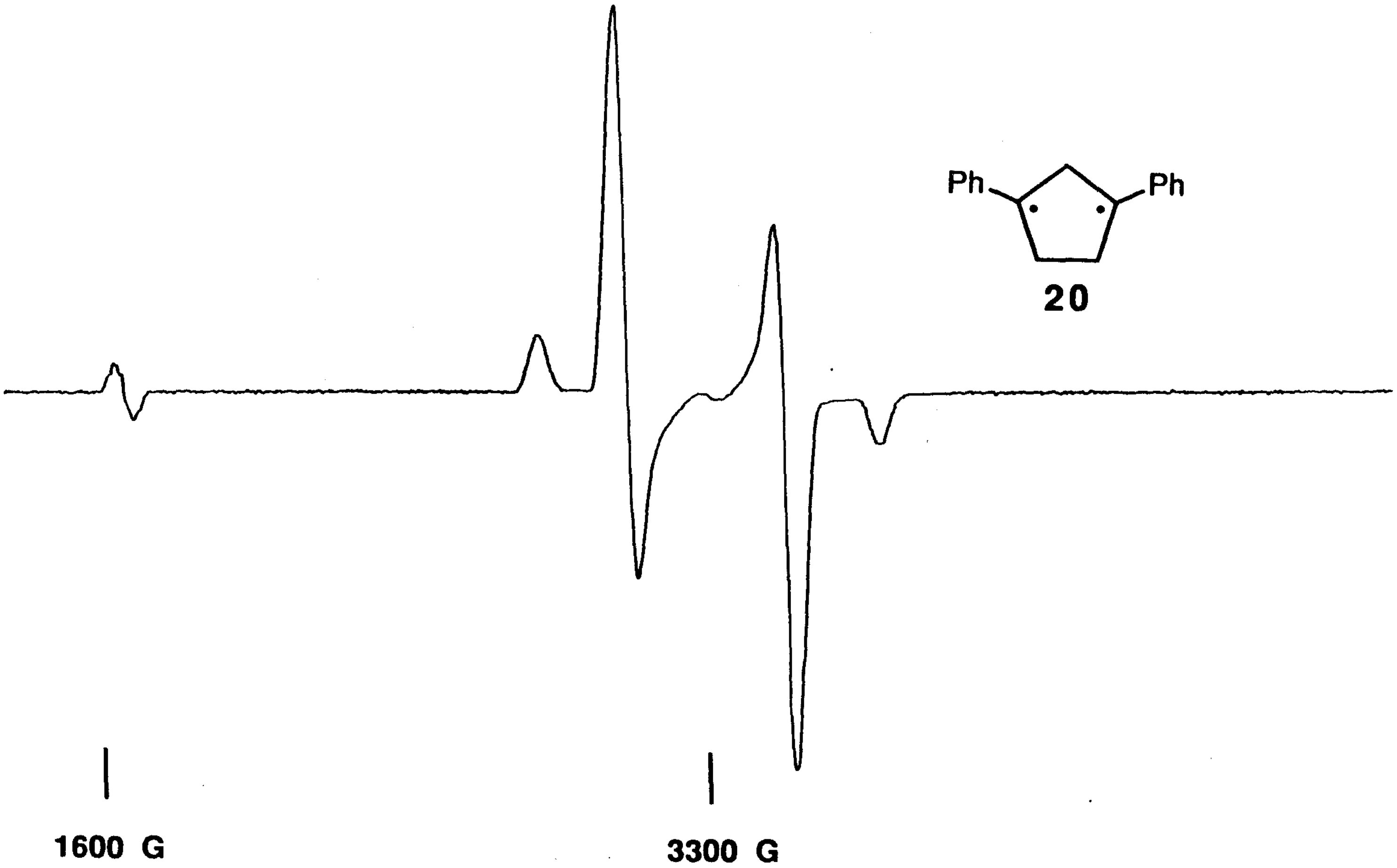

Figure 3-1. Triplet EPR spectrum of **20** obtained upon photolysis of a frozen MTHF solution of **21** at 77 K.

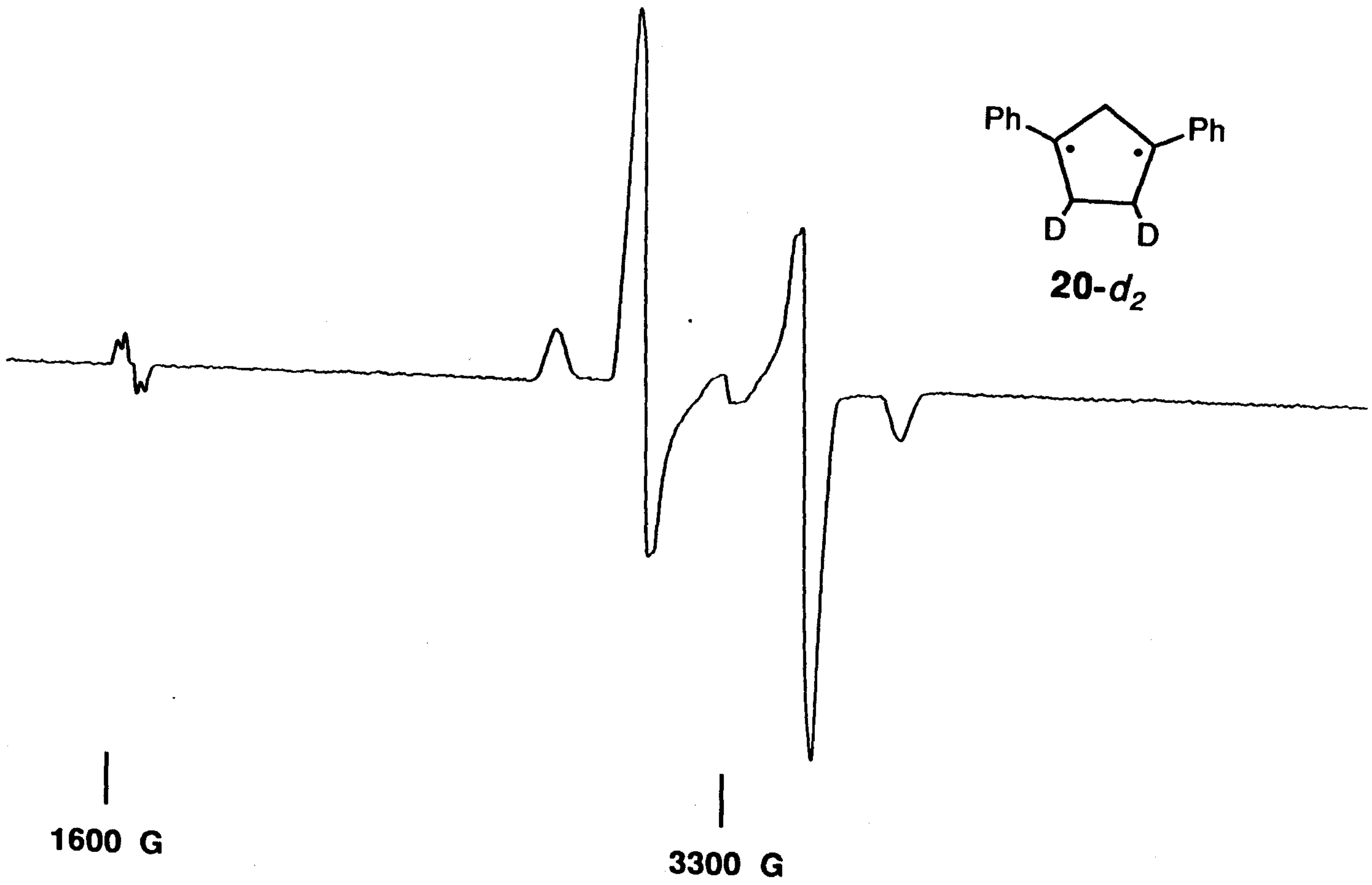

Figure 3-2. Triplet EPR spectrum of **20**-d_2 obtained upon photolysis of a frozen MTHF solution of **21**-d_2 at 77 K.

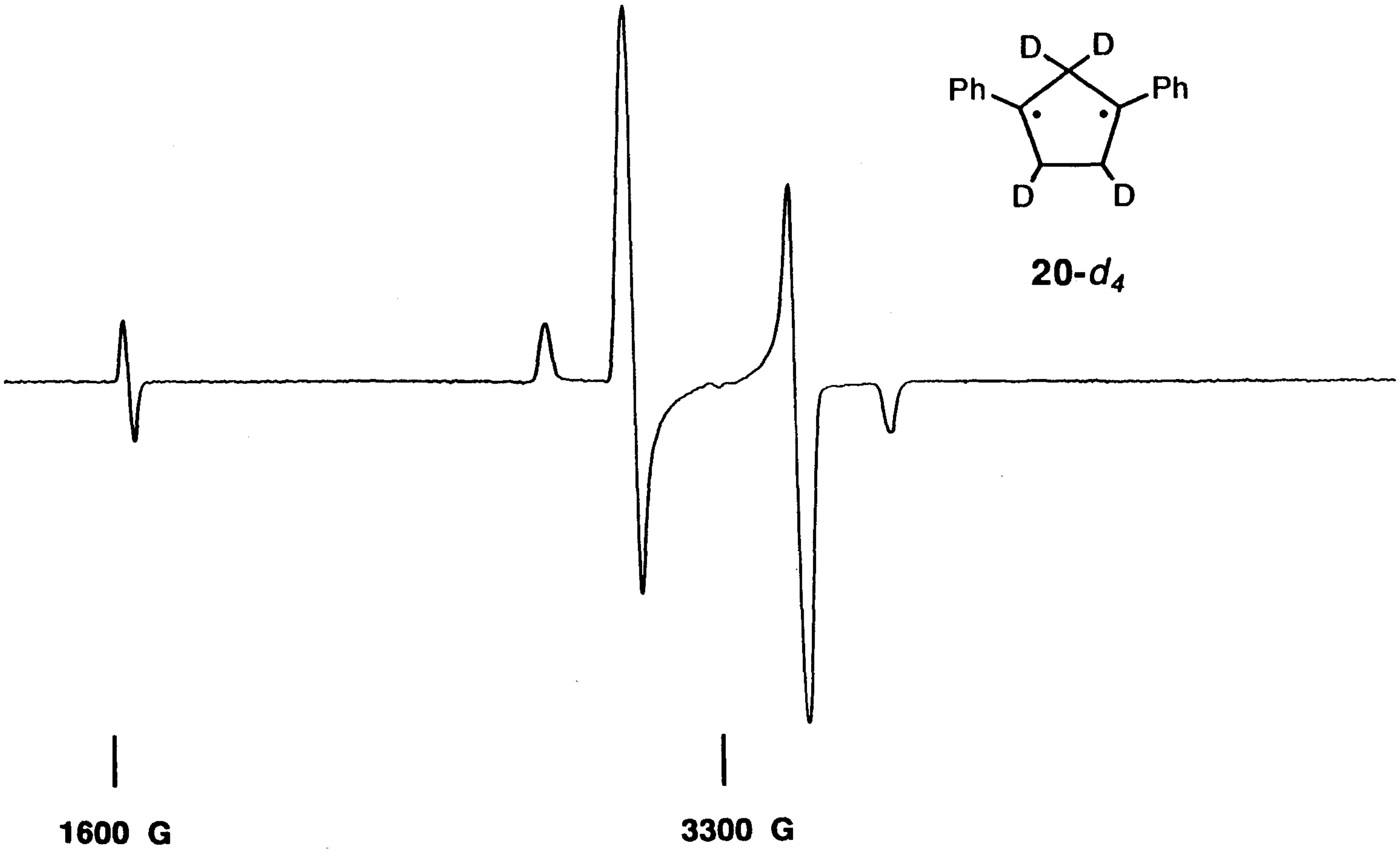

Figure 3-3. Triplet EPR spectrum of 20-d_4 obtained upon photolysis of a frozen MTHF solution of 21-d_4 at 77 K.

Table 3-1. Zero-Field Splitting Parameters (cm^{-1}) for Localized Biradicals

	 **6**	 **20**	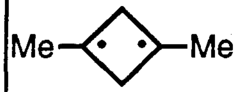 **24-Me**	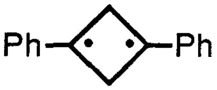 **24-Ph**
$\|D/hc\|$	0.084	0.045	0.112	0.060
$\|E/hc\|$	0.002	0.001	0.005	0.002

nonexponentially at 77 K, but nevertheless, this still represents a monumental increase in stability relative to diphenylcyclobutanediyl **24-Ph**, which cannot be generated at 77 K and is predicted to have a lifetime of less than one second at this temperature.[17] We assume that **20** has a triplet ground state, based on that fact that it is readily observable at 3.8 K.

Hyperfine Coupling. As with most cyclobutanediyls **24**, and with **6**, the half-field transition of **20** (Figure 3-4) clearly shows splittings due to hyperfine coupling (hfc). We have simulated this splitting pattern by using our previously described procedure (Chapter 2). As expected, the protons attached to C2, which can, in effect, couple to both radical centers of **20**, exhibit a hyperfine splitting (24 G) that is equivalent in magnitude to that observed in an analogous free radical. This splitting is somewhat larger than the 22.5 G observed for **24-Ph** and most likely reflects the better overlap between the π_{CH_2} orbital and the radical orbitals of the five-membered ring.[18] The protons attached to C4 and C5 produce splittings (14 G) that are essentially one half those for C2. The smaller splittings (3 G) due to coupling with the *ortho* and *para* protons of the phenyl groups contribute only to line broadening.

The simulation, though not perfect, does reproduce several important features of the pattern quite well. First, the overall width of the transition is correct. Second, all interpeak spacings match quite well with the experimental spectrum. Third, the relative intensities of the individual peaks follow the same trends as the experimental spectrum. The major discrepancy between the calculated and experimental spectra concerns the resolution of the individual peaks. This is quite evident in the outermost peaks of the transition. Simulations that correctly reproduced the resolution of outer peaks proved grossly unsatisfactory in the reproduction of overall width and

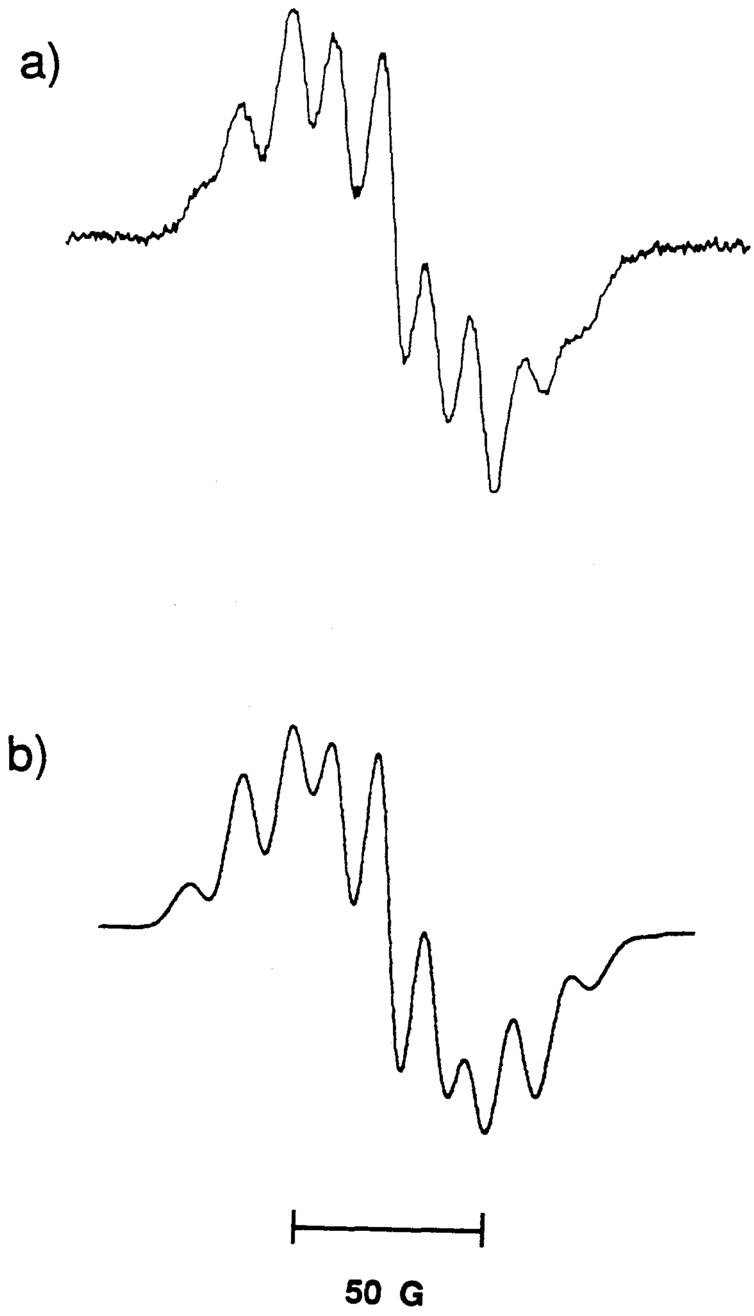

Figure 3-4. Observed (a) and calculated (b) hyperfine patterns of the $\Delta m_S = 2$ region of biradical **20**. The coupling constants used in the simulation are 24 G (2H, methano), 14 G (4H, ethano), 3 G (6H, *ortho, para*).

interpeak spacing, criteria which were judged to be the most important components of an accurate simulation. The shortcomings of the simulation are most probably the result of our simplifying assumptions of uniform transition probabilities and isotropic hyperfine coupling (Chapter 2). It should also be mentioned that the simulation of Figure 3-4 assumed a planar cyclopentanediyl geometry. We do not believe that this is a severe restriction because the zfs values of ^{3}**20** are quite consistent with a planar geometry. Although simulations involving four different coupling constants for the six hydrogens of the five-membered are quite possible, they are quite time consuming since our simulations are performed by manual iteration. In spite of the above mentioned restrictions and limitations, we feel the simulation Figure 3-4 is quite good.

The $\Delta m_s = 2$ transitions of deuterated biradicals **20**-d_2 and **20**-d_4 are shown in Figures 3-5 and 3-6, respectively. Also shown in the figures are the corresponding simulated spectra which were calculated using parameters derived from the simulation of **20**. For deuterium splitting, a coupling constant one-sixth of the corresponding proton coupling was employed and the intensity pattern was adjusted to comply with the allowed nuclear spin states of I = 1. It is clear that there are large discrepancies between the experimental and simulated spectra. For **20**-d_2 the simulation reproduces the overall width well but has incorrect peak spacing and too many lines (Figure 3-5). All simulations that incorporate coupling to two protons on C2 and two on C4 and C5 gave a strong central peak that is not present in the experimental spectrum. Also, the low-field outer peak of the experimental spectrum is far broader than that produced by any simulation. These findings suggest that the observed spectrum is actually a superposition of two or more spectra. The per protio biradical ^{3}**20** is a logical candidate as a contaminant. The presence of

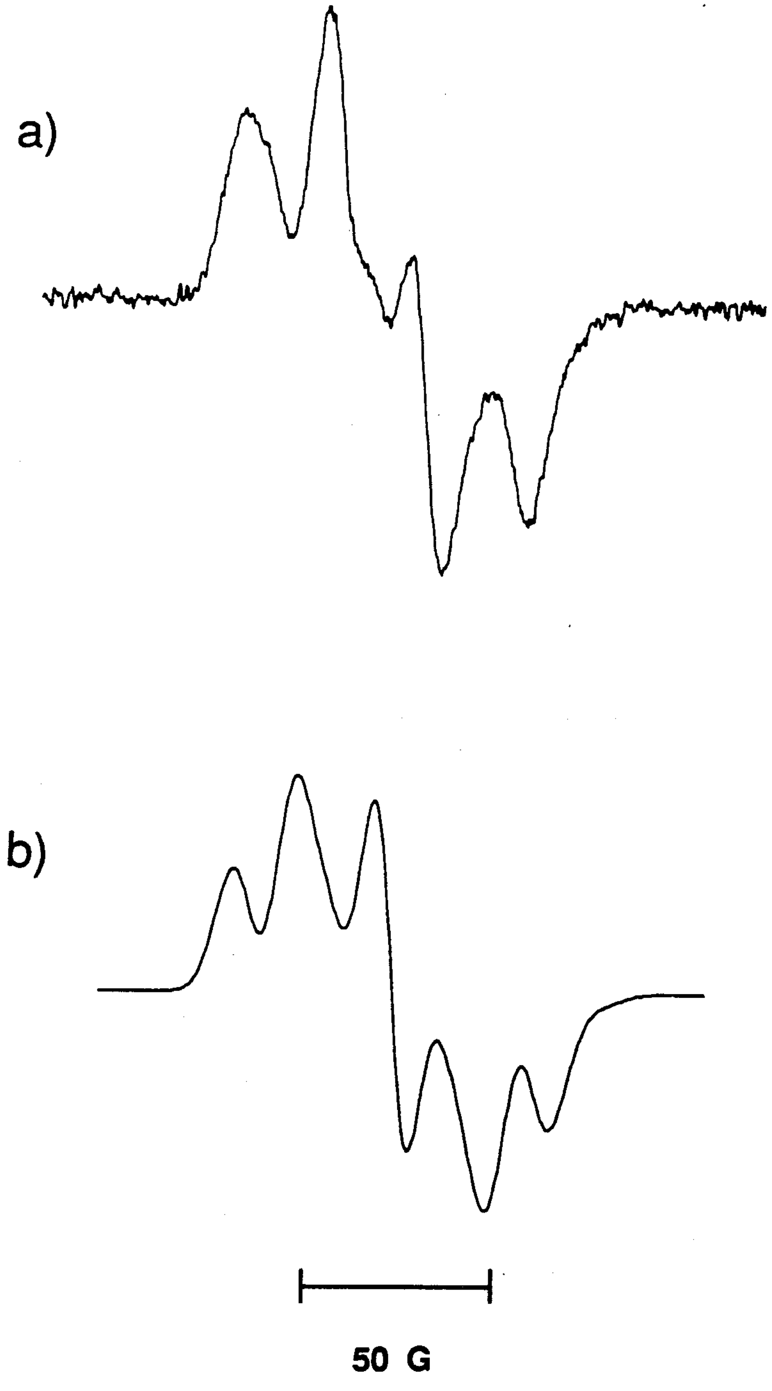

Figure 3-5. Observed (a) and calculated (b) hyperfine patterns of the $\Delta m_s = 2$ region of biradical **20**-d_2. The coupling constants used in the simulation are 24 G (2H, methano), 14 G (2H, ethano), 2.5 G (2 D, ethano), 3 G (6H, *ortho, para*).

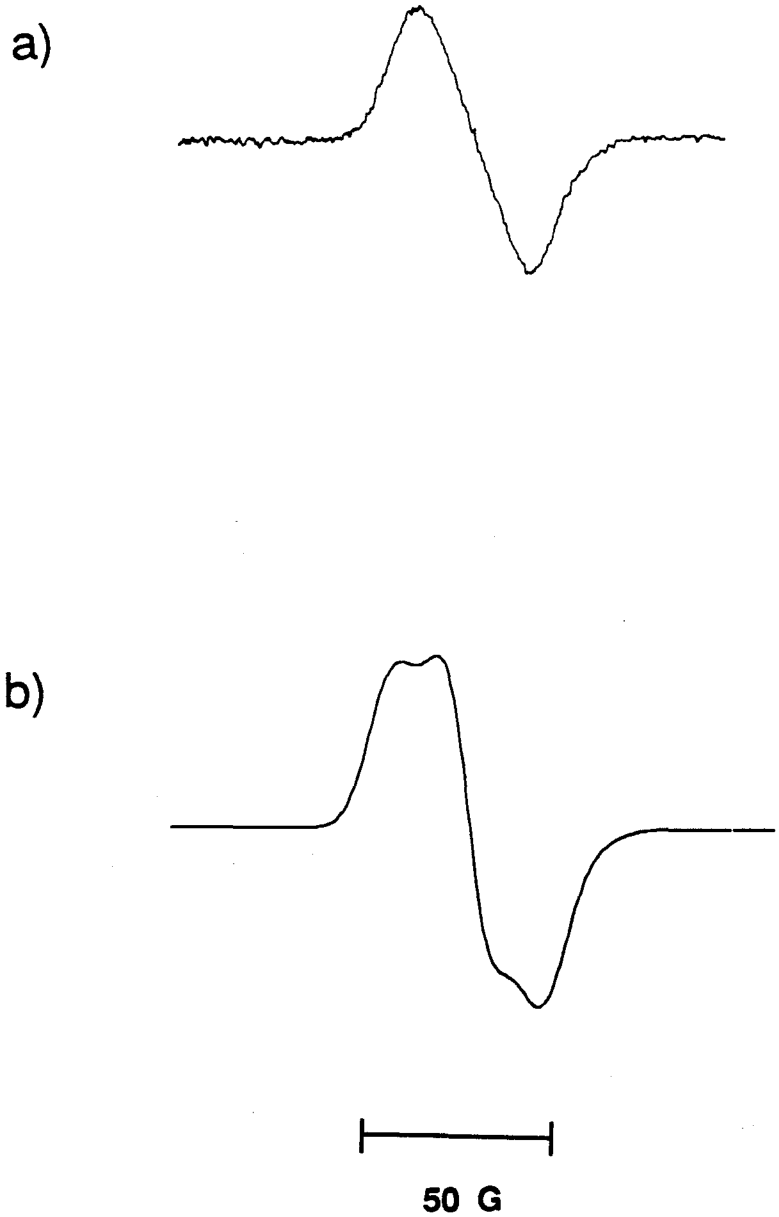

Figure 3-6. Observed (a) and calculated (b) hyperfine patterns of the $\Delta m_s = 2$ region of biradical **20**-d_4. The coupling constants used in the simulation are 4 G (2D, methano), 14 G (2H, ethano), 2.5 G (2 D, ethano), 3 G (6H, *ortho, para*).

a small amount of ^{3}**20** could very easily account for the broadness of the lines, but does not explain the lack of a strong central line in the observed spectrum because ^{3}**20** also exhibits a strong central line. Perhaps some other, unknown impurity in the sample accounts for this strange half-field signal. The simulation of the half-field transition of **20**-d_4 exhibits some poorly resolved fine structure that the experimental spectrum does not (Figure 3-6). This discrepancy may also be caused by the presence of other, incompletely deuterated isomers in the sample. Although the poor agreement between the observed and calculated spectra for these deuterated biradicals is somewhat disturbing, it does not cause us to question our simulation of **20**. Labeled biradicals with a very high percentage incorporation of deuterium ($>$ 99%) should produce spectra more closely resembling the simulations of Figure 3-5 and 3-6.

Electronic Spectroscopy

When a frozen solution of **21** is photolyzed with UV light, a persistent yellow color develops. Figure 3-7a shows the absorption spectrum of **21** in an MTHF glass at 77 K. Upon photolysis ($324 \le \lambda \le 346$ nm), an intense peak at 326 nm develops and a very weak, structural band also appears from 360 to 470 nm (Figure 3-7bc). These bands are quite similar to those observed for benzyl radicals.[19] Any benzyl radicals/biradicals generated from **21** would be most closely related to the cumyl radical. In fact, the 324 nm transition observed for the cumyl radical[19a] agrees very well with the transition observed here.

Based on three lines of evidence, the observed optical spectrum is assigned to triplet 1,3-diphenylcyclopentanediyl. First, the appearance of the UV spectrum and the EPR signal occur simultaneously upon photolysis. Second, upon bleaching the sample with visible light ($400 \le \lambda \le 470$ nm), both the UV and EPR signals decay rapidly. Finally, a qualitative study of the 77 K decay kinetics of the UV signal at 466 nm reveals that its rate of decay is virtually identical to the decay rate of the EPR signal. These findings are consistent with the assignment, but do not rule out the possibility that the UV signal is due to the singlet biradical in equilibrium with the triplet. It is, however, highly unlikely that a localized singlet biradical would have a lifetime of many hours at 77 K.

Wirz and Adam have recently studied the absorption, excitation and emission spectra of ^{3}**20** in EPA at 77 K.[20] They found that the fluorescence lifetime of ^{3}**20** (*ca.* 220 ns) was typical for benzyl radical chromophores[19b] and hence concluded that there is no significant interaction between the benzylic moieties. Thus, their finding of non-interacting radical subunits, agrees with

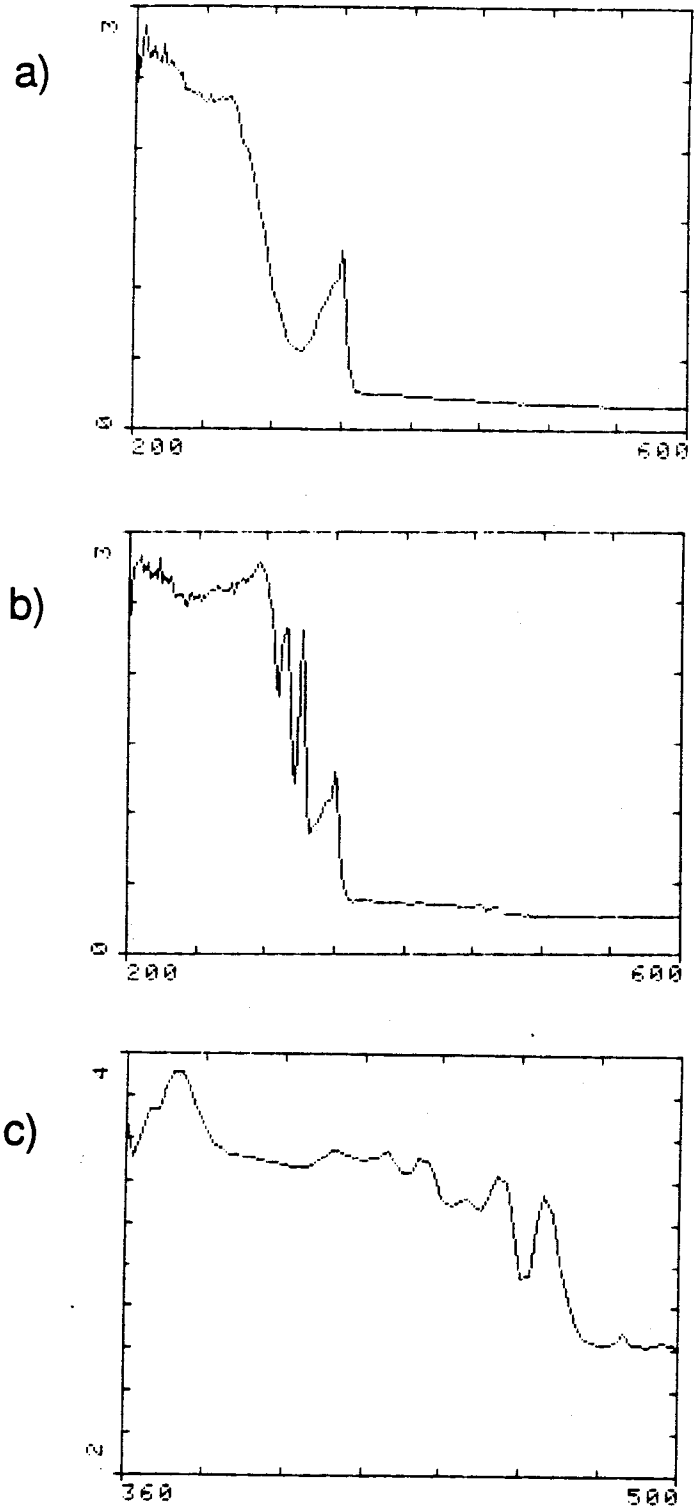

Figure 3-7. (a) UV-Visible spectrum of diazene **21** in a frozen MTHF glass at 77 K. (b) Spectrum obtained after 2 min of photolysis. (c) Expansion of the region $360 \leq \lambda \leq 500$ nm to show the weak, long-wavelength band.

the conclusions we have drawn for ^{3}**20** and cyclobutanediyls **24**, which are based upon observed zero-field splittings and hyperfine coupling patterns.

Matrix-Isolation Decay Kinetics

As mentioned previously, ^{3}**20** decays very slowly and nonexponentially at 77K in MTHF as monitored by EPR spectroscopy. We have also studied the decay behaviors of ^{3}**20**-d_2 and ^{3}**20**-d_4 under identical conditions and have discovered that, in certain instances, the decays are quite sensitive to isotopic substitution. We now report in detail the results of these kinetics studies.

When samples of diazenes **21**, **21**-d_2, and **21**-d_4 in MTHF are irradiated ($324 \leq \lambda \leq 346$ nm) for short intervals (10-40 sec) at 77 K, the corresponding triplet EPR signal grows in rapidly. When the lamp is shuttered, signal growth ceases and nonexponential decay commences. The EPR generation and decay profiles are shown in Figure 3-8. Qualitatively, it is apparent that ^{3}**20** and ^{3}**20**-d_2 exhibit virtually identical decay profiles. The amount of decay observed and the shapes of these two decay traces are very similar. Interestingly ^{3}**20**-d_4 exhibits a noticably different decay profile. Its decay trace shows considerably less decay over the same time interval and is also flattened relative to that observed for ^{3}**20** and ^{3}**20**-d_2.

We have employed our previously described[21] (Chapter 2) decay trace fitting procedure to examine these decays quantitatively. It is important to note, that for these studies we have not performed the complementary distribution slicing experiments as was done for **24-Ph** and other cyclobutanediyls (Chapter 2). We therefore have no data concerning distribution width nor decay trace normalization. This does not pose a problem in the present study because, at 77 K, very little decay occurs for these biradicals during the short photolysis intervals. As was done for cyclobutanediyls, we will assume that these dispersive kinetics can be quite adequately modeled using a Gaussian distribution over activation energy.

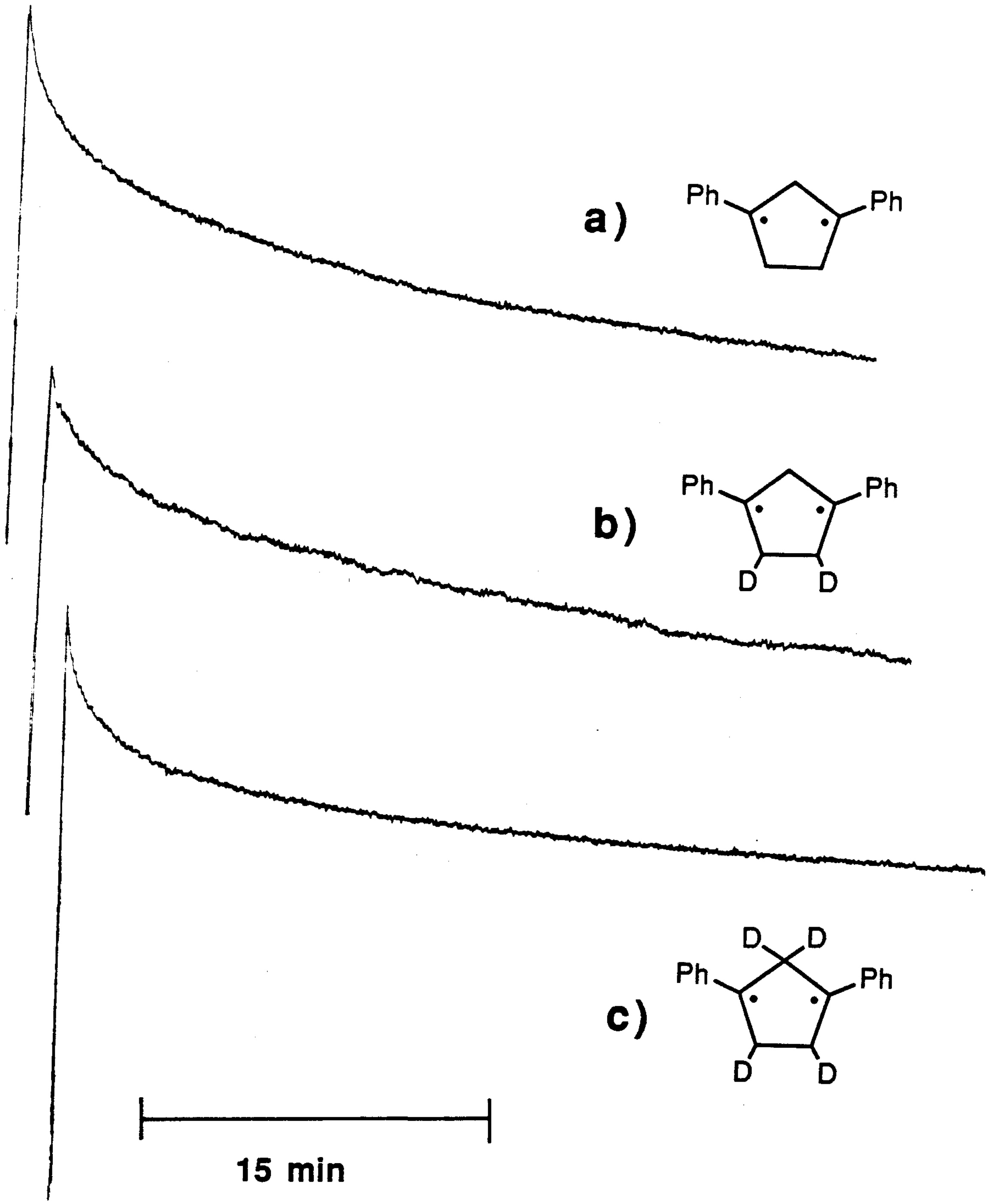

Figure 3-8. Experimental decay traces for biradicals **20** (a), **20**-d_2 (b), and **20**-d_4 (c) obtained at 77 K in MTHF matrices.

Thus, the decay trace fitting described here will simultaneously optimize the Gaussian width and position over an E_a scale.

Three separate decay traces were recorded for **^{3}20** with decay times spanning 26 to 46 min. When subjected to the fitting procedure, the optimized standard deviations ranged from 0.39 to 0.41 kcal/mol. Shown in Figure 3-9 are the fits obtained when the decay traces were refit to the average standard deviation, 0.4 kcal/mol. Satisfyingly, the fits are very good and the most probable rate constants ($k°$) obtained from these fits agree remarkably well. In all future discussions we will refer only to the average of these values, 4.8 x 10^{-4} s^{-1}. This value of $k°$ can be compared to that of its cyclobutanediyl analog (**24-Ph**) which, based on its activation parameters ($\log A$ = 7.8, E_a = 2.29 kcal/mol), would exhibit a $k°$ of 20 s^{-1} at 77 K. Thus, at liquid nitrogen temperature, 1,3-diphenylcyclopentanediyl (**^{3}20**) is over four orders of magnitude more stable than its four-membered ring analog. Our simulations show that, by assuming a $\log A$ = 8.0 for this spin forbidden process, the decay rate observed at 77 K can be well reproduced with an activation energy of 4.0 kcal/mol.

The width of the Gaussian that describes the distribution over E_a for **^{3}20** in MTHF (σ = 0.4 kcal/mol) is considerably smaller than that employed for the analysis of **24-Ph** in MTHF (σ = 0.600 kcal/mol). This implies that upon its unimolecular reaction at 77 K to form an EPR silent species, **^{3}20** experiences less of a matrix perturbing effect than does **24-Ph** from 27 to 54 K. This pronounced difference in the distribution width over E_a between **20** and **24-Ph** is surprising given the shape and size similaritites of these biradicals. This may reflect a difference in the decay processes or different matrix properties in the different temperature regions.

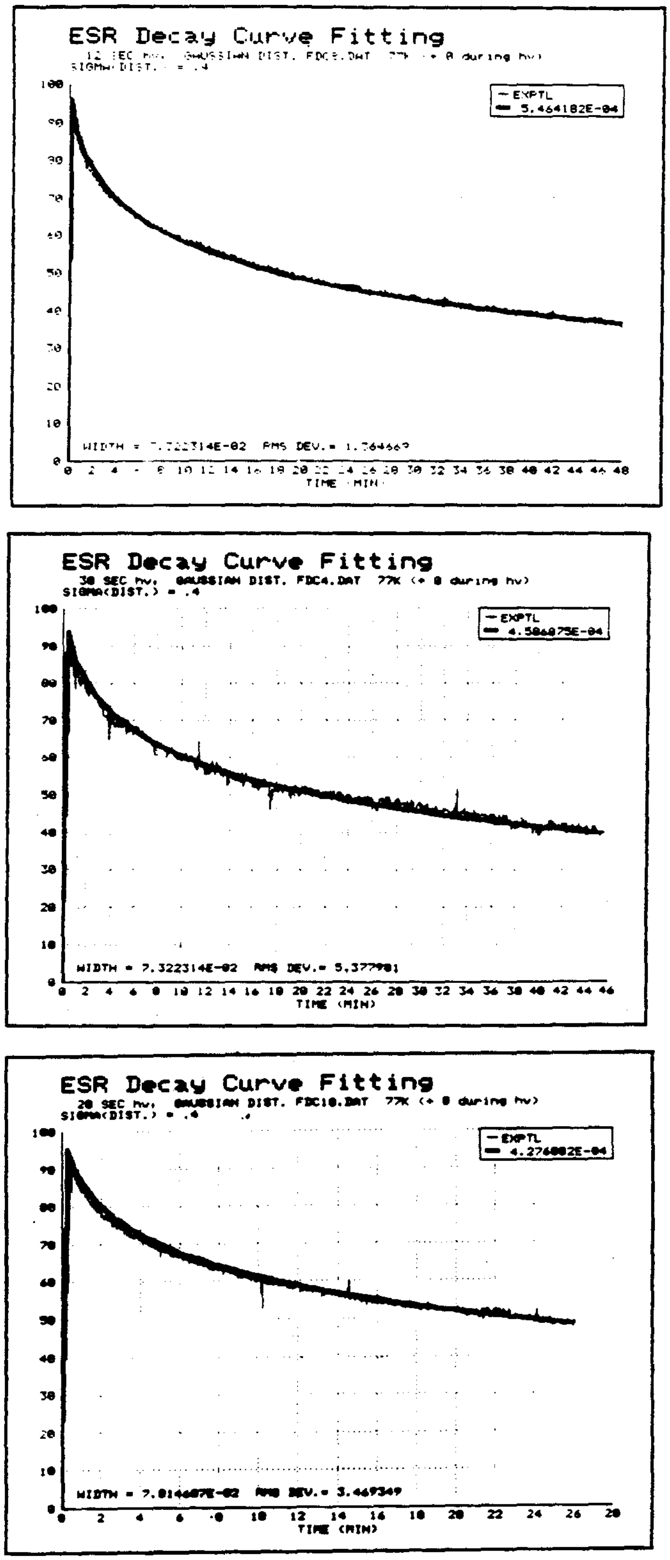

Figure 3-9. Experimental and calculated decay traces for **20** in MTHF. The distribution width employed in the fits is 0.4 kcal/mol.

Another procedure that has been employed to analyze other reactions that exhibit dispersive kinetics involves plotting the decay of the signal as ln I vs $t^{1/2}$.[22] If such a plot is linear, the most probable rate constant (k°) can be extracted from the slope. For this analysis, the shape of the distribution is a stretched Gaussian which has a fixed width over $\ln(k/k^\circ)$. Subjecting the decay trace data obtained from **^{3}20** to such an analysis provides the results shown in Figure 3-10. Although the plot closely approximates a linear function, there is definitely a noticeable amount of curvature. From a linear fit to the data, the slope is related to k° by

$$\text{slope} = (6\,k^\circ)^{1/2}$$

to give a most probable rate constant of 5.4×10^{-5} s^{-1}. This is almost a full order of magnitude slower than the k° obtained from our fitting procedure described above. Because of the curvature exhibited by this plot, we do not consider the derived value of k° to be reasonably accurate.

The plot of Figure 3-10 is curved because the true width of the $\ln(k/k^\circ)$ distribution for **^{3}20** is greater than the width of the $t^{1/2}$ distribution, which, at half maximum, is only 2 $\ln(k/k^\circ)$ units. Recall from Chapter 2 that the $\ln(k/k^\circ)$ distribution is related to the E_a dispersion by

$$\ln(k/k^\circ) = \Delta E_a/RT$$

where $\Delta E_a = E_a{}^\circ - E_a$. We can therefore obtain the $\ln(k/k^\circ)$ distribution width for **^{3}20** that is implied by our Gaussian fitting procedure. If we take ΔE_a to be the range of activation energies which fall within one standard deviation (± 0.4 kcal/mol) of the most probable E_a, we obtain a $\ln(k/k^\circ)$ distribution width of 5.2 units or over 2.5 times greater than the $t^{1/2}$ distribution. Note that for the same ΔE_a, the $\ln(k/k^\circ)$ distribution will change with temperature. For instance, at 30 K, the same E_a distribution leads to a $\ln(k/k^\circ)$ distribution of 13.3 units. Because of the fixed width of the $t^{1/2}$ distribution, we feel that it

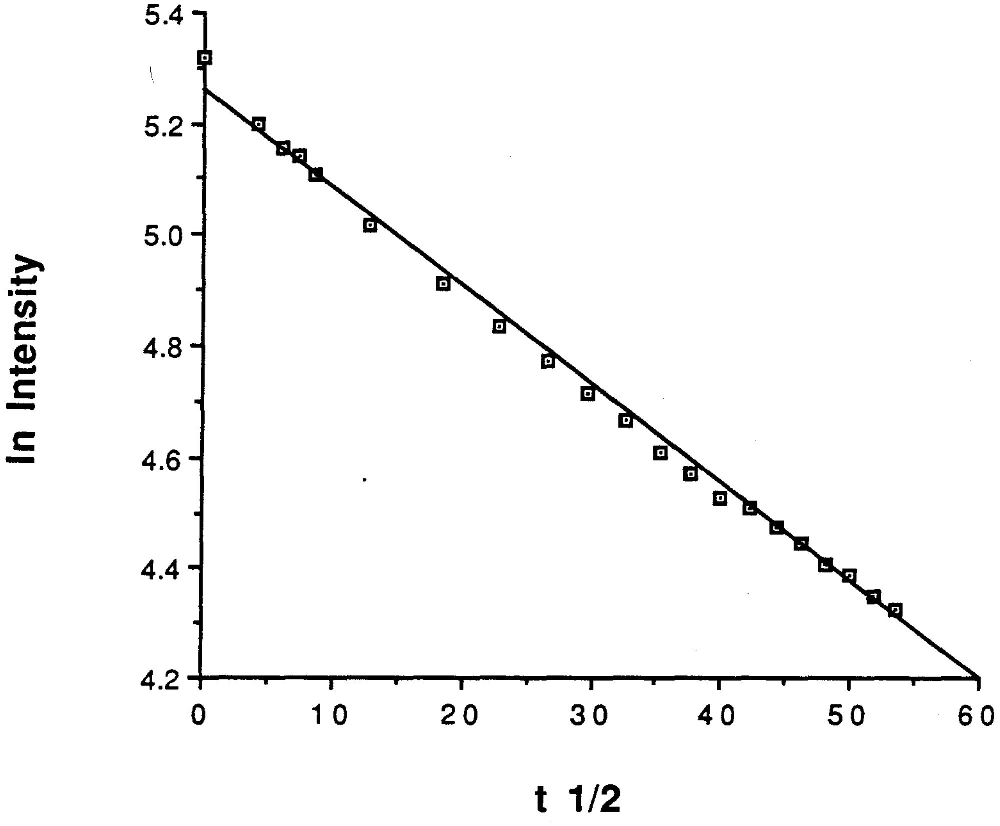

Figure 3-10. Plot of *l*n intensity **20** vs $t^{\frac{1}{2}}$ at 77 K in MTHF.

should not be considered as a general method to be employed for modeling dispersive kinetics. As shown in Figure 3-10, very nearly linear plots alone do not justify its use.

As anticipated, when the decay trace for ^{3}**20**-d_2 was subjected to the fitting procedure, it too produced an optimized standard deviation of 0.4 kcal/mol (Figure 3-11). The most probable rate of $k° = 4.2 \times 10^{-4}$ s^{-1} is virtually identical to that obtained for **20.**

When the two decay traces for ^{3}**20**-d_4 were fit, they produced much larger optimized widths of $\sigma = 0.7$ kcal/mol and a significantly lower $k°$ of 8.8×10^{-5} s^{-1} (Figure 3-12). Again, assuming log $A = 8.0$, our simulations show that this rate is well reproduced with an activation energy of 4.25 kcal/mol. The anomalously large standard deviation found for this tetradeutero biradical was quite unexpected because, even at very low temperatures (*ca.* 20K), we have never observed such a large matrix effect. Thus, phenomenologically ^{3}**20**-d_4 is fundamentally different form ^{3}**20** and ^{3}**20**-d_2. This can also be seen by inspection of decay Figures 3-9, 3-11, 3-12. After 40 min of decay, 60% of the signal for ^{3}**20** and ^{3}**20**-d_2 has decayed, compared to roughly 45% for ^{3}**20**-d_4. A related observation was reported by Buchwalter and Closs in their study of **6**. They found that while **6** decayed fairly rapidly at 5.5 K, the deuterated derivative **6**-d_8 decayed too slowly at 5.5 K to study.[1] The results obtained for the three biradicals are summarized in Table 3-2.

The large difference in the distribution width (matrix effect) between the two sets of biradicals suggests that they react along different paths to give different products. At this point it should be mentioned that in none of the biradical decay traces was there any accompanying radical signal growth. This rules out hydrogen-atom abstraction as the decay process. Of course the two logical unimolecular reaction paths of a 1,3-biradical are closure, which in

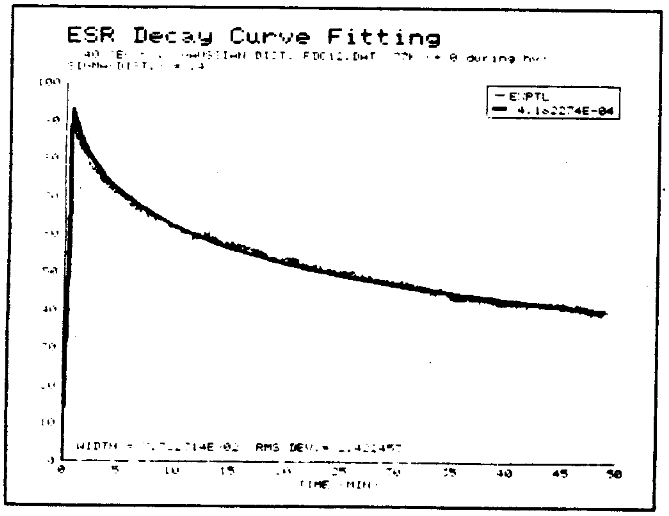

Figure 3-11. Experimental and calculated decay trace for **20**-d_2 in MTHF. The distribution width employed in the fit is 0.4 kcal/mol.

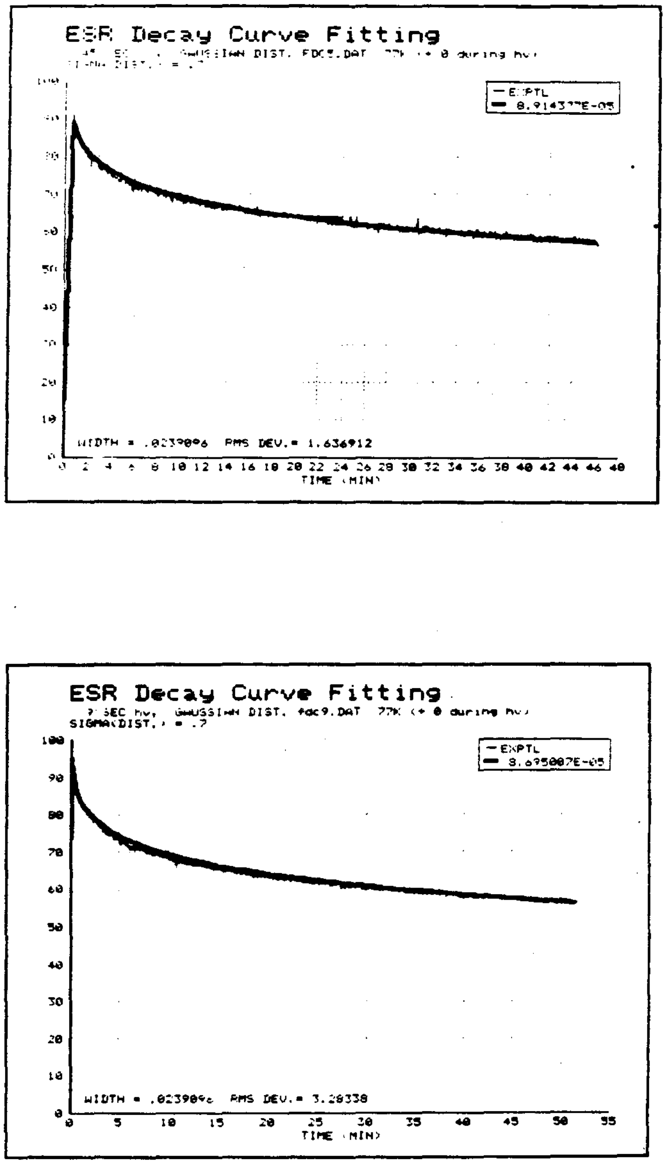

Figure 3-12. Experimental and calculated decay traces for **20**-d_4 in MTHF. The distribution width employed in the fit is 0.7 kcal/mol.

Table 3-2. Most Probable Rate Constants for Triplet Diphenylcyclopentanediyl decay

Biradical	k°, s^{-1}	E_a[a]
^{3}**20**	4.8 x 10^{-4} [b]	4.0
^{3}**20**-d_2	4.2 x 10^{-4}	4.0
^{3}**20**-d_4	8.8 x 10^{-5} [c]	4.25

[a] Obtained from a simulation assuming log $A = 8.0$ [b] Average over three decay traces. [c] Average over two decay traces.

this case would lead to 1,4-diphenylbicyclo[2.1.0]pentane (**22**), and a 1,2 hydrogen shift to give 1,3-diphenylcyclopentene (**52**). As mentioned in Chapter 2, Fischer and Michl have observed both processes in a naphthoquinodimethane.[23] In their study, the hydrogen shift reaction occurred exponentially (*i.e.*, no matrix effect), while the closure process was characterized by nonexponential kinetics. They also noted that the hydrogen shift reaction exhibited a deuterium kinetic isotope effect of 1300 near 100K. These results, along with our observations led us to wonder if matrix isolated ^{3}**20** and ^{3}**20**-d_2 undergo a 1,2-hydrogen shift reaction, while ^{3}**20**-d_4 undergoes a closure reaction. This hypothesis is consistent with the smaller matrix effect observed for ^{3}**20** and ^{3}**20**-d_2 and with an anticipated large deuterium isotope effect for ^{3}**20**-d_4 toward a 1,2-hydrogen shift. To investigate this further, product studies were performed.

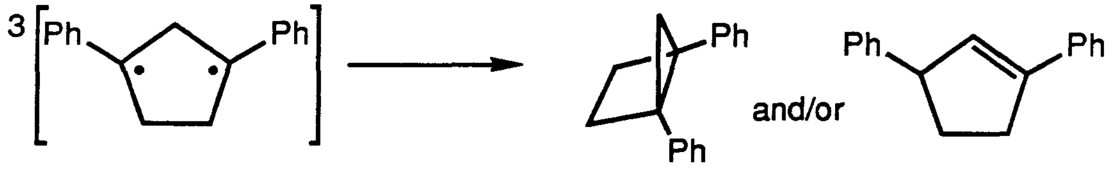

20 **22** **52**

Product Studies. The object of these product studies is to determine the product distributions that arise from biradical decay *in the rigid matrix*. This means that once the triplets are generated, the sample must be allowed to stand at 77 K for extended periods of time. Simulations show that the degree to which this goal can be accomplished is highly dependent upon the activation parameters of decay. Figure 3-13 shows that for ^{3}**20** and ^{3}**20**-d_2, 95% of the original biradical signal will decay thermally after about 40 h (2400 min) at 77K. Tetradeutero biradical ^{3}**20**-d_4, on the other hand, will experience

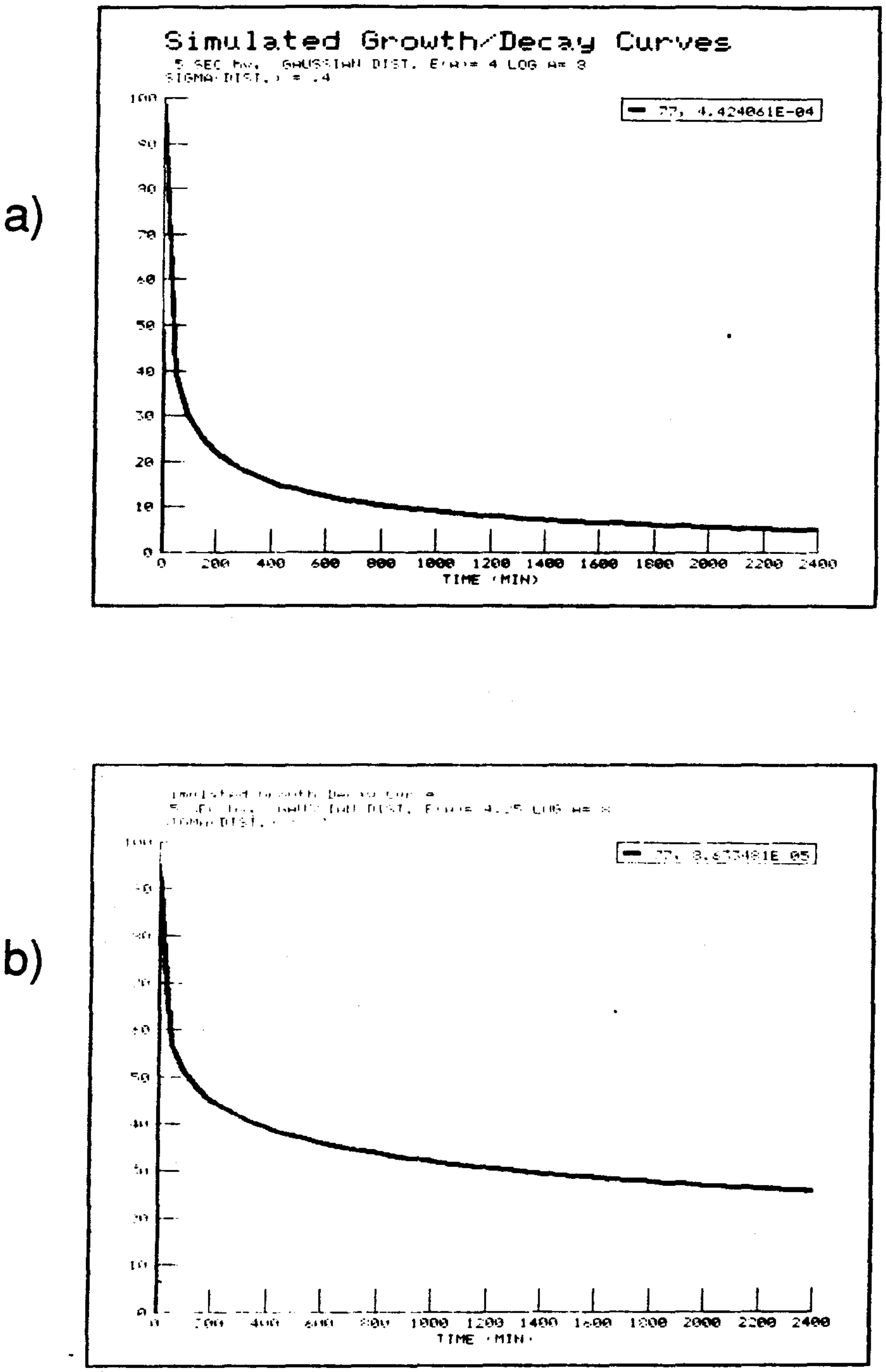

Figure 3-13. (a) Simulated decay of **20** assuming log $A = 8.0$, $E_a = 4.0$, and $\sigma = 0.4$ kcal/mol (b) Simulated decay of **20**-d_4 assuming log $A = 8.0$, $E_a = 4.25$, and $\sigma = 0.7$ kcal/mol.

only about 73% decay over the same interval and about 17% of the original signal will persist even after seven days at 77 K. It is obvious that we will not be able to realize the complete thermal decay of ^{3}**20**-*d*$_{4}$ at 77 K. This does not present a problem because this study is aimed at being only semi-quantitative.

The biradical samples (^{3}**20** and ^{3}**20**-*d*$_{4}$) were generated by photolysis ($305 \leq \lambda \leq 386$ nm) of the corresponding diazenes in MTHF at 77 K until near depletion of the diazenes as monitored by UV spectroscopy.[24] The intensity of the EPR signal was monitored periodically over the decay interval. At the end of the decay interval the samples were thawed. The solvent was then replaced with $CDCl_3$ and the products analyzed by high-field ^{1}H NMR. Gas chromatography could not be used for the analysis because at the temperatures required to elute the bicyclopentane it undergoes rearrangement to the cyclopentene.

Two samples of ^{3}**20** generated as described above were allowed to remain at 77K for 40 hours. Analysis by high-field ^{1}H NMR revealed that the product mixture consisted of $27 \pm 2\%$ cyclopentene **52** and $73 \pm 2\%$ bicyclopentane **22** and products derived therefrom. This result is quite interesting because neither direct nor sensitized photolysis of diazene **50** produces any detectable cyclopentene at 273 K.[25] Buchwalter and Closs also observed cyclopentene in their EPR samples, but in a much smaller amount (*ca.* 3%).[1]

A sample of ^{3}**20**-*d*$_{4}$ was allowed to decay for five days (119.25 h, 7155 min) at 77 K. From the end of the photolysis interval to thawing (*ca.* 117 h), the EPR signal was observed to decay only 37%. Much to our surprise, the composition of the product mixture obtained from this sample was virtually identical to that of ^{3}**20** giving 29% cyclopentene and 71% bicyclopentane and its associated products.[25] We find this result quite unusual because we would expect at least some kinetic isotope effect for the 1,2-hydrogen shift but, within experimental error, we find none.

The results of these product studies are somewhat disturbing, because they tell us very little about the products of decay from the triplet biradical. Presumably, upon direct photolysis of the diazenes at 77 K, most of the photochemistry takes place within the singlet manifold. In fact, the triplet biradicals we observe at 77 K probably arise from that small fraction of excited diazenes which undergo intersystem crossing (ISC) to excited triplet before they expel nitrogen. It should be noted that a similar product study conducted via benzophenone sensitized photolysis of **21** gave qualitatively the same results. At this point, we do not know the nature of the decay process, it could be closure, a 1,2-hydrogen shift, or some other process that we cannot detect by high-field ^{1}H NMR.

Discussion. In order to determine what factors contribute to the enhanced stability of ^{3}**20**-d_4 relative to ^{3}**20** and ^{3}**20**-d_2, it is perhaps best to concentrate on the *first* elementary process which must occur before the triplet biradicals can react to give covalent products. Of course, this process is intersystem crossing (ISC) from the triplet surface to the singlet surface.[26,27] Because these biradicals possess triplet ground states, ISC is necessarily an endothermic process.[27] Therefore, ISC will require distortion from the idealized triplet geometry (planar ring, parallel *p* orbitals) to some new geometry where the singlet and triplet surfaces are nearly degenerate. Intersystem crossing from such a representative point then quickly leads to product formation. Thus, the rate determining step for product formation of such biradicals is ISC. Two different mechanisms give rise to ISC, namely, electron-nuclear hyperfine coupling (HFC) and spin-orbit coupling (SOC).

Recently, SOC has been identified as the primary ISC mechanism in biradicals.[28] This dominance of SOC in ISC of biradicals can be attributed to its ability, even in pure hydrocarbon systems, to effect singlet ⇆ triplet interconversions between states that differ in energy by one wave number or more, while the HFC mechanism can only induce ISC between states that are within 0.01 cm^{-1} of each other.

The first qualitative theoretical discussion of SOC applied to hydrocarbon biradicals was presented by Salem and Rowland.[26] Their classic study identified three important features: SOC is proportional to the ionic character (and hence, overlap, see Chapter 1) of the singlet wavefunction; it is proportional to the degree of interorbital perpendicularity; and it decreases sharply as the distance between the radical centers increases. An in-depth study of SOC in the trimethylene biradical (**5**) has recently been reported by Doubleday and coworkers.[27] In this study, the individual contribution of through-space and through-bond effects to SOC were determined by comparing SOC values for the biradical **5** with a pair of methyl radicals with identical orbital geometries. Upon examining the through-space effect they found that SOC is maximized (0.7 cm^{-1}) for the conformation shown below. In agreement

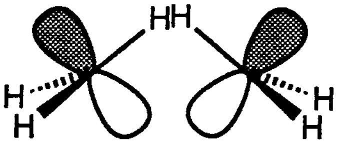

with the factors outlined by Salem and Rowland, this conformation maximizes both orbital overlap and orthogonality. The geometry dependence of SOC for trimethylene was virtually identical to that of the radical pair, but the absolute magnitude of the SOC matrix element was found to be a factor of 2.5 greater than that observed for the radical pair at all geometries. Thus, the principal effect of through-bond coupling by a single CH_2 group is to increase SOC by a factor of 2.5, and it therefore plays a very important role in ISC of trimethylene biradicals.

Through-bond coupling and hyperconjugation are two terms used to describe the same phenomenon, which is simply the first-order mixing between a filled bonding orbital and another orbital of the same symmetry.[16,27] This second orbital may either be filled, half-occupied or empty. Hyperconjugation is invoked to explain the marked stability difference between the methyl and ethyl cations. Through their mixing with the empty *p* orbital, the π_{CH_3} orbitals of the ethyl cation donate electron density to the electron deficient center. There is also a substantial stability decrease observed on replacing the CH_3 group of the ethyl cation with a CD_3 group. This effect can be explained by first noting that hyperconjugation serves to weaken the interacting C-H bonds somewhat. Deuterium, being heavier than hydrogen, prefers to reside in the more strongly bound site and, as a consequence, a C-D bond is less able than a C-H bond to participate in hyperconjugation.[29] The poorer hyperconjugative ability of a C-D bond relative to a C-H bond has also been observed in biradical chemistry by Baldwin and Carter.[30] In their study of the one-center epimerizations of 1-cyano-2-phenylcyclopropanes, they observed a secondary deuterium isotope effect of $(k_H/k_D) = 1.13$ upon substitution at C3 with deuterium. They

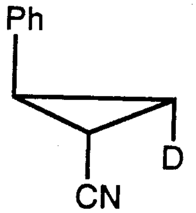

attributed this rate retardation to the poorer hyperconjugative ability of the C-D bond.

We are now led to ask whether the intervening CD_2 group of ^{3}**20**-*d*$_4$ contributes to its unique behavior relative to ^{3}**20** and ^{3}**20**-*d*$_2$. If, in fact, the CD_2 group is a poorer hyperconjugating group than the CH_2 group, then the SOC matrix element of the CD_2-containing biradical will be smaller than that of a CH_2-containing biradical at the same geometry. Therefore, to obtain the same magnitude SOC interaction as the protio biradical, the deutero biradical will have to distort further from the idealized triplet geometry than will the protio biradical. This rationalization may explain the observed larger matrix effect and the larger activation energy of ^{3}**20**-*d*$_4$. Of course, this is an oversimplification because, if the CD_2 group is a poorer hyperconjugating group, the S-T gap[16,31] of **20**-*d*$_4$ would most likely be different from that of ^{3}**20** and ^{3}**20**-*d*$_2$, greatly complicating the analysis. This discussion does serve to illustrate, however, that the substitution of the intervening CH_2 group of a trimethylene biradical with a CD_2 group is probably not an "innocent" substitution at all. Given this, it would be quite worthwhile to study the decay kinetics of ^{3}**24-Ph**-*d*$_4$ to determine if it also is significantly stabilized relative to its all protio analog.

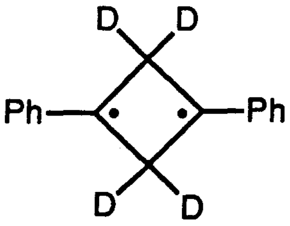

24-Ph-*d*$_4$

Concerning the Stability of 1,3-Diphenylcyclopentanediyl

As mentioned previously, 1,3-diphenylcyclopentanediyl ^{3}**20** is much more stable than 1,3-diphenylcyclobutanediyl ^{3}**24-Ph.** While ^{3}**24-Ph** is only marginally stable at 65K, ^{3}**20** can be readily generated at 77 K and decays only slowly at this temperature. One may ask what factors contribute to the enhanced persistence of ^{3}**20** relative to ^{3}**24-Ph.** Certainly, one factor that must contribute generally is the distance between the radical centers. The larger separation between the radical centers in the five-membered ring (2.37[15] vs 2.11[32] Å) will require a much larger geometrical distortion to achieve the requisite orbital overlap for ISC to occur. Also, given the decreased driving force for ring closure in the five-membered ring system,[8] this geometrical distortion may incorporate more strain than the analogous distortion in the four-membered ring. It is also worth noting that ^{3}**20** is anticipated to have a *smaller* S-T gap than **24-Ph.** This is a consequence of reduced exchange repulsions in the five-membered ring due to the greater distance between the radical centers. Thus, a greater S-T gap does not necessarily imply greater stability.

Thermal Decompostion of Diazene 21

Diazene **21** loses nitrogen to give 1,4-diphenylbicyclo[2.1.0]pentane (**22**) with first-order kinetics, as monitored by ^{1}H NMR between 25 and 45°C. The derived activation parameters are $\Delta H^\ddagger = 20.7 \pm 1.0$ kcal/mol, $\Delta S^\ddagger = -8.2 \pm 3.1$ eu (Figure 3-14). Table 3-3 lists the corresponding activation parameters for a series of 1,2-diazenes. As expected, based on the anticipated transition state stabilizing effect of the phenyl groups,[33] **21** is substantially more thermally labile than the parent diazene **7**. In fact, based on the decrease in $\Delta H^\ddagger$ observed going from **7** to **21**, one can see that most of the resonance stabilization energy expected from two benzyl radicals (20.4 kcal/mol)[34] is manifested in the transition state for the thermolysis of diazene **21**. These activation parameters suggest that the transition state for the thermolysis is late and that the expulsion of nitrogen takes place in a concerted, if not synchronous, manner.[35] An interesting aspect of the thermolysis of **21**, is its negative entropy of activation. It seems counter intuitive that a negative entropy of activation could be observed for a fragmentation reaction. However, upon inspection of Table 3-3 it is clear that, relative to the parent diazenes, a substantial decrease in $\Delta S^\ddagger$ is observed upon placing delocalizing substitutions at the α carbon of 1,2-diazenes. This is consistent with the notion that, in order for the delocalizing group to exhibit the maximum possible stabilizing effect in the transition state, it must adopt a specific orientation with respect to the breaking bond(s). As described below, this effect has also been observed for other fragmentation reactions.

The thermolysis activation parameters obtained for **21** provide a useful benchmark against which to compare the thermal stabilities of two related derivatives **53**[36] and **54**[37]. While **21** has a half life of about 45 min at 35°C, compounds **53** and **54** must be heated above 120°C to effect deazetization.

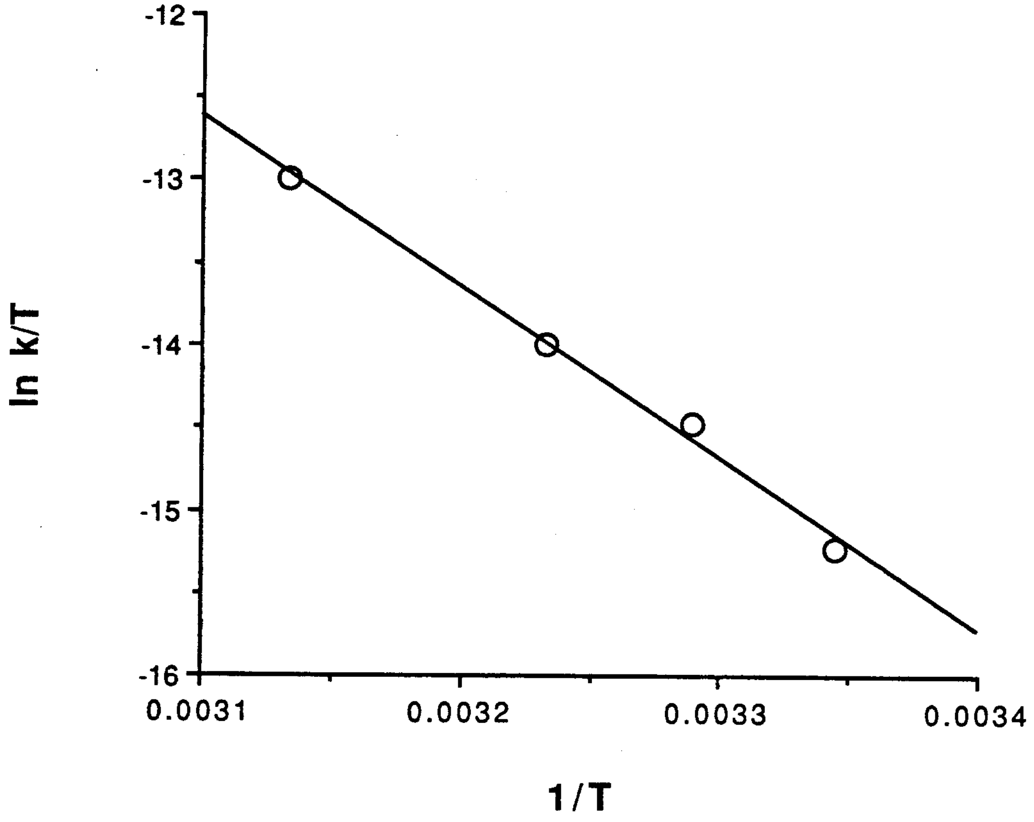

Figure 3-14. Eyring plot of the thermal decomposition kinetics of diazene 21 between 25 and 45 °C in $CDCl_3$. The activation parameters are $\Delta H^{\ddagger} = 20.7 \pm 1.0$ kcal/mol and $\Delta S^{\ddagger} = -8.2 \pm 3.1$ eu.

Table 3-3. Activation Parameters of Diazene Decomposition.

Diazene	$\Delta H^{\ddagger}$	$\Delta S^{\ddagger}$	$\Delta\Delta H^{\ddagger}$	$\Delta\Delta S^{\ddagger}$	ref.
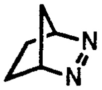	36.0	5.6	—	—	*a*
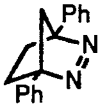	20.7	-8.2	-15.3	-13.8	this work
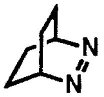	45.0	10.6	—	—	*b*
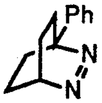	34.1	1.7	-10.9	-8.9	*c*
	28.8	1.5	-16.2	-9.1	*d*
	41.5	11.3	—	—	*a*
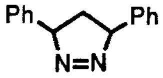	25.0	0.0	-16.5	-11.3	*e*
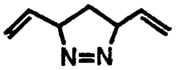	22.3	-4.5	-19.2	-15.8	*f*

a Roth, W. R.; Martin, M. *Justus Liebings Ann. Chem.* **1977**, *702*, 1. *b* Engel, P. S.; Hayes, R. A.; Kiefer, L.; Szilagyi, S.; Timberlake, J. W.; *J. Am. Chem. Soc.* **1978**, *100*, 1876. *c* Engel, P. S.; Nalepa, C. J.; Horsey, D. W.; Keys, D. E.; Grow, R. T. *J. Am. Chem. Soc.* **1983**, *105*, 7102. *d* Engel, P. S.; Allgren, R.; Chae, W. K.; Leckonby, R. A.; Marron, N. A. *J. Org. Chem.* **1979**, *44*, 4233. *e* Schneider, M.; Strohäcker, H. *Tetrahedron* **1976**, *32*, 619. *f* Crawford, R. J.; Ohno, M. *Can. J. Chem.* **1974**, *52*, 3134.

The thermal stabilities of these compounds, which rival that of **7**, must, in part, be due to geometric constraints which prevent full utilization of the benzyl resonance energy in the transition state for thermolysis.

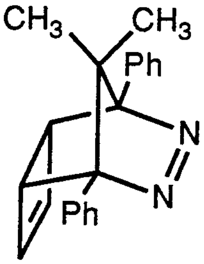

53

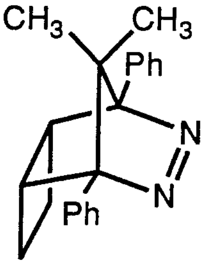

54

Bridge-Flip Reaction of 1,4-Diphenylbicyclo[2.1.0]pentane

The bicyclo[2.1.0]pentane structure is unsurpassed among simple ring systems in the amount of strain energy (SE) released upon a single bond homolysis.[8,38] In the parent, **8**, C1-C4 bond cleavage to produce 1,3-cyclopentanediyl **6** relieves *ca.* 50 kcal/mol of SE.[8] This is manifest in the low barrier for the bridge-flip process (Figure 3-15), for which $\Delta H^{\ddagger} = 36.3$ kcal/mol, $\Delta S^{\ddagger} = 2.1$ eu.[39] As shown in (Figure 3-15), 36 kcal/mol represents an upper limit to the bond dissociation energy (BDE) in **8**.

Introduction of phenyl groups at the bridgehead positions to give **22** should preferentially stabilize the derived biradical **20** by *ca.* 20 kcal/mol due to benzylic resonance.[34] One would expect most or all of this stabilization to be felt in the bridge-flip transition state,[39c] and so diphenylbicyclopentane **22** should have a quite low barrier to bond cleavage. Note that such a bridge-flip reaction interconverts endo-exo pairs of protons, and therefore, if the barrier is near 16 kcal/mol, it should be observable by dynamic NMR methods over a readily attainable temperature range. Through a combination of ^1H NMR complete line-shape analysis and magnetization transfer studies, we have determined the activation parameters for the bridge-flip reaction of **22**. This study has revealed that **22** does, indeed, possess a very weak C1-C4 bond and as a consequence, it has some very interesting properties.

DNMR Studies. Shown in Figure 3-16 is the aliphatic portion of the 400 MHz ^1H NMR spectrum of **22** obtained in $CDCl_3$ solution at 20°C. An interesting feature of the spectrum of **22** is the long-range W coupling (^4J = 1.96 Hz) between the 5_x and $2,3_x$ protons.. The sharpness of the lines indicate that the bridge-flip reaction is slow on the NMR time scale at room temperature. As the temperature is raised and the rate of the bridge-flip

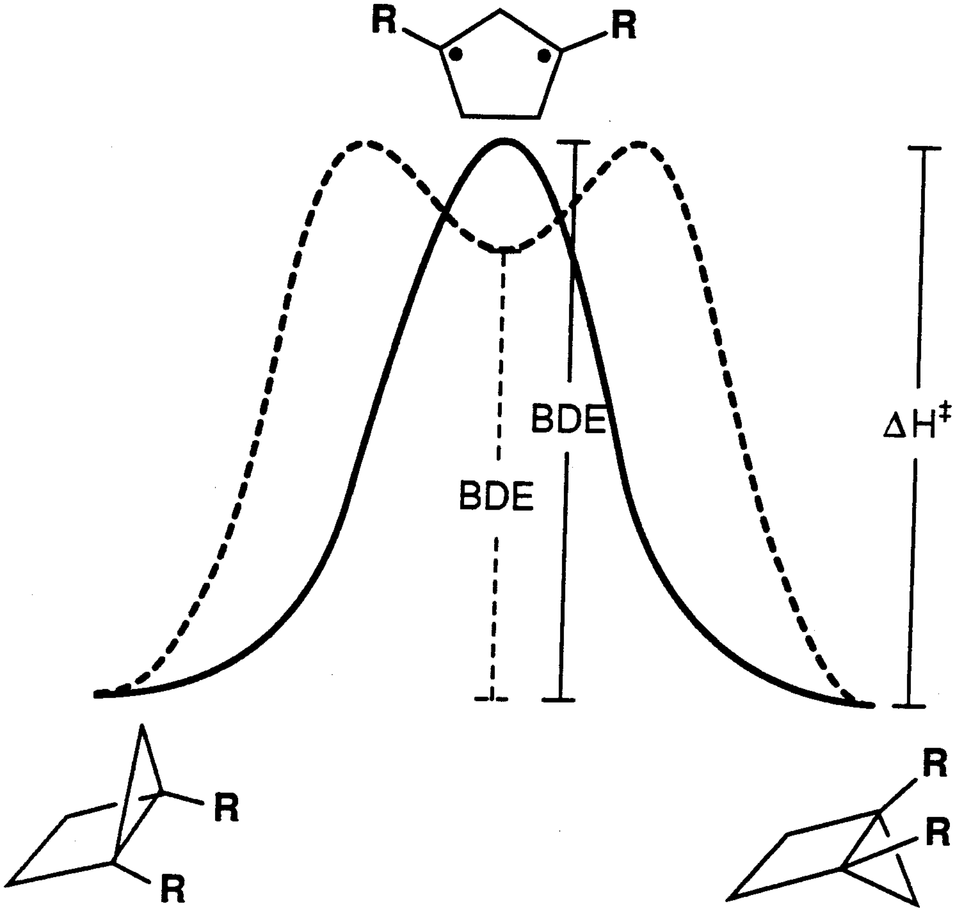

Figure 3-15. Schematic potential energy surfaces for the bridge-flip of a bicyclo[2.1.0]pentane. As shown, the BDE is less than or equal to $\Delta H^{\ddagger}$, depending on whether there is (dashed line) or is not (solid line) a biradical minimum on the singlet surface.

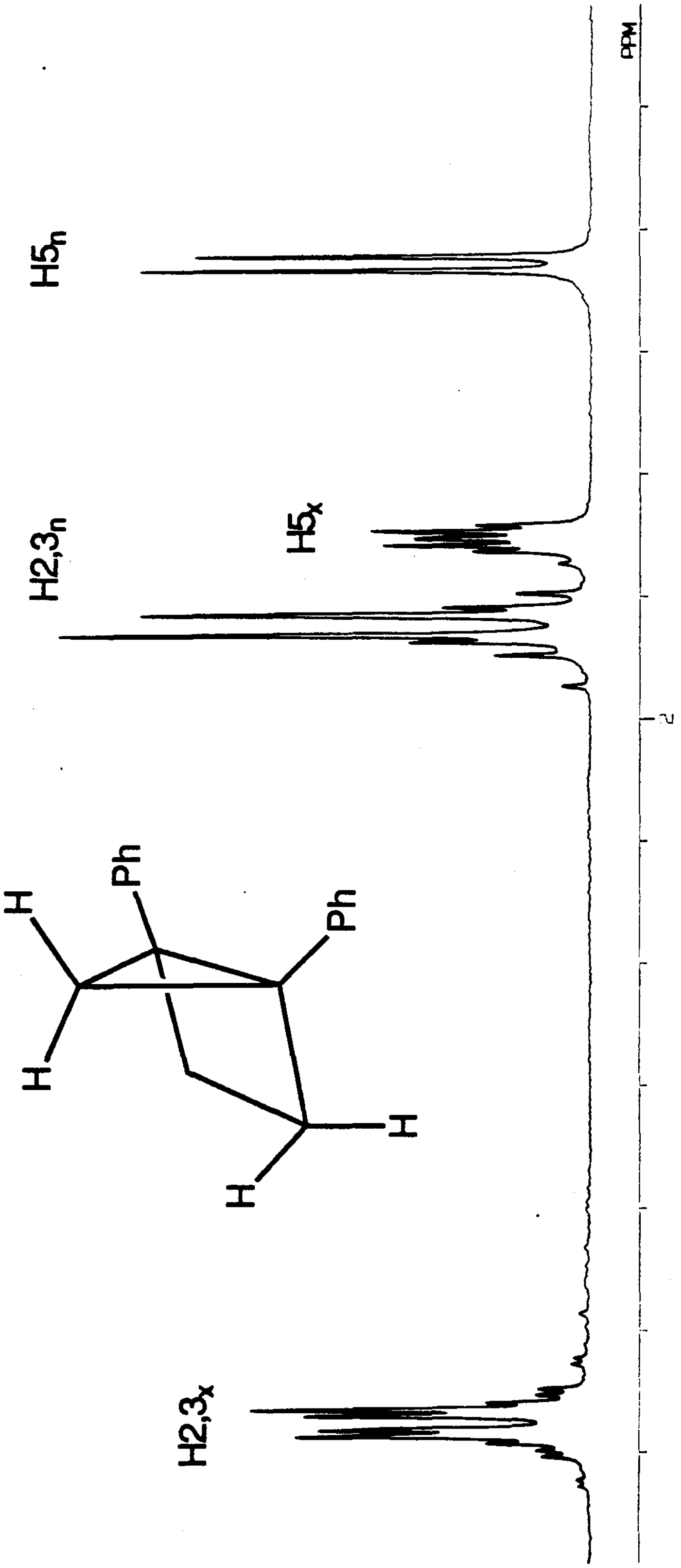

Figure 3-16. 400 MHz ^1H NMR spectrum of **22** in $CDCl_3$ at 20 °C.

process increases, we would expect the $5_{x,n}$ proton pair to gradually broaden and eventually coalesce. The $2,3_{x,n}$ pair is expected to exhibit the same behavior but coalescence will occur at a higher temperature because the chemical shift difference ($\Delta\nu$) between $2,3_x$ and $2,3_n$ is considerably greater than that of $5_{x,n}$. Preliminary DNMR studies[40] conducted at 200 MHz confirm these predictions and also indicate that at 400 MHz, coalescence of the $5_{x,n}$ signals should occur at temperatures near 110°C.

In order to obtain meaningful activation parameters from a complete line-shape (CLS) analysis, the observed coalescence should take place over a broad temperature range which requires that $\Delta\nu$ between the exchanging signals be large ($\Delta\nu > 50$ Hz).[40,41] It was therefore desired to perform the DNMR experiments at 400 MHz, where $\Delta\nu$ between 5_x and 5_n at ambient temperature is 90 Hz. Such an experiment requires the use of an NMR solvent that can withstand a minimum temperature of 110°C. It is worth noting that because the DNMR experiments are performed in medium-walled sealed tubes, it is not necessary to use a solvent that has a boiling point above 110°C. Under these experimental conditions, a solvent can be raised to temperatures 50° or more above its boiling point. Three other requirements of a potential NMR solvent are: 1) it must be able to dissolve the bicyclopentane, 2) it must adequately resolve the four multiplets of the static spectrum, 3) it must remain nonviscous at temperatures below ambient so that the variation of $\Delta\nu$ with temperature can be examined.

Five solvents were examined: benzene-d_6, toluene-d_8, chlorobenzene-d_5, *o*-dichlorobenzene-d_4 and 1,1,2,2-tetrachloroethane-d_2. All five solvents failed to meet the third criterion -- they were unable to separate the 5_x from the $2,3_n$ resonance. Of all solvents employed, even those with low boiling points, the one that proved most effective in separating the NMR signals of **22** was deuterochloroform. We had previously established that $CDCl_3$ solutions in medium-walled sealed NMR tubes could easily withstand temperatures up to 120°C. Thus, $CDCl_3$ became the solvent for our DNMR experiments.

In order to simulate spectra of an equally-populated two-configuration system undergoing chemical exchange, four parameters must be determined:[40,41] 1) the rate of exchange *k*, 2) the separation of the signals ($\Delta\nu$) undergoing exchange, 3) the effective line width of the signals undergoing exchange as indicated by $T2_{eff}$, 4) the coupling constants. As described below, $\Delta\nu$, $T2_{eff}$ and the coupling constants can be easily obtained from the experimental spectra so the observed line shape is a function of only one unknown parameter, *k*.

Quite often the chemical shift parameters vary considerably with temperature, therefore, accurate simulations must account for this behavior. The chemical shift separation between exchanging signals in the fast exchange region is usually determined by performing a linear extrapolation from a plot of $\Delta\nu$ versus temperature obtained in the slow exchange region. For **22** we have found that while the chemical shifts of the $2,3_{x,n}$ protons are temperature invariant, those of the $5_{x,n}$ protons are quite temperature dependent. Shown in Figure 3-17 are the plots of $\Delta\nu$ versus temperature for the $5_{x,n}$ protons obtained from -30 to 30°C. Over this temperature range, the coupling constants of the spin system did not change significantly. In a complete line shape study, the $T2_{eff}$ values are usually determined by measuring the width (in Hz) of a peak not affected by the exchange process. The $T2_{eff}$ value used in the simulations is determined by scaling the observed width of this reference signal by the ratio (reference signal width/exchanging

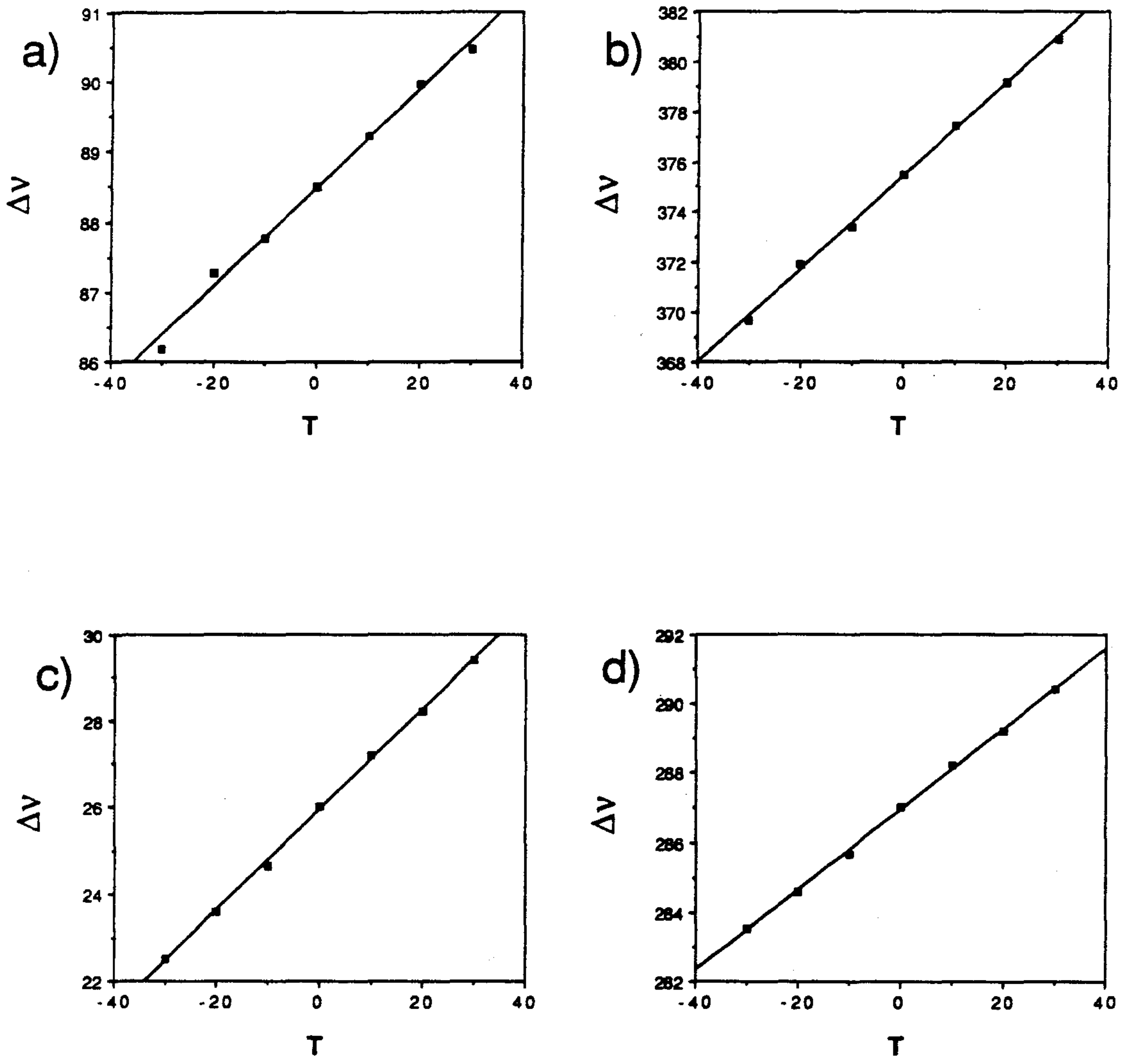

Figure 3-17. Variation of the relative chemical shifts (expressed in Hz) of the aliphatic protons of **22** with temperature. Chemical shift of the 5_n proton relative to (a) the 5_x proton and (b) the $2,3_x$ protons. Chemical shift of the 5_x proton relative to (a) the $2,3_n$ protons and (b) the $2,3_x$ protons.

signal width) observed in the slow exchange limit. In the present study, the width of the $CHCl_3$ signal was employed to determine $T_{2_{eff}}$ values.

In order to make use of all the line-shape information available from a coalescence study of **22**, we needed to simulate a six-spin system. At present, there are no six-spin DNMR simulators available and there is a good reason for this. Such a calculation is very large and therefore, even a single point calculation would be prohibitively expensive. This situation is not acceptable because a complete line-shape study requires many iterative simulations. To circumvent this problem, we dissected our simulation into two separate systems: one consisting of two spins ($5_{x,n}$), and the other containing four spins ($2,3_{x,n}$). The full spectrum could then be produced by plotting the sum of the two simulations. This treatment required that the 1.96 Hz coupling between 5_x and $2,3_x$ be omitted. This restriction did not present a problem because, in the rate regime studied, the line shape is very insensitive to J coupling and most sensitive to k.[40-42]

The 400-MHz ^1H NMR spectra of **22** in $CDCl_3$ obtained from 343.1 to 382.6 K are shown in Figure 3-18 along with the corresponding simulated spectra. As predicted by our preliminary studies, coalescence of the $5_{x,n}$ pair occurs at temperatures very near 383 K. Unfortunately, we were unable to study the process at higher temperatures and observe the coalescence of the $2,3_{x,n}$ protons because the sample decomposed rapidly above 385 K. This decomposition process involves a 1,2-H shift to give 1,3-diphenylcyclopentene (**52**).[43] In fact, this process can be clearly observed in the two highest temperature spectra of Figure 3-18 in the form of significant deviations from the calculated line-shape for the $2,3_{x,n}$ protons. It is worth emphasizing that it is not a conformational process giving rise to these exchange broadened spectra, but rather, it is the *rapid breaking and reforming of a carbon-carbon*

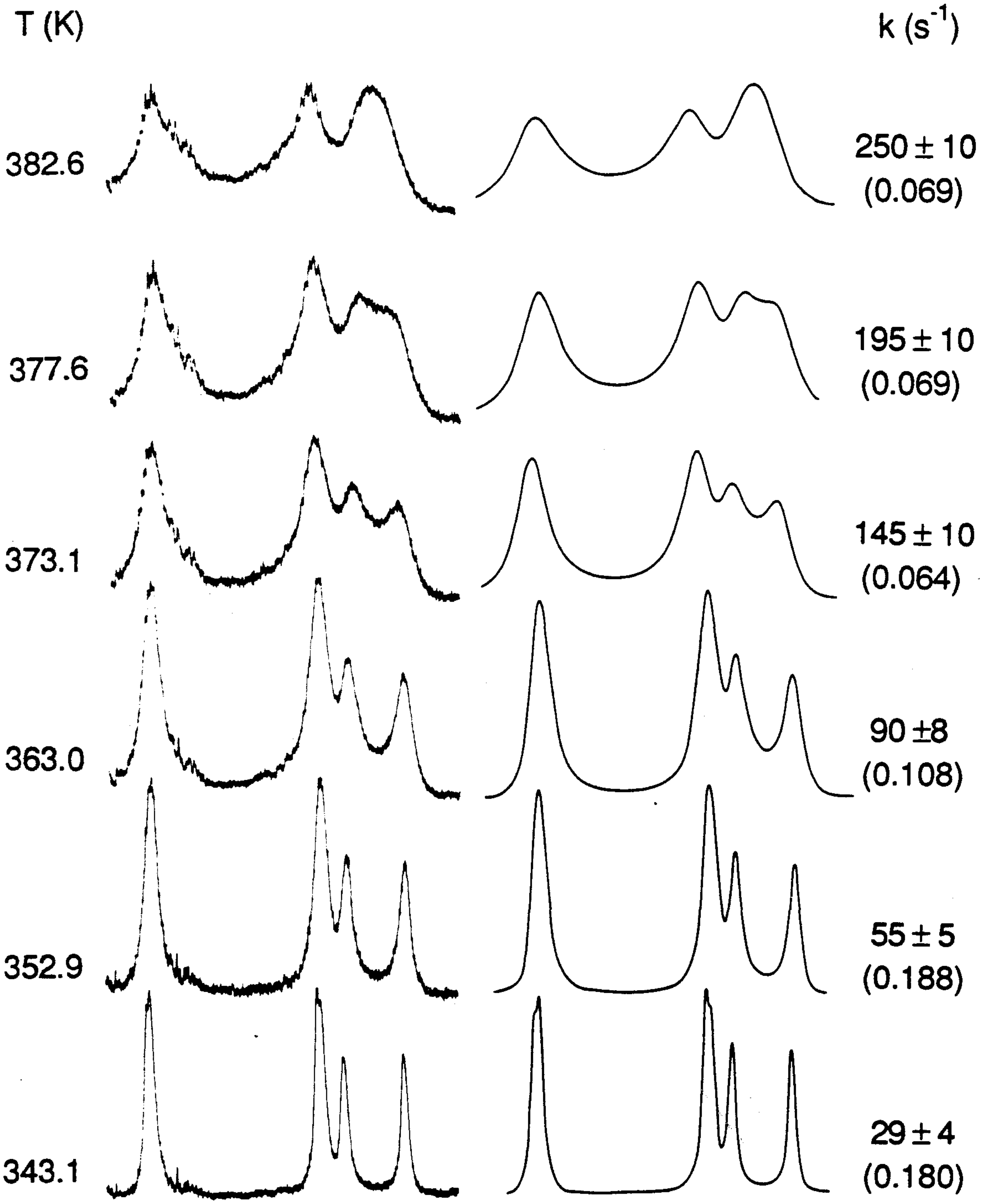

Figure 3-18. Observed (left) and simulated (right) 400 MHz ^{1}H NMR spectra of **22** in $CDCl_3$ from 343.1 to 382.6 K. Also shown are the corresponding rates obtained from the simulations and the T_{2eff} values (in parentheses).

bond. The rates are listed in Table 3-4, and the derived activation parameters and related data are collected in Table 3-5. A complete discussion of these results will be presented below, but we note at this point that a good correlation is obtained (Table 3-5).

Magnetization Transfer Studies. Like other NMR-based analytical methods such as DNMR, the magnetization transfer (MT) technique[44] provides an opportunity to measure the rates of chemical exchange between components in an equilibrium state. These methods depend on being able to attach an innocuous label to an atom or group of atoms that is being carried to another site by chemical exchange. Unlike DNMR, which uses the phase of nuclear precession as a label, magnetization transfer uses a population disturbance as its label. Because the return of the spin system to its equilibrium state is governed, in part, by longitudinal (spin lattice) relaxation, the exchange rates of processes probed by magnetization transfer are roughly comparable to $1/T_1$. This is in contrast to the DNMR (coalescence) approach, which measures rates that are roughly comparable to the chemical shift separation. The two methods therefore work in different rate regimes, and together they can cover a very broad kinetic range.

Consider the simple case of two exchanging sites (A and X) with equal populations, so that the forward and reverse exchange rates, *k*, are

$$AX \underset{k}{\overset{k}{\rightleftharpoons}} XA$$

equal, and the spin-lattice relaxation times, T_1, are also equivalent. The experiment is performed by selectively inverting the magnetization of the X spins with a 180° pulse, followed by a variable delay time τ before a non-

Table 3-4. Bridge-Flip Rates Derived From a Complete Lineshape Analysis

T, K[a]	*k*, s^{-1}
343.1	29 ± 4
352.9	55 ± 5
363.0	90 ± 8
373.1	145 ± 10
377.6	195 ± 10
382.6	250 ± 10

[a] ± 1 K

Table 3-5. Activation Parameters for the Bridge-Flip Reaction

	$\Delta H^{\ddagger}$ [a]	$\Delta S^{\ddagger}$ [a]	$\Delta G^{\ddagger}_{297}$ [a]	ρ [c]	$\sigma\Delta H^{\ddagger}$ [d]	$\sigma\Delta S^{\ddagger}$ [d]	pts [e]	ΔT [f]
400 MHz CLS	13.2	-13.5	17.2	0.9988	0.3	0.8	6	39.5
500 MHz MT	12.8	-14.2	17.0	0.9997	0.1	0.4	3	16.9
CLS + MT	12.2	-16.4	17.1	0.9993	0.2	0.5	9	84.5

[a] kcal/mol. [b] cal/mol·K. [c] Correlation coefficient. [d] Standard deviation. [e] Number of data points. [f] Temperature range

selective 90° observe pulse. Under these conditions the longitudinal magnetizations of the two sites can be described by equations 3-1 and 3-2.

$$M_\infty(A) - M_z(A) = M_\infty(A)[\exp(-\tau/T_1) - \exp(-\tau/T_1 - 2kT)] \qquad (3\text{-}1)$$

$$M_\infty(X) - M_z(X) = M_\infty(X)[\exp(-\tau/T_1) + \exp(-\tau/T_1 - 2kT)] \qquad (3\text{-}2)$$

Note that when τ is infinite, both signals reach their equilibrium values $M_\infty(A)$ and $M_\infty(X)$. Also when $k=0$, $M_Z(A) = M_\infty(A)$ throughout while

$$M_z(X) = M_\infty(X)\,[1 - 2\exp(-\tau/T_1)]$$

This is the expression describing normal longitudinal relaxation after population inversion. As shown in equations 3-1 and 3-2, when exchange and relaxation occur simultaneously, the recovery of the signals is no longer exponential. The X resonance recovers from its initial inversion quite quickly at first as exchange and relaxation reinforce, and then more slowly as the exchange becomes less effective because the transferred spins are less and less perturbed. The A signal loses intensity and passes through a minimum before gong back to $M_\infty(A)$ as spin-lattice relaxation takes over. Analysis of these two curves allows the exchange rate to be extracted.[44a]

For the magnetization transfer study of **22**, we decided to study the exchange between the $5_{x,n}$ pair of protons in $CDCl_3$ solution. This decision was based on the fact that the 5_n proton, being a simple doublet and far removed from other signals, could most easily be inverted with a selective pulse. Preliminary saturation transfer experiments indicated that the most reliable exchange rates would be obtained by performing the magnetization transfer experiments between 20 and 45°C. Given this, a ^{1}H NMR T_1 study of **22** in $CDCl_3$ was conducted over this temperature range. As shown in Figure 3-19, the T_1's of the 5_x and 5_n protons are very similar and vary considerably with temperature.

A typical magnetization transfer experiment obtained using a 500-MHz NMR spectrometer is shown in Figure 3-20. The exchange rate constants (k_{ex}) were calculated by fitting the integration data to the magnetization equation using a non-linear least squares procedure.[45] The exchange rate constant is related to the bond-breaking rate constant by $k_{ex} = 1/2\ k$. This is so because, upon bond cleavage, only one-half of the molecules actually undergo a bridge-flip reaction, while other half return to their original configuration. Table 3-6 lists the rate constants obtained for the three temperatures studied along with the T_1 values (obtained from the plot of Figure 3-19) employed in the calculation of the rate constants.

As in previous studies,[46] the results from the MT method are in excellent agreement with those from the CLS. This can be seen in Table 3-5, which includes activation parameters for the MT data, and for the combined MT and CLS data. Agreement between the two methods can also be seen in Figure 3-21 which shows the Eyring plot for the combined data. The combined method allows us to span an 84° temperature range and over a factor of 100 in rates, instilling confidence in the derived activation parameters.

Error Limits. The DNMR method has long been recognized as a valuable tool for obtaining rate data.[40,41] There are, however, many hazards in using such data to obtain reliable activation parameters from the complete line shape method.[41] The difficulty arises because several factors other than

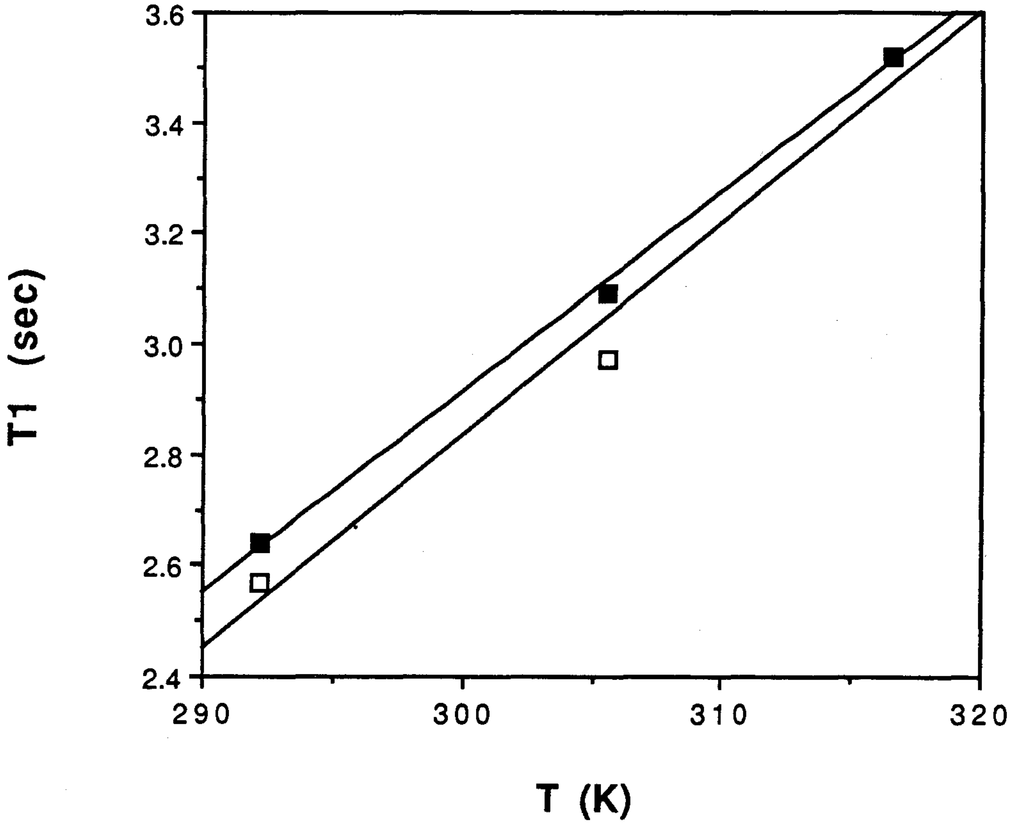

Figure 3-19. Variation of the T_1's of the 5_x (open squares) and 5_n (filled squares) protons with temperature in a degassed $CDCl_3$ solution. At 316.5 K, both protons exhibit the same T_1 value.

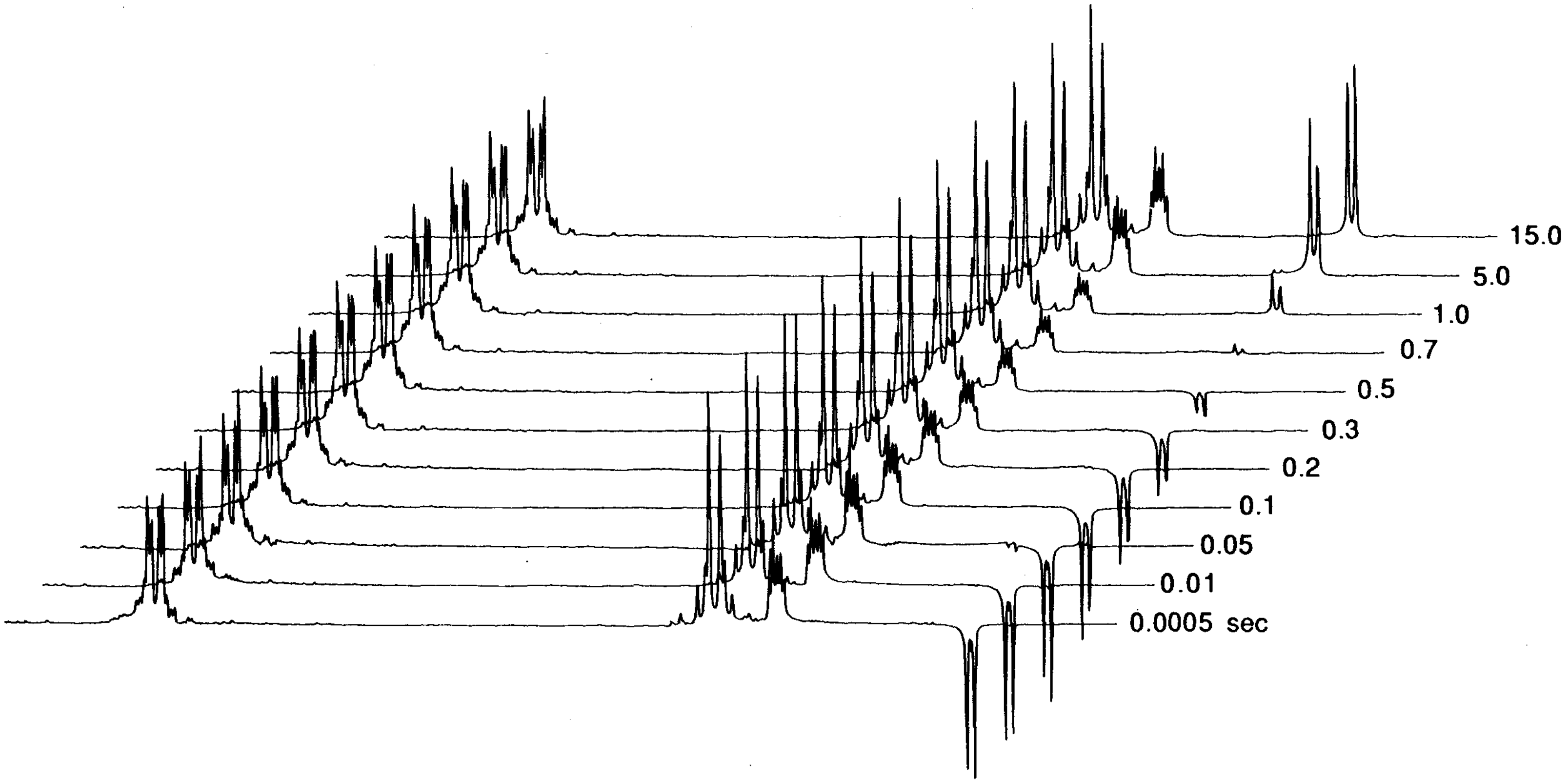

Figure 3-20. Magnetization transfer experiment for **22** obtained at 298.1 K. The numbers beside the spectra correspond to the time delay between the selective inversion of the 5_n proton and aquisition.

Table 3-6. Bridge-Flip Rates Derived From Magnetization Transfer Studies

T, K[a]	k, s^{-1}	T, 5_n[b]	T 5_x[b]
298.1	1.91 ± 0.26	2.76	2.84
308.5	4.16 ± 0.44	3.16	3.22
315.0	6.44 ± 0.65	3.42	3.44

[a] ± 1 K. [b] Obtained from plot of Figure 3-19.

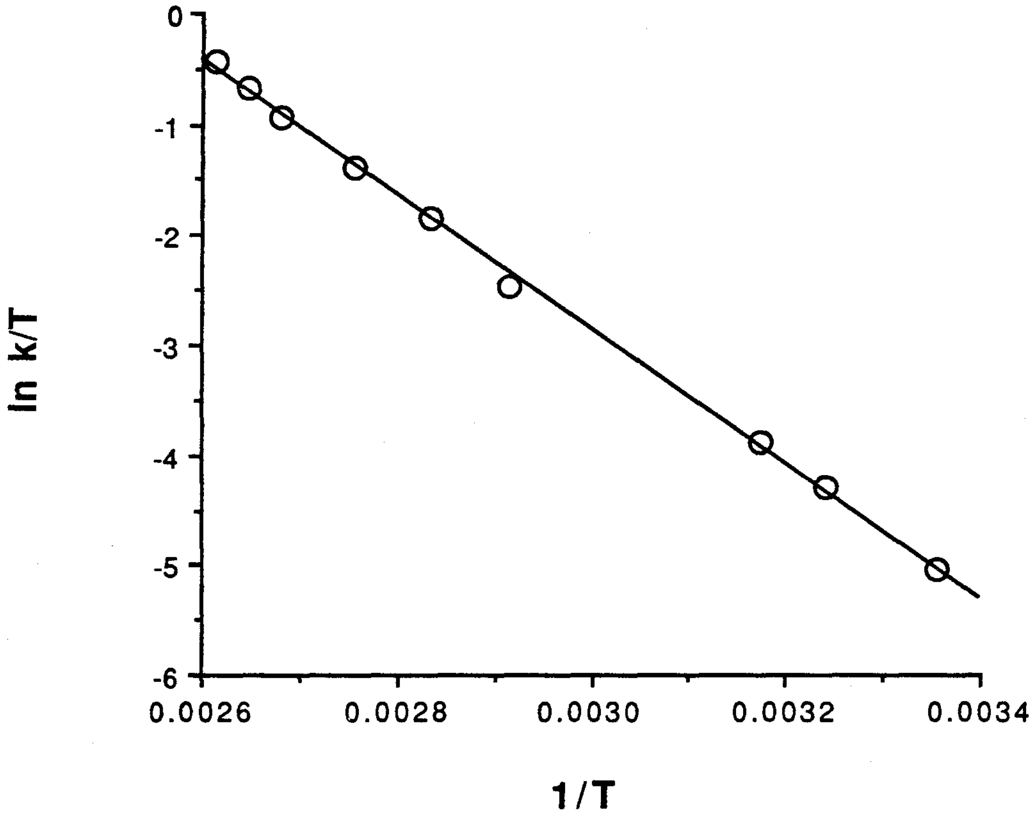

Figure 3-21. Eyring plot for the combined CLS and MT data.

the exchange rate can affect line shape. These factors include $\Delta\nu$, $T2_{eff}$ and the coupling constants. These complications are particularly acute in the region where the exchange rate is slow ($k < 10\ s^{-1}$) and the extent of line broadening is small, because this is where the line shape is *least sensitive* to *k* and *most sensitive* to the other parameters.[41,42] The contribution of these non-rate parameters to the line shape decreases dramatically as the exchange rate increases.[42] Therefore, in accord with the guidelines established by Binsch and Kessler,[41] we have ignored the early regions of the coalescence and have considered only spectra for which the line width is at least 6 times greater than the line width under slow exchange conditions. In this region the line shape is much more sensitive to *k* than any other parameter.

There are also several inherent sources of error that accompany the MT method. The complicating factors include imperfect and non-selective 180° pulses, uncorrectable phasing errors and integration errors. Because of the multiple sources of error, our reported error bars for the MT rates (Table 3-6), represent at least two standard deviations as given by the non-linear least squares fitting routine.

It is generally agreed that, given the possibilities for systematic error in coalescence and magnetization transfer studies, the standard deviations in $\Delta H^\ddagger$ and $\Delta S^\ddagger$ derived from an Eyring plot are inadequate measures of probable error.[40,41] We have adopted the approach suggested by Sandström[47] to obtain more realistic values. This method assumes maximal errors of 10% in rate constants and 1.0 K in temperatures to determine a maximal error in $\Delta G^\ddagger$. It further assumes the error in all points equals the maximum error for deriving errors for $\Delta H^\ddagger$ and $\Delta S^\ddagger$. Using this approach we arrive at the best estimates for activation parameters for the combined analysis listed in Table 3-7.

Table 3-7. Activation Parameters with Estimated Error Limits

$\Delta G^{\ddagger}_{297}$ [a]	$\Delta H^{\ddagger}$ [a]	$\Delta S^{\ddagger}$ [b]
17.1 ± 0.1	12.2 ± 0.6	-16.4 ± 1.5

[a] kcal/mol. [b] cal/mol·K.

Discussion. The derived activation parameters (Table 3-7) indicate that **22** does indeed possess an extremely weak C1-C4 bond. We put an upper limit of *only* 12 kcal/mol on the BDE. Yet, the bicyclopentane is indefinitely long-lived (persistent) at room temperature even though its C1-C4 bond is breaking at a rate of about 2 s^{-1}. Only above 100°C does any noticable decomposition occur.

The 12 kcal/mol bridge-flip barrier is significantly less than the 16 kcal/mol predicted by the qualitative analysis is given above. This results, at least in part, from the ground state destabilization of **22** due to steric repulsions between the phenyls. Simple molecular mechanics calculations[48] suggest that the effect should be worth about 4 kcal/mol, in good agreement with observation.

The value of $\Delta S^{\ddagger}$ (-16.4 eu) for the bridge-flip reaction of **22** is surprisingly large and negative for a unimolecular reaction. For example, the parent, bicyclo[2.1.0.]pentane exhibits an entropy of activation quite typical of a unimolecular process ($\Delta S^{\ddagger}$ = 2.1 eu). Berson and coworkers have also reported on anomalously large, negative $\Delta S^{\ddagger}$ of -16 eu for the thermal decomposition of 5-isopropylidenebicyclo[2.1.0]pentane (**55**).[49] Upon decomposition, **55** gives a mixture of dimers via the triplet biradical **56**. The formally spin-forbidden nature of this process manifests itself in a low

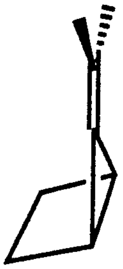

55

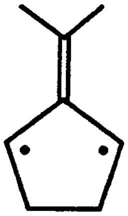

56

probability (*i.e.*, a large negative $\Delta S^{\ddagger}$) of achieving the transition state for bond cleavage. These observations led us, at first, to wonder if ^{3}**20** was involved in the bridge-flip reaction. This was found not to be the case. A survey of the literature reveals that a phenyl substituent α to a bond undergoing homolytic cleavage results in a substantial decrease in $\Delta S^{\ddagger}$ for that process relative to the unsubstituted case[33] (Table 3-8). For example, $\Delta S^{\ddagger}$ for the stereomutation of cis-1,2-diphenylcyclopropane is *ca.* 24 eu[50] *less* than the corresponding value for 1,2-dideuteriocyclopropane.[51] Thus, in order for the delocalizing group to exhibit its stabilizing effect, it must adopt a specific orientation with respect to the breaking bond. As previously mentioned, a very similar effect has been observed in azoalkane thermolyses. There is thus no reason to invoke ^{3}**20**, and we assume that the bridge-flip reaction is spin conservative proceeding through ^{1}**20**.

Several other, more highly substituted, 1,4-diphenylbicyclo-[2.1.0]pentanes (**57**-**60**)[36,52-54] have also been reported to undergo bridge-flip reactions. In all cases, however, the reactions are much slower ($\Delta H^{\ddagger} \geq 25$ kcal/mol) than for **22**. For example, the bridge-flip reaction of **57** gives rise to activation parameters of $\Delta H^{\ddagger} = 26.0$ kcal/mol, $\Delta S^{\ddagger} = -4.2$ eu.[55] The relatively high bond strengths of these compounds most likely originate from steric

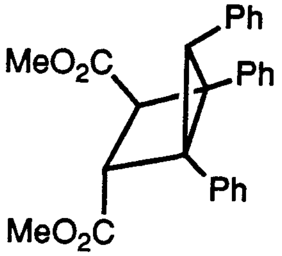

57

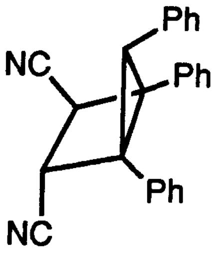

58

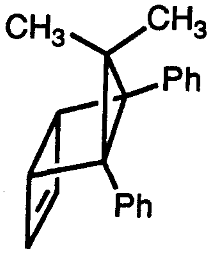

59

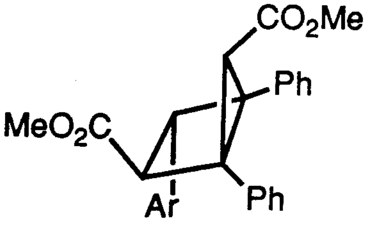

60

Table 3-8. Activation Parameters for Bond Homolysis

	log *A*	E_a	$\Delta\Delta S^{\ddagger a}$	ref.
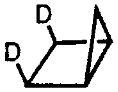	13.9	37.8	—	*b*
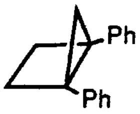	9.7	12.9	-19.2	this work[c]
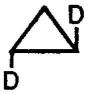	16.4	65.1	—	*d*
	11.2	33.5	-23.8	*e*
	15.6	62.5	—	*f*
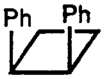	12.9	35.6	-12.3	*g*

a $\Delta S^{\ddagger}$ values computed according to: $\Delta S^{\ddagger} = R(\ln A - 30.4627)$. *b* ref 39a. *c* Obtained from a separate Arrhenius plot. *d* ref 51. *e* ref 50. *f* Doering, W. von E. *Proc. Natl. Acad. Sci. USA* **1981**, *78*, 5279. *g* Jones, G., II; Chow, V. L. *J. Org Chem.* **1974**, *39*, 1447.

constraints which prevent full utilization of benzyl resonance in the transition state for bond cleavage.

Because the bridge-flip process of **22** proved so facile, we decided to attempt the observation of the bridge-flip reaction of the next smaller homolog, 1,3-diphenylbicyclo[1.1.0]butane (**19**). Earlier work by Woodward and Dalrymple on the *exo-exo*-2,4-dicabromethoxy derivative (**61**) of **19** indicated that the activation parameters for its bridge-flip to the *endo,endo* isomer are $\Delta H^{\ddagger}$ = 26 kcal/mol, $\Delta S^{\ddagger}$ = 9 eu.[56] Considering that **22** has a much weaker bond than its substituted derivatives, **19** might also have a weaker bond than **61**. Using the technique of saturation transfer,[57] we estimate that the bridge-flip process can be detected if it is occurring at a rate greater than 0.5 s^{-1}. However, upon decoupling either the endo or the exo signal of **19** at 150°C, we found no intensity decrease of the corresponding multiplet indicating that, if the process is indeed occurring, it is slower than 0.5 s^{-1} at this temperature. Simple thermochemical considerations based on strain energies also indicate that the bridge-flip reaction of **19** should be very slow at 150°C. Cleavage of the strained central bond of a bicyclobutane (SE ≈ 65 kcal/mol)[8] to give a 1,3-cyclobutanediyl (SE ≈ 30 kcal/mol)[58] relieves about 35 kcal/mol of strain. This strain relief upon cleavage is about 15 kcal/mol less than the amount of strain released upon the homolysis of the central bond of bicyclo[2.1.0]pentane.[8] Therefore, if we add this difference to the $\Delta H^{\ddagger}$ observed for **22**, the bridge-flip activation parameters for **19** become $\Delta H^{\ddagger}$ ≈ 27 kcal/mol, $\Delta S^{\ddagger}$ ≈ -16 eu. Thus, at 150°C, the rate constant of the bridge-flip reaction is predicted to be about 1

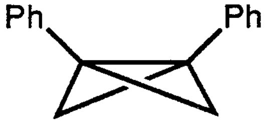

19

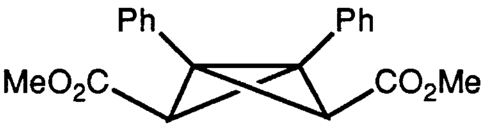

61

$\times 10^{-4}$ s^{-1}, far too slow to be detected by any NMR method. Even if $\Delta S^{\ddagger}$ for this process were near zero, the bridge-flip would still be undetectable by these methods. This discussion serves to underscore the profound differences between the bicyclopentane-cyclopentanediyl and bicyclobutane-cyclobutanediyl systems. The reason for the difference resides in the fact that bicyclobutane, while considerably more strained than bicyclopentane, is unable to relieve as much strain upon a single bond homolysis as bicyclopentane.[8] The converse of this statement may also explain the observed stability differences between ^{3}**24-Ph** and ^{3}**20**, if the decay process of ^{3}**20** can be attributed to ring closure.

Reactivity of 1,4-Diphenylbicyclo[2.1.0]pentane

Reaction With Olefins. Like bicyclo[2.1.0]pentane (**8**),[59] diphenylbicyclopentane **22** reacts with electron-deficient olefins to form 1:1 adducts. When a degassed acetone-d_6 solution of **22** was heated to 60°C for several hours with a 10-fold excess of maleic anhydride, a 1:1 mixture of cycloadducts **62** and **63** were obtained in about 80% yield. In order to confirm the assignment the Diels-Alder adduct of **48** and maleic anhydride, **64**, was reduced with hydrogen to yield a sample of **62** which was identical to that obtained from **22**. The high yield of cycloadducts produced by **22** is in marked contrast to **8** where the corresponding *endo*- and *exo*- cycloadducts comprise only 5% of the product mixture. Bicyclopentane **8** also requires a reaction temperature of 120°C for its reaction with maleic anhydride.

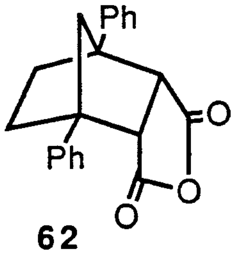

62

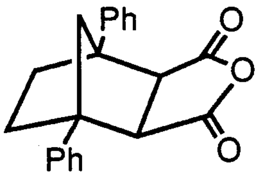

63

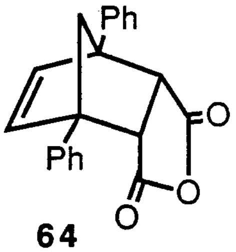

64

Reaction With Oxygen. When air is admitted to solutions of **22**, a rapid and irreversible reaction occurs to give mainly endoperoxide **23** along with a smaller amount of (*ca.* 13%) of hydroperoxide **65**.[60] Such an uncatalyzed oxidation reaction is quite unusual for a closed-shell organic

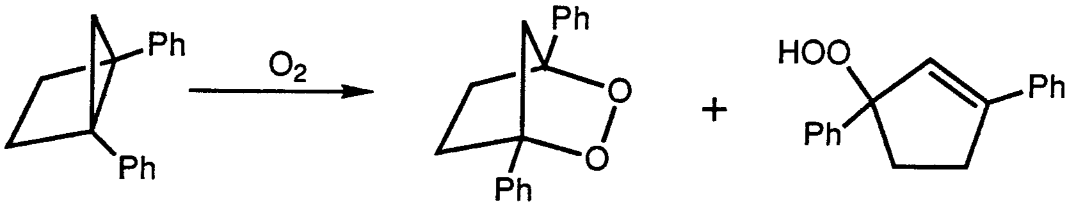

22 **23** **65**

molecule. However, as discussed above, 1,4-diphenybicyclopentane is not an ordinary organic molecule. Its C1-C4 bond is breaking and reforming quite rapidly at room temperature. This led us to wonder if this oxidation reaction might involve trapping of the singlet biradical **^{1}20** with oxygen. Herein, we report the results of our investigation into this reaction. Also discussed, are the results of a more detailed analysis of the O_2-trapping reaction performed by Adam and Wirz.[20] Their data, combined with our activation parameters obtained for the bridge-flip reaction, result in the development of a detailed model of the kinetic and thermodynamic relationships among **22**, **^{1}20** and **^{3}20** .

Shown in Scheme 3-2 is a probable biradical mechanism by which oxidation products **23** and **65** could arise from **22**. If the singlet biradical (**^{1}20**) is assumed to be a steady-state intermediate such that

$$[^{1}\mathbf{20}] = \frac{k_1[\mathbf{22}]}{k_{-1} + k_2[\mathrm{O_2}]}, \tag{3-3}$$

the rate of bicyclopentane and oxygen consumption can be described by

$$-\frac{d[\mathbf{22}]}{dt} = -\frac{d[\mathrm{O_2}]}{dt} = k_2[^{1}\mathbf{20}][\mathrm{O_2}] = \frac{k_1 k_2[\mathbf{22}][\mathrm{O_2}]}{k_{-1} + k_2[\mathrm{O_2}]}\ . \tag{3-4}$$

Two limiting cases may now be envisioned. First, if the trapping step is much faster than reclosure of the singlet biradical ($k_2[O_2] >> k_{-1}$), equation 3-4 reduces to

$$-\frac{d[\mathbf{22}]}{dt} = k_1[\mathbf{22}], \tag{3-5}$$

In this case the reaction is first-order in bicyclobutane and the trapping rate is equal to the rate of bond breaking. In contrast, a second-order reaction occurs

Scheme 3-2

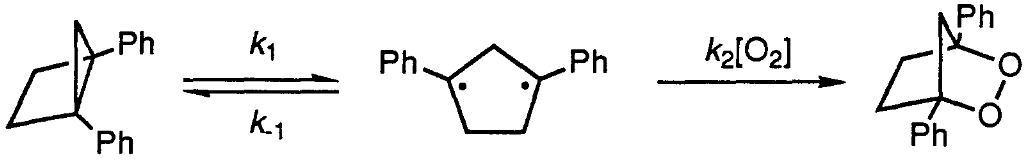

22 **20** **23**

if $k_{-1} >> k_2[O_2]$ $-d[\mathbf{22}]/dt = k_1k_2[\mathbf{22}][O_2]/k_{-1} = Kk_2[\mathbf{22}][O_2] = k_{obs}[O_2]$

if $k_{-1} << k_2[O_2]$ $-d[\mathbf{22}]/dt = k_1[\mathbf{22}]$

for the opposite situation where the rate of singlet biradical closure is much faster than the trapping rate ($k_{-1} >> k_2[O_2]$). Noting that the equilibrium constant (K) between 22 and ^{1}20 is simply k_1/k_{-1}, the rate expression becomes

$$-\frac{d[22]}{dt} = \frac{k_1 k_2[22][O_2]}{k_{-1}} = K k_2[22][O_2]. \qquad (3\text{-}6)$$

Thus, the two scenarios are quite distinct. Described below are two simple experiments we performed to differentiate between the two possibilities for this oxidation reaction.

The first experiment involves introducing oxygen into a cold (-78°C) CD_2Cl_2 solution of the bicyclopentane and then monitoring its disappearance as the solution is allowed to warm. If the reaction rate is governed by ring-opening (eq 3-5), we estimate (using the activation parameters determined for the bridge-flip reaction) that the half-life of the bicyclopentane would be about 30 min at -60°C. We found, however, that upon warming the oxygenated solution to -60°C no reaction occurred. Not until the solution was warmed to -10°C was the oxidation reaction observed to occur at a reasonable rate (k ~ 10^{-4} s^{-1}). At -10°C the C1-C4 bond is breaking at a rate near 0.1 s^{-1}, thus, each ring opening reaction does not lead to trapping. To confirm this result we performed a second experiment where we monitored the kinetics of the reaction at -10°C. Shown in Figure 3-22 is the plot of the disappearance of 22 according to the first-order rate law. The pronounced curvature of the plot indicates that the rate of the oxidation reaction does not depend on the [22] alone and it appears that the rate of oxidation is also dependent on $[O_2]$ (eq 3-6). When studying the kinetics of a second-order reaction, it is often desirable to do so under pseudo first-order conditions, where one of the reactants is present in large excess and the concentration of the other reactant is

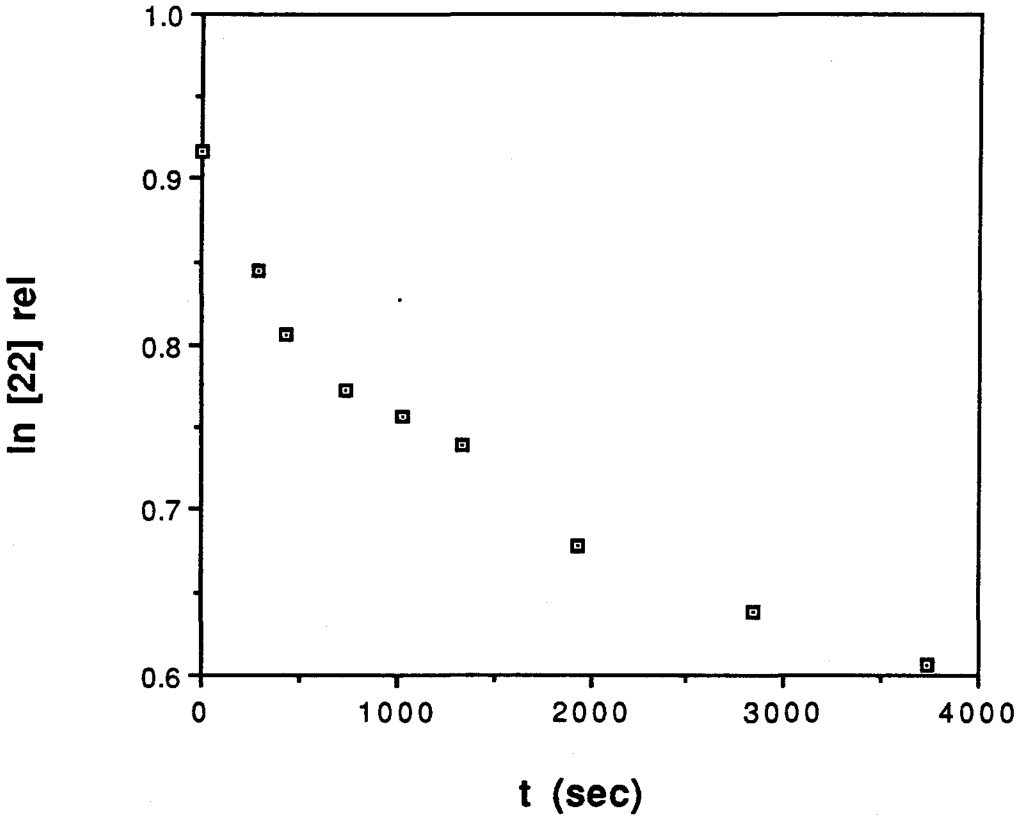

Figure 3-22. Plot of ln[22] vs. t(sec) for the reaction between **22** and oxygen at −10 °C in CD_2Cl_2 solution.

monitored as a function of time. In the present case, where we monitor the concentration of **22** by ^{1}H NMR, this is virtually impossible because we are limited by the solubility of oxygen (*ca.* 10 mM)[61] in organic solutions. We therefore discontinued our investigation of the kinetics of this oxidation reaction. Of course, the other approach to this problem would involve using an excess of **22** and monitoring the oxygen concentration with time.

Concurrent with our study of **22**, Adam and Wirz had undertaken a detailed study of the oxidation of **22** to **23**.[20] Their study was performed under pseudo first-order conditions where **22** was present in excess. The lifetime of triplet tetracene, τ_{tet}, was used as an indicator of the concentration of oxygen. They found that τ_{tet} increased exponentially with time. The slope of the $\ln(\tau_{tet})$ vs time plot gave the pseudo first-order rate constant, $^1k_{obs}$, where $^1k_{obs} = K\ k_2\ [\mathbf{22}]$. Using these observed rate constants, and calculated rate-constants for the diffusion of oxygen, they were able to calculate the equilibrium constant (K) between **22** and ^{1}**20** at three different temperatures. A van't Hoff plot of the data produces $\Delta H = 10.9$ kcal/mol, $\Delta S = -9.8$ eu and $\Delta G_{297} = 13.7 \pm 0.1$ kcal/mol. Comparing this free energy difference with the free energy of activation of the bridge-flip process $\Delta G^{\ddagger}{}_{297} = 16.7 \pm 0.1$ kcal/mol,[62] suggests that the singlet biradical resides in a 3.0 kcal/mol free energy well, implying a singlet biradical lifetime of *ca.* 25 ps. Viewed alternatively, the activation parameters for ring closure of the singlet biradical are *ca.* $\Delta H^{\ddagger} = 1.3 \pm 1.0$ kcal/mol, $\Delta S^{\ddagger} = -6 \pm 2$ eu. Note that the activation barriers for the cyclization of the singlet biradical should be considered as lower limits because the rate constant for oxygen trapping of **22**, k_2, represents the upper limit of diffusion control.[20] For example, if the trapping rate constant is an order of magnitude slower than diffusion, ΔG_{297} drops from 13.7 to 12.4 kcal/mol, increasing the well depth to 4.3 kcal/mol. The kinetic and thermodynamic parameters derived from this combined analysis are summarized in Figure 3-23. It is worth emphasizing that this model predicts the singlet biradical, ^{1}**20**, to be a true intermediate on the potential energy surface. Furthermore, these findings are also consistent with the conclusions we have drawn for stabilized cyclobutanediyls **24** (Figure 2-22). This is in marked contrast to the prototypical 1,3-biradical, trimethylene (**5**), for which no minimum is indicated by theory or experiment.[63] As mentioned in Chapter 2, this singlet minimum is the result of selective stabilization of the planar biradical by delocalization into the phenyl rings.

It may at first seem surprising that we are invoking the trapping of a singlet biradical with oxygen, because virtually all examples of biradical trapping with oxygen involve the triplet state of the biradical.[64] This is not a consequence of a "spin allowed" triplet-triplet interaction, but rather, it is due to the long lifetime of triplet biradicals relative to singlets. That is, many triplet biradicals live long enough in solution to experience many diffusional encounters with oxygen, whereas most singlet biradicals do not. However, exceptionally long lived singlet biradicals can and do react with oxygen in solution. For example, 3,4-dimethylenefuran **66**,[65] a non-Kekulé molecule which has an intrinsic lifetime of about 3-4 µs in solution, reacts rapidly with oxygen to form peroxide **67**. Singlet 1,4-perinaphthadiyl **68**,[66] which has a

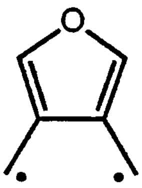

66

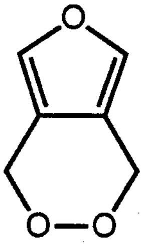

67

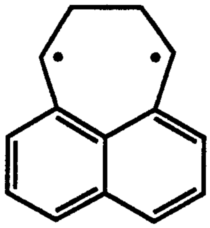

68

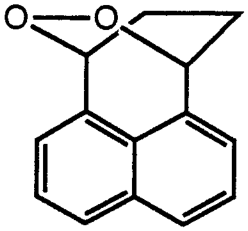

69

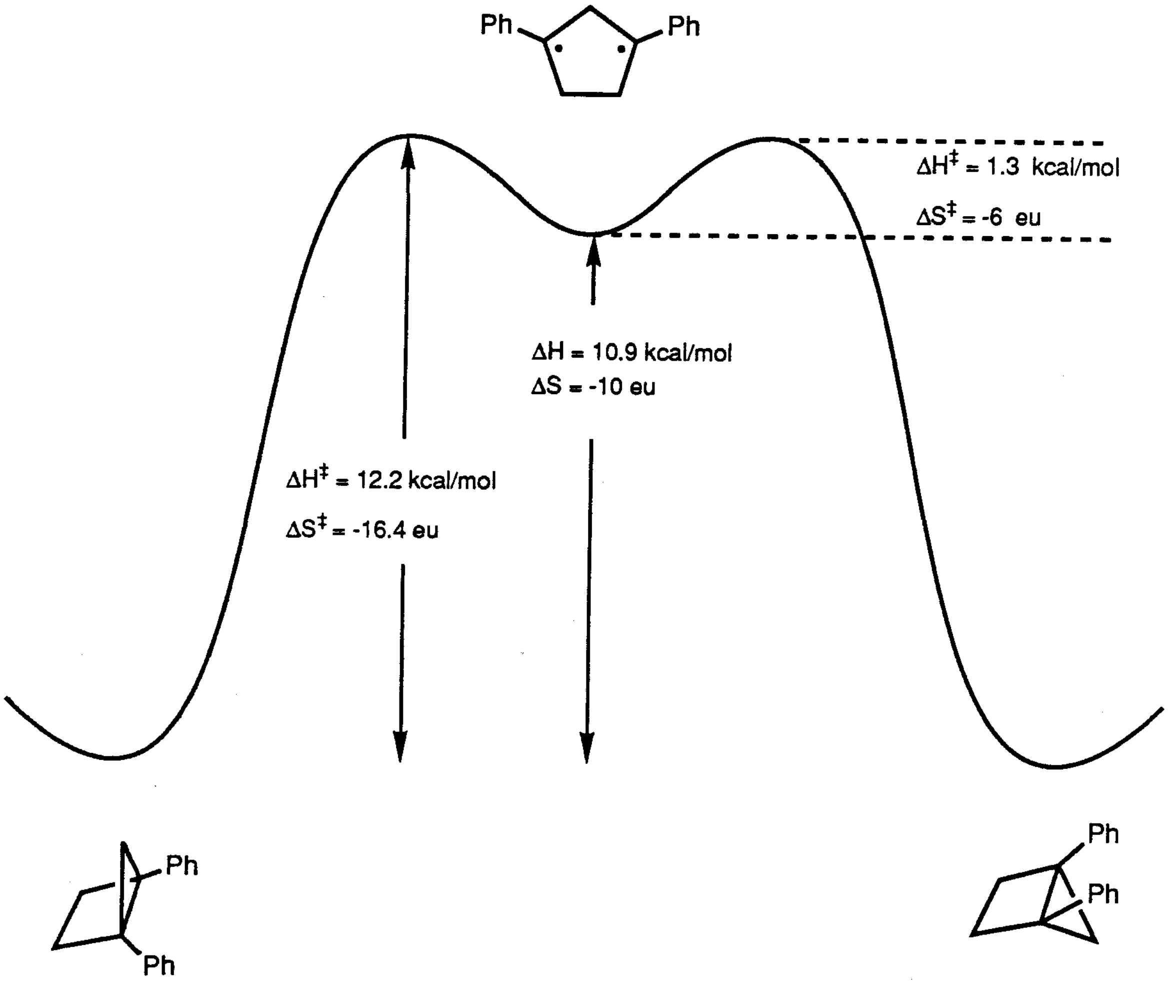

Figure 3-23. Potential energy diagram for the bridge-flip reaction of 22.

lifetime of about 1 ns at room temperature, also reacts with oxygen to give about a 50% yield of endoperoxide **69** in competition with cleavage and closure products.

The trapping of ^{1}**20** with triplet oxygen takes place in a stepwise fashion. A logical candidate for a reactive intermediate of such a reaction is triplet biradical **70**.[64] Rapid ISC from ^{3}**70** produces the singlet biradical ^{1}**70** which can either collapse to the endoperoxide or abstract a hydrogen to form the hydroperoxide **65**.

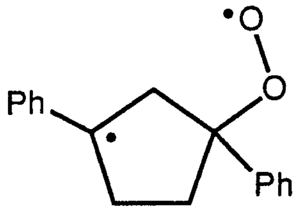

70

The unusual feature about the oxygen trapping reaction of ^{1}**20** is that even though it does not have an exceptionally long singlet lifetime (we estimate that an upper limit of the lifetime is 0.3 ns),[67] the trapping reaction is virtually quantitative. The reason for this behavior is obvious -- unlike all other singlet biradicals which decay irreversibly, **20** decays to bicyclopentane **22** which regenerates the biradical at a rate near 2 s^{-1} at room temperature. Therefore, even though only a small fraction of the available biradical is trapped at any given time, the constant regeneration of ^{1}**20** ensures that the reaction will eventually go to completion.

Although the experimental details of the oxidation reaction of **22** to **23** are consistent with the biradical mechanism discussed above, a second mechanism that involves the direct addition of oxygen across the strained central bond of **22** warrants discussion. This second-order reaction is strictly analogous to the addition of olefins across the strained bonds of bicyclopentanes and bicyclobutanes. This would be quite an unusual reaction, but again, the very weak bond of **22** makes it a very unusual molecule, and at this time we cannot rule out this alternative mechanism. Recall, however, from Chapter 2 that 1,3-diphenylbicyclo[1.1.0]butane (**19**) also undergoes an oxidation reaction to give epoxyketone **26**. A logical precursor to **26** was shown to be the endoperoxide **27**. We may now ask the question -- how does **19** react with oxygen to give **27**? First, let us examine the biradical mechanism. We

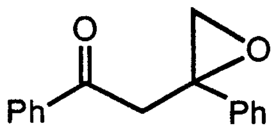

26

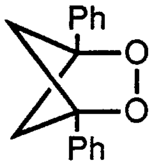

27

know that the C1-C3 bond strength of **19** is at least 27 kcal/mol and therefore predict that the pseudo first-order rate constant ($^1k_{obs}$, $= k_1 k_2 [\mathbf{19}]/k_{-1}$) will be *ca.* 10^{-8} s^{-1} [68] assuming [**19**] = 1M. This compares to the corresponding value for **22** of 0.2 s^{-1}. The oxidation reaction of **19** is observed to be only 10 to 100 times slower than the oxidation of **22** so it seems highly unlikely that the oxidation of **19** proceeds via the singlet biradical ^{1}**24-Ph.** At this point it would be very appealing to say that the oxidation of **19** proceeds via the direct addition of oxygen to the strained bond. At this time, however, we do not have enough data (endoperoxide **27** is only a presumed intermediate) to support such an alternative mechanism. The purpose of this discussion is simply to acknowledge that one can envision alternative mechanisms for these strained-hydrocarbon oxidations which merit consideration.

In a related investigation, Adam and Wirz have undertaken a study of the solution-phase lifetimes of ^{1}**20** and ^{3}**20** by using time-resolved laser flash spectroscopy.[69] Consistent with the above findings regarding the short lifetime of ^{1}**20**, they observed no transient absorptions upon direct excitation of diazene **21**. This indicates that the lifetime of ^{1}**20** is less than 25 ns under these conditions. However, upon benzophenone sensitized photolysis in CH_3CN, they observed a transient absorption with a lifetime of 25 µs which was attributed to ^{3}**20**.[69] In agreement with the results we have obtained, they find that the sole product of the direct and sensitized photolyses is bicyclopentane **22**. This implies that, in solution, the triplet biradical (^{3}**20**) makes a jump from the triplet to the singlet surface on the path to product formation.

Thus, with the lifetime data of ^{3}**20** in hand, and knowledge of an S-T surface crossing on the path to **22**, we can now postulate how the entire potential energy surface (^{1}**20**, ^{3}**20** , **22**) might appear. The first issue to address is the S-T gap. Unlike non-Kekulé molecules, where the S-T gap may be several kcal/mol,[70] localized biradicals have S-T gaps on the order of one kcal/mol. In fact, the calculated S-T gap for the parent, 1,3-cyclopentanediyl (**6**) is only 0.9 kcal/mol.[15] Because of the decreased spin density at the ring carbons of **20** relative to **6**, the exchange repulsions will also decrease.[16,31] This leads to a decrease in the S-T gap. Therefore, we estimate that the S-T gap of **20** is near 0.5 kcal/mol at the planar geometry.

We will now turn our attention to the activation parameters of ^{3}**20** decay in solution. A 25 µs lifetime of ^{3}**20** implies a free energy of activation for the spin-forbidden ring closure of $\Delta G^{\ddagger}_{297} = 11.7$ kcal/mol. Shown in Table 3-9 are several combinations of $\Delta H^{\ddagger}$ and $\Delta S^{\ddagger}$ that can give rise to this $\Delta G^{\ddagger}$. Also shown are the corresponding log *A* values for comparison purposes. We are now in a position to construct a composite potential energy diagram (Figures 3-24).[71] With an enthalpic barrier of 1.3 ± 1.0 kcal/mol to singlet biradical

Table 3-9. Combinations of Possible Activation Parameters for the Decay of ^{3}**20** in CH_3CN Solution at 297 K

$\Delta H^{\ddagger}$ [a]	$\Delta S^{\ddagger}$ [a]	log *A* [b]
1.0	-36.0	5.4
1.5	-34.3	5.7
2.0	-32.7	6.1
2.5	-31.0	6.5
3.0	-29.3	6.8
3.5	-27.6	7.2
4.0	-25.9	7.6
4.5	-24.2	7.9
5.0	-22.6	8.3

[a] kcal/mol. [b] cal/mol·K.

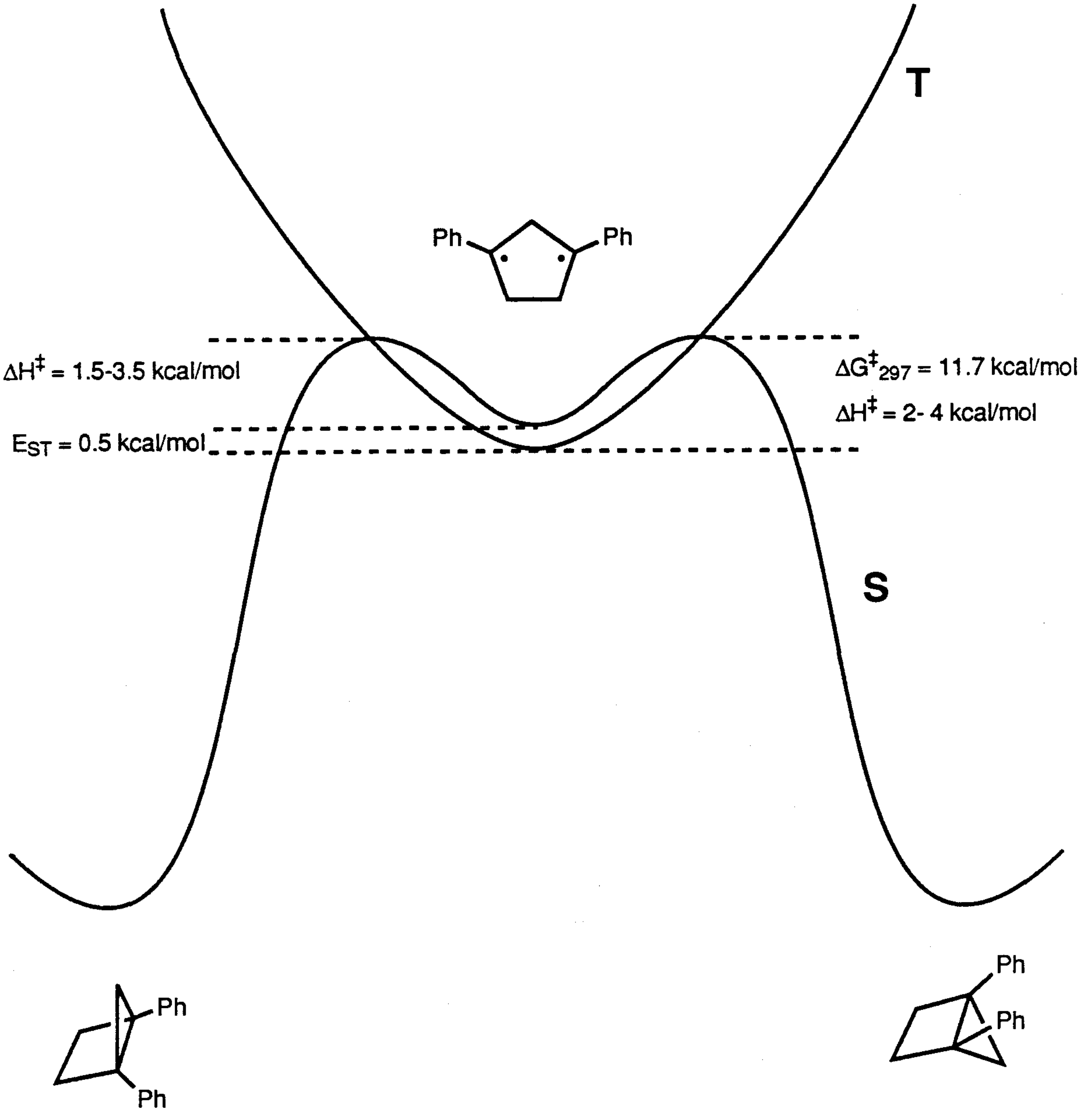

Figure 3-24. Postulated potential energy diagram describing the kinetic and thermodynamic relationships among ^{1}**20**, ^{3}**20** and **22**.

closure and a 0.5 kcal/mol S-T gap, the maximum enthalpic barrier to an S-T crossing point that ^{3}**20** could encounter is *ca.* 2 kcal/mol. This value seems low, especially when compared to the much less stable parent compound ^{3}**6**, which is reported to encounter a barrier of 2.3 kcal/mol to the S-T crossing point. Recall, however, that the enthalpic barrier to singlet closure determined from the oxygen trapping results represents a lower limit. Given this, and possible errors in the activation parameters for the bridge-flip reaction, we feel that it is best to report the enthalpic barrier to triplet reaction as being somewhere between 2 and 4 kcal/mol. Such barriers correspond to entropies of activation that range from -26 to -33 eu. Because the activation parameters for most spin forbidden reactions are reported in terms of E_a and log A, it is convenient to view the entropic barriers in terms of log A. As shown in Table 3-9, the log A values that correspond to the enthalpic barriers range from 6.1 to 7.6. Comparing these values to those listed in Table 2-7 reveal that they are in very good agreement with those of other spin-forbidden thermal reactions and the log A value of 7.8 determined for the ring closure reaction of ^{3}**24-Ph** (Chapter 2). We thus feel that the potential energy diagram of Figure 3-24 is quite realistic.

Conclusion

Triplet 1,3-diphenylcyclopentanediyl **20** has proven to be a remarkably stable localized biradical. Strong triplet EPR signals of the biradical can be generated even at 77 K. This represents a great increase in stability relative to its four-membered ring analog 1,3-diphenylcyclobutanediyl (**^{3}24-Ph**) which is only marginally observable at a temperature of 60 K. Tetradeuterodiyl **^{3}20-d_4** is even more persistent than **^{3}20**. Strong triplet EPR signals of **^{3}20-d_4** persist even after five days at 77 K. The stability of **^{3}20-d_4** may be a result of the poorer hyperconjugative ability of the C2 CD_2 group relative to a CH_2 group at the same position.

1,4-Diphenylbicyclo[2.1.0]pentane (**22**), the closed-shell isomer of **20**, possesses a very weak C1-C4 bond. At room temperature, this bond is breaking and reforming at a rate of about 2 s^{-1}. Through a combination of ^{1}H NMR complete lineshape analysis and magnetization transfer studies of the degenerate bridge-flip reaction, we have placed an upper limit of only 12 kcal/mol on the C1-C4 bond dissociation energy of **22**.

In the presence of oxygen, **22** undergoes a rapid second-order reaction to predominantly give endoperoxide **23** via the singlet biradical (**^{1}20**). Using the activation parameters determined for the bridge-flip reaction along with data concerning the oxygen trapping reaction[20] and the solution-phase lifetime of **^{3}20**,[69] we have developed a fairly detailed model to describe the kinetic and thermodynamic relationships among **^{1}20**, **^{3}20** and **22**. This model, which could not have been developed if the C1-C4 bond weren't so weak, predicts the singlet biradical **^{1}20** to be a true intermediate that resides in an enthalpic well of 1.5-3.5 kcal/mol.

Experimental

General. Fourier transform NMR spectra (^1H and ^{13}C) were obtained on a JEOL GX-400 or Varian XL-200 spectrometer. An INEPT pulse sequence[72] was employed to determine carbon-hydrogen coupling constants. Ultraviolet spectra were recorded on a Hewlett-Packard 8451A diode array spectrophotometer. Mass spectra were obtained at the University of California, Riverside Analytical Facility. Analytical gas chromatography was performed on a Hewlett-Packard 5890 chromatograph equipped with a flame ionization detector. Melting points are uncorrected.

Tetrahydrofuran was distilled from benzophenone ketyl prior to use. All other solvents were reagent grade or better and used as purchased unless otherwise noted. Column chromatography was performed by the method of Still[72] employing 230-400 mesh silica gel.

NMR solvents employed in the studies of **21** and/or **22** were purified as described below. Deuterochloroform and methylene chloride-d_2 were vacuum transferred from CaH_2. Benzene-d_6 and toluene-d_8 were vacuum transferred from sodium benzophenone ketyl. All other NMR solvents were used as supplied after drying over 4A sieves.

1,4-Diphenylcyclopentadiene (48). Diene **48**[74] was prepared according to the method of Cohen *et.al.*[5] ^1H NMR ($CDCl_3$) δ 3.78 (t, 2 H, $J = 1$ Hz), 6.92 (t, 2 H, $J = 1$ Hz), 7.30 (m, 6 H), 7.60 (m, 4 H); UV (hexane) λ_{max} 239, 350 nm; mp 158-159°C.

1,4-Diphenyl-2,2,5,5-tetradeuterocyclopentadiene (48-*d₄*). To 160 mg (0.73 mmol) of **48** suspended in 10 mL of a 1:1 hexane/benzene solution was added benzyltriethylammonium chloride (10 mg, 0.044 mmol). To the suspension were added 4.5 mL of a 5 N NaOD solution. The resulting two-phase solution allowed to stir for 40 h. After removal of the aqueous solution, the organic solution was washed with D_2O (2 x 5 mL), then dried over $MgSO_4$. The crude material was purified by column chromatography (15% benzene/ethyl acetate) to yield 83 mg (51%) of a slightly yellow crystalline solid. ^1H NMR analysis revealed that the deuterium incorporation was greater than 95%. ^2H NMR (CH_2Cl_2) δ 3.76, 6.96; mass spectrum (EI) *m/e* 222.

1,7-Diphenyl-2,4,6-triazatricyclo[5.2.1.0^{2,6}]dec-8-ene-3,5-dione (49). To a suspension of diene **48** (200 mg, 0.92 mmol) in 100 mL of hexane was added an ethereal MTAD solution (105 mg, 0.93 mmol, in 40 mL of ether) until the pink color persisted. The solvent was then removed to leave a white solid that was either used immediately or stored at -25°C. ^1H NMR ($CDCl_3$) δ 2.12 (d, 1 H, J = 9 Hz), 2.55 (d, 1 H, J = 9 Hz), 3.93 (s, 3 H), 6.72 (s, 2 H), 7.42 (m, 6 H), 7.70 (m, 4 H).

1,7-Diphenyl-2,4,6-triazatricyclo[5.2.1.0^{2,6}]decane-3,5-dione (50). To a solution of olefin **49** (200 mg, 0.060 mmol) in 10 mL of an ice-cold ethyl acetate solution (made from 15 mL ethyl acetate and 10 drops of glacial acetic acid) were added 50 mg of 5% Rh/Al_2O_3. The solution was then subjected to 45 psi of hydrogen gas for 30 min while shaking. The reaction mixture was then filtered through celite and concentrated to leave a colorless oil. The crude material was purifed by column chromotagraphy (7:3 benzene/ethyl acetate)to afford 136 mg (67% from **48**) of a white crystalline solid. ^1H NMR ($CDCl_3$) δ 2.35 (d, 1 H, J = 10.5 Hz), 2.39 (m, 2 H), 2.65 (m, 2 H), 2.93 (dt, 1 H, J = 10.5, 2.7 Hz), 3.01 (s, 3 H), 7.40 (m, 6 H), 7.60 (m, 4 H); ^{13}C NMR ($CDCl_3$) δ 25.38 (q, $^1J_{CH}$ = 141.6 Hz), 31.54 (t, $^1J_{CH}$ = 133.9 Hz), 56.38 (tt, ${}^1J_{CH}$ = 140.1 Hz, ${}^3J_{CH}$ = 5.9 Hz), 73.78 (s), 126.79 (d, ${}^1J_{CH}$ = 160.7 Hz), 128.45 (d, ${}^1J_{CH}$ = 159.9 Hz), 128.50 (d, ${}^1J_{CH}$ = 159.9 Hz), 135.06 (s), 156.15 (s); mass spectrum (EI) *m/e* 333, 220, 219 (100), 141, 91; exact mass calcd for $C_{20}H_{19}N_3O_2$ 333.1477, found 333.1480.

Semicarbazide 51. To a 10 mL flask containing **50** (47 mg, 0.14 mmol) were added *ca.* 70 mg of freshly-crushed KOH and 3 mL of degassed 2-propanol. The contents of the flask were brought to reflux under an argon atmosphere for 1 h. The cooled solution was then acidified by dropwise addition of 3 N HCl until CO_2 evolution ceased (*ca.* 300 µL). The solution was then neutralized by dropwise addition of degassed 1 N NH_3. Degassed water was then added to dissolve the salts followed by extraction of the solution with two 4 mL portions of CH_2Cl_2 (distilled from CaH_2). The organic solution was dried over $MgSO_4$ then concentrated to afford a yellow solid. The crude solid was purified by column chromatography (ether) to afford 38 mg (88%) of a white crystalline solid. ${}^1H$ NMR ($CDCl_3$) δ 2.04 (m, 1 H), 2.14 (m, 2 H), 2.43 (m, 1 H), 2.44 (dt, 1 H, J = 10.5, 2.5 Hz), 2.48 (d, 1 H, J = 10.5 Hz), 2.60 (m, 1 H), 2.76 (d, 3 H, J = 5.1 Hz), 4.43 (bs, 1 H), 6.4 (bs, 1 H), 7.40 (m, 10 H); mass spectrum (EI) *m/e* 307 (219 (100), 202, 115, 91; exact mass calcd for $C_{19}H_{21}N_3O$ 307.1685, found 307.1669.

1,4-Diphenyl-2,3,-diazabicyclo[2.2.1]hept-2-ene (21). To a 10 mL two-necked oven-dried flask was fitted with an addition ampule charged with 120 mg (*ca.* 0.55 mmol of active oxident) of nickel peroxide.[9b] The atmosphere was replaced with argon then **51** (15 mg, 0.044 mmol) in 3.5 mL of CH_2Cl_2 (distilled from CaH_2) was added via syringe. After the solution was cooled to 0°C, the contents of the ampule were added over 1 min. After stirring for 30 min, the cold slurry was transferred via a teflon cannula to a precooled (0°C) filtration frit and vacuum filtered into a cold (-50°C) receiving flask. The solvent was removed under high vacuum at -50°C to leave a white crystalline solid. ^{1}H NMR ($CDCl_3$, -15°C) δ 1.59 (m, 2 H), 1.80 (dt, 1 H, J = 10.5, 2.4 Hz), 2.06 (d, 1 H, J = 10.5 Hz), 2.09 (m, 2 H), 7.45 (m, 6 H), 7.68 (m, 4 H); ^{13}C NMR ($CDCl_3$, -15°C) δ 30.,21 (t, $^1J_{CH}$ = 137.9 Hz), 48.51 (tt, $^1J_{CH}$ = 136.1 Hz, $^3J_{CH}$ = 5.5 Hz), 91.32 (s), 126.77 (d, $^1J_{CH}$ = 160.7 Hz), 127.97 (d, $^1J_{CH}$ = 161.4 Hz), 128.67 (d, $^1J_{CH}$ = 159.5 hz), 137.95 (s); UV (MTHF) λ_{max} = 350 nm.

1,4-Diphenylbicyclo[2.1.0]pentane (22). Gentle thermolysis (60°C) of a degassed $CDCl_3$ solution of diazene **21** over a period of 1 h cleanly produced the bicyclobutane in quantitative yield. ^{1}H NMR ($CDCl_3$) δ 1.63 (d, 1 H, J = 4.64 Hz), 1.86 (dt, 1 H, J = 4.64, 1.96 Hz), 1.92 (m, 2 H), 2.58 (m, 2 H), 7.09 (m, 6 H), 7.20 (m, 4 H); ^{13}C NMR ($CDCl_3$) δ 26.11, 29.24, 38.14, 125.55, 127.03, 128.07, 140.88.

2,3-Dioxa-1,4-diphenylbicyclo[2.2.1]heptane (23). Through a $CDCl_3$ solution of bicyclopentane **22** was bubbled oxygen for 5 min. Analysis by ^{1}H NMR immediately after this treatment revealed that all of the bicyclopentane had been consumed and had been replaced predominantly (*ca.* 90%) by endoperoxide **23**. ^{1}H NMR ($CDCl_3$) δ 2.37 (m, 2 H), 2.58 (m, 2 H), 2.73 (d, 1 H, J = 10.3 Hz), 2.89 (dt, 1 H, J = 10.3, 2.6 Hz), 7.36 (m, 6 H), 7.49 (m, 4 H). A spectrum obtained in C_6D_6 agrees very well with the values reported by Salomon.[75] (C_6D_6) δ 1.89 (m, 2 H), 2.15 (d, 1 H, J = 10.3 Hz), 2.38 (m, 2 H), 2.63 (dt, 1 H, J = 10.3, 2.6 Hz), 7.12 (m, 6 H), 7.38 (m, 4 H); mass spectrum (NH_3 CI) *m/e* 253, 237, 222, 105 (100), 91, 77, exact mass calcd for $C_{17}H_{17}O_2$

253.1229, found 253.1240. The spectrum also contained a small amount (*ca.* 13%) of hydroperoxide **65**. ^{1}H NMR (CD_2Cl_2) δ 3.08 (m, 2 H), 3.29 (m, 2 H), 6.21 (m, 1 H), 7.45 (m, 10 H).

***exo,exo*-8,9-Dideutero-1,7-diphenyl-2,4,6-triazatricyclo-[5.2.1.0^{2,6}]decane-3,5-dione (50-*d*$_2$).** To a solution of olefin **49** (53 mg, 0.16 mmol) in 4.5 mL of ice-cold ethyl acetate were added 30 mg of 5% palladium-on-carbon. After replacing the atmosphere with nitrogen, the vessel was charged with 40 psi of deuterium gas. After stirring for 30 min, the slurry was vacuum filtered through a pad of celite and the resulting solution concentrated to leave a colorless oil. The oil was purified by column chromatography (7:3 benzene/ethyl acetate) to afford 36 mg (68% from **48**) of a white crystalline solid. ^{1}H NMR analysis revealed that the deuterium was incorporated at the *exo* positions and that the extent of deuteration was 94 ±2%. ^{1}H NMR ($CDCl_3$) δ 2.35 (d, 1 H, J = 10.5 Hz), 2.36 (bs, 2 H), 2.93 (dt, 1 H, J = 10.5, 2.7 Hz), 3.01 (s, 3 H), 7.40 (m, 6 H), 7.60 (m, 4 H); mass spectrum (EI) *m/e* 335, 221 (100), 92, exact mass calcd. for $C_{20}H_{17}D_2N_3O_2$ 335.1603, found 335.1593.

Semicarbazide 51-*d*$_2$. The dideuterosemicarbazide **51**-*d*$_2$ was prepared in the same manner at **51**. Mass spectrum (EI) *m/e* 309, 221 (100), 143, 119, 92; exact mass calcd. for $C_{19}H_{19}D_2N_3O_2$ 309.1810, found 309.1809.

2,3-Diaza-*exo,exo*-5,6-dideutero-1,4-diphenylbicyclo[2.2.1]hept-2-ene (21-*d*$_2$). Dideuterodiazene **21**-*d*$_2$ was prepared in the same manner as **21**. UV (MTHF) λ_{max} = 350.

2,4,6-Triaza-1,7-diphenyl-*endo,endo*-8,9,10,10-tetradeuterotricyclo[5.2.1.0^{2,6}]decane-3,5-dione (50-*d₄*). Starting with 48-d_4, tetradeuterourazole 50-d_4, was prepared in the same manner as **50**. ^{1}H NMR ($CDCl_3$) δ 2.63 (bs, 2 H), 3.01 (s, 3 H), 7.40 (m, 6 H), 7.60 (m, 4 H); ^{13}C NMR ($CDCl_3$) δ 25.37, 31.14 (t, J_{CD} = 20 Hz), 73.61, 126.81, 128.44, 129.50, 135.08, 156.18.

Semicarbazide 51-*d₄*. Tetradeuterosemicarbazide 51-d_4 was prepared in the same manner as **51**. Mass spectrum (EI) *m/e* 311, 222 (100), 205, 144, 121, 92; exact mass calcd for $C_{19}H_{17}D_4N_3O$ 311.1936, found 311.1938.

2,3-Diaza-1,4-diphenyl-*endo,endo*-5,6,7,7-tetradeuterobicyclo-[2.2.1]hept-2-ene (21-*d₄*). Tetradeuterodiazene 21-d_4 was prepared in the same manner as **21**. ^{1}H NMR ($CDCl_3$) δ 2.06 (bs, 2 H), 7.45 (m, 6 H), 7.68 (m, 4 H); UV (MTHF) λ_{max} = 350 nm.

1,3-Diphenylcyclopentene (52). A C_6D_6 solution of **21** in a sealed NMR tube was heated to 140°C for 10 min. Upon cooling to room temperature, high-field ^{1}H NMR analysis revealed that the sample had partially (*ca.* 35%) decomposed to **52**. ^{1}H NMR ($CDCl_3$) 1.90 (m, 1 H), 2.56 (m, 1 H), 2.80 (m, 1 H), 2.87 (m, 1 H), 4.06 (m, 1H), 6.21 (m, 1H), 7.30 (m, 8 H), 7.50 (m 2H); mass spectrum (EI) *m/e* 220, 219 (100), 205, 141, 115, 91.

NMR Samples. All NMR samples of **21** were prepared as described below. The volume of the CH_2Cl_2 solution containing diazene **21** was concentrated to a volume of 1-3 mL under high vacuum at -50°C. This cold solution was then transferred via 30-gauge teflon tubing into several NMR tubes (*ca.* 500 µL into each tube). The sample tubes were Wilmad glass 701-PQ 5-mm o.d., 3.5-mm i.d. quartz tubes fitted with quartz ground glass joints. The tubes had been previously base-washed, rinsed thoroughly with distilled water and methanol, and dried under vacuum. The tubes containing the diazene solutions were then fitted with vacuum stopcocks and the remaining solvent removed under high vacuum at -50°C to leave a white solid coating the inner surface. The appropriate NMR solvent was then vacuum transferred into the tube. After thoroughly degassing the sample with three freeze-pump-thaw cycles, the tube was sealed under vacuum using an oxygen-gas torch. NMR samples of bicyclopentane **22** were prepared from these diazene samples by gentle thermolysis at 60°C for 1 h.

Decomposition Kinetics of Diazene 21. Samples of **21** (*ca.* 20 mM) in $CDCl_3$ were inserted into the GX-400 NMR probe and allowed to equilibrate for *ca.* 5 min at the temperature of the experiment. After each kinetic run, the temperature of the probe was measured with a standard ethylene glycol sample. Typically 8 to 12 spectra were recorded for a run at a given temperature. Each spectrum was acquired with 4 scans, 15 sec apart to allow for sufficient relaxation. The intensity of the $2,3_{x,n}$, 5_x multiplet at δ 2.07 was monitored vs. an internal standard. All rate plots gave correlation coefficients of 0.996 or higher. The following data were obtained: *k* (T(K)), 7.25 ($\pm$ 0.12) x 10^{-5} s^{-1} (299.0), 1.56 ($\pm$ 0.02)x 10^{-4} s^{-1} (304.0), 2.54 ($\pm$ 0.04) x x 10^{-4} s^{-1} (309.3), 7.28 ($\pm$ 0.23) x 10^{-4} s^{-1} (319.1). The reported errors in rate represent standard deviations of the ln[**21**] vs. t plots. The derived activation parameters from an Eyring plot are: $\Delta H^{\ddagger} = 20.7 \pm 1.0$ kcal/mol, $\Delta S^{\ddagger} = -8.2 \pm 3.1$ eu. The errors represent one standard deviation derived from the plot.

Reactions of 22 With Olefins. to a 5 mm quartz NMR tube containing solid diazene **21**, was added a ten-fold excess of olefin and 0.5 mL of dry acetone-d_6. The sample was degassed in the usual manner and sealed. The diazene was then transformed into bicyclopentane **22** by direct photolysis at 0°C. The samples were then heated in an oil bath at 70° until the reaction was complete as monitored by high-field ^{1}H NMR. Adducts **62** and **63** were separated by colmn chromatography (3:1 pet. ether/ethyl acetate).

62: ^{1}H NMR (CDCl$_3$) δ 2.2 (m, 4 H), 2.4 (d, 1 H, J = 10.5 Hz), 2.65 (dt, 1 H, J = 10.5, 2.5 Hz), 3.7 (bs, 2 H), 7.4 (m, 10 H); mass spectraum (EI) *m/e* 318, 290, 219 (100), 91, exact mass calcd for $C_{21}H_{18}O_3$ 318.1256, found 318.1271. **63:** ^{1}H NMR (CDCl$_3$) δ 2.05 (m, 2 H), 2.20 (m, 3H), 2.33 (dt, 1 H, J = 11.0, 2.5 Hz), 3.40 (d, 2 H, J = 1.2 Hz), 7.35 (m, 10 H); mass spectrum (EI) *m/e* 318, 219 (100), exact mass calcd for $C_{21}H_{18}O_3$ 318.1256, found 318.12.64.

Photolysis Experiments. Photolyses of **21** were performed in CD$_2$Cl$_2$ solution using an Oriel 1000-W mercury-xenon arc lamp. Direct photolyses utilized the Schott filter combination WG-305/KG-5/UG-11/Hg-int ($324 \leq \lambda \leq 346$ nm) while for sensitized photolyses the WG-305/GG-375/KG-5/UG-11 ($360 \leq \lambda \leq 386$ nm) combination was used. Direct or sensitized photolysis of **21** at 0°C led to the production of only **22** as indicated by high-field ^{1}H NMR. Photolysis of **21**-d_4 in CD$_2$Cl$_2$ at -78°C, gave rise to a slight excess (*ca.* 60%) of the bicyclopentane isomer with retention of configuration (*i.e., endo* protons). Warming this sample to room temperature led to the random distribution of the proton label.

DNMR Studies. The quantitative DNMR study of 22 in degassed $CDCl_3$ solution was performed using a JEOL GX-400 spectrometer. The temperature controller on the probe was calibrated using an ethylene glycol standard. The program DNMR4 (Bushweller, C.H. *et al.*, QCPE 466) was employed in the lineshape analysis. As described in text, the simulation was divided into separate two-spin ($5_{x,n}$) and four spin ($2,3_{x,n}$) simulations. The simulated spectra shown in Figure 3-18 were obtained by plotting the sum of the two simulations. The range of rate constants that gave acceptable fits tc the experimental spectra were determined visually by overlapping the experimental and simulated spectra on a light table.

Magnetization Transfer Studies. The magnetization transfer experiments were performed using a Bruker AM-500 spectrometer in $CDCl_3$ ([22] ~ 30 mM) from 298 to 315 K. A DANTE pulse sequence[76] was employed to selectively invert the magnetization of the 5_n proton at 1.63 ppm. An acquisition time of 1.6 s and a pulse delay of 12 s were employed. The magnetizations of the 5_n and 5_x protons were then monitored as a function of the delay time (τ) before the non-selective 90° observe pulse (21 to 23 τ's ranging from 0.0005 to 15 s were employed). The magnetizations were measured by standard integrations. The exchange rates were then extracted from the raw data by fitting to the magnetization data using a non-linear least squares procedure. The reported errors in the rates are at least two times greater than the standard deviations given by the fitting routine.

The T_1's of the 5_x and 5_n protons were obtained using a Varian XL-200 spectrometer and employing the standard inversion-recovery pulse sequence. The probe was calibrated with an ethylene glycol standard.

EPR Studies. Triplet EPR spectra recorded below 77 K were obtained using a liquid helium cryostat as described in Chapter 2. Spectra recorded at 77 K were obtained by placing an MTHF solution of the diazene into a liquid N_2-filled quartz finger dewar that had been mounted in the EPR cavity. The sample was then photolyzed with light from a 1000-W mercury-xenon arc lamp directed through either a WG-305/KG-5/UG-11 ($305 \leq \lambda \leq 386$ nm) or WG-305/KG-5/UG-11/Hg-int ($324 \leq \lambda \leq 346$ nm) filter combination. The decay traces of biradicals **20**, **20-d_2**, and **20-d_4** were obtained by photolysis (9-40 s) of the corresponding diazenes and monitoring the rise and fall of signal at 3050 G (9.27 GHz) with 0.2 mW microwave power. The signal intensities were monitored for *ca.* 45 min. The decay traces were digitized and stored on disk as collected using a Compaq Plus computer. The decay traces were analyzed according to the decay-trace fitting procedure described in Chapter 2.

77 K Product Studies. Glassy MTHF solutions of diazenes 21 and 21-d_4 were photolyzed for 90 to 105 min with light ($305 \leq \lambda \leq 386$ nm) from a 1000-W mercury-xenon arc lamp while inside a liquid N_2-filled quartz finger dewar. The sample was moved vertically within the light beam periodically (10-20 min) so as to ensure uniform diazene depletion. After photolysis, the samples were quickly transferred to a large liquid N_2-filled dewar and allowed to stand for their respective decay intervals. The MTHF was then removed from the thawed samples under high vacuum at -50°C. The NMR solvent ($CDCl_3$) was then vacuum transferred into the tubes. The $CDCl_3$ solutions were then transferred via 30-gauge teflon tubing into 5 mm NMR tubes and analyzed by high-field ^1H NMR.

References and Notes

1. Buchwalter, S. L.; Closs, G. L. *J. Am. Chem. Soc.* **1975**, *97*, 3857-3858. Buchwalter, S. L.; Closs, G. L. *J. Am. Chem. Soc.* **1979**, *101*, 4688-4694.
2. Although not purely hydrocarbons, a series of triplet 4,5-diaza-1,3-cyclopentanediyls were the first localized organic biradicals to be characterized by EPR. (Arnold, D.R.; Evnin, A.B.; Kasai, P.H. *J. Am. Chem. Soc.* **1969**, *91*, 784-785.) The radical centers are in conjugation with a urazole ring, and comparison of the zfs values reported with those described here indicate a considerable, but variable degree of delocalization into the urazole.
3. Jain, R., Ph.D. Thesis. California Institute of Technology, 1987.
4. Much of the work described in this chapter has been reported in the following publications (a) Coms, F. D.; Dougherty, D. A. *Tetrahedron Lett.* **1988**, *29*, 3753-3756. (b) Coms, F. D.; Dougherty, D. A. *J. Am. Chem. Soc.* submitted for publication.
5. There was, however a report of an attempted synthesis of **21**. Cohen, S. G.; Zand, R.; Steel, C. *J. Am. Chem. Soc.* **1961**, *83*, 2895-2900.
6. Early attempts at this reduction using palladium-on-carbon as catalyst led to some (*ca.* 50%) hydrogenolysis of the benzyl amine. The rodium catalyst[7] was then employed to minimize the unwanted cleavage. It was later found that, with proper conditions, this cleavage reaction could be eliminated with palladium-on-carbon.
7. Stocker, J.H. *J. Org. Chem.* **1962**, *27*, 2288-2289.
8. Wiberg, K. B. *Angew. Chem. Int. Ed. Engl.* **1986**, *25*, 312-322.

9. (a) Snyder, G. J.; Dougherty, D. A. *J. Am. Chem. Soc.* **1985**, *107*, 1774-1775. (b) George, M. V.; Balachandran, K. S. *Chem. Rev.* **1975**, 491-519.

10. Baldwin, J. E.; Belfield, K. D. *J. Org. Chem.* **1987**, *52*, 4772-4776.

11. Engel, P.S. *J. Am. Chem. Soc.* **1969**, *91*, 6903-6907.

12. Rule, M.; Matlin, A. R.; Seeger, D E.; Hilinski, E. F.; Dougherty, D. A.; Berson, J. A. *Tetrahedron* **1982**, *38*, 787-798.

13. For the zfs calculation, the phenyl groups were coplanar with the cyclopentanediyl ring. A "spin polarized wave function" derived from experimental hyperfine measurements of benzyl radical[14] was used in the calculation. The distance between the radical centers was taken to be 2.37Å.[15]

14. Snyder, L. C.; Amos, T. *J. Chem. Phys.* **1965**, *42*, 3670-3683.

15. Conrad, M. P.; Pitzer, R. M.; Schafer, H. F., III *J. Am. Chem. Soc.* **1979**, *101*, 2245-2246.

16. (a) Goldberg, A. H.; Dougherty, D. A. *J. Am. Chem. Soc.* **1983**, *105*, 284-290. (b) Sponsler, M. B., Ph.D. Thesis, California Institute of Technology, 1987.

17. Based on the activation parameters of decay, log $A = 7.8$, $E_a = 2.29$ kcal/mol (Chapter 2).

18. Wertz, J.E.; Bolton, J.R. *Electron Spin Resonance: Elementary Theory and Practical Application*; McGraw-Hill: New York, 1972.

19. (a) Hodgkins, J.E.; Megarity, E.D. *J. Am. Chem. Soc.* **1965**, *87*, 5322-5326. (b) Huggenberger, C.; Fischer, H. *Helv. Chim. Acta* **1981**, *64*, 338-353. (c) Hiratsuka, H.; Okamura, T.; Tanaka, I.; Tanizaki, Y. *J. Phys. Chem.* **1980**, *84*, 285-289. (d) Irie, M.; Shimizu, M.; Yoshida, H. *J. Phys. Chem.* **1976**, *80*, 2008-2014.

20. Adam, W.; Wirz, J. personal communication. Adam, W.; Platsch, H.; Wirz, J. *J. Am. Chem. Soc.* submitted for publication.

21. Sponsler, M. B.; Jain, R.; Coms, F. D.; Dougherty, D. A. *J. Am. Chem. Soc.* **1989**, *111*, 2240-2252.

22. Doba, T.; Ingold, K. U.; Siebrand, W.; Wildman, T. A. *J. Phys. Chem.* **1984**, *88*, 3165-3167. Doba, T.; Ingold, K. U.; Siebrand, W. *Chem. Phys. Lett.* **1984**, *103*, 339-342.

23. Fisher, J. J.; Michl, J. *J. Am. Chem. Soc.* **1987**, *109*, 583-584.

24. This photolysis wavelength range was employed because the filter combination which produced it has a much higher transmittance (trans=0.3) at the diazene λ_{max} (350 nm) than does the mercury interference filter combination ($\text{trans}_{350\ \text{nm}} \leqq 0.01$, see experimental section). This filter combination allowed us to decrease the photolysis time required to deplete the diazene, but also led to some photolysis of the biradical as evidenced by the appearance of a radical signal in the g=2 region of the EPR spectrum.[1]

25. We cannot rule out that the cyclopentene is the product of biradical photolysis.[24]

26. Salem, L.; Rowland, C. *Angew. Chem., Int. Ed. Engl.* **1972**, *11*, 92-111. Salem L. *Pure Appl. Chem.* **1973**, *33*, 317-328.

27. Carlacci, L.; Doubleday, C., Jr.; Furlani, T.R.; King, H. F.; McIver, J. W., Jr. *J. Am. Chem. Soc.* **1987**, *109*, 5323-5329.

28. Zimmt, M. B.; Doubleday, C., Jr.; Gould, I.; Turro, N. J. *J. Am. Chem. Soc.* **1985**, *107*, 6724-6726. Zimmt, M. B.; Doubleday, C.; Jr.; Turro, N. J. *J. Am. Chem. Soc.* **1985**, *107*, 6726-6727. Closs, G. L.; Redwine, O. D. *J. Am. Chem. Soc.* **1985**, *107*, 4543-4544, 6131-6133.

29. For a discussion of isotope effects see: Carpenter, B. K. *Determination of Organic Reaction Mechanisms*; Wiley: New York, 1884; Chapter 5.

30. Baldwin, J. E.; Carter, C. G. *J. Am. Chem. Soc.* **1979**, *101*, 1325-1327.

31. Doubleday, C.,Jr.; McIver, J. W., Jr.; Page, M. *J. Am. Chem. Soc.* **1982**, *104*, 6533-6542.

32. Pranata, J.; Dougherty, D. A. *J. Phys. Org. Chem.* **1989**, in press.

33. Engel, P.S. *Chem. Rev.* **1980**, *80*, 99-150.

34. McMillen, D. F.; Golden, D. M. *Ann Rev. Phys. Chem.* **1982**, *33*, 493.

35. Thermolysis of tetradeutero diazene **21**-d_4 at 310.1 K produced a first order rate constant of $2.36 \times 10^{-4}\ s^{-1}$. This can be compared to a rate constant obtained for **21** at 309.3 K of $2.56 \times 10^{-4}\ s^{-1}$. Thus, the minimum secondary deuterium isotope effect is $k_H/k_D = 1.08$.

36. Paquette, L. A.; Leichter, L. M. *J. Am. Chem. Soc.* **1971**, *93*, 5128-5136.

37. Paquette, L. A.; Leichter, L. M. *J. Org. Chem.* **1974**, *39*, 461-467.

38. Greenberg, A.; Liebman, J. F. *Strained Organic Moelcules*; Academic Press: New York, 1978.

39. (a) Baldwin, J.E.; Ollerenshaw, J. *J. Org. Chem.* **1981**, *46*, 2116-2119. See also: (b) Chesick, J.P. *J. Am. Chem. Soc.* **1962**, *84*, 3250-3253. (c) Roth, W.R.; Enderer, K. *Justus Liebigs Ann. Chem.* **1969**, *730*, 82-90.

40. For an excellent overview of the DNMR method, see: Sandström, J. *Dynamic NMR Spectroscopy*; Academic Press: New York, 1982.

41. Binsch, G.; Kessler, H. *Angew. Chem., Int. Ed. Engl.* **1980**, *19*, 411-428.

42. Dimitrov, V.S. *J. Magn. Reson.* **1976**, *22*, 71-79.

43. Halberstadt, M L.; Chesick, J. P. *J. Am. Chem. Soc.* **1962**, *84*, 2688-2691. Steel, C.; Zand, R.; Hurwitz, P.; Cohen, S. G. *J. Am. Chem. Soc.* **1964**, *86*, 679-684.

44. (a) Campbell, I.D.; Dobson, C.M.; Ratcliffe, R.G.; Williams, R.J.P. *J. Magn. Reson.* **1978,** *29*, 397-417. (b) Lambert, J. B.; Neinhaus, R. J.; Keepers, J. W. *Angew. Chem. Int. Ed. Engl.* **1981,** *20*, 487-500. (c) Led, J. J.; Gesmar, H. *J. Magn. Reson.* **1982,** *49*, 444-463.

45. Doherty, N.M., Ph.D. Thesis, California Institute of Technology, 1984.

46. Anet, F.A.L.; Bourn, A.J.R. *J. Am. Chem. Soc.* **1967**, *89*, 760-768. Chang, M.H.; Masek, B.B.; Dougherty, D.A. *J. Am. Chem. Soc.* **1985,** *107*, 1124-1133.

47. Berg, U.; Karlsson, S.; Sandström, J. *Org. Magn. Reson.* **1977,** *10*, 117-121.

48. Steric repulsions between the phenyls were estimated by a homodesmotic reaction, in which **8** plus **22** were converted to two molecules of 1-phenylbicyclo[2.1.0]pentane. ΔH for this process was calculated to be −4.1 kcal/mol using MACROMODEL and the standard MM2 force field.

49. Rule, M.; Mondo, J. A.; Berson, J. A. *J. Am. Chem. Soc.* **1982,** *104*, 2209-2216.

50. Rodewald, L. B.; DePuy, C. H. *Tetrahedron Lett.* **1964,** *5*, 2951-2953.

51. Rabinovitch, B. S.; Schlag, E. W.; Wiberg, K. B. *J. Phys. Chem.* **1958,** *28*, 504-505.

52. Arnold, D. R.; Morchat, R. M. *Can. J. Chem.* **1977,** *55*, 393-406.

53. Wong., P.C.; Arnold, D. R. *Can. J. Chem.* **1979,** *57*, 1037-1049.

54. Brown-Wensley, K. A.; Mattes, S. L.; Farid, S. *J. Am. Chem. Soc.* **1978,** *100*, 4162-4172.

55. The activation parameters were derived from the rate information provided in ref. 52.

56. Woodward, R. G.; Dalrymple, D. L. *J. Am. Chem. Soc.* **1969**, *91*, 4612-4613.

57. Mann, B.E. *J. Magn. Reson.* **1976**, *21*, 17-23.

58. Chang, M. H.; Jain, R.; Dougherty, D. A. *J. Am. Chem. Soc.* **1984**, *106*, 4211-4217.

59. Gassman, P. G. *Acc. Chem. Res.* **1971**, *4*, 128-136.

60. At this time the structural assignment is tentative because the compound has resisted isolation and purification.

61. Adam, W.; Hannemann, K.; Wilson, R. M. *J. Am. Chem. Soc.* **1986**, *108*, 929-935.

62. The activation parameters for the bridge-flip reaction give $\Delta G^{\ddagger}_{297}$ = 17.1 ± 0.1 kcal/mol. However, if ^{1}**20** is a true intermediate, a transmission coefficient 0.5 must be attributed to the bridge-flip process. In other words, there are two paths by which ^{1}**20** may collapse to **22**. Hence, the free energy of activation for the *formation* of ^{1}**20** is reduced by RT ln2 = 0.4 kcal/mol to give $\Delta G^{\ddagger}_{297}$ = 16.7 kcal/mol.[20]

63. Dervan, P. B.; Dougherty, D. A. in *Diradicals*; Borden, W. T., Ed., Wiley: New York, 1982; Chapter 3 and references therein.

64. Wilson, R. M in *Organic Photochemistry*; Padwa A., Ed.; Dekker: New York, 1985; Vol. 7, Chapter 5.

65. Stone, K. J.; Greenberg, M. M.; Goodman, J. L.; Peters, K. S.; Berson, J. A. *J. Am. Chem. Soc.* **1986**, *108*, 8088-8089.

66. Burnett, M. N.; Boothe, R.; Clark, E.; Gisin, M.; Hassaneen, H. Am.; Pagni, R. M.; Persy, G.; Smith, R. J.; Wirz, J. *J. Am. Chem. Soc.* **1988**, *110*, 2527-2538.

67. Based on the probable errors in the activation parameters for the bridge-flip reaction and the values of ΔH and ΔS provided by Adam

and Wirz,[20] we estimate that the singlet biradical could reside within a 5.0 kcal/mol free energy well. This leads to a lifetime for ^{1}**20** of 0.3 ns.

68. Assuming that the activation parameters for a bridge-flip reaction of 19 are $\Delta H^{\ddagger} = 27$ kcal/mol, $\Delta S^{\ddagger} = 0$ eu; k_1 at 300 K becomes $4 \times 10^{-7}\ s^{-1}$. By assuming $k_2 = 10^{10}\ s^{-1}$, $k_{-1} = 10^{11}\ s^{-1}$, and [**19**] = 1 M; $^{1}k_{\mathrm{obs}}$ becomes $4 \times 10^{-8}\ s^{-1}$.

69. Adam, W.; Grabowski, S.; Platsch, H.; Hannemann, K.; Wirz, J.; Wilson, R. M. *J. Am. Chem. Soc.* **1989,** *111*, 751-753.

70. Feller, D.; Davidson, E. R.; Borden, W. T. *Isr. J. Chem.* **1983,** *23*, 105-108. Feller, D.; Davidson, E. R.; Borden, W. T. *J. Am. Chem. Soc.* **1982,** *104*, 1216-1218. Kato, S.; Morokuma, K.; Feller, D.; Davidson, E. R.; Borden, W. T. *J. Am. Chem. Soc.* **1983,** *105*, 1791-1795. Du, P.; Hrovat, D. A.; Borden, W. T. *J. Am. Chem. Soc.* **1986,** *108*, 8086-8087. Du, P.; Borden, W. T. *J. Am. Chem. Soc.* **1987,** *109*, 930-931.

71. Because we are not certain of the decay products of triplet biradical decay in a solid matrix at 77 K, it does not seem wise to map this solid-state decay data onto a potential energy diagram derived from data obtained in solution. Furthermore, it is not apparent how the most probable rate constant (k°), obtained in the condensed phase, is related to the rate constant obtained in solution, if at all.

72. Morris, G. A.; Freeman, R. *J. Am. Chem. Soc.* **1979** *101*, 760-762. Benn, R.; Günther, H. *Angew. Chem., Int. Ed. Engl.* **1983,** *22,* 350-380.

73. Still, W. C.; Kahn, M.; Mitra, A. *J. Org. Chem.* **1978,** *43*, 2923-2925.

74. Drake, N. L.; Adams, J.R., Jr. *J. Am. Chem. Soc.* **1939,** *61*, 1326-1329.

75. Salomon, R. G.; Salomon, M. F. *J. Am. Chem. Soc.* **1977,** *99,* 3501-3503.

76. Morris, G. A.; Freeman, R. *J. Magn. Reson.* **1978,** *29*, 433-462.

Appendix A

1,4-Dibromo-2,3-diazabicyclo[2.1.1]hex-2-ene

This chapter presents the results of our preliminary study of 1,4-dibromo-2,3-diazabicyclo[2.1.1]hex-2-ene (**71**). At the outset of this work, it was recognized that the thermal chemistry and photochemistry of **71** could deviate significantly from its "all hydrocarbon" analogs such a **10** and **14** for at least two reasons. First, bromine, being a "heavy atom", will greatly enhance spin-orbit coupling relative to pure hydrocarbon systems, and hence effect S ⇆ T interconversions in the diazene and any subsequent biradical species.[1] Second, as an electronegative substituent, bromine will lead to the moderate pyramidalization of radical centers.[2] These significant deviations from planarity of the radical centers may lead to altered product distributions from these intermediates relative to the unperturbed hydrocarbon systems. Indeed, as described below, **71** does exhibit dramatically novel chemistry.

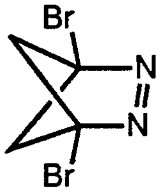

71

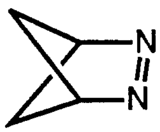

10

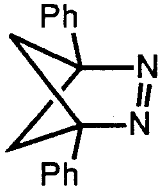

14

Synthesis

The preparation of diazene **71** begins with the readily available dicarbomethoxy urazole (**72**)[3] (Scheme A-1). The ester groups of **72** were selectively hydrolyzed by treatment with refluxing 0.5 N HCl to afford the very water soluble diacid **73**. Subjecting **73** to the conditions of the modified Hunsdiecker reaction[4] then gave dibromourazole **74** in good yield along with a small amount of bromourazole **75**. Urazole **74** can also be synthesized by thermolysis of the pyridine-2-thione diester (**76**) in refluxing bromotrichloromethane.[5] The diester is prepared *in situ* from the bis-acid chloride (**77**). Hydrolysis of urazole **74** using the standard conditions of potassium hydroxide in refluxing 2-propanol did not give the desired semicarbazide, but instead gave pyrazole **78** as the sole product (Scheme A-2). This rearrangement upon urazole hydrolysis is very similar to that observed in the phenyl-substituted series (Chapter 2), as it also involves the cleavage of a C-C bond β to a nitrogen atom. In this case, however, the formerly bridgehead substituent is expelled rather than being retained in the product. Transformation of urazole **74** into semicarbazide **79** is simply accomplished under milder conditions by performing the hydrolysis at room temperature. Diazene **71** is then prepared by treating **79** with nickel peroxide[6] at room temperature.

Scheme A-1.

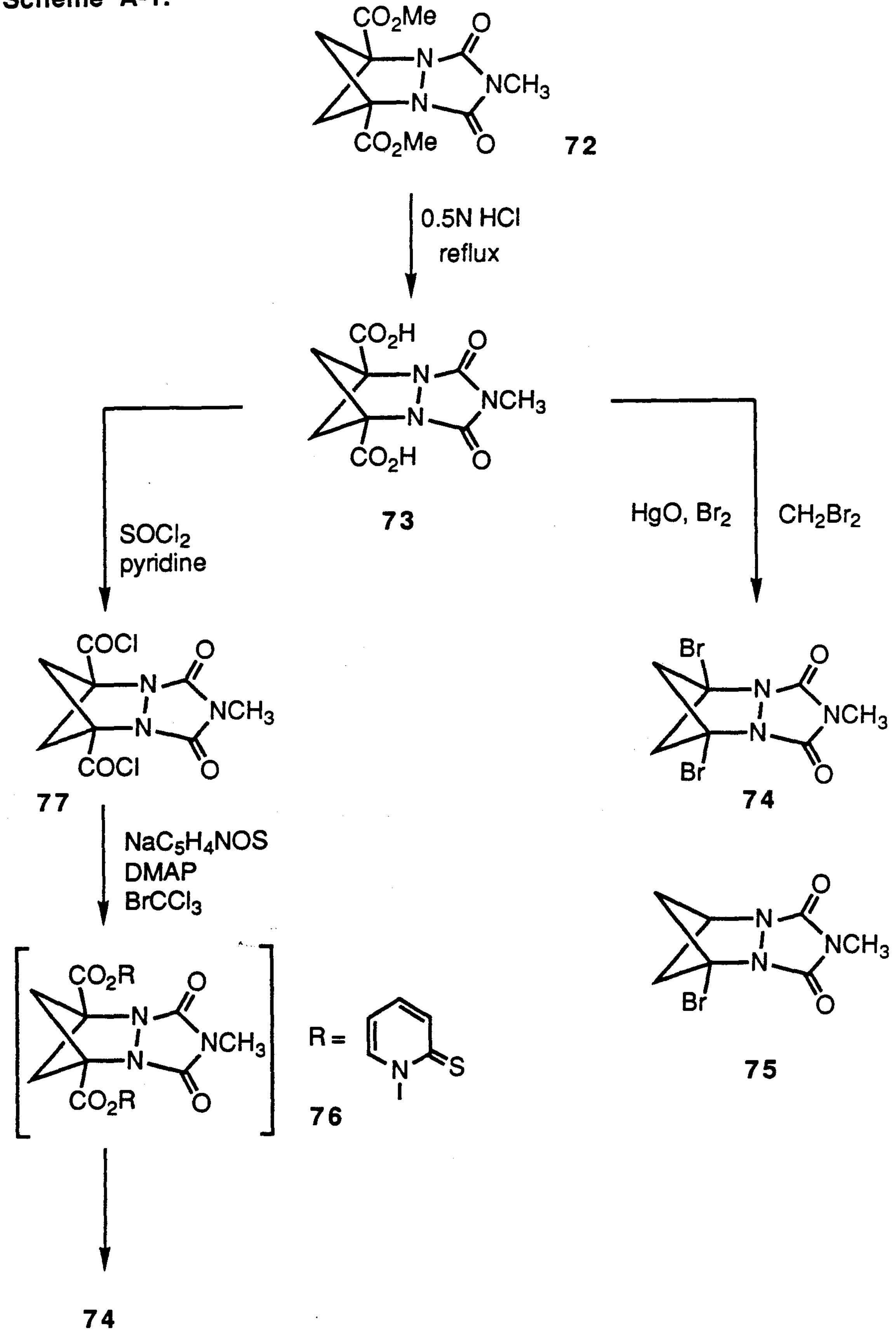
CO2Me
O
N
N
NCH3
CO2Me
O
72
0.5N HCl
reflux
CO2H
O
N
N
NCH3
CO2H
O
73
SOCl2
pyridine
HgO, Br2
CH2Br2
COCl
COCl
77
NaC5H4NOS
DMAP
BrCCl3
Br
Br
74
Br
75
CO2R
CO2R
76
R =
N
S
74

Scheme A-2.

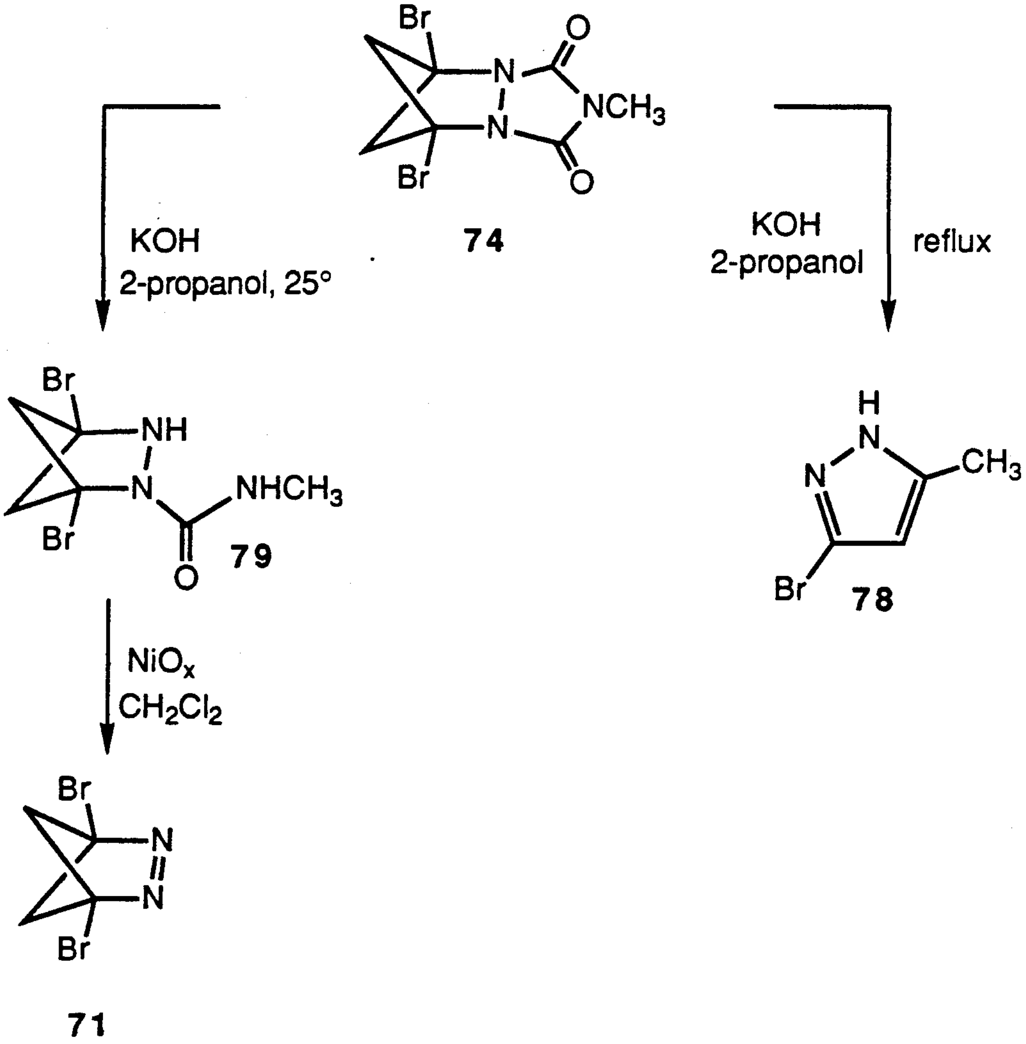
Br
Br
O
O
NCH3
N
N
74
KOH
2-propanol, 25°
KOH
2-propanol
reflux
Br
Br
NH
N
NHCH3
O
79
H
N
N
CH3
Br
78
NiOx
CH2Cl2
Br
Br
N
N
71

Thermal Chemistry

Solution-Phase. Thermal decomposition of **71** in $CDCl_3$ or C_6D_6 solution produces the corresponding bicyclobutane **80**. However, unlike all other 2,3-diazabicyclo[2.1.1]hexenes studied,[3a,7] **71** also produces a small amount (*ca.* 10%) of 1,3-dibromocyclobutene[8] (**81**, Scheme A-3). The cyclobutene 81 could arise via a 1,2-hydrogen shift from the biradical **82**. Such a hydrogen shift is well precedented in 1,3-biradical chemistry,[9] but, as stated above, has never been previously observed in a 1,3-cyclobutanediyl.[10] The lack of a 1,2-hydrogen shift in cyclobutanediyls can perhaps be attributed to poor overlap between the Π_{CH_2} orbital and the radical orbital where the migration terminates. This suggests that perhaps in **82**, this overlap has increased.

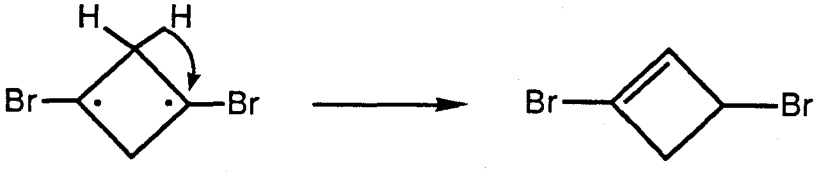

82 **81**

Although the decay kinetics were not studied quantitatively, it should be noted that the first-order rate constant of decay for **71** in solution is about 100 times that of **10** at 100°C.[7] This result is consistent with previous observations of radical stabilization by α-halogen atoms.[11,12]

Gas-Phase. Thermal decomposition of **71** in the gas phase is remarkably different from that in solution (Scheme A-3). Thermolysis of **71** at very low pressure (P ~ 10 torr) gives no bicyclobutane. The product mixture

Scheme A-3.

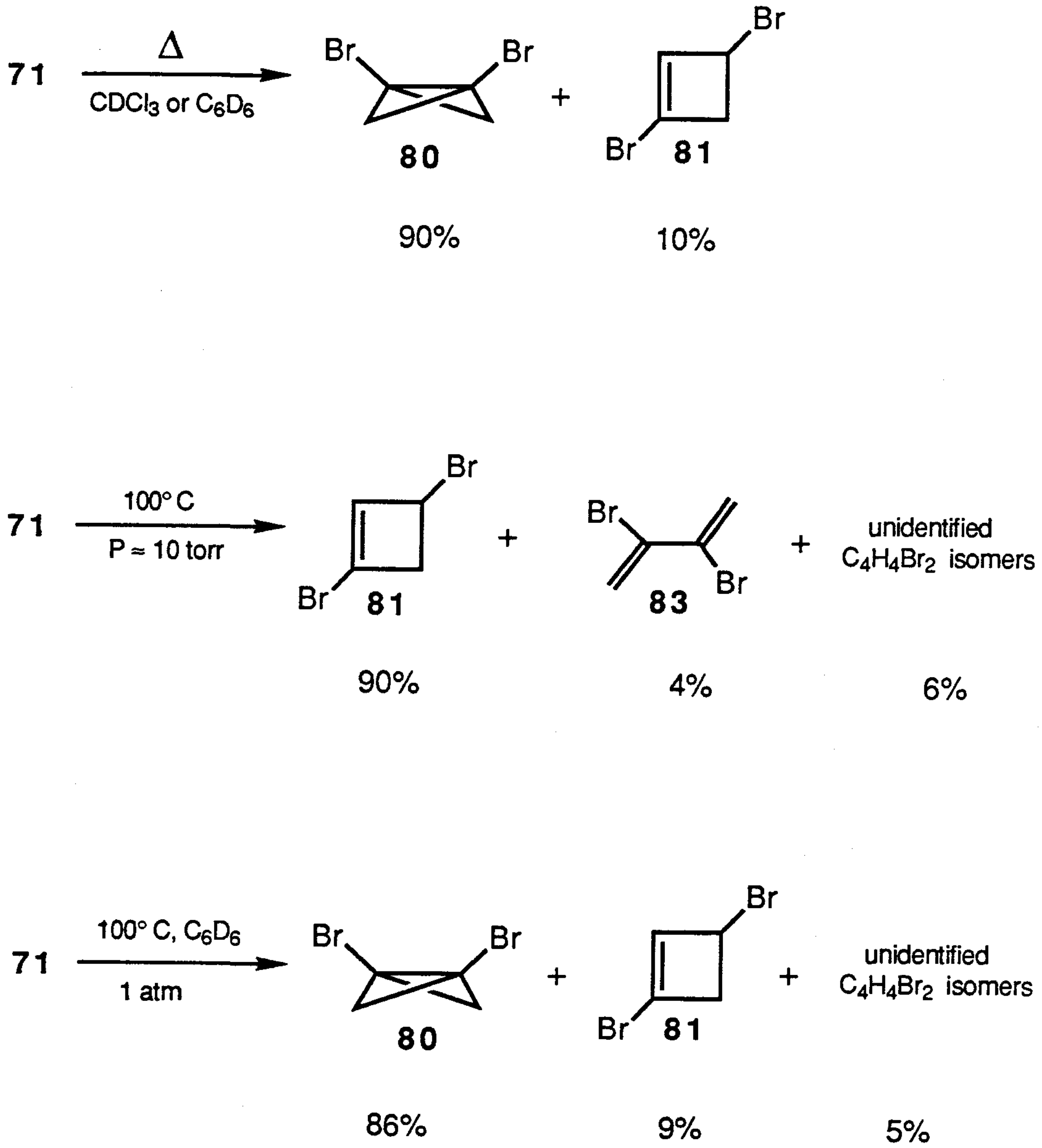
71
Δ
CDCl3 or C6D6
Br
Br
80
+
Br
Br
81
90%
10%
71
100° C
P ≈ 10 torr
Br
Br
81
+
Br
Br
83
+
unidentified
C4H4Br2 isomers
90%
4%
6%
71
100° C, C6D6
1 atm
Br
Br
80
+
Br
Br
81
+
unidentified
C4H4Br2 isomers
86%
9%
5%

consists of **81** (*ca.* 90%), 2,3-dibromo-1,3-butadiene (**83**) (*ca.* 4%), and two other unidentified $C_4H_4Br_2$ isomers (*ca.* 6%). However, when the thermolysis is performed at a pressure of one atmosphere using C_6D_6 as a bath gas, the product mixture is very similar to that obtained in the solution experiments. This gas phase experiment also contains a small amount (*ca.* 5%) of unidentified isomers. These data, suggest that the gas-phase thermolysis of **71** produces a vibrationally-excited (chemically activated) intermediate which goes on to give product distributions that differ from those obtained by thermolysis in solution.[7]

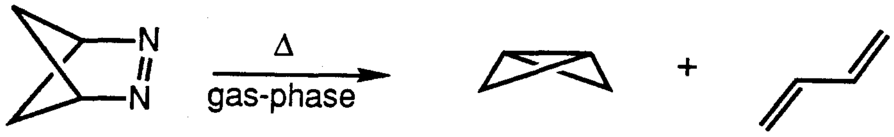

10 **82** **83**

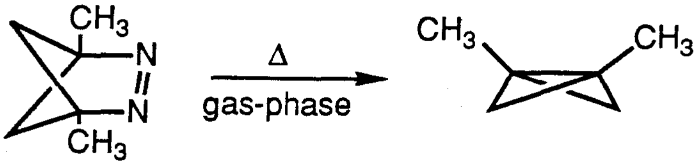

11 **13**

A similar effect has been previously observed in these laboratories when diazene **10** was thermolyzed in the gas phase to give chemically activated bicyclobutane **84** which rearranges to the "hot-molecule" product, 1,3-butadiene (**85**), in competition with collisional deactivation by a bath gas.[7] At low pressures ($P \leq 200$ torr), using N_2 as a bath gas, 1,3-butadiene is the major product. In contrast, when a good collisional deactivator such as C_6D_6 was used as a bath gas, bicyclobutane was, by far, the major product even at very low pressures. It was also shown that, at any pressure, gas phase thermolysis of the dimethyl derivative **11** gave 1,3-dimethylbicyclobutane (**13**) as the sole product. The lack of reactivity of **11** relative to **10** can be attributed to the greater number of oscillators in 1,3-dimethylbicyclobutane, which thereby decreases the probability of accumulation of energy into the reactive mode.

It is instructive to compare and contrast the results obtained from **10** and **71**. First, the respective bicyclobutanes have the same number of vibrational degrees of freedom. Therefore, it is quite plausible that, like **10**, chemical activation could be observed upon gas-phase thermolysis of **71**. Also, one of the "hot-molecule" products observed from **71**, 2,3-dibromobutadiene (**83**), could quite possibly arise via a [$\sigma 2s + \sigma 2a$] cycloreversion from 1,3-dibromobicyclobutane (**80**). In fact, the 1,3-butadiene obtained from **10** is believed to originate from this path. The dibromide system, however, deviates significantly from the parent system in that one of the presumably "hot-molecule" products, 1,3-dibromocyclobutene, is also present in the solution-phase thermolysis, albeit in small amount. Furthermore, in addition to 1,3-dibromocyclobutene, there are at least three other unsaturated $C_4H_4Br_2$ isomers present in the low-pressure thermolysis. Thus, the basic chemistries of the two systems do not appear to be strictly analogous. This is most likely a result of the non-innocent nature of bromine mentioned previously.

At this point, we cannot unequivocally state that the gas-phase thermal behavior of **71** is ascribable to chemical activation. Primarily, this is because we do not know the identity of all of the products or the pathways by which they arise. Clearly, more experiments must be performed before one can fully understand the intriguing thermal chemistry of this dibromodiazene.

Photochemistry

The photochemistry of **71** in $CDCl_3$ and C_6D_6 has been investigated. Before discussing the results, however, it is useful to review the photochemistry of other 2,3-diazabicyclo[2.1.1]hex-2-enes.

Direct or sensitized photolysis of the parent diazene **10** gives bicyclobutane (**84**), butadiene (**85**), and 1,2-diazabicyclo[3.1.0]hex-2-ene (**86**).[13] The relative yields of the photoproducts are dependent on the temperature and spin multiplicity. One unusual aspect of this photochemistry is the presence of the nitrogen-retained photoproduct **86** which is formed by β C-C cleavage to a biradical. It is this product that is formed primarily from the triplet state of photoexcited **10**.[13] Photoexcited **10** also undergoes a formal retro-[3+2] cycloaddition to give diazoalkene **87**. This diazoalkene then eliminates nitrogen photolytically to give secondary photoproducts **84** and **85**. Dimethyl diazene **11** shows very similar behavior.[3a] In contrast, diazabicyclo[2.1.1]-hexenes which have at least one delocalizing substituent (phenyl or vinyl) at a

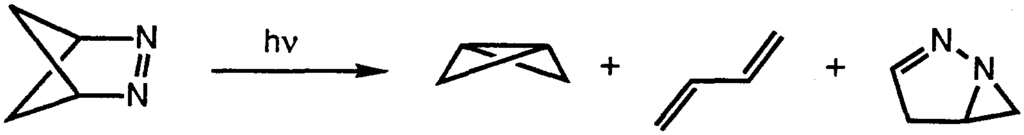

10 **82** **83** **84**

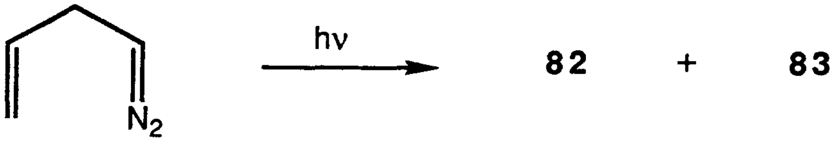

87

bridgehead position give the corresponding bicyclobutane as the sole product upon direct or sensitized photolysis.[3a]

Direct photolysis ($324 \geq \lambda \geq 346$ nm) of **71** in either $CDCl_3$ or C_6D_6 gives 1,3-dibromocyclobutene (*ca.* 60%) and an unidentified product (*ca.* 40%).[14] Analysis of the product mixture by high-field ^1H NMR reveals that unidentified product has a signal in the olefinic region and at least two signals in the aliphatic region. Unfortunately, because all of the signals are singlets, little structural information is available.

Thioxanthone-sensitized photolysis of **71** gives a a much more complex product mixture. In this case, 1,3-dibromocyclobutene is the only identifiable component of the photolysate and represents only a small fraction (*ca.* 5-10%) of the mixture. Again the NMR spectrum of the product mixture mainly consists of singlets in the olefinic and aliphatic regions.

The photochemistry is of **71** is quite complex and bears no homology with the photochemistry of other 2,3-diazabicyclo[2.1.1]hex-2-enes.[3a,13] In neither the direct nor sensitized photolyses were any trace of butadienes or nitrogen-retained products detected. Before more can be learned about this unique photochemistry, the products must be identified. Larger scale, preparative photolyses will, no doubt, aid in the identification of these products. Low-conversion photolyses should also be employed to determine what the *primary* photoproducts are. It is quite possible that the photochemistry of **71** proceeds via carbene intermediates.[13] This could easily be determined by performing the photolyses in an alcoholic solvent. Finally, acid catalysis may play an important role in this chemistry. This qualitative study has only scratched the surface of the unusual reactivity manifold of **71**.

EPR Spectroscopy

Photolysis of a frozen MTHF solution of **71** at 4 K did not produce a triplet EPR spectrum of 1,3-dibromocyclobutanediyl (**82**), but instead gave only a radical signal in the g=2 region of the spectrum.[15] This result was not unexpected and at least three reasons can be given for the failure to observe a triplet EPR spectrum. First, the triplet state of 1,3-dibromocyclobutanediyl (**82**) may not be the ground state. Second, the photoexcited triplet state of **71** may not lose N_2 at 4 K to produce the cyclobutanediyl. Finally, the triplet cyclobutanediyl, if formed, may undergo ISC to the singlet too rapidly to be detected.[1] The rapid ISC may be a consequence of the enhanced spin-orbit coupling brought about by bromine or a non-planar preferred geometry of the diyl.

Conclusion

From the above discussion, it is clear that the simple substitution of bromine for hydrogen leads to dramatic changes in chemistry. At this time, we do not know what factors (*i.e.*, heavy atom effects, radical center pyramidalization) are responsible for the unusual chemistry exhibited by **71**. One compound that may aid in the unraveling of these issues is dichlorodiazene **88**. We feel that the chemistry of **88** will deviate significantly from that of **71** for two reasons. First, because of chlorine's lower atomic number, spin-orbit coupling (and hence, intersystem crossing) in this system will be very much attenuated relative to **71**.[1] Second, because chlorine is more electronegative than bromine, we expect greater pyramidalization of the radicals centers relative to the bromine case. It is easy to see that much could be learned from a study of this system. Initial attempts at the synthesis of dichlorourazole **89** from **73**, however, failed. Many synthetic alternatives exist, and perhaps further work will lead to the synthesis of **88** and a complete understanding of this unusual chemistry.

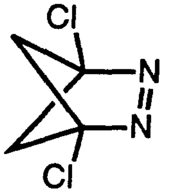

88

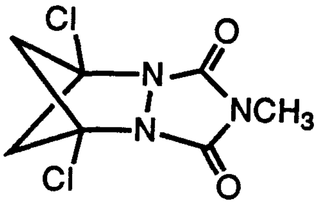

89

Experimental

General. Fourier transform NMR spectra (^{1}H and ^{13}C) were obtained on a JEOL GX-400 or Varian XL-200 spectrometer. An INEPT pulse sequence[16] was employed to determine carbon-hydrogen coupling constants. Ultraviolet spectra were recorded on a Hewlett-Packard 8451A diode array spectrophotometer. Mass spectra were obtained at the University of California, Riverside Analytical Facility or at the Caltech Analytical Facility. Analytical gas chromatography was performed on a Hewlett-Packard 5890 chromatograph equipped with a flame ionization detector. GCMS analyses were performed with a Hewlett-Packard 5890 chromatograph equipped with a Hewlett-Packard 5970 mass-selective detector. Melting points are uncorrected.

All solvents and reagents were reagent grade or better (except as noted) and used as purchased unless otherwise noted. Column chromatography was performed by the method of Still employing 230-400 mesh silica gel.

3,5-Dioxo-4-methyl-2,4,6-triazatricyclo[5.1.1.0^{2,6}]nonane-1,7-dicarboxylic Acid (73). A suspension of diester **72** (213 mg, 0.75 mmol) in 5 mL of 0.5 N HCl was refluxed for 2 h under an argon atmosphere. The resulting solution was freeze-dried to give 185 mg (96%) of **73** as a white solid: ^{1}H NMR (acetone-*d*$_6$) δ 2.30 (m, 2 H), 2.86 (m, 2 H), 3.03 (s, 3 H); ^{13}C NMR (D_2O) δ 27.58 (CH_3), 46.34 (CH_2), 71.48 (bridgehead), 162.27 (CO), 168.73 (CO_2H).

1,7-Dibromo-4-methyl-2,4,6-triazatricyclo[5.1.1.0^{2,6}]nonane-3,5-dione (74). To a refluxing suspension of diacid **73** (173 mg, 0.678 mmol) and red mercuric oxide (352 mg, 1.63 mmol) in 5.5 mL of dibromomethane (distilled from P_2O_5) was added a solution of bromine (540 mg, 3.4 mmol) in 2 mL of dibromomethane over 2 h under an argon atmosphere. The solution was allowed to reflux for an additional hour. The cooled solution was then filtered to remove the precipitated $HgBr_2$. The filtrate was washed with 1 N HCl (2 x 10 mL) and water (2 x 10 mL) to remove the dissolved $HgBr_2$. The resulting solution was dried over $MgSO_4$, filtered and concentrated to give a yellow solid which upon flash chromatography (7:3 petroleum ether-ethyl acetate) gave 126 mg (58%) of dibromide **74** as a white crystalline solid and 10 mg of bromourazole **75**. **74**: ^1H NMR ($CDCl_3$) δ 2.63 (m, 2 H), 2.78 (m, 2 H), 3.09 (s, 3 H); ^{13}C NMR ($CDCl_3$) 26.44 (q, J_{CH} = 142 Hz), 55.80 (t, J_{CH} = 152 Hz), 62.19 (s), 157.66 (s); mass spectrum (EI), *m/e* 327 (M + 4), 325 (M + 2), 323 (M), 187 (100, M - 136); exact mass calcd for $C_7H_7Br_2N_3O_2$ 322.8905, found 322.8899. **75**: ^1H NMR ($CDCl_3$) δ 2.20 (m, 2 H), 2.53 (m, 2 H), 3.08 (s, 3 H), 4.81 (t, 1 H, J = 2.2 Hz); ^{13}C NMR ($CDCl_3$) δ 26.24, 48.56, 59.98, 65.88, 158.67, 159.97; mass spectrum (EI) *m/e* 247, 245, 166, 109 (100), 82.

Preparation of 74 Via Bis-Acid Chloride 77. To 25 mg (98 µmol) of diacid **73** in 500 µL of thionyl chloride were added 16 µL of pyridine (distilled from BaO). The apparatus was placed under an argon atmosphere and the contents were brought to reflux for 1 h. The thionyl chloride was removed from the cooled reaction mixture under reduced pressure to leave **77** as an orange-brown oil. To the bis-acid chloride were added 3 mL of distilled $BrCCl_3$ and 1.5 mg of dimethylaminopyridine. After the contents of the flask were brought to reflux, sodium 2-mercaptopyridine N-oxide (Fluka technical 90-95%) was added in 2-5 mg solid portions until no decarboxylation was observed upon addition (*ca.* 50 mg over 50 min). The solvent was then removed and and the crude material purified by column chromatography to yield 7.5 mg (24% from diacid) of **74** as a white crystalline solid.

Semicarbazide 79. To a 10-mL flask containing **74** (26 mg, 0.080 mmol) and freshly-crushed potassium hydroxide (38 mg, 0.6 mmol) was added 3 mL of degassed 2-propanol. The atmosphere was replaced with argon, and the mixture was allowed to stir for 1.5 h. The solution was then carefully acidified by dropwise addition of degassed 3 N HCl until decarboxylation ceased. The solution was brought to neutrality by addition of 1 N NH3. Enough degassed water was added to dissolve the salts, and the solution was extracted with CH_2Cl_2 (2 x 2 mL). The extracts were passed through a column of $MgSO_4$ during filtration into a 10-mL flask. The solution was concentrated by passing a stream of argon over it, and then the last traces of solvent were removed under high vacuum to leave 24 mg (100%) of **79** as a white crystalline solid: ^1H NMR ($CDCl_3$) δ 2.58 (m, 4 H), 2.82 (d, 3 H, $J = 5$ Hz), 4.75 (bs, 1 H), 6.57 (bs, 1 H).

Employing the above procedure in refluxing 2-propanol for 10 min gives pyrazole **78** as the only product as a white crystalline solid: ^1H NMR ($CDCl_3$) δ 2.36 (s, 3 H), 6.05 (s, 1 H), 11.75 (bs 1 H); ^{13}C NMR ($CDCl_3$) δ 11.50 (q, $J_{CH} = 128$ Hz), 106.94 (d, $J_{CH} = 181$ Hz), 126.25 (s), 141.47 (s); mass spectrum (EI), *m/e* 162 (M + 2), 160 (100, M), 81 (M - 79).

1,4-Dibromo-2,3-diazabicyclo[2.2.1]hex-2-ene (71). To a 10-mL two-necked flask fitted with an addition ampule charged with nickel peroxide (300 mg) under an argon atmosphere was added **79** (24 mg, 0.080 mmol) in 4.5 mL of dry CH_2Cl_2 (distilled from CaH_2). The nickel peroxide[6a] was then added to the stirring semicarbazide solution over 1 min. The slurry was allowed to stir at room temperature for 20 min, then transferred to a filtration frit via cannula, and vacuum filtered into a 10-mL flask. The solvent was removed under high vacuum at -50°C to leave a slightly yellow, volatile oil: ^{1}H NMR ($CDCl_3$) δ 2.66 (m, 2 H), 3.04 (m, 2 H); UV ($CDCl_3$) λ_{max} 334 nm.

Preparation of NMR Samples of 71. All NMR samples of **71** used in photolysis and solution-phase thermolysis studies were prepared as described below. To a flask containing solid diazene **71** was added the appropriate NMR solvent ($CDCl_3$ or C_6D_6, Aldrich) via syringe. The resulting solution was divided among several quartz NMR tubes (tube specificaitons given in Chapter 3). The samples were degassed using at least three freeze-pump-thaw cycles and then sealed under vacuum.

Photolysis Experiments. Photolyses of **71** were performed at room temperature using a 1000-W mercury-xenon arc lamp. Direct photolyses utilized the Schott filter combination WG-305/KG-5/UG-11/Hg-int ($324 \leq \lambda \leq 346$ nm) while for thioxanthone sensitized photolyses the GG-375/KG-5/UG-11 ($360 \leq \lambda \leq 386$ nm) combination was used.

Solution-Phase Thermolysis Experiments. Thermolyses of sealed NMR samples of **71** were conducted from 82 to 100°C in a silicon oil bath. The progress of the reactions were monitored by UV spectroscopy.

Gas-Phase Thermolyses. Gas-phase thermal studies were conducted in a 50 or 100 mL pyrex flask fitted with a vacuum stopcock. The vessel was pretreated with Et_3N for 20 h at 120°C and then evacuated. Small amounts of diazene **71** (3-4 mg) were vacuum transferred into the flask with or without a measured amount of C_6D_6 both gas. The apparatus was then heated to 100°C for 1.5 h. The products were condensed in liquid nitrogen and an NMR solvent was vacuum transferred into the flask. Products were analyzed by high-field ^1H NMR and GCMS (oven temp 40°C, 12.5 m, OV-101 column). All detectable products were $C_4H_4Br_2$ isomers with the same mass spectrum (EI) *m/e* 214, 212, 210, 133 (100), 131 (100), 51.

References and Notes

1. Turro, N. J. *Modern Molecular Photochemistry*; Benjamin Cummings: Menlo Park, 1978; Chapter 5.
2. Kaplan, L. in *Free Radicals*, Kochi, J. K., Ed.; Wiley: New York, 1973; Vol. 2, Chapter 18.
3. (a) Jain, R.; Sponsler, M. B.; Coms, F. D.; Dougherty, D. A. *J. Am. Chem. Soc.* **1988**, *110*, 1356-1366. (b) Sponsler, M. B., Ph.D. Thesis, California Institute of Technology, 1987.
4. Della, E. W.; Patney, H. K. *Synthesis* **1976**, 251-252.
5. Barton, D. H. R.; Crich, D.; Motherwell, W. B. *Tetrahedron Lett.* **1983**, *24*, 4979-4982.
6. (a) George, M. V.; Balachandran, K. S. *Chem. Rev.* **1975**, *75*, 491-519. (b) Snyder, G. J.; Dougherty, D. A. *J. Am. Chem. Soc.* **1985**, *107*, 1774-1775.
7. Chang, M. H.; Jain, R.; Dougherty, D. A. *J. Am. Chem. Soc.* **1984**, *106*, 4211-4217.
8. Thermolyses performed at 82 and 100°C gave virtually identical product distributions.
9. See for example: Schlag, E. W.; Rabinovitch, B. S. *J. Am. Chem. Soc.* **1960**, *82*, 5996-6000. Halberstadt, M L.; Chesick, J. P. *J. Am. Chem. Soc.* **1962**, *84*, 2688-2691. Steel, C.; Zand, R.; Hurwitz, P.; Cohen, S. G. *J. Am. Chem. Soc.* **1964**, *86*, 679-684.
10. Sponsler, M. B.; Jain, R.; Coms, F. D.; Dougherty, D. A. *J. Am. Chem. Soc.* **1989**, *111*, 2240-2252.
11. O'Neal, H. E.; Benson, S. W. in *Free Radicals*, Kochi, J. K. Ed.; Wiley: New York, 1973; Vol. 2, pp. 338-340.

12. Engel, P. S. *Chem. Rev.* **1980**, *80*, 99-150.
13. Chang, M. H.; Dougherty, D. A. *J. Am. Chem. Soc.* **1982**, *104*, 2333-2334.
14. On one occasion, during the direct photolysis of **71** in C_6D_6, a small amount of 1,3-dibromobicyclobutane (**80**) was observed in the product mixture after half of the starting diazene had been decomposed. Upon complete photolysis, no bicyclobutane was detected, suggesting that **80** is a primary photoproduct. A control photolysis of bicyclobutane in $CDCl_3$, however, revealed that the bicyclobutane is inert to the radiation employed in the photodecomposition of **71**. These results may indicate the intervention of acid catalysis in the decomposition of 1,3-dibromobicyclobutane, although more studies are required.
15. On two separate occasions when the quartz EPR sample tube fractured violently on cooling to 4K, a signal centered at 820 G grew in upon photolysis ($324 \leq \lambda \leq 345$ nm). This signal decayed when the lamp was turned off. The origin of this signal is unknown.
16. Morris, G. A.; Freeman, R. *J. Am. Chem. Soc.* **1979** *101*, 760-762. Benn, R.; Günther, H. *Angew. Chem., Int. Ed. Engl.* **1983**, *22*, 350-380.